

PARAMETERIZATION OF BUILT ENVIRONMENT
FOR WIND RESOURCE ASSESSMENT

A THESIS SUBMITTED TO
THE GRADUATE SCHOOL OF NATURAL AND APPLIED SCIENCES
OF
MIDDLE EAST TECHNICAL UNIVERSITY

BY

ŞAFAK SAKÇAK

IN PARTIAL FULFILLMENT OF THE REQUIREMENTS
FOR
THE DEGREE OF MASTER OF SCIENCE
IN
BUILDING SCIENCE
IN
ARCHITECTURE

FEBRUARY 2018

Approval of the thesis:

**PARAMETERIZATION OF BUILT ENVIRONMENT FOR WIND
RESOURCE ASSESSMENT**

submitted by **ŞAFAK SAKÇAK** in partial fulfillment of the requirements for the degree of **Master of Science in Building Science in Architecture Department, Middle East Technical University** by,

Prof. Dr. Gülbin Dural Ünver
Dean, Graduate School of Natural and Applied Sciences

Prof. Dr. Fatma Candaş Bilisel
Head of Department, Architecture

Assoc. Prof. Dr. Ali Murat Tanyer
Supervisor, Architecture Dept., METU

Assist. Prof. Dr. Mehmet Koray Pekerli
Co-Supervisor, Architecture Dept. METU

Examining Committee Members:

Prof. Dr. Arzu Gönenç Sorguç
Architecture Dept. METU

Assoc. Prof. Dr. Ali Murat Tanyer
Architecture Dept. METU

Assist. Prof. Dr. Mehmet Koray Pekerli
Architecture Dept. METU

Assist. Prof. Dr. İpek Gürsel Dino
Architecture Dept. METU

Assist. Prof. Dr. Timuçin Harputlugil
Architecture Dept. Çankaya University

Date: 07.02.2018

I hereby declare that all information in this document has been obtained and presented in accordance with academic rules and ethical conduct. I also declare that, as required by these rules and conduct, I have fully cited and referenced all material and results that are not original to this work.

Name, Last name: Şafak Sakçak

Signature :

ABSTRACT

PARAMETERIZATION OF BUILT ENVIRONMENT FOR WIND RESOURCE ASSESSMENT

Sakçak, Şafak

M. Sc. in Building Science, Department of Architecture

Supervisor: Assoc. Dr. Ali Murat Tanyer

Co-Supervisor: Assist. Dr. Mehmet Koray Pekerli

February 2018, 298 pages

Use of wind power for energy generation in urban areas is gaining importance considering the energy consumption and environmental impact behaviors of built environments. Therefore, assessment of urban wind resource is crucial. The study of air flows in cities is also related to other concerns as natural ventilation, air contamination and pedestrian comfort. Two of primary research topics proposed in feasibility studies for urban wind energy are improvement on the understanding of urban wind flows with developed methods; also, an enhanced knowledge on the interaction of urban geometry with air movements. Related literature points out that there is a need for better communication between disciplines concerned with research and design. As an interface which help both sides to configure their studies, algorithm aided design tools may offer opportunities. The aim of this study is to propose a framework for parameterization of built forms for wind related studies with the use of parametric model algorithms by visual programming interfaces. Thus, a faster and diversified production of sample models can be provided by changing values of geometric variables. An example model within this framework was developed. To achieve this, a literature survey was conducted with a focus on extracting and aggregating possible shape attributes, architectural form and urban formation parameters. UML diagrams were used before translating parameters into the interface

of Dynamo software. Simple flow simulations made on samples derived from parametric models. By comparing results with parameter sensitivity analysis, influences of the parameters and relevancy of the example model were observed.

Keywords: Urban wind resource, Building geometry, Urban morphology, Algorithm aided architecture, Visual programming

ÖZ

RÜZGAR DEĞERLENDİRMELERİ İÇİN YAPILI ÇEVRENİN PARAMETERİZASYONU

Sakçak, Şafak
Yüksek Lisans, Mimarlık Bölümü, Yapı Bilimleri

Tez Yöneticisi: Doç. Dr. Ali Murat Tanyer
Ortak Tez Yöneticisi: Yrd. Doç. Dr. Mehmet Koray Pekerçli

Şubat 2018, 298 sayfa

Yapılı çevrenin enerji tüketimi ve çevresel etki davranışları değerlendirildiğinde, kentsel bölgelerde rüzgar ile enerji üretimi önem kazanmaktadır. Bu sebeple, kentsel rüzgar kaynağının değerlendirilmesi kritik hale gelmiştir. Kentlerdeki hava akımlarının incelenmesi aynı zamanda doğal havalandırma, hava kirliliği ve yaya konforu gibi konularla da ilgilidir. Kentsel rüzgar enerjisi uygulanabilirlik değerlendirmelerinde araştırma yapılması önerilen alanlardan ikisi; kentlerdeki hava akımlarının daha iyi incelenmesi ve yapı geometrisi ile kent örüntüsünün hava hareketlerine olan etkisinin daha iyi anlaşılmasıdır. Çeşitli alanlardaki yayınlar, rüzgar çalışmalarıyla ilgili disiplinler ile tasarım, yenileme ve planlama ile ilgili disiplinler arasında güçlendirilmiş bir iletişime ihtiyaç duyulduğuna işaret etmektedir. Bu bağlamda, algoritma destekli tasarım araçları fırsatlar sunabilir. Bu çalışmanın amacı, rüzgar analizlerinde kullanılmak üzere, görsel programlama ile yapılı çevrenin parameterizasyonu için bir çerçeve önermektir. Bu çerçevede esas olarak görsel programlama arayüzleri ile üretilen parametrik model algoritmaları kullanılacaktır. Böyle bir yöntem, parametre değerlerinin değişimi ile daha hızlı ve daha çok sayıda değişkenle üç boyutlu modeller üreterek her iki taraftaki ilgililere fayda sağlayabilir. Önerilen çerçevenin denemesi örnek bir modelle gerçekleştirilmiştir. Mimari biçim ve

kentsel örüntünün olası deęişkenlerini derlemek üzere bir literatür taraması yapılmıştır. Belirlenen parametreler, UML şemaları aracılığıyla ilişkilendirilmiş, daha sonra Dynamo yazılımı arayüzü kullanılarak parametrik model elde edilmiştir. Modellerden türetilen örnekler üzerinde basit rüzgar simülasyonları uygulanmış, simülasyonların sonuçları hassasiyet analizi ile incelenerek parametrelerin etki düzeyleri ve modelin amaca uygunluğu gözlemlenmiştir.

Anahtar kelimeler: Kentsel rüzgar kaynağı, Bina geometrisi, Kent biçimbilgisi, Algoritma destekli mimarlık, Görsel programlama

ACKNOWLEDGEMENTS

Firstly, I would like to thank Assoc. Prof. Dr. Ali Murat Tanyer for his guidance and criticism throughout my research process. Without his understanding and contribution, this study may have never been completed. I also would like to express my gratitude for Assist. Prof. Dr. Mehmet Koray Pekerçli for his comments and guidance from the very beginning of my graduate education.

I am grateful to all individuals of Çankaya University Department of Architecture, for their invaluable support, patience and guidance. I owe special thanks to Assist. Prof. Dr. Timuçin Harputlugil and Assoc. Prof. Dr. Gülsu Ulukavak Harputlugil for their constructive comments in this research, and also to Assist. Prof. Dr. Cengiz Özmen for his support and understanding.

I am also grateful to Merve Eşmebaşı, whose contributions and accompany was essential for me during both my undergraduate and graduate years in Middle East Technical University.

Finally, I owe deepest gratitude to my beloved family. My father was the person who taught me the importance of the education and science with his open-mindedness, idealism and vision. Then, there is no way to rightfully address the invaluable support of my mother. Without her patience, care and love, any accomplishments in my life would have been never realized.

TABLE OF CONTENTS

ABSTRACT	v
ÖZ.....	vii
ACKNOWLEDGEMENTS	ix
TABLE OF CONTENTS	x
LIST OF TABLES	xiii
LIST OF FIGURES.....	xvii
LIST OF ABBREVIATIONS	xxii

CHAPTERS

1. INTRODUCTION	1
1.1 Background Information.....	1
1.2 Motivation.....	3
1.3 Aim and Objectives	5
1.4 Contribution.....	5
1.5 Procedure and Disposition.....	6
2. LITERATURE REVIEW	7
2.1 Wind Energy in Urban Environment.....	9
2.1.1 Introductory Information on Wind Resource	9
2.1.2 Feasibility Studies and Practices of Urban Wind Energy	17
2.2 Built Forms and Their Properties.....	27
2.2.1 Classes.....	31
2.2.2 Operations	41
2.2.3 Properties.....	46
2.3 Review of Urban Wind Studies for Morphology Parameters.....	52
2.3.1 Building Form Parameters from Wind Flow Studies.....	52
2.3.2 Urban Morphology Parameters from Wind Flow Studies	56
2.4 Examples of Algorithms for Producing Generic Forms	62
2.5 Conclusions Deducted From Literature Review.....	74
3. MATERIAL AND METHOD.....	79

3.1 Material.....	79
3.1.1 Categorized Parameters.....	79
3.1.2 Software Used.....	80
3.1.3 3D Model Samples.....	81
3.2 Method.....	83
3.2.1 Parameter Aggregation and Constructing Parametric Model Algorithm.....	87
3.2.2 Sensitivity Analysis on Wind Flow Simulations	107
4. RESULTS AND DISCUSSION	119
4.1 Samples Produced by the Model for Primary Form Types	119
4.2 Results of Wind Flow Simulations.....	124
4.2.1 Measured Values.....	124
4.2.2 Observations Made During Simulations.....	128
4.3 Results of Statistical Tests.....	138
4.3.1 Curve Estimations	138
4.3.2 Assessment of Parameters' Effects by Relative Importance Values	141
4.4 Inferences from Analysis of Results.....	153
4.4.1 A Critical Review of Proposed Method.....	153
4.4.2 Inferences on Interactions Between Building Form and Wind Flows	156
5. CONCLUSION	161
5.1 Summary of the Research.....	161
5.2 Main Outcomes.....	162
5.3 Limitations of the Study	165
5.4 Recommendations for Further Research	166
6. REFERENCES	169

APPENDICES

A. PARAMETERS FROM LITERATURE SURVEY.....	189
A.1 Survey of Parameters in Wind Flow Studies.....	189

A.2 UML Diagrams of Reviewed Form Parameters	195
B. PARAMETRIC CONFIGURATION OF SAMPLE MODELS.....	199
C. SIMULATION RESULTS	205
D. DATA ANALYSIS RESULTS	271
D.1 Multiple Regression Analyses	271
D.2 Correlation Matrices	292

LIST OF TABLES

TABLES

Table 1: Type definitions, application definitions and test methods of building mounted / integrated wind turbines until 2005, interpreted from Dutton et al., (2005).....	22
Table 2: Various definitions for urban morphology. (Adapted from: Marshall & Çalışkan, 2011).....	30
Table 3: Surface types and primary solids as categorized by Ching (2014).	31
Table 4: Composition possibilities of architectural forms according to Eckler (2012).....	32
Table 5: Architectural composition types as specified by Hanlon (2009)	32
Table 6: Architectural form types in generative design (Agkathidis, 2016).....	33
Table 7: Building types according to adjacency conditions from two research studies. Interpreted from Wurm et al. (2016); Steadman (2014).....	35
Table 8: Classification of buildings based on daylight use characters of buildings in a defined region (Steadman, 1994).....	36
Table 9: Some of Reference Building Types in U.S. Department of Energy National Building Stock, interpreted from Deru et al. (2011).....	38
Table 10: Land use classes from the database of Los Angeles, California (Burian, Brown, & Linger, 2002).	39
Table 11: Current residential forms in urban pattern evolution of metropolitan regions in United States (Wheeler, 2008).....	40
Table 12: Additive transformation possibilities according to (Ching, 2014).....	42
Table 13: A classification for acts of architectural form manipulation. Adapted from Eckler (2012)	42
Table 14: A review of form and pattern components and variables. Interpreted from Çalışkan (2013).....	44
Table 15: Properties of urban forms and formations. (Çalışkan, 2013).....	48
Table 16: Comparison of three research studies by proposed properties of basic building geometry in generalization.	49

Table 17: Morphological Properties And Corresponding Indicators for urban fabrics characterization based on buildings footprints (Hamaina et al., 2012).	50
Table 18: Building specific features and neighborhood features in automatic classification of building types (Henn et al., 2012).	50
Table 19: Some of the parameters defined with site survey in San Francisco Bay Area for a procedural city model (Kunze et al., 2012).	51
Table 20: Geometric sensitivity index variables and ranges for evaluation of basic building geometry on energy use (Hemsath & Bandhosseini, 2015).	52
Table 21: Plan types and form types as used in wind flow experiments by Tamura et al. (2017).	54
Table 22: Land use classes, functions, properties for urban parameterization (Brown, 1999).	59
Table 23: Some constraint values and correlation functions for geometric parameters of urban surfaces deduced from wind flow simulations. Interpreted from (Kanda et al., 2013).	60
Table 24: Definition of the proposed framework in a form of a matrix.	84
Table 25: Lists of architectural form types, form attributes and transformative operations after first aggregation from literature.	90
Table 26: Form types based on proposed origin algorithmic model after second aggregation.	91
Table 27: Examples of essential form types with their parametric configuration in model algorithm.	120
Table 28: Simulation outputs of samples 1 – 25.	125
Table 29: Simulation outputs of samples 25 – 50.	126
Table 30: Values of parameters for samples 51-66.	127
Table 31: Curve estimation results for output parameter WS.SpeedUpRegions vs. input parameter SC.DegreeOf Curve	139
Table 32: Curve estimation results for output parameter WS.MaxSpeed vs. input parameter SC.EaveDepthRatioFront	139
Table 33: Curve estimation results for output parameter WS.MaxLocation vs. input parameter H.TotalHeight	139

Table 34: Curve estimation results for output parameter WS.MaxLocation vs input parameter SC.VertexPositionRatio	140
Table 35: Curve estimation results for output parameter RL.MaxSpeed vs V.ElevationRatio	140
Table 36: Table showing predictor importance values of model parameters for each simulation output as targets.	143
Table 37: Parameters from wind flow studies based on reference source.	189
Table 38: Parametric configuration of sample models for samples 1-10.....	199
Table 39: Screenshots of first 50 simulations used in sensitivity analysis.	205
Table 40: Screenshots of simulations 51- 66	255
Table 41. Model summary for Regression Model 1	272
Table 42: Effects, Regression Model 1	272
Table 43: Coefficients, Regression Model 1	273
Table 44. Model summary for Regression Model 2	274
Table 45: Effects, Regression Model 2	274
Table 46: Coefficients, Regression Model 2.....	275
Table 47. Model summary for Regression Model 3	276
Table 48: Effects, Regression Model 3	276
Table 49: Coefficients, Regression Model 3.....	277
Table 50. Model summary for Regression Model 4	278
Table 51: Effects, Regression Model 4	278
Table 52: Coefficients, Regression Model 4.....	279
Table 53. Model summary for Regression Model 5	280
Table 54: Effects, Regression Model 5	280
Table 55: Coefficients, Regression Model 5.....	281
Table 56. Model summary for Regression Model 6	282
Table 57: Effects, Regression Model 6	282
Table 58: Coefficients, Regression Model 6.....	283

Table 59. Model summary for Regression Model 7	284
Table 60: Effects, Regression Model 7	284
Table 61: Coefficients, Regression Model 7	285
Table 62. Model summary for Regression Model 8.....	286
Table 63: Effects, Regression Model 8	286
Table 64: Coefficients, Regression Model 8	287
Table 65. Model summary for Regression Model 9.....	288
Table 66: Effects, Regression Model 9	288
Table 67: Coefficients, Regression Model 9	289
Table 68. Model summary for Regression Model 10.....	290
Table 69: Effects, Regression Model 10	290
Table 70: Coefficients, Regression Model 10	291
Table 71: Correlation matrix of simulated dataset.	292
Table 72: Correlation matrix for samples 51-54	296
Table 73: Correlation matrix for samples 55-58.	297
Table 74: Correlation matrix for samples 59 – 62.....	297
Table 75: Correlation Matrix for Samples 63 – 66	298

LIST OF FIGURES

FIGURES

Figure 1: Power equation for an ordinary wind turbine (Campbell et al., 2009)....	10
Figure 2: World-wide annual wind speed (m/s) map at 100 m height depended on macroclimatic meteorological statistics from MERRA reanalysis between 1997-2013 (Badger, Badger, Kelly, & Guo Larsén, 2016).	11
Figure 3: A partial map of wind energy density (GW-h / km ²) in Europe (European Energy Agency, 2007).	12
Figure 4: Cumulative wind power capacity and future scenarios for wind power utilization in EU countries (Kaldellis, Zafirakis, Kondili, & Papapostolou, 2012)	13
Figure 5: Conventional formula of height- wind speed relation with definitions of inputs. (Hau, 2013).....	14
Figure 6: Overview of the energy prediction process for wind sites.	15
Figure 7: Total cumulative capacity as kW of small wind energy facilities between 2010 and 2013 from Small Wind World Report 2014. (Gsänger & Pitteloud, 2014).....	17
Figure 8: Generic options for the placement of building mounted / augmented wind turbines. (Campbell et al., 2009)	20
Figure 9: Green Building, Temple Bar, Dublin, 1995. Three turbines (each 1,5 kW) developed by Murray O’Laoire Associates (Dutton et al., 2005)	23
Figure 10: “Aeolian Roof” designs with cross-flow turbines (left), HAWTs (middle) and with a façade concentrator plane (left) by Altechnica (Dutton et al., 2005).....	23
Figure 11: Bahrain World Trade Center, designed by Atkins at 2008, image retrieved from Urban Wind Design by Campbell et al. (2009).....	24
Figure 12: A representation of the conceptual design that was re-illustrated by Campbell et al. (2009) after (N Campbell, Stankovic, & Graham, 2001).....	25
Figure 13: Oklahoma Medical Research Foundation building. The flow is channeled to wind turbines by planes designed on roof.	26
Figure 14: San Francisco Public Authority Commission Headquarters by KMD architects (Casini, 2015)	26

Figure 15: A prototype of EWICON displayed on EWI faculty building in front of Delft University (Accessed from: http://www.mecanoo.nl/Projects/project/61/Ewicon?t=6 , at 30.08.2017).....	27
Figure 16: A basic shape vocabulary of primitive solids for grammar rules to be applied on to derive different geometries (Müller, Wonka, Haegler, Ulmer, & Van Gool, 2006).	28
Figure 17: Illustrations of different opening positions in building envelope. (Ching, 2014)	47
Figure 18: Flow patterns around buildings with roof pitches of 15°, 30°, 45° (Ozmen et al., 2016).	54
Figure 19: Building height distribution and the occurrence of sheltered zones in facades behind (Millward-Hopkins et. al., 2011).	56
Figure 20: Roughness lengths and roughness classes according to terrain type.	58
Figure 21: Building array models used in flow simulations from the study of Carpentieri & Robins (2015)	61
Figure 22: “An example model from a scene-based system” (P. Janssen & Stouffs, 2015).....	63
Figure 23: “An example model from a feature-based system” (P. Janssen & Stouffs, 2015).....	64
Figure 24: Randomly generated buildings by Random3DCity in four different level of details. (Biljecki et al., 2016).....	66
Figure 25: City model produced by ESRI CityEngine and an example control panel for object parameters of selected building.	67
Figure 26: An example of a parametric model tested with sensitivity analysis for daylight qualities by multiple linear regression method. (Nault, Moonen, Rey, & Andersen, 2017).....	68
Figure 27: Plan and section profile inputs for constructing a building form with an algorithm. (Kelly & Wonka, 2011)	70
Figure 28: Automated service core generator algorithm produced in Autodesk Dynamo visual programming interface. (Das et al., 2016).....	70
Figure 29: Explanation of the design of the St. Mary Axe with a parametric model. (Giedrowicz, 2015)	72
Figure 30: Explanation of the EEPFD’s experimental process (Lin & Gerber, 2014).	73

Figure 31: Problem formulation for a design process by EEFPD (Lin & Gerber, 2014).....	73
Figure 32: Model used as Sample 1	81
Figure 33: Model used as Sample 19.	82
Figure 34: Model used as Sample 37	82
Figure 35: Definition of parameterization steps with IDEF0 diagram.	84
Figure 36: IDEF0 diagrams explaining three consequent stages with nine processes in total.....	86
Figure 37: Initial sketches for central form (left) and linear form (right) layouts.	91
Figure 38: UML Flowchart of pre-configuration step for Central Form model algorithm.....	93
Figure 39: UML flowchart explaining pre-configured Linear Form model algorithm (not produced).....	94
Figure 40: The UML diagram showing the structure of resulted parametric model algorithm.....	95
Figure 41: Polycurve of tower footprint.....	97
Figure 42: Two tower footprints with different irregularity conditions.....	98
Figure 43: Different base - tower configurations.....	100
Figure 44: Form properties of building section except the roundness, each controlled by an independent parameter explained under Section Curve Module.	104
Figure 45: Section curve and loft curves to construct the building solid in a decreased amount.....	105
Figure 46: Explanation of the ideal tunnel sizes in Autodesk Flow Design. (Autodesk Knowledge Network, accessed in 2018).....	110
Figure 47: Model status bar appears in the top-right corner of the simulation window, showing the flow condition.	110
Figure 48: An example from simulation results showing the legend, color banding and contours.....	111
Figure 49: Horizontal planes used in simulations.	112
Figure 50: Vertical planes used in simulations.	112

Figure 51: View of windward section plane from side view in sample 43, showing two speed up regions.	113
Figure 52: Location categories shown in windward section for WS_Max_Location.	114
Figure 53: An IDEF0 scheme representing the flow of Monte Carlo process in this study.	114
Figure 54: Spherical, vaulted and conic examples	121
Figure 55: Pyramidal, cubic and square based examples.	122
Figure 56: Cylindrical, circular based and triangular based examples.....	123
Figure 57: Predictor Importance comparison for Average Drag coefficient, among top ten standardized effects.....	144
Figure 58: Predictor Importance comparison for WS.SpeedUpRegions among top ten standardized effects.....	144
Figure 59: Predictor Importance comparison for WS.MaxSpeed among top ten standardized effects.....	145
Figure 60: Predictor Importance comparison for WS.MaxLocation among top ten standardized effects.....	146
Figure 61: Predictor Importance comparison for NS.SpeedUpRegions among top ten standardized effects.....	147
Figure 62: Predictor Importance comparison for NS.MaxSpeed among top ten standardized effects.....	148
Figure 63: Predictor Importance comparison for RL.SpeedUpRegions among top ten standardized effects.....	149
Figure 64: Predictor Importance comparison for RL.MaxSpeed	150
Figure 65: Predictor Importance comparison for PL.SpeedUpRegions among top ten standardized effects.....	150
Figure 66: Predictor Importance comparison for PL.MaxSpeed among top ten standardized effects.....	151
Figure 67: Building solid as a cross product of footprint layout and section curve, after reverse tapered with S.NormalTapering parameter and void opened.....	156
Figure 68: Change of the maximum speed region in windward section, depending on the building dimension.	163

Figure 69: Examples of wind flow patterns over the building base.....	164
Figure 70: Three different concentrator effects of building forms.	164
Figure 71: UML diagram showing parameters derived from literature for urban area formation.....	195
Figure 72: UML diagram showing parameters derived from literature for block formation.	196
Figure 73: UML diagram showing form parameters derived from literature for building form.	197
Figure 74: Residuals graph compared to a normal distribution, Regression Model 1.....	273
Figure 75: Residuals graph compared to a normal distribution, Regression Model 2.....	275
Figure 76: Residuals graph compared to a normal distribution, Regression Model 3.....	277
Figure 77: Residuals graph compared to a normal distribution, Regression Model 4.....	279
Figure 78: Residuals graph compared to a normal distribution, Regression Model 5.....	281
Figure 79: Residuals graph compared to a normal distribution, Regression Model 6.....	283
Figure 80: Residuals graph compared to a normal distribution, Regression Model 7.....	285
Figure 81: Residuals graph compared to a normal distribution, Regression Model 8.....	287
Figure 82: Residuals graph compared to a normal distribution, Regression Model 9.....	289
Figure 83: Residuals graph compared to a normal distribution, Regression Model 10.....	291

LIST OF ABBREVIATIONS

B	Base
B.HR	Base. Height Ratio
B.YR	Base. Y Ratio
BAWT	Building Augmented Wind Turbine
BIM	Building Information Modelling
BUWT	Building Mounted Wind Turbine
CAAD	Computer Aided Architectural Design
CAD	Computer Aided Design
CCLRC	Council for the Central Laboratory of the Research Councils
CFD	Computational Fluid Dynamics
CGA	Computer Generated Architecture
EEA	European Energy Agency
EU	European Union
EUJRC	European Union Joint Research Center
EWEA	European Wind Energy Association
GPM	Generalized Parametric Model
GW	GigaWatt
H	Height
H.TH	Height. Total Height
HAWT	Horizontal Axis Wind Turbine
ICAM	Integrated Computer Aided Manufacturing
IDEF0	ICAM Definition for Function Modeling 0
IFC	Industry Foundation Classes
MERRA	Modern-Era Retrospective Analysis for Research and Applications
NS	Normal Section
NURBS	Non-Uniform Rational B-Spline
PL	Pedestrian Level
RL	Roof Level
S	Solid

S.NT	Solid. Normal Tapering (ratio)
SAT	Standard ACIS Text (digital file extension)
SC	Section Curve
SC.CTRB	Section Curve. Concavity Translation Ratio, Back
SC.CTRF	Section Curve. Concavity Translation Ratio, Front
SC.DOC	Section Curve. Degree of Curve
SC.EDRF	Section Curve. Eave Depth Ratio, Front
SC.FETRB	Section Curve. Facade Endpoint Translation Ratio, Back
SC.FETRF	Section Curve. Facade Endpoint Translation Ratio, Front
SC.SDRB	Section Curve. Setback Depth Ratio, Back
SC.SDRF	Section Curve. Setback Depth Ratio, Front
SC.SHR	Section Curve. Setback Height Ratio
SC.VHR	Section Curve. Vertex Height Ratio
SC.VPR	Section Curve. Vertex Position Ratio
SC:EDRB	Section Curve. Eave Depth Ratio, Back
T	Tower
TF	Tower Footprint
TF.IR	Tower Footprint. Irregularity (ratio)
TF.R	Tower Footprint. Roundness (ratio)
TF.V	Tower Footprint. Vertice (count)
TF.X	Dimension of Tower Footprint in X axis of Coordinate System
TF.Y	Dimension of Tower Footprint in Y axis of Coordinate System
UML	Unified Modelling Language
UN	United Nations
V	Void
V.ER	Void. Elevation Ratio
V.HR	Void. Height Ratio
V.WR	Void. Width Ratio
VAWT	Vertical Axis Wind Turbine
WECS	Wind Energy Conversion System
WS	Windward Section

CHAPTER 1

INTRODUCTION

In this chapter, the background information is presented and followed by motivation, aim and objectives, contribution, procedure and disposition.

1.1 Background Information

Use of wind power for energy needs comes with two considerable benefits. While it reduces the dependence of economies to fuel price instability, it also reduces the carbon footprint of energy conversion, especially during generation. Wind energy has certain advantages about its operation as well. For instance, it does not require a significant policy of waste management (EWEA, 2009). The wind resource, future projections and its comparison with other energy sources are encouraging research studies in related fields.

According to UN Commission on Sustainable Development (2007), cities are territories that energy consumption is significantly concentrated, relatively to rural settlements and inhabited regions. Concordantly to this definition, they are one of the primary origins of the global warming. Since urban areas are where the energy is most needed and consumed, taking the advantage of wind energy by local means would have both economic and environmental benefits (Dutton, Halliday & Blanch, 2005; Campbell, Stankovic & Harries, 2009).

There are various issues that the wind flows can aid in urban areas. Energy conversion is one of them but it is not the only. Natural ventilation, pollution dispersion, onshore cooling, dehumidification of coastal cities are some of the possible exploitation of wind power in favor of sustainable urban developments. (Ishugah, Li, Wang, & Kiplagat, 2014)

Obviously, there are challenges and needs in the utilization of wind energy for urban environments. Turbulent characteristic of wind flows due to the increased roughness

might be one of the major problems encountered. (Smith, Forsyth, Sinclair, & Oteri, 2012), (Stathopoulos, Zisis, & Wang, 2005) However, cities also have the potential of concentrator effects for wind flows, driven by buildings and tall structures (Grayson & Garcia, 2014, Mertens, 2002). Current trends in urban wind energy are focused on micro generation (Brandon, 2015; Turan, Peacock, & Newborough, 2006) and small scale, building integrated / augmented wind turbines (Dutton et al., 2005; Grieser, Sunak, & Madlener, 2015).

Urban wind conditions are studied primarily by three methods as wind tunnel simulations, computational fluid dynamics (CFD) simulations, and field measurements (Baniotopoulos, Borri, & Stathopoulos, 2011).

Procedure of modelling the sample environment for wind studies is also subject to change according to conditions, sensitivity and the purpose of the research. Physical models in different resolutions are employed for wind tunnel measurements. Digital models can be provided by various software tools and methods for CFD simulations. It is even possible to trace 3D information data from satellite imagery for a defined area (Houda, Zemmouri, Athmani, & Belarbi, 2011) or use convert a digital model of an urban from a local administrative institution (Kanda, Inagaki, Miyamoto, & Gryscha, 2013).

Recently, practices by parametric models of architectural objects increasing in number and variety, mainly because of the development in the visual programming languages and the integration of them into parametric modelling tools (Dino, 2012). Visual programming is an intermediary tool between the programmer and the algorithm, which operates based on providing real time display of graphical representations for algorithmic data flows (Hils, 1992; Myers, 1986; Shu, 1988). Thanks to the algorithms' ability of constituting geometries, algorithm aided design has earned place in many disciplines including architecture and urban design. In general, algorithms of design process originate from a parametric diagram of relations, as the name "parametric architecture" implies (Tedeschi, 2014). Janssen & Stouffs (2015) define two categories for the types of interfaces used in parametric modelling as "scene based systems" and "feature based systems"

1.2 Motivation

Building integrated wind turbines and wind energy in urban areas are gaining importance. With necessary technology developing, design of the new turbine types or innovative utilization models of wind energy, future expectation is the increase in the use of urban wind resource; not only as designs dedicated to host conventional large scale wind turbines, but also with micro-generation and retrofitting with small scale wind energy conversion systems (Campbell et al., 2009). Besides, study of the air flows in urban environment is also associated with some other reasonable concerns like pedestrian comfort, structural analysis, passive ventilation systems, contamination and pedestrian comfort.

In a 2005 feasibility report of urban wind energy prepared for EU by CCLRC¹ research and development priorities and challenges are listed. Need for improvement in the analysis of urban wind flows together with need for improvement in knowledge on the interactions of built geometry with air movements are emphasized in both sections (Dutton et al., 2005). On the other hand, there is an observable lack of knowledge in designers and other decision makers in city planning and construction sector on similar issues. It is argued that, wind flows are represented by “smart arrows” in design process sketches or presentations of most architects depend on their predictions; while the correct prediction for wind flows in such cases requires adequate knowledge of fluid dynamics together with experience, for most cases these predictions differ from reality significantly (Chen, 2004). With the recent developments in computer aided design, building information and building information modeling software it became possible to analyze early form decisions in terms of many environmental parameters including the wind. However, there is still need for a better understanding on the correlations among types and attributes of built geometry and wind flow characteristics around them.

There is a two-way need for augmented communication between fields related to urban wind. Engineering and physics studies can become more comprehensible for architecture, building science and urban design studies to support building simulations,

¹ CCLRC was a science and engineering research body in UK government.

planning, pre-design and renovation decisions. Whereas, wind flow research and future urban wind energy innovations might benefit from the enhanced knowledge of wind related generic form and formation parameters of urban environment to develop their experimental setup. Moreover, collecting information on building types, form attributes and urban formations from various fields like urban morphology, geo-information and photogrammetry is also considered beneficial for potential developments.

In order to provide a noteworthy contribution to improvement needs mentioned, a relatively recent trend in architecture and design practices may be considered utilizable in accelerating and diversifying research methods. Algorithm aided architectural design, especially with the help of parametric models, created with algorithms by visual programming tools likes of Grasshopper and Dynamo, can become very constructive in producing interfaces between the studies of built geometry and urban wind. It is possible to integrate a large number of variables into a single algorithmic model. So that, simplified models of generic architectural and urban form samples as they can be used in wind flow simulations can be modeled with increased speed and variety in a considerably shorter time. Possible benefits of such algorithmic tools are to support:

- Simplified estimation of wind resource and potential to host wind energy conversion systems for any building or urban area.
- Design exploration, pre-design decisions of architectural forms and urban formations upon configuration for intended use with additional algorithms or BIM tools.
- Enhanced communication and understanding about wind - built form interaction to help researchers and designers in future studies.
- Acting as a core structure, allowing more sophisticated methods to be integrated onto them with optimization and decision support purposes.

1.3 Aim and Objectives

The principal aim of the study is to propose a framework on parameterization of built environment for wind flow studies by using algorithm aided tools as a step forward in wind resource assessment within urban areas.

In order to achieve this aim, these are research objectives:

- Investigating various fields of literature related to architectural forms, compositions and urban forms with a concern of determining possibly significant form parameters for wind flow studies.
- Aggregating form parameters to be included in algorithmic models and designing an algorithm for a parametric model based on these. Developing parametric model algorithm with visual programming by considering its inclusiveness on generic form types in its scope, and its relevance on wind flow behaviors
- Analyzing the influence of proposed parameters by parameter sensitivity analysis on simple flow simulations to be able to validate model considerations. This objective includes gaining inferences on building form – wind interactions as a secondary motivation.

1.4 Contribution

Contributions that this study endeavors for:

- Review and classification of building form and urban morphology parameters with concern of urban wind studies.
- Proposing a method framework on the use of algorithm aided tools to parameterize the built environment for wind-related studies.
- An example parametric model algorithm based on proposed framework, utilizable for producing experimental setups in urban wind energy potential assessment studies.

1.5 Procedure and Disposition

There are five chapters in this thesis. The first of these chapters is this introduction part. Second chapter covers a review of literature from various fields that contributed to the aim and purposes of the study. These fields include feasibility of urban wind energy, estimation of wind source, wind flow analysis, architectural aerodynamics, classification of architectural form, urban morphology studies, geo-information studies, building simulation, algorithm aided architecture and visual programming. The overall approach to the literature is based on analysis with a concern on extracting possible parameters of built environment from each domain and then relating them with the definitions on flow related parameters and variables used in wind flow studies. That process also constitutes the first part of the research methodology.

Chapter 3 is about material and method and divided into two sections. In material part, information provided for tools used in research together with the information on parameters and sample models prepared for simulations are provided. The second section, method, explains the research procedure with proposed three-step framework and research process composed of three major parts as construction of parametric model algorithm, flow simulations and parameter sensitivity analysis. In essence, an example model algorithm based on proposed framework was developed with UML and visual programming, then examined with observations and statistical tests on flow simulations. Scope and the procedure for the example model as well as the experimental setup are explained in that chapter.

Results of the processes in research are presented in the fourth chapter. Discussions and data presented include information and assessment on resulted parametric model, wind flow simulation results and a comparative evaluation of parameters' effects within the context of this study.

Lastly, the fifth chapter is the conclusion part which is comprised of judgments on conducted research with a brief summary, main outcomes, limitations of the study and recommendations for further study.

CHAPTER 2

LITERATURE REVIEW

This chapter covers the literature review, on which the latter stages of the research is based. The interpretation of literature divided into five major parts as:

- **Wind energy in urban environment:** This is configured as the first heading of the chapter. This is because the potential of the increased benefit from urban wind resource locally in urban areas, where the energy needed and consumed at most (UN Commission on Sustainable Development, 2007), was the main factor driven the motivation of the study at the beginning. Two sub-headings included in this part are:
 - **Built forms and their properties:** Within this heading, definitive approaches for architectural form, composition, urban pattern and formation types and attributes is comparatively reviewed from studies of various fields, with different purposes and methods. This part analyzes relevant literature with a more explanatory and narrative approach.
 - **Review of Urban Wind Studies for Morphology Parameters:** Similar to the former, this section is also aiming to determine form parameters for urban structures. Although, content of this section are sourced from knowledge based approaches on urban winds, architectural aerodynamics as well as wind flow analysis studies investigating variables of urban areas (See Appendix A).
 - **Algorithm Aided Models of Built Environment:** This heading provides required introductory information for the origin of the method proposed in the study. After a brief introduction with definitions and different approaches for the field, some example models from relatively similar purposed studies are interpreted.

About second and third headings, upon which the parameter aggregation is conducted, additional explanation for the nature of literature review process is needed. For a subject that requires a wide range of scanning through various fields of research literature to selectively incorporate in a Master's thesis, it is important to follow a

systematical approach to remain reliable and valid about the concerned issues. During this study that review system is based on some considerations.

Considering the possibly large amount of relevant sources, the bibliography is processed through a multi-step elimination. Google Scholar, Web of Science and Science Direct databases are used for searching with specified criteria explained as below:

- If both keywords and abstract related with the search content, the study added to a categorized pool with the help of Mendeley Desktop reference assistance tool (For this first stage, the number of quickly reviewed material was 710.).
- Secondly, in each category, if the publishing year of the content is after 2012, the reference is selected for further reading.
- Content with publishing year dated between 2002 and 2012 is sorted according to their citation number shown in databases. Among them, first 50 are reviewed.
- When the publishing year is older than 2002, the content is sorted according to their citation number similarly to explained above, then first 10 are selected for reviewing.
- Sources read are analyzed in terms of whether their content in any way includes direct inferences for “geometry based” type or attribute definitions of architectural forms and urban formations or not. A considerable number of references eliminated in this phase due to the difference of their approaches while classifying and defining forms. Since they have preferred not to use geometrical characteristics or shape attributes, rather proposing other types of determiners such as structural system or syntactic analysis.

As exceptions; books found in METU Library with a comprehensive material related to searched subject, were added to the selection. Furthermore, a few references are explored to be cited almost all of the reviewed papers in a category, they were also added to the selection without considering their publishing year and other features. After final review, sources with mostly overlapping or very similar content were eliminated for the sake of coherence of expressions.

2.1 Wind Energy in Urban Environment

This section is about facts, statistics, important terms and approaches for wind, wind energy and its urban uses. In first sub-section, 2.1.1., basic facts, statistics and terms about wind resource is presented. Starting from the definition of wind power, types of wind in atmosphere and wind resource data; continues with the estimation procedure of wind resource. 2.1.2. is rather related to studies on feasibility of urban wind energy conversion; suggestions and challenges. Content related with analysis and surveys about precedent studies of implemented wind turbines in urban areas and classification of urban wind turbines also included in this part.

2.1.1 Introductory Information on Wind Resource

Stathopoulos (2007) defines wind as atmospheric circulations created by pressure differences, hence by temperature differences in first place. Therefore, sun is the main source of the wind energy as solar radiation produces temperature differences. He continues with listing other reasons of variations of atmospheric circulations as seasonal effects, geographical effects and the rotation of earth. According to his descriptions; these three factors affect winds due to annual movement of sun between north and south of the equator, positioning of water and land masses and the rotational speed differences between equator and poles.

According to Ahrens (2012), winds divided into two groups as local and global winds. Global winds are the major and rather constant movements of huge air masses. Whereas, local winds are caused by thermal pressure systems found in the shallower regions of atmosphere. They are the wind types occurred under the effect of local geographic conditions. Ahrens classifies the most significant local wind types as below;

- Land and sea breezes due to the daily temperature difference between land and water,
- Valley breezes and mountain breezes produced by heating & cooling variations caused by topography,
- Winds driven by compressional heating like Foehn or Santa Ana,

- Seasonal winds (or monsoon winds). (pp. 241-253)

Campbell, Stankovic & Harries (2009) explain the utilizable power content of wind with respect to a basic equation valid on wind turbines:

The power in ‘free-flowing’ wind (i.e. not locally accelerated) is given by the well-known kinetic power term $\frac{1}{2}m.v^2$ where m is the mass flow rate (kg/s) of the air passing through the swept area of the turbine blades and v is the velocity of the free wind (m/s). For convenience the wind turbine power equation is expressed in terms of swept area. Therefore, the mass m is replaced with ρAv where ρ is the density of the air (kg/m³) and A is the swept area of the blades (m²). (p. 34)

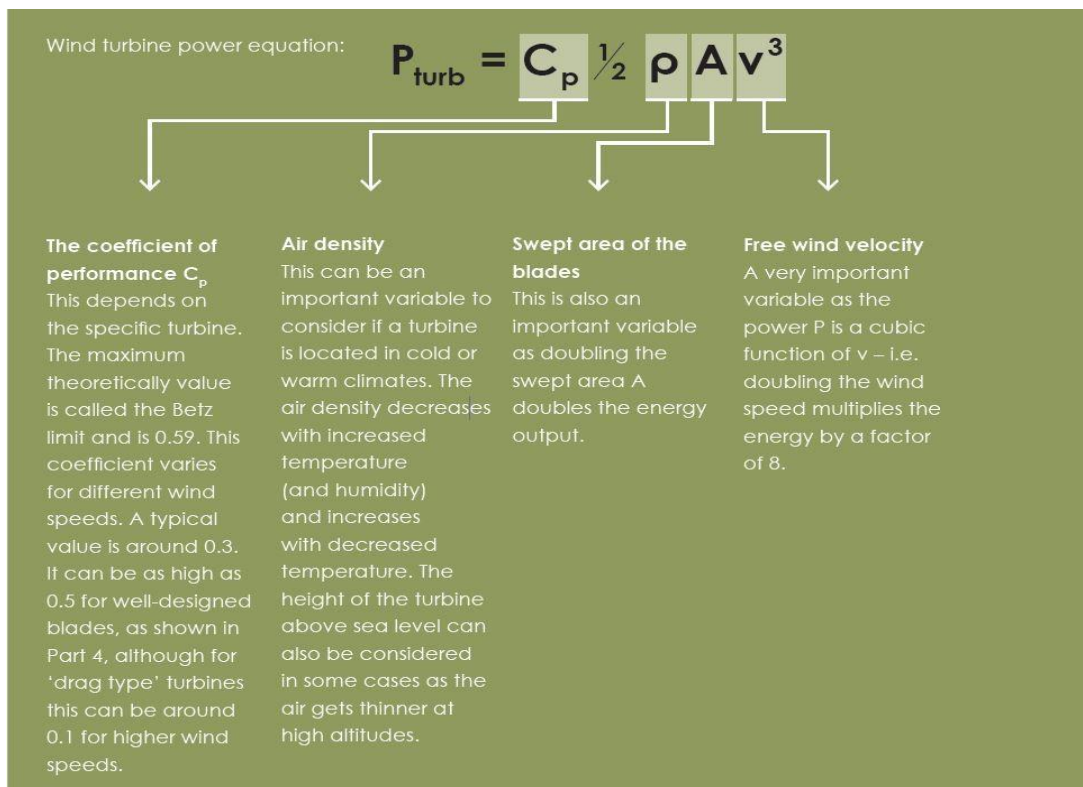


Figure 1: Power equation for an ordinary wind turbine (Campbell et al., 2009)

The wind is variable in terms of both geography and consistency. The cubic relationship of the wind speed to available energy amplifies the effects of this variety.

There are many different climatic regions in the world and this brings in the variability of sources. On the other hand, physical geography defines substantial amount of additional variation due to land and sea sizes, topography and vegetation. Open seas are the locations for highest wind velocities, whereas above land surfaces the velocity is significantly decreased (Hau, 2013). Technical University of Denmark Department of Wind Energy presents maps of global distribution in wind speed from four different statistic sets in the web site named “globalwindatlas.com”

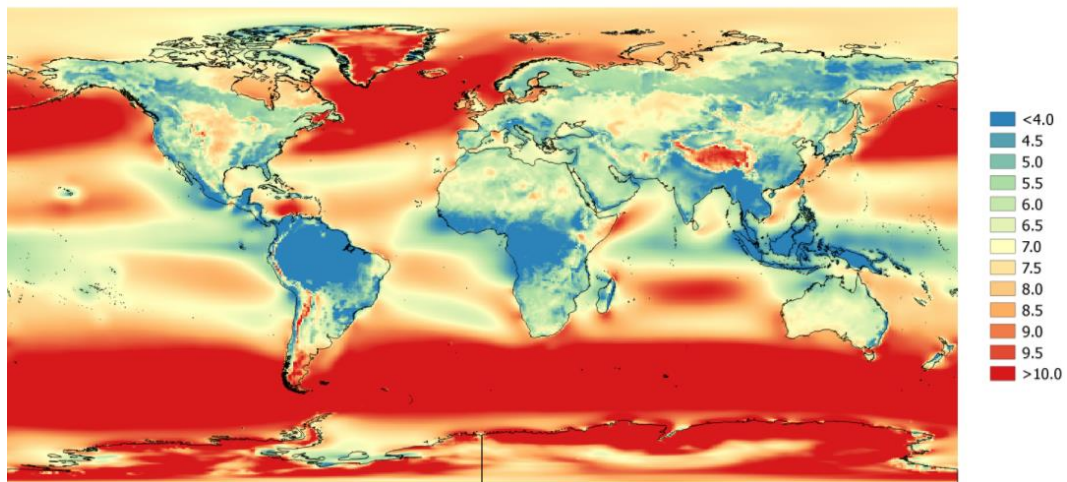


Figure 2: World-wide annual wind speed (m/s) map at 100 m height depended on macroclimatic meteorological statistics from MERRA reanalysis between 1997-2013 (Badger, Badger, Kelly, & Guo Larsén, 2016).

Also, a wind energy density map for Europe is provided in Figure 5 from a 2012 report of European Energy Agency. Beaufort Scale for the classification of wind speeds is widely used in related literature. (Hau, 2013)

According to EWEA report on 2012, there are variations and huge differences between wind power installation numbers of EU countries. The accumulated number of wind power installations is changed from 12887 to 56535 in a seven years' time period after 2000. In the same report, a prediction has been made for the future shares of wind power use in European Union until 2030 as seen in Figure 4.

EWEA (2012) describes three alternative scenarios for the future of wind power utilization of EU countries. In the study, reference values in GW were calculated according to 2007 statistics and two models developed for low and high rated development of wind energy use according to the analysis over investment potentials. The lowest expectation points 200 GWs as total, while if the highest estimations become true, this value can reach to 350 GWs. According to these estimations, possible shares of wind power in EU's energy demand are also subject to change.

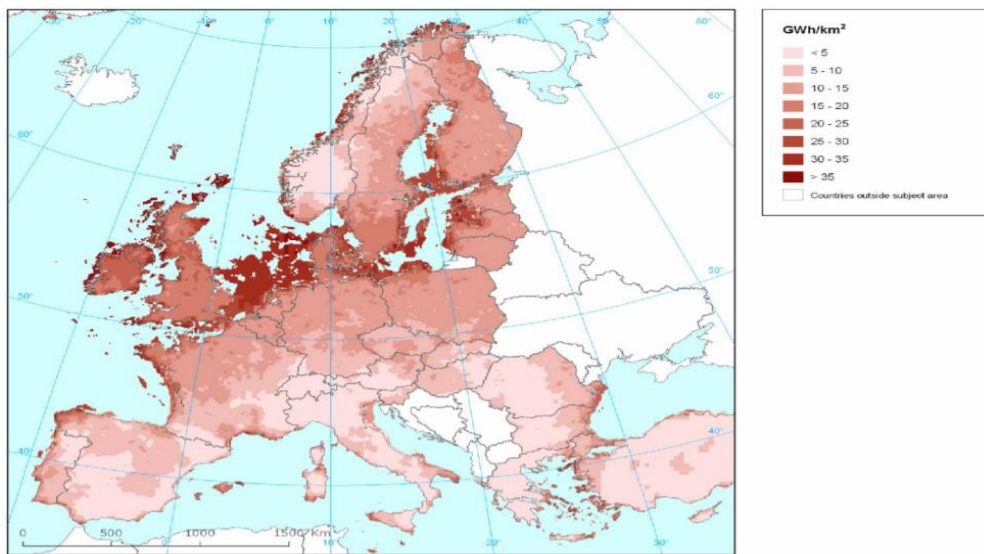


Figure 3: A partial map of wind energy density (GW-h / km²) in Europe (European Energy Agency, 2007).

It is possible to predict the energy conversion from a wind resource in a systematic way. There are various methodologies and procedures according to the context of wind resource, as well as the aim and features of proposed wind energy conversion systems. A classification can be implemented to these methods as:

- Numerical weather prediction & wind forecasting
- Ensemble forecasting
- Physical methods
- Statistical and learning approach methods

- Benchmarking and uncertainty analysis

Generic inputs for most of these procedures are contextual such as site data, short term and long term meteorological estimations and local concentrators or constraints (Foley, Leahy, Marvuglia, & McKeogh, 2012).

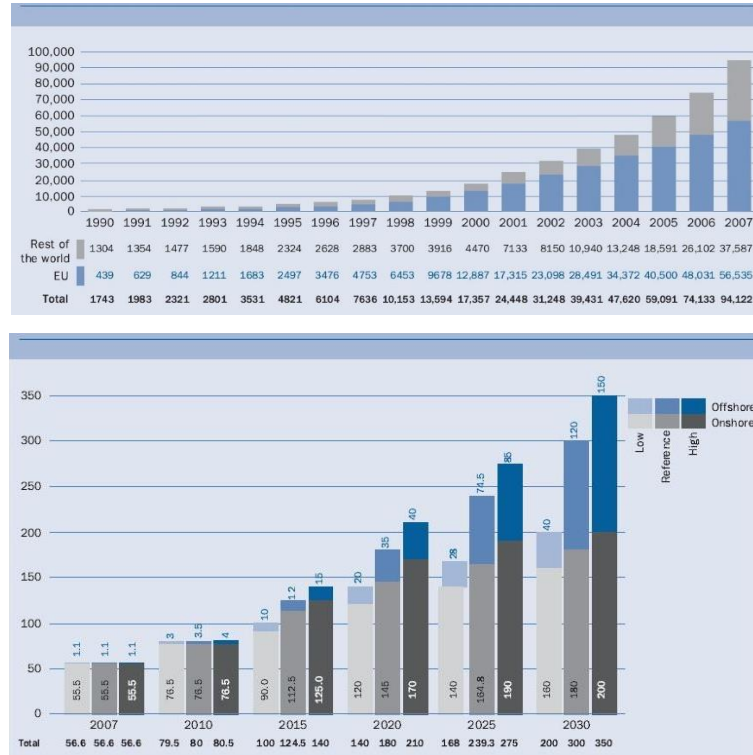


Figure 4: Cumulative wind power capacity and future scenarios for wind power utilization in EU countries (Kaldellis, Zafirakis, Kondili, & Papapostolou, 2012)

Relation of wind speed and altitude is computational by a formula which uses an elevation and a reference elevation as inputs.

$$\bar{v}_H = \bar{v}_{\text{ref}} \cdot \frac{\ln \frac{H}{z_o}}{\ln \frac{H_{\text{ref}}}{z_o}}$$

where:

\bar{v}_H = mean wind velocity at elevation H (m/s)
 \bar{v}_{ref} = mean wind speed at reference elevation H_{ref} (m/s)
 H = height (m)
 H_{ref} = reference elevation (measuring elevation) (m)
 \ln = natural logarithm (base $e = 2.7183$)

Figure 5: Conventional formula of height- wind speed relation with definitions of inputs. (Hau, 2013)

Mathew (2006), lists four factors considered in determining the energy potential of wind regimes with a concern on basic principles of a wind turbine as:

- Wind energy density which is the available energy for unit rotor area in unit rotor time.
- Most frequent wind velocity.
- Maximum wind energy reached in the specific regime.
- Design wind velocity of WECS in use. (p. 80)
- Similarly, according to Hau (2013), significant parameters for assessment of wind energy potential can be defined as:
 - The mean annual wind speed and wind speed frequency distribution.
 - Increase in wind speed with altitude
 - Steadiness of wind
 - Wind turbulence

Below, a schematic overview of the energy prediction analysis steps for wind resources as given in Figure 6.

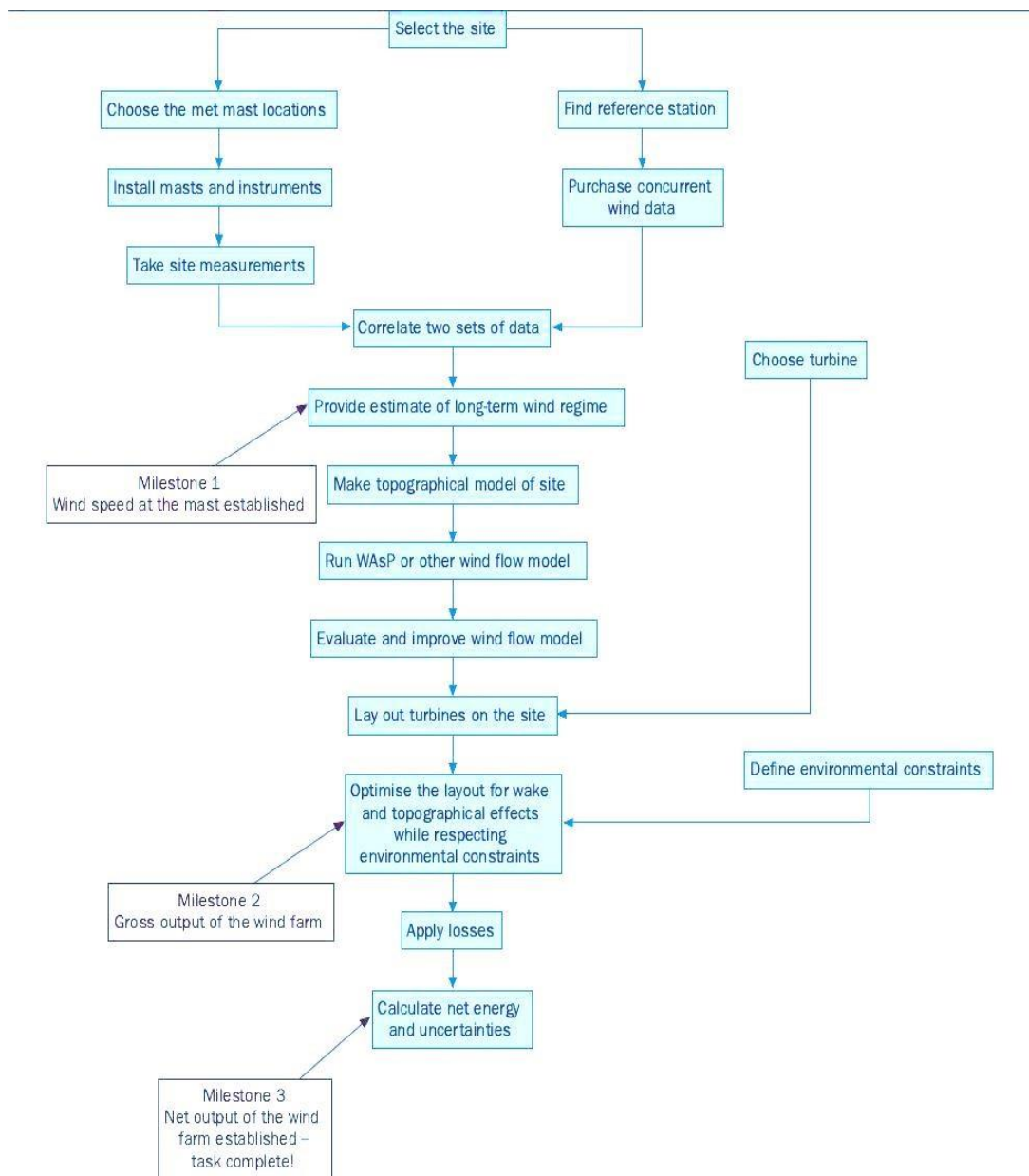


Figure 6: Overview of the energy prediction process for wind sites. (“Local Wind Resource Assessment and Energy Analysis,” accessed from <https://www.wind-energy-the-facts.org/introduction-2.html> at 29.05.2015.)

Size of the wind energy conversion systems is a parameter of classification in wind energy studies (Campbell et al., 2009). Together with the improvement of wind energy conversion technology, turbine types and mechanisms are changing. Smaller sized wind turbines have been found more suitable for the urban wind conditions. Small-scale urban wind energy generation is used as a term for such practices, (Allardyce, 2011; Moriarty, 2009) especially for the conditions that the turbine hosted by a building (Campbell et al., 2009) While innovation and development continues for wind energy conversion systems, new pioneer types which will not use the terminology of “turbine” anymore are also expected to be designed in future. According to Moriarty (2009), types of turbines are in use in urban areas generally named depending on their rotational axis as:

- Horizontal axis wind turbines (HAWT).
- Vertical axis wind turbines (VAWT).
- Building augmented wind turbines (BAWT).

The third item listed above is an exception to that naming since it represents rather a broader category. It can imply more than one siting preference likes of: On top of or alongside of a building, in between two buildings with concentrator effects, inside a building or its duct having the fundamental advantage of the stack effect (Mertens, 2002)

The term “small wind” or “small scale wind” is used in the wind energy sector to specify the small amounts of wind energy conversion with small and/ or irregular wind flows, as well as facilities dedicated for wind energy conversion which either having smaller sizes relatively to more usual wind turbines which are familiar from wind farms. Therefore, most of the wind energy conversion systems implemented, designed or thought about in urban context can be considered in that category (Dutton et al., 2005; Gsänger & Pitteloud, 2014; Mertens, 2005) However, the term certainly does not consist only urban uses, since rural areas with or without a built environment are also hosts small scale wind energy initiatives (Gsänger & Pitteloud, 2014)

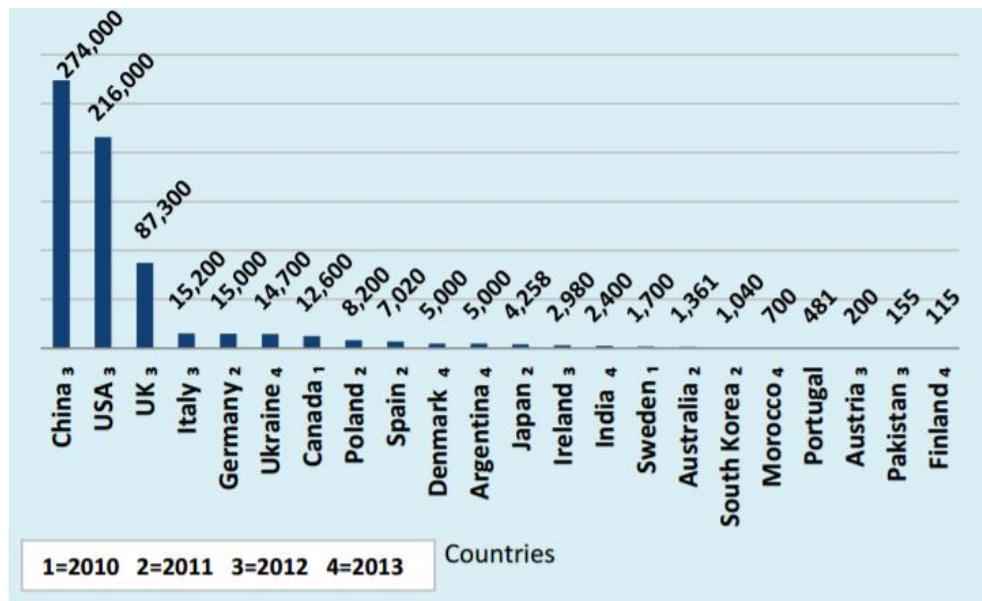


Figure 7: Total cumulative capacity as kW of small wind energy facilities between 2010 and 2013 from Small Wind World Report 2014. (Gsänger & Pitteloud, 2014)

2.1.2 Feasibility Studies and Practices of Urban Wind Energy

For urban conditions, in most cases, analysis of architectural aerodynamics and wind site assessment methodology were combined to assess wind energy potential (Neil Campbell et al., 2009; Mertens, 2006; Stewart, Haupt, & Cole, 2011). On the other hand, it is difficult to assess potential energy production of a wind turbine sited in an urban area due to three factors:

- Doubts on the knowledge of wind flow characteristics in built areas.
- Elusive nature of building – wind flow interactions
- The need for classification of building stocks based on their potential to host BUWTs. (Dutton et al., 2005)

A 2005 report by CCLRC named as “The Feasibility of Building-Mounted/Integrated Wind Turbines: Achieving their potential for carbon emission reductions” recommends four broad areas of research and development as quoted in the list below:

- Assessment of the wind regime in urban areas and isolated buildings.

- Assessment of the structural and noise implications of mounting wind turbines on or within a building structure.
- Optimization of wind turbine design for building applications
- Addressing non-technical barriers to BUWT installations

(Dutton et al., 2005)

Similarly, Günel, Ilgın and Sorguç (2007) addressed research and development priorities in ten items. Among them two are related to the study of building form as:

- Utilizing CFD tests in research of wind flows around buildings, research on different roof forms on model building structures.
- Development of guidelines for architects, designers and engineers, research on prevention of the turbine propagated noise.

Campbell et al. (2009), argue that; although urban wind energy may evoke visions of small size, three bladed wind turbines on thin columns attached to house roofs or facades; it is probably the least realistic scenario for wind energy conversion system installations in urban areas. In current situation building-mounted wind turbines requires great deal of knowledge and investment to be able to avoid unwanted complications and unsatisfactory energy supplies. These complications include structural damage together with economic drawbacks and environmental problems. Property owners may suffer disappointment and frustration after erecting small turbines on their roofs. For most of the built facilities, standard constructions of architectural elements like walls or chimneys are not capable to withstand the loading and stresses caused by a turbine mast. Unless the building structure is designed for the purpose of hosting a WECS, the only safe way for them to be utilized in that purpose is the assessment by structural experts. The unstable turbulent structure of boundary layer wind may lead to irregular stresses on turbine blades and these stresses are possibly transmitted to their connections to the host structures. They also give place to suggestions for placement of building integrated wind turbines as seven generic options and design considerations according to them (See Figure 8).

- Option A is the wind turbine on top of building. In this option, increased height of the wind conversion may eliminate local turbulence, considering fall-over distance, sustaining maintenance access and dealing with increased vibration are the important challenges. High wind turbine towers located on top of buildings makes the visual impacts another concern.
- Option B is the wind turbine on top of a building with rounded facing edge on roof. In this case the increased quality of higher altitude wind is combined with the local acceleration effect of building top form. To achieve this, additional costs for facade and roof construction may become design concerns. However, the rounded shape of the building top helps decreasing the tower height for wind turbine, and may eliminate visibility issues. Fall-over distance, maintenance access, erection process and vibration problem will be easier to overcome.
- Option C is the placement of wind turbine on top of a building with concentrator form. This option also has a local accelerator effect especially when the wind resource is bi-directional. Acoustic buffers should be provided for the building spaces in the role of concentrator. A VAWT type of turbine can be used instead of a HAWT to be able utilize wind form both directions.
- Option D is the Square concentrator within a building façade. The implementation of this option might be possible for buildings with vertical courtyards or sky gardens etc. and results better for narrower buildings. However, due to the limitations of the wind turbine technology, the size of the opening should be significantly big. Blade shedding, maintenance access and safety will be major concerns.
- Option E is very similar with the D, only the shape of the opening is circular to generate a cylindrical air movement through building. Acceleration occurs in a slightly higher rate and direction of the wind flows become a lesser concern. Hence, the use of HAWTs is also possible, but YAWTs still will be performing better.
- Option F includes turbine placements on the side of a building. For the buildings with sharper edges, this option is less realistic. The swept area needs to be increased and therefore increasing the number of turbines is suggestible. To eliminate yawing VAWTs are preferable. Safe and reliable turbines should be used

to avoid possible accidents. The material and the structure of the building facade must have required strength and consistency against dynamic effects transmitted from turbines. Adjacent facades must be thermally and acoustically insulated.

- Option G presents wind turbines between multiple buildings. Same considerations with option F are valid. Additionally, connecting two separated bodies of structures brings further challenges and requires utmost precautions.

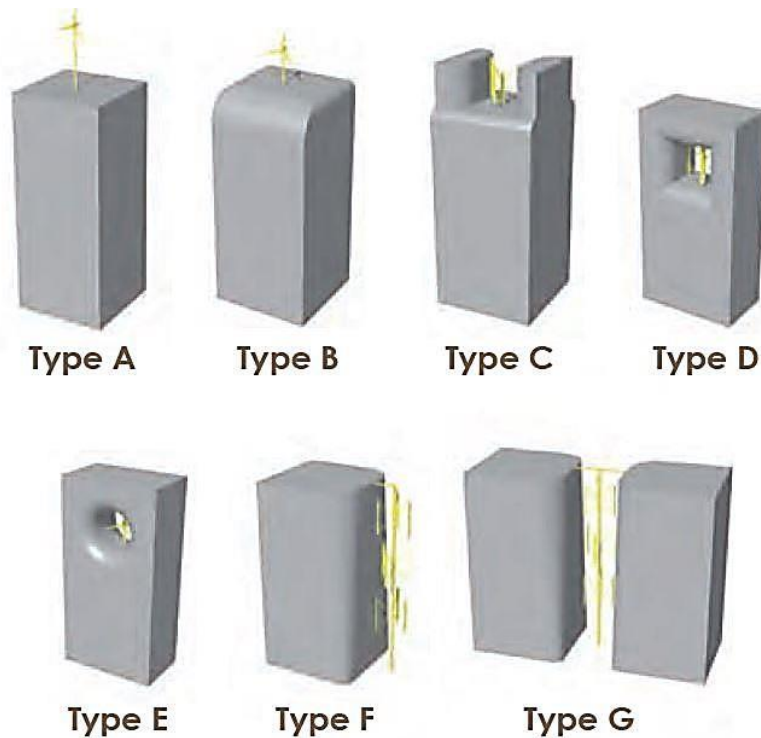


Figure 8: Generic options for the placement of building mounted / augmented wind turbines. (Campbell et al., 2009)

An important term which is expected to have a significant role in the future of urban wind energy is micro-generation. Domestic scale micro-generation, although being at an earlier stage of development, facing challenges in terms of technology and economic feasibility, have the potential of realizing considerable progress in cost, efficiency and carbon emission levels of energy production (Brandon, 2015). In this respect, most of the implemented building integrated or building augmented wind

turbines can be counted as examples of micro-generation practice. That is primarily because of the use of small scale wind energy facilities in retro-fitting wind turbines into existing building structures or designing new buildings with wind turbine components. Despite that there are examples of HAWT use on buildings, the micro-generation is usually provided by various types of VAWT designs (Bussel & Mertens, 2005; Moriarty, 2009)

Advances in wind turbine design is a crucial subject for the development of urban wind energy implementations (Baskaran, Davis, Long, & Steiner, 2009). While the variability in means of production is a broader concern which relates other areas of wind energy research such as off-shore wind energy conversion (Kaldellis et al., 2012), for urban areas it is expected that an increase in integration possibilities of wind turbines with buildings will bring innovative opportunities (Bobrova, 2015; Chaudhry, Calautit, & Hughes, 2014).

There are some studies in literature based on surveys of implemented or prototyped wind turbines in terms of their operating principles, efficiencies, noise and vibration values etc. Among them, the most comprehensive one is perhaps the related part included in 2005 CCLRC report on the feasibility of urban wind energy. Dutton et al., (2005), provides a nine page long table covering a selection of implemented building integrated wind turbines before 2005 mostly from UK with related statistical data and explanations. Table 1 presents an interpretation of this table including different types of turbines specified and other types of attributes like relative position of building and application procedure.

Following figures show some of the types involved the research mentioned above by additional information. According to Campbell et al. (2009), the most famous implementation after that era is the Bahrain World Trade Center Building with three larger horizontal axis wind turbines mounted on bridges between two symmetrical blocks of towers which augmenting the wind flow in favor of the efficiency of turbines.

Table 1: Type definitions, application definitions and test methods of building mounted / integrated wind turbines until 2005, interpreted from Dutton et al., (2005)

Type Definitions	Application Definitions	Test Definitions
HAWT	Building Mounted	Numerical models
HAWT downwind	Tested as a prototype	Wind tunnel tests
VAWT	Tested as a building mounted commercial machine	Field Measurements
VAWT (caged, augmented)		Commercial feasibility analysis
Ducted	Installed near building	
Cross-flow turbine	Aligned with corner of a tall building	
Aeolian, Bi-plane concentrator	Aligned with apex of a low-rise roof	
Tri-plane concentrator	Between adjacent buildings	
Multi-plane concentrator	Projecting out from façade	
Yawable	Projecting out from roof	
V-Type VAWT	Free-standing	
Single bladed teetered	Mounted with (or without) support structures	
Ducted Fan WT		
Slanted bladed		
Darrieus		
Savonius		
WARP (Wind Amplified Rotor Platform)		
Hellical VAWT		



Figure 9: Green Building, Temple Bar, Dublin, 1995. Three turbines (each 1,5 kW) developed by Murray O’Laioire Associates (Dutton et al., 2005)

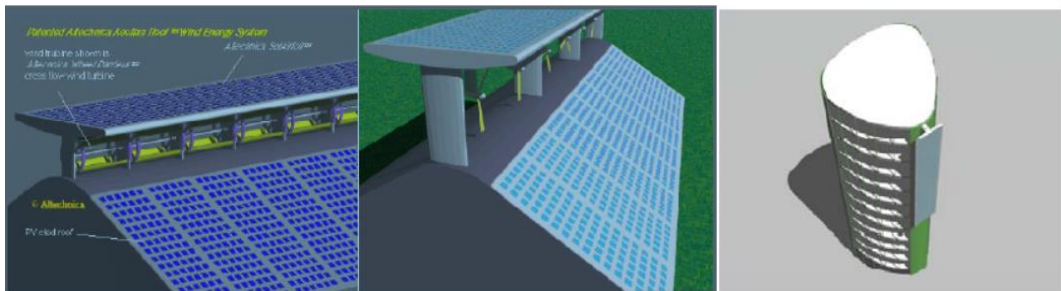


Figure 10: “Aeolian Roof” designs with cross-flow turbines (left), HAWTs (middle) and with a façade concentrator plane (left) by Altechnica (Dutton et al., 2005)



Figure 11: Bahrain World Trade Center, designed by Atkins at 2008, image retrieved from Urban Wind Design by Campbell et al. (2009)

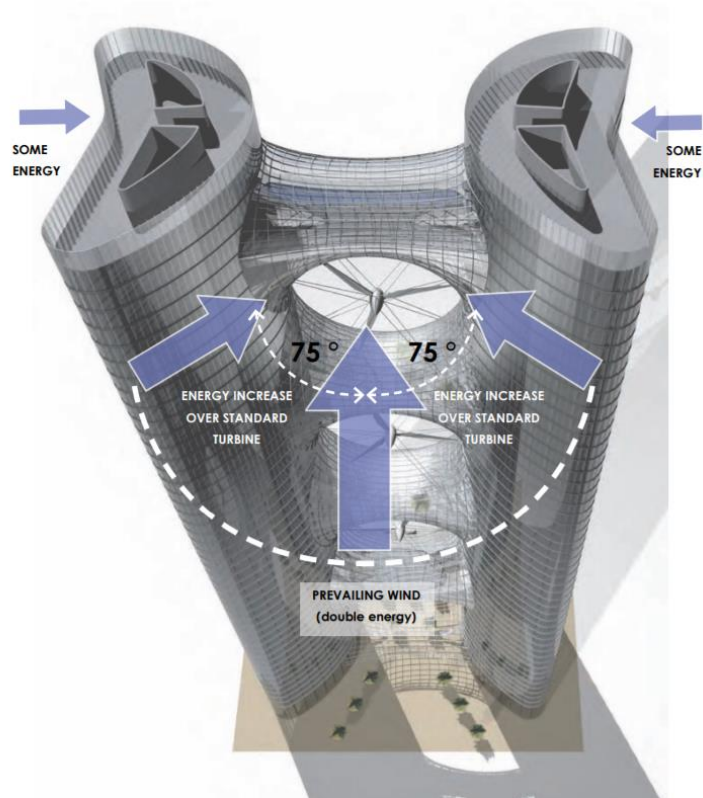


Figure 12: A representation of the conceptual design that was re-illustrated by Campbell et al. (2009) after (N Campbell, Stankovic, & Graham, 2001)

A very similar design concept to Bahrain World Trade Center; which benefits from two identical vertical components for wind augmentation was studied previously in a research and development project called “Project Web” in 2000 (Campbell, Stankovic, & Graham, 2001).

There are also examples of building which enables the augmentation of wind turbines with additional building components like panels or projections. Casini (2015) has reviewed some of the latest implementations of vertical axis wind turbines augmented by building forms by use of additional planes designed parallel to building envelope. Two of the examples from his article are: Oklahoma Medical Research Foundation building and Francisco Public Authority Commission Headquarters building. Images of both buildings are presented in next page.



Figure 13: Oklahoma Medical Research Foundation building. The flow is channeled to wind turbines by planes designed on roof. Source: <http://perkinswill.com/work/oklahoma-medical-research-foundation.html>, accessed at 15.03.2016



Figure 14: San Francisco Public Authority Commission Headquarters by KMD architects (Casini, 2015)

Djairam, Hubacz, Morshuis, Marijnisen, & Smit (2005) proposed an electrostatic wind energy converter. Unlike conventional methods, there is no moving parts on this converter for wind energy harvesting.



Figure 15: A prototype of EWICON displayed on EWI faculty building in front of Delft University (Accessed from: <http://www.mecanoo.nl/Projects/project/61/Ewicon?t=6>, at 30.08.2017).

2.2 Built Forms and Their Properties

This section is a brief review of an exploration on definitive components of forms in built environments based on literature of various fields.

It is possible to overview the geometry-based classification and parameterization of forms as the act of decomposing the observable shape into its constituent components. Metaphorically, the procedure is similar with linguistic analysis practices like decomposing the structure of a word or a sentence. In this sense, an approach developed during the second half of the 20th century which defines shapes algorithmically, uses the name of shape grammars. In a shape grammar there is a primary geometric object like a word root, takes actions onto itself to develop into

another geometry. There are acts resembling suffixes and prefixes for a word or verbs and clauses for a sentence. Their role is to transform the primary object into other shapes according to sets of rules defined by the shape grammar in use (Stiny, 1980).



Figure 16: A basic shape vocabulary of primitive solids for grammar rules to be applied on to derive different geometries (Müller, Wonka, Haegler, Ulmer, & Van Gool, 2006).

Form and morphology, however, hosts contextual meanings in addition. For fine arts, design and architecture; there are more qualities and properties attached to the form rather than merely the shape of objects (Ching, 2014; Krier, Schnerider, & Vorreiter, 1988).

Morphology is a superset term which also includes the form within. In biology the form and structure of an organism together composes the morphology which is also the name of a branch in biological sciences (Brady, 1994; Nyhart, 1995; Richards, 2008). In linguistics, morphology is related with linguistic elements, their structure like stems, suffixes, prefixes, patterns of word formations mostly based on syntactic relationships (Anderson, 1992). For geographic information studies the condition is similar; forms like trees, buildings, water bodies with several structural properties associating them into patterns and clusters are subject to morphological analysis (Tulloch, 2016). The term geomorphology denotes the area of geography studying landforms, mostly with an emphasis on un-built objects of nature (Summerfield, 2014). Whereas, various definitions available for “urban morphology” is provided

from literature in a 2011 study by Marshall & Çalişkan (2011) as quoted, with the table as it is, in Table 2.

Building forms can be analyzed in terms of their primary architectural form components, parent geometry that they are generated from; as primary shapes. (Ching, 2014) Or archetypical characteristics that may aggregate them into classes and types may be preferred as an analytic tool (J. P. Steadman, 1994). The existence of built forms in urban context manifests more ingredients than each form has independently; as they become constituent parts of urban pattern. Nevertheless, a similar kind of an analysis is possible for the formation of urban forms whether depending on their shared primary components (Kropf, 2009) or their observed similarities to abstract them into archetypes (Steiniger, Lange, Burghardt, & Weibel, 2007). However, for the analysis of urban formation, a classification of its constituents also necessary as they also include their own variables. Together with the form, characteristics of the structure, which defines the order that forms come together, characteristics of the pattern since the whole behaves different than its components.

To analyze the possibilities of exploring generic form parameters for buildings and urban patterns for an algorithmic set-up utilizable in urban wind studies; related literature is reviewed from various fields, throughout following sections of this chapter. In three sections, following subsets are followed to interpret from a wide range of relevant literature:

- Class; to select from (Object, type, base geometry, components etc.)
- Operation; to apply on (Form giving operations, generative acts, transformative acts etc.)
- Property; to change (Attributes, variables, values, qualities etc.)
- Second degree property (Properties of components, reviewed together with the previous item in 2.2.3).

Table 2: Various definitions for urban morphology. (Adapted from: Marshall & Çalışkan, 2011)

	Definition	Source
General	‘The study of urban form.’	(Cowan, 2005)
	‘The science of form, or of various factors that govern and influence form.’	(Lozano, 1990, p. 209)
	‘The study of the physical (or built) fabric of urban form, and the people and processes shaping it.’	(Urban Morphology Research Group, 1990)
	‘Morphology literally means ‘form-lore’, or knowledge of the form ... what is the essence of that form; does certain logic in spatial composition apply, certain structuring principles?’	(Meyer, 2005, p. 125)
Focus on the manner and purpose of study	‘... an approach to conceptualizing the complexity of physical form. Understanding the physical complexities of various scales, from individual buildings, plots, street-blocks, and the street patterns that make up the structure of towns helps us to understand the ways in which towns have grown and developed.’	(Smailes, 1955, p. 101; cited in Chapman, 2006, p. 24)
	‘Urban morphology ... is not merely two dimensional in scope. On the contrary, it is through the special importance which the third dimension assumes in the urban scene that much of its distinctiveness and variety arise.’	
	‘A method of analysis which is basic to finding out principles or rules of urban design.’	(Gebauer and Samuels, 1981; cited in Larkham, 1998)
Focus on the manner and purpose of the study	‘... the study of the city as human habitat... Urban morphologists ... analyze a city’s evolution from its formative years to its subsequent transformations, identifying and dissecting its various components.’	(Moudon, 1997)
	‘First, there are studies that are aimed at providing both (i.e. cognitive contributions); and secondly, there are studies aimed at determining the modalities according to which the city should be planned or built in the future (i.e. normative contributions).’	(Gauthier and Gilliland, 2006, explanations or developing explanatory frameworks or p. 42)

2.2.1 Classes

One of the frequent qualitative approaches in architecture literature investigates architectural forms by their geometry based generative components. In that case, there are primary elements behave as constituent elements of all forms. Definition or classification of those primary objects vary in literature. Line, plane and volume are mentioned in multiple studies (Ching, 2014; Çalışkan, 2013).

Definitions of form classes based on their resemblance to a primal geometric shape is also a preferred approach. Ching (2014) and Krier et al. (1988) suggest circle, triangle and square to behave like stems for other geometries while Achten (2012) uses a more versatile definition as a n sided regular polygon together with circle. (Eckler, 2012), on the other hand, named these constituents as “tectonic elements of assembly” which are listed as:

- mass,
- plane,
- frame
- stereotomy.

Ching (2014), similarly, provides definitions of primary surfaces and primary solids as quoted in Table 4.

Table 3: Surface types and primary solids as categorized by Ching (2014).

Types of Surfaces	Primary Solids
Cylindrical surfaces	Sphere
Translational surfaces	Cylinder
Ruled surfaces	Cone
Rotational surfaces	Pyramid
Paraboloids, Hyperbolic paraboloids	Cube
Saddle surfaces	

Likewise, elements can also be distinguished based on the regularity of their primary geometry. In this sense Krier et al. (1988), divided architectural compositions into three groups as: Regular (geometric), irregular (chaotic) and mixed.

Types of compositions and arrangements of architectural form is also an agent of classification. This approach is exemplified in Table 4 and Table 5 from the studies of Eckler (2012) and Hanlon (2009).

Table 4: Composition possibilities of architectural forms according to Eckler (2012).

Structured Arrangement Possibilities	Generative Possibilities in Simplified Form
Central	Curvilinear
Cluster	Diagonal
Grid	Orthogonal
Linear	Horizontal
Radial	Vertical

Table 5: Architectural composition types as specified by Hanlon (2009)

Squared Composition	Linear Composition	Clustered Composition	Layered Composition
Four quartered square	Spinal organization	Radial focus on a central point	Horizontal layers
Nine square diagram	Segmental organization	A shared axis as a centerline	Vertical layers
	Branched organization	Perpendicular relations of their sides or axes of symmetry	Concentric layers
		Parallel relations of their sides or axes of symmetry	Radial layers
		Tangential relations of their sides or axes of symmetry	

Table 6: Architectural form types in generative design (Agkathidis, 2016).

Continuous surfaces		
Soft mesh	Double curved shells	Hyper paraboloids
Modular and Accumulated		
Interlocking units	Irregular units	
Deformed and Subtracted		
Twisted block	Porous space	
Algorithmic Patterns		
Tessellated planes	Voronoi surface	
Triangulated Forms		
3D Penrose pattern	Faceted loft	

Even the representation of architectural information can be a determining factor in form production. Conventionally, representations can be translated into three type of medium as 3D, planar plane (horizontal section), sectional plane (vertical section) (Özdemir & Önal, 2016).

Quantitative approaches for classification of building forms are usually found in geo-information or urban morphology studies. Depending on the purpose of the study, definitions of the object classes may vary. A common approach is to categorize built forms by generalization of their shape based features (Gaffuri & Trévisan, 2004; Wurm, Schmitt, & Taubenböck, 2016) Yet, some parameters can be encountered in most of these studies. Height of a building is one of the significant parameters used in quantitative classification. Buildings can be distinguished by their heights as:

- Low- rise buildings (Wen Zhang et al., 2017)
- Multi-storey buildings (Steadman et al., 2000; Wen Zhang et al., 2017)
- High-rise buildings (Burian, Brown, & Velugubantla, 2002; Wen Zhang et al., 2017)

Concordantly to the height variables mentioned above, Szalay's (2008) study can be referred as an example of differences in rules for quantitative parameter definitions depending on the purpose and the sample size of research. As the study proposes a

model of building stock geometry for energy, emission and mass calculations for residential buildings, a combination of density and height classes defined as below:

- Single family houses, one storey
- Single family houses, two storeys
- Low-rise, high-density buildings, one storey
- Low-rise, high-density buildings, two storeys
- Low multi-family buildings
- Medium-high multi-family buildings.

To categorize the size, various criteria can be adapted other than exact dimensional values. When generalized based on site data like satellite imagery, function or the use of the building can also be associated to its size (Belgiu, Tomljenovic, Lampoltshammer, Blaschke, & Höfle, 2014). In their 2014 study based on three major cities, London, Istanbul and Paris, Belgiu et. al. provided three classes for that kind of an approach: Residential (small buildings), apartment (block buildings), industrial and factory buildings.

Similar to the height and size, adjacency condition of a building can serve the purpose of categorical generalization in quantitative studies (Steadman, 2014; Wurm et al., 2016). Terminology employed and sensitivity of distinction may differ in each research depending on the context and aim as exemplified in Table 7. Adjacency is also a parameter for urban formations.

Other than adjacency, for a built unit, another parameter for its surrounding can be derived from the definition of the type of its regional context. Gaffuri and Trévisan (2004), suggested a classification which converts the affinity to urban character into a determinant measure for the blocks they defined in their research as:

- Isolated building (unitary blocks)
- Farm blocks
- Urban blocks
- Suburban blocks

Table 7: Building types according to adjacency conditions from two research studies. Interpreted from Wurm et al. (2016); Steadman (2014).

Title of the reference	Building types according to adjacency
Wurm, M., Schmitt, A., & Taubenböck, H. (2016). Building types' classification using shape-based features and linear discriminant functions.	Perimeter Block Development
	Block Development
	Terraced houses/row houses
	Detached/ semi-detached houses
	Halls
Steadman (2014) Building Types and Built Forms	Back to back (detached by single facade)
	Quarter detached
	Semi detached
	Terraced (row houses)
	Detached

Shape of a building footprint can also be an object of generalization by resemblance. Hamaina, Leduc, & Moreau (2012) used the resemblance to letters which they call template; to classify building fabrics. Match-up definitions they provided are:

- L shaped footprint
- I shaped footprint
- H shaped footprint
- A shaped footprint
- V shaped footprint

It is possible that shape definitions and number of shape based types are mounted up, mostly in research studies based on much specified areas and an elaborate reason. Steadman et al. (2000), implemented that kind of a classification in their research, based on daylight use characters of buildings in a defined region. Other than the variety and number of proposed categories, which are inevitably valid on the limited context of the study, the novelty of analytic rule behind this categorization should be mentioned. Built forms are grouped in three major type as principle forms, parasitic forms and composite assemblies as major classes, before deciding on further sortation (See Table 8).

Table 8: Classification of buildings based on daylight use characters of buildings in a defined region (Steadman, 1994).

Principle Forms	Parasitic forms	Composite Assemblies
Daylit (sidelit) cellular strip, 1 to 4 storeys	AC Attached open-sided canopy	Principle (n) + Parasitic (n)
CS5 Daylit (sidelit) cellular strip, 5 storeys or more	AG Attached glasshouse or conservatory	
OD4 Daylit (sidelit) open-plan strip, 1 to 4 storeys	AI Monopitch aisle	
OD5 Daylit (sidelit) open-plan strip, 5 storeys or more	AR Covered street or arcade	
CT1 Toplit cellular, single-storey	AT Atrium	
HD Daylit hall, either sidelit or toplit (or both)	BA Basement	
HA Artificially lit hall	BL Large balcony	
OS Open-plan space in a single shed	CB Circulation bridge	
OC1 Open-plan continuous single-storey space	CL Covered enclosed ground-level circulation link	
OG Open-plan car parking or trucking deck	CT Attached circulation tower	
OA Artificially lit open-plan multistorey space	EX Small single-storey extension	
SR Single-room form	OR Occupied pitched roof or attic	
SSR String of single-room forms	PC Porte cochere	
RA Railway arch	PR Roof-level plant room	
Composite form types with special codes		
CDO Daylit (sidelit) cellular strip around some or all edges of artificially lit or toplit		
Open-plan space		
CDH Daylit (sidelit) cellular strip around some or all edges of artificially lit or toplit hall		

Shape attributes of forms might be related to their functions as well. Hence the function can be used as a device of classification for architectural forms (Moussavi & Lopez, 2009).

The type of use or the function of the building also often used for classifying buildings, it is also possible to correlate this classification with generic form categories (Moussavi & Lopez, 2009). A categorization which derive from an analogous approach, can be reviewed on reference building types defined by U.S. Department of Energy National Building Stock (Deru et al., 2011). In this report, the reference building type is described by computable statistical values directly related with shape properties of each function definition differing from other uses (See Table 10).

Similarly but more concisely, Kunze, Dyllong, Halatsch, Waddell, & Schmitt, (2012) presented four major building types in a research that they studied parameterization of archetypical buildings in San Francisco Bay Area by function as:

- Single family house
- Multi-family house
- Office
- School

As in the architectural form classifications, an approach which tends to explore primary constituents to define urban formation classes is also familiar. Kropf (2009), defines primary components of urban forms as line, area, space and module. Whereas similarly to the primary components mentioned previously for architectural forms line, plane and volume are also considered as constituent variables for urban compositions. Additionally framework (network) and grain (texture) are also included (Çalışkan, 2013).

From the point of view on masterplans and design codes specified in literature, primary components shaping urban structure can be listed as objects which can host form variations according to their primary type:

- Land uses

- Streets
- Blocks
- Plots
- Buildings

(Carmona, Marshall, & Stevens, 2006)

Table 9: Some of Reference Building Types in U.S. Department of Energy National Building Stock, interpreted from Deru et al. (2011)..

Reference Building Types (Commercial)	Floor Area (m²) Aspect Ratio	Number of Floors Floor-to-Floor Height	Glazing Fraction
Small Office	511 1,5	1 3,05	0,21
Medium Office	4982 1,5	3 3,96	0,33
Large Office	46320 1,5	12 3,96	0,38
Primary School	6871 E-Shape	1 3,96	0,35
Secondary School	19592 E-Shape	2 3,96	0,33
Stand-Alone Retail	2294 1,3	1 6,10	0,07
Supermarket	4181 1,5	1 6,10	0,11
Full Service Restaurant	511 1	1 3,05	0,17
Small Hotel	4013 3	4 3,35	0,11
Large Hotel	11345 5,1	6 3,96	0,27
Hospital	22422 1,3	5 4,27	0,15
Warehouse	4835 2,2	1 8,53	0,006
Midrise Apartment	3135 2,7	4 3,05	0,15

As the site of interest expands, from single building to larger instances like neighborhood, town, city; a structure of defined zones begin to be more significant for classifying urban formations. Morphological indices which are used to parameterize urban structures can operate upon a selected type as a mathematical switch. Type, in this case, can be simply the definition of prevalent urban character for any given zone (Steiniger et al., 2007). An example procedure based on discriminant analysis

technique from a geo-information research by Steiniger et al. (2007), have defined primary zones with the name of “types of urban structures” as below:

- Inner city areas
- Industrial and commercial areas
- Urban areas
- Suburban areas
- Rural areas

Within congruent grouping, generic land uses with more specific definitions can also act as class components of urban formations as exemplified by Burian, Brown, & Linger (2002). Possible approaches for defining urban formation types are not limited with that kind of a generic classification, based on the context and aim of the study. For example, Wheeler (2008), gave a type classification with the concern of an explanation of typical urban pattern evolution in US with definitions and computational comparison inputs (See Table 11).

Table 10: Land use classes from the database of Los Angeles, California (Burian, Brown, & Linger, 2002).

Residential	Commercial & Services	Other Urban or Built-up
Low-density Single-family (<8 units/hectare)	Industrial	Predominantly Vegetated
High-density Single-family (>8 units/hectare)	Transportation / Communications / Utilities	Urban High-rise
Multifamily	Mixed Industrial & Commercial	Downtown Core Area
Mixed		

Table 11: Current residential forms in urban pattern evolution of metropolitan regions in United States (Wheeler, 2008).

Current Residential Forms	Street Pattern / Building Size	Typical Unit Size and Lot Layout	Subdivision Scale
Rural Sprawl	Haphazard street pattern; street connectivity varies	Small to midsized houses; 1,000-2,500 square feet; wide variety of structure types and lot layouts	Small scale; 1-20 lots
Upscale fringe	“Loops and lollipops”; loose street patterns; low connectivity; large, irregular blocks;	Large houses; 2,000-5,000 sq. feet; lot layouts often vary due to custom construction	Small to medium scale; 10-100 lots
Suburban tracts	“Loops and lollipops”; tight street patterns; low connectivity;	Midsized houses; 1,500-3,000 square feet; repetitive housing forms and lot layouts	Medium to large scale; 20-1,000+ lots
Multifamily	Looping access roads; moderate block size and street connectivity	Small to midsized apartments and condos; 500-1,500 square feet	Medium scale; 20-500 lots
Trailer parks	Very tight, linear lanes; small blocks; moderate connectivity	Small units; 500-1000 square feet	Medium scale; 50-200 lots
New urbanist	Grid-like street pattern; small blocks; high street connectivity	Varying housing forms including second units and row houses;	Large scale; 100-1,000+ lots
Incremental subdivision	Haphazard street pattern; incremental addition of streets; block size and street connectivity vary	Small to midsized; 1,000-2,500 square feet	Small scale; 1-20 lots

2.2.2 Operations

Within this heading, a brief scanning on possible generic operations to apply on forms, more specifically on their geometric properties, of built structures and urban formations is compiled. Definitions of the acts included in that kind of a content can be diversified from literature, like examples below:

- Acts of creation, generative operations (Çalışkan, 2013)
- Transformation of form (Ching, 2014)
- Organizing and enclosing principles, form giving and transformative operations (Krier et al., 1988)
- Formative strategies (Özdemir & Önal, 2016)

Whereas, for some studies like building simulations, cartographic studies or building stock aggregations, definitions might contain different kind of acts in terms of their manner and purpose:

- Shape approximations (Wurm et al., 2016)
- Characterization methods (Hamaina et al., 2012)
- Generalization methods (Bard, 2004; Gaffuri & Trévisan, 2004)

It is possible to observe differences among definitions attached to these operative acts from studies with different scientific fields and different purposes. Similarly to the distinctions explained in previous part for class definitions, there are also modality changes between more qualitative, often “intuitive” (Steadman, 2014), approaches and more quantitative, often computational approaches on exploring forms.

As an example for the qualitative approaches from architectural field, Ching (2014), classified possible operations on architectural forms under three major types:

- Dimensional transformation
- Subtractive transformation
- Additive transformation.

Among them, Ching elaborates additive transformation with explanations for addition types and additive forms as in Table 11. The addition is sometimes explained as an act of combining different forms together. Basically, these acts can be named as organizing and enclosing principles (Krier et al., 1988). Seven principles of such are proposed by Krier et al.'s work (1988):

- Central / axial
- Linear
- Central and Linear Overlap
- Fork-like representation
- Network
- Superimposition
- Labyrinth

Table 12: Additive transformation possibilities according to (Ching, 2014)

Addition types	Additive forms
Spatial tension	Centralized form
Edge to edge contact	Linear form
Face to face contact	Radial form
Interlocking volumes	Clustered form
	Grid form

Table 13: A classification for acts of architectural form manipulation. Adapted from Eckler (2012)

Generative possibilities in simplified form	Operative types
Curvilinear	Expansion
Diagonal	Compression
Orthogonal	Extension
Horizontal	Contraction
Vertical	Filter
	Transition

To continue in a similar kind of approach exploring the methodology of architectural form creation, Eckler (2012) can be referred for the classification of operations on form. (See Table 13)

For architectural design, the possibilities of form modification are defined with similar but different names in many studies, either in a deductive way, which analyses form by dividing into its components; or in an inductive way, while describing form properties by according to their occurrence processes. Former is mostly derived from explanatory studies dealt with the architectural or urban form and its components. While, latter is mostly encountered in studies that not directly related with the definition of form and morphology, but related to fields like energy efficiency decisions according to architectural form. In the following pages these names of form giving acts will be listed:

- Cutting (Krier et al., 1988), (Aliaga, Vanegas, Lei, & Niyogi, 2013) , (Özdemir & Önal, 2016), Breaking (Krier et al., 1988) (Eckler, 2012) (Futcher & Mills, 2013)
- Extruding (also as extending or elevating) (Eckler, 2012), (Özdemir & Önal, 2016)
- Subtraction (Ching, 2014), (Çalışkan, 2013), (Özdemir & Önal, 2016)
- Bending (also as twisting) (Krier et al., 1988), (Özdemir & Önal, 2016)
- Cycling (looping) (Özdemir & Önal, 2016)
- Segmentation (also as segmenting or separation) (Ching, 2014), (Krier et al., 1988), (Özdemir & Önal, 2016)
- Integration (Özdemir & Önal, 2016), addition (Ching, 2014), (Krier et al., 1988), friction, accumulation, stacking (Krier et al., 1988)
- Orienting / rotating (Özdemir & Önal, 2016), (Eckler, 2012)
- Penetration, superimposition (Krier et al., 1988)
- Interlacing, meshing (Krier et al., 1988)
- Alienation (Distortion in scale) (Krier et al., 1988)

For urban morphology. similar content about possible operations can be summarized by referring the study of Çalışkan, (2013). With a concern of functional segregation, these actions can be grouped into three broad categories as generative operations, acts of creation and tools of generation which are linked with objects that manipulated by

them. Table 14, quoted from this study, is a summarized framework for this purpose; divided into three parts for form and composition, structure, pattern and fabric.

Correspondingly to the new class definitions of contemporary architectural design practice as mentioned in 2.2.1. form giving operation possibilities are also shaping around newer definitions. Agkathidis (2016) names five principal form finding tools for generative design studies, while some of them being same with former definitions:

- Continuous surface
- Modularity and accumulation
- Deformation and subtraction
- Algorithmic pattern
- Triangulation

Table 14: A review of form and pattern components and variables. Interpreted from Çalışkan (2013).

	Objects	Generative Operation	Acts of Creation	Tools of Generation
Form and Composition	Line Plane Volume	Articulation (Massing & layout)	Combination Subdivision Assemblage Coupling Mounting Alliance Overlapping Subtraction Amalgamation	Axial lines Generic grid Zones System of proportioning
Structure	Framework or network	Organization (Ordering & structuring)	Connection Separation Distantiation Linkage	Unitary types and rules of assemblage
Pattern and Fabric	Grain and texture	Propagation	Tessellation Iteration Translation Reflection Interweaving Multiplication Knitting Superimposition Gradation	Code and algorithm

An analysis on operative schemes of computational tools providing volumes as closed surfaces and/or solids would be beneficial. Hence, this analysis can aid a better perception of how operations act in constructing different shapes. For a classification of these schemes, 1980 dated article of Requicha is cited in many of the related papers given that it provides an essential categorization still in use as terminology in various practices like solid modelling, CAD (computer aided design) and CAAD (computer aided architectural design). Some of these schemes are:

- Parameterized primitive instancing: This scheme operates based on primitive instances called a generic primitive, which can have their own parameters distinguishable to others and can transform according to that, into a limited geometric variability.
- Cell decompositions: A solid is represented and manipulated by units called cells on a spatial grid (also known as spatial array). Since the size of cells as smallest units constituting every possible geometry, this approach is usually preferable for approximations.
- Boundary representation: It is a surface based approach, which uses boundaries to create volumes. Similar procedures of primitive instancing or cell decompositions can be implemented for the surfaces instead of volumes. Also, surfaces can be constructed by parameters of their components like vertexes and edges or with the help of a gridal frame.
- Surface mesh modeling: This scheme is a particular type of boundary representation. However, the method of producing meshes according to topological parameters which will compose surfaces and volumes subsequently is the reason of naming it as a separate class.

(Requicha, 1980)

Other types that are not described in detail here are: Constructive solid geometry, sweeping, implicit representation, parametric and feature based modeling (Requicha, 1980).

2.2.3 Properties

In architectural theory, knowledge based explanatory approaches examines geometry related properties of forms similarly to each other. For instance, Ching (2014) lists eight essential properties of architectural form, among six can be treated as geometry defining attributes:

- Shape
- Size
- Texture
- Position
- Orientation
- Regularity

Likewise, Hanlon (2009) states five basic properties of architectural compositions as number, geometry, proportion, hierarchy and orientation.

Generic representations of forms also have their shape attributes defined in literature. An example for that kind of an approach is presented in a list below:

- Shape: Simple contour, contour
- Structure: Grid, zone, axis, subdivision
- System: Circulation, structure, functions

Scalar form attributes, which can be defined and changed by numeric values are generally available from the studies of urban morphology (including geo-information and photogrammetry) and building stock researches. These research studies are generally conducted on a specific geographic context with purposes of parameterization, characterization and generalization of urban forms. Numerous simplified models of urban morphology are proposed in different studies. In one case, Adolphe (2001) proposed a set of morphological indicators to be used in analysis of built-up areas in terms of their environmental performance:

- Density:

- Rugosity:
- Porosity
- Sinuosity
- Occlusivity
- Compacity
- Contiguity
- Solar admittance
- Mineralization

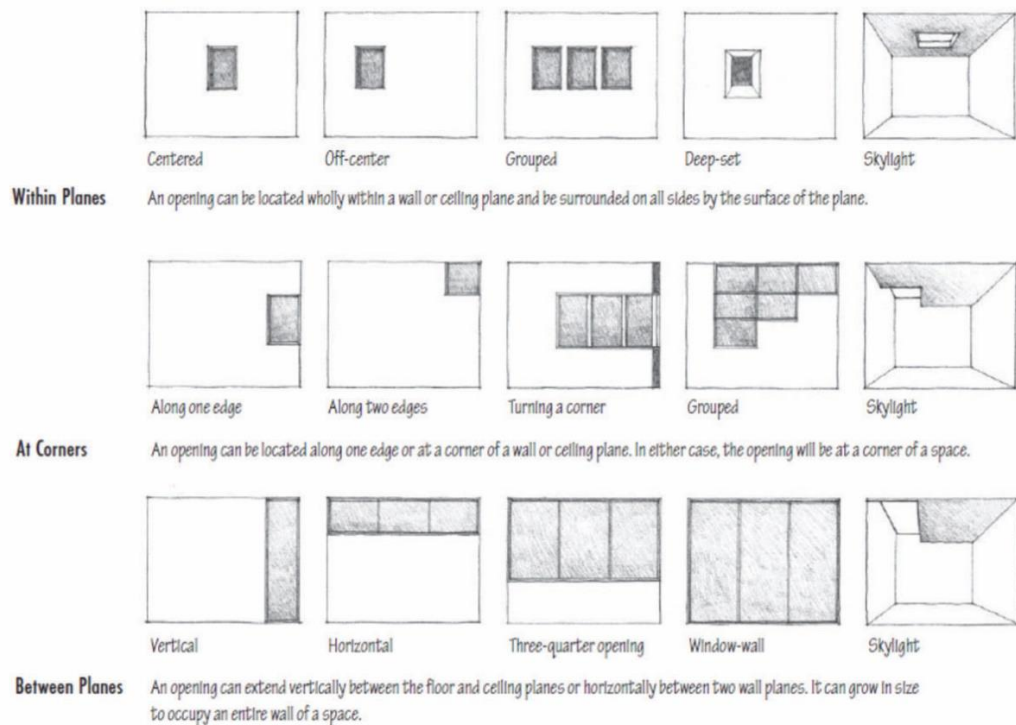


Figure 17: Illustrations of different opening positions in building envelope. (Ching, 2014)

Properties related to components of buildings are also provided in some of the same sources. Ching (2014), listed edge and corner types as: Unadorned corner, reinforced (projected) corner, contactless corner, rounded corner. Whereas, for opening

placement he states three types of positioning: within planes, between planes and at corners.

After a comprehensive literature review, Çalışkan (2013) has provided an aggregation of urban formation properties outlined in three sections as form and composition, structure and pattern. In this classification, many of the attributes effects the boundary geometry.

Table 15: Properties of urban forms and formations. (Çalışkan, 2013)

	Form and Composition	Structure	Pattern and Fabric
Basic Properties	Shape Size Color and texture Position and orientation Coverage (density) Proportion Contrast Enclosure Porosity	Typology Hierarchy Datum Depth (topological) Symmetry Distributedness Connection	Regularity Variation Succession Periodicity Frequency (Local) symmetry Rhythm Betweenness Closeness Granularity
Basic qualities	Harmony Balance Unity Variety Permeability Contiguity Porosity Continuation	De-centrality Continuity Integrity Intelligibility Segregation Diffusion	Proximity Legibility Consistency Coherence Self-similarity Diversity

Several classification and generalization studies provide simplified computational definitions that determine building geometry. Motivations of these research may differ. Some examples are: classification of residential building types based on LIDAR scan (Tooke, Van der Laan, Coops, Christen, & Kellett, 2011), building footprint shape based characterization of urban fabric (Hamaina et al., 2012) and developing building stock geometry models for calculations of energy efficiency, carbon emissions and heat mass (Szalay, 2008). Three studies of such are compared with their proposed parameters in Table 16.

Table 16: Comparison of three research studies by proposed properties of basic building geometry in generalization.

Reference source.	Type of included building form properties	Properties of building geometry
Tooke, T. R., Coops, N., Christen, A., & Kellett, R. (2011). Classification of residential building architectural typologies using LiDAR	Building Morphological Characteristics	Area Volume Mean height Max height Height standard deviation Building-lot area ratio Roof slope External surface area Compacity
Hamaina, R., Leduc, T., & Moreau, G. (2012). Towards urban fabrics characterization based on buildings footprints	Simple Building Descriptors	Length Width Area (of footprint) Height Volume
Szalay, Z. (2008). Modelling building stock geometry for energy, emission and mass calculations.	Main Geometric Parameters Describing Buildings	Floor area Number of storeys Ceiling height Perimeter-to-floor area ratio Ratio of adjacent walls Window ratio and Frame ratio Roof slope

Wurm et al. (2016), named these geometric features used in building types' classification:

- Footprint area
- Perimeter length
- Building volume
- VarZ (a function of the differences in height values from different locations of building)
- Length and width of footprint polygon
- Length and width of main line
- Vertices count of footprint polygon

Hamaina et al. (2012), also presents properties and corresponding indicators for urban morphology (See Table 17).

Likewise, similar geometry parameters were used in a study which proposes an automatic classification method operate on digital 3D city models (Henn, Römer, Gröger, & Plümer, 2012). This study divided building related geometric variables into two groups one of which is also related to surrounding.

Table 17: Morphological Properties And Corresponding Indicators for urban fabrics characterization based on buildings footprints (Hamaina et al., 2012).

Buildings Geometry	Minimum Enclosing Rectangle of footprint	
	Compactness indicator	
Open Space Geometry	Voronoi cells area	
Buildings Adjacency	Party walls ratio	Shared walls length / Building footprint perimeter
Density	Ground Space Index	Building's Footprint area / corresponding cell's area
	Floor Space Index	Building's volume / Corresponding cell's area
Neighboring	Mean buildings distance	
	Generalized Width/ Height	
Open Space Morphology (Spatial openness)	Sky Openness: Sky view factor	Visible sky / Sky masked by other buildings (at a POV)
	Ground Openness	Isovist Area / Disk area

Table 18: Building specific features and neighborhood features in automatic classification of building types (Henn et al., 2012).

Building specific features	Neighborhood features
Length of footprint	Number of buildings in building block
Area of footprint	Number of direct neighbors along street
Width of footprint	Number of touching buildings
Volume of BRep	Distance to the nearest opposing building
Height of Building	Distance to the nearest right building
Number of Vertices in footprint	Distance to the nearest left building
Slimness of footprint (length / width)	
Degree of perpendicularity	
Building usage	
Number of Storeys	

In addition, research on urban form generalization also provides scalar parameters for urban pattern. These approaches will be exemplified on following pages:

Steiniger et al. (2007) implemented a method of classification for urban structures in four countries with discriminant analysis techniques. In order to analyze building geometry, they employed a cognitive approach which referring to principles of Gestalt psychology.

Based on San Francisco area, a study for determining possible parametric building typologies was conducted as a preliminary step of a procedural city model which operates on a parametric algorithm (Kunze et al., 2012). The study depends on site surveys and analysis on selected samples of each type definition.

Table 19: Some of the parameters defined with site survey in San Francisco Bay Area for a procedural city model (Kunze et al., 2012).

Survey Based Design Parameters of Block and Lot	Values of S.F. Survey	Design Parameters of Private Frontage	Values from example
Average Block Dimension	625 x 265 ft.	Private Frontage Type	Front Garden & Garage
Units per Acre	0,65 units	Principal Building H	25 ft.
Average Lot Size	165000 sqft	Outbuilding height	10 ft
Average Lot Coverage	45%	First floor above grade	2 ft
Parked cars per Acre	1	Watermark level	None
Trees per Acre	5	Building disposition	Front and back yard
		Lot Size	164 600 sqft
		Lot Coverage	45%
		Front Setback	25 ft
		Side Setback	13 ft
		Rear Setback	2 ft
		Outbuilding Setback	70 ft

Sensitivity analysis as a method of determining the influence of parameters on a specified subject is implemented on similar property definitions. For example, in a study investigating the effect of basic building geometry on the energy use, sensitivity

analysis employed with four basic properties and their ranges as explained in the Table 22. (Hemsath & Bandhosseini, 2015)

Table 20: Geometric sensitivity index variables and ranges for evaluation of basic building geometry on energy use (Hemsath & Bandhosseini, 2015).

	Local	Global
Stacking	1 to 4 levels	1,2,3,4
Orientation	0 to 135 degrees rotation	0,120,240,360 degrees
Eave	0 to 2 m	0,0.66, 1.33, 2.0 m
Aspect ratio	4:20 to 4:4	0.2, 1.8, 3.4, 5.0

2.3 Review of Urban Wind Studies for Morphology Parameters

Under this section, the literature survey conducted on wind flow studies are briefly summarized with some key references selected. A more detailed and comprehensive inventory of form parameters used in wind studies is given in Appendix A.

2.3.1 Building Form Parameters from Wind Flow Studies

The literature on this field is generally from experimental wind studies, mostly in engineering and physics. In most cases, on idealized urban environments, (Millward-Hopkins, Tomlin, Ma, Ingham, & Pourkashanian, 2013) or very simplified variables for a single building element like the difference of a pitched roof vs. a cube shaped object (Stewart et al., 2011) or the impact of an edge type like chamfered corners vs. perpendicular ones (Stathopoulos, 1985) is used in each study.

Mean wind speed around a specific building is primarily related to:

- Distance to the boundary of urban area
- Heights and orientations of surrounding buildings relatively to the wind flow and each other
- Height and orientation of subject building

(Dutton et al., 2005)

The interaction of wind flows and buildings is not only concern for urban wind energy studies, but also significant as a field of research for building structure in terms of safety considerations against wind loads. Factors determining the effects of wind loads to the buildings can be listed as:

- Wind characteristics
- Size and geometry of the building
- Stiffness value of the structure and mass distribution of building
- Inherent characteristics of structural system and material in terms of damping
- Topography and neighboring buildings. (Günel & Ilgin, 2014)

The height of a building is an important factor effecting the wind flow characteristic around, which is also directly or indirectly related to many geometrical or aerodynamic parameters. (Grimmond & Oke, 1999) (Stathopoulos, 2007) Simply, for the unexceptional conditions, the exposure of a built object against wind flows is proportioned with the increase of its height. Whereas, taller buildings has additional effects on the wind conditions of nearby pedestrian environment. (Stathopoulos & Blocken, 2016)

In association with the importance of height variable; the geometry of the topmost part of the buildings, in most cases; roofs, has considerable interaction with the wind flows above. Pitched roofs influence mean velocity, turbulence and kinetic energy profiles in relation with the angle of roof surfaces to the vertical or horizontal axis. (Ozmen, Baydar, & van Beeck, 2016)

Instead of using an angle parameter for a building's roof definition, Ledo, Kosasih, & Cooper (2011), used three categorical types as pitched roofs, flat roofs and pyramidal roofs. They produced three samples for each type and based on CFD simulations, they argued about site analysis procedure of roof mounted wind turbines.

Huang, Hu and Zeng (2009) stated the importance of the roof vertex's relative position to a building form for pitched roofs by CFD simulations and wind tunnel tests on wedge shaped roofs.

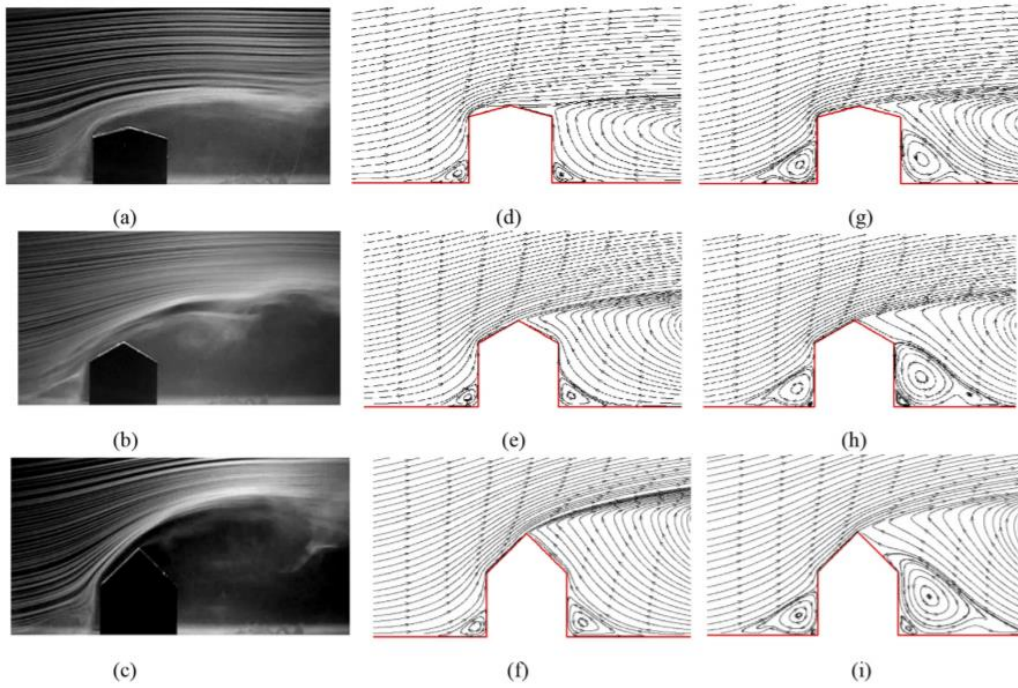


Figure 18: Flow patterns around buildings with roof pitches of 15°, 30°, 45° (Ozmen et al., 2016).

There are various wind flow studies on limited number of building shape variable sets:

Tamura et al. (2017), applied wind tunnel tests on 40 building form samples. Their work is the one including most samples among wind flow studies reviewed by this study. They produced super tall building models which are results of a cross-production between form categories and form types specified as in:

Table 21: Plan types and form types as used in wind flow experiments by Tamura et al. (2017).

Plan Type	Form Type
Square plan,	Tilted
Elliptic plan	Tapered
Plan with corner chamfered	Inverse tapered
Rectangular plan	With setback
Plan with cornet cut	Hellical

A study for the evaluation of pedestrian wind environment around tall buildings analyzed a building with 8 design features (Stathopoulos & Blocken, 2016). Authors implemented 5 generic form variables and produced 9 sample forms with them:

- Positioning of opening
- Ground floor setback
- Podium size
- Height
- Adjacency

Another set of similar number for building form parameters is proposed by Irwin, Kilpatrick, Robinson, & Frisque (2008). Five form samples representing generic building types were produced by these variables:

- Corner roundness
- Tapering
- Porosity
- Projections

Building footprint type is also used with categorical variables in many studies (Gan & Chen, 2016; Biao Li, Liu, & Gao, 2015). Li et al. (2015) used two different footprint type as a rectangle and an H shaped layout to propagate various urban formations with vertical extrusions.

Projections from buildings with different names were implemented as form parameters for wind flow studies. Blocken, Janssen and van Hooff (2012), tested canopy size and canopy height variations on digital model of a real building in Chambéry. Their results show correlations between pedestrian comfort with buildings' canopy form properties. Similarly, effects of generic facade projections were also tested in an experimental configuration on a prismatic solid (Montazeri & Blocken, 2013).

It is also possible for wind studies to select real cases representing generalized building categories by referring to urban morphology literature (Gao et al., 2012). This approach is used in field measurements as a site selection criterion.

2.3.2 Urban Morphology Parameters from Wind Flow Studies

Three critical route of flows and movements including wind in urban areas relatively to a subject boundary are; along the boundary, parallel to the boundary or perpendicular to the boundary (Forman, 2014). Movement of a flow through a boundary is affected by the form of the object or its boundary shape.

Among other meteorological impacts, buildings cause significant changes in flow dynamics, effecting drag and turbulence as well as thermodynamically driven winds due to the temperature differences between heat island created by urban areas and surrounding environment. While parameterizing the urban environment for mesoscale boundary layer meteorology studies, parameter definitions that are more universal and in-depth are still questionable in terms of the need for more or new specific parameters (Brown, 1999).

The two most significant geometrical factors can be specified as surface area density and building height variability since they are related to aerodynamic parameters as roughness length and zero-plane displacement length. The effect of building height variability is studied with models which use it as a generic parameter, yet it should be considered contextually. When an urban configuration analyzed using a simplified site section, the significant relation of building height distribution with wind sheltered areas on successive building facades is illustrated by Millward-Hopkins et. al. (2011).

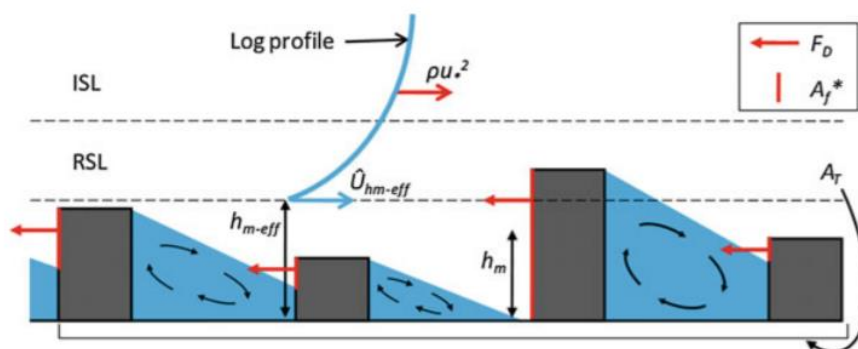


Figure 19: Building height distribution and the occurrence of sheltered zones in facades behind (Millward-Hopkins et. al., 2011).

An urban morphology index system was proposed for research on natural ventilation in block scale (Gan & Chen, 2016). As an example application, they produced 14 formation samples with two types of prismatic solids and eventually determined five parameters as:

- Footprint shape (as type categories)
- Spacing differences
- Comprehensive porosity
- Relative rugosity
- Ventilation obstruction

Roughness is a determinant parameter for wind energy assessments in urban areas. That is primarily because the boundary layer in urban zones is generally tend to have greater roughness lengths. Therefore the wind flows in urban zones acquire a feature of producing turbulent zones more than the unbuilt geography (Campbell et al., 2009; Dutton et al., 2005; Toja-Silva, Colmenar-Santos, & Castro-Gil, 2013).

Hau (2013), has provided a ruler shaped diagram for classification of different terrain types according to their roughness lengths (z_0) (see Figure 20).

Direction of the wind have the utmost importance for concerns related with urban wind energy. An assessment should take it into consideration while deciding the optimal location of a wind turbine.

CFD simulations showed the significance of the wind direction impact to the decision of siting the turbine around a building depends on the distance to the host building. Energy conversion potentials of turbines until 1 m. height from a building is more influenceable from the direction of prevalent wind flow. Whereas, for the turbines sited 2 m. above their host building, or in cases that 1/3 of the building height exceeded, it is advisable that the optimal location for an integrated wind turbine is usually coincides with the geometric center of the host structure (Stewart et al., 2011).

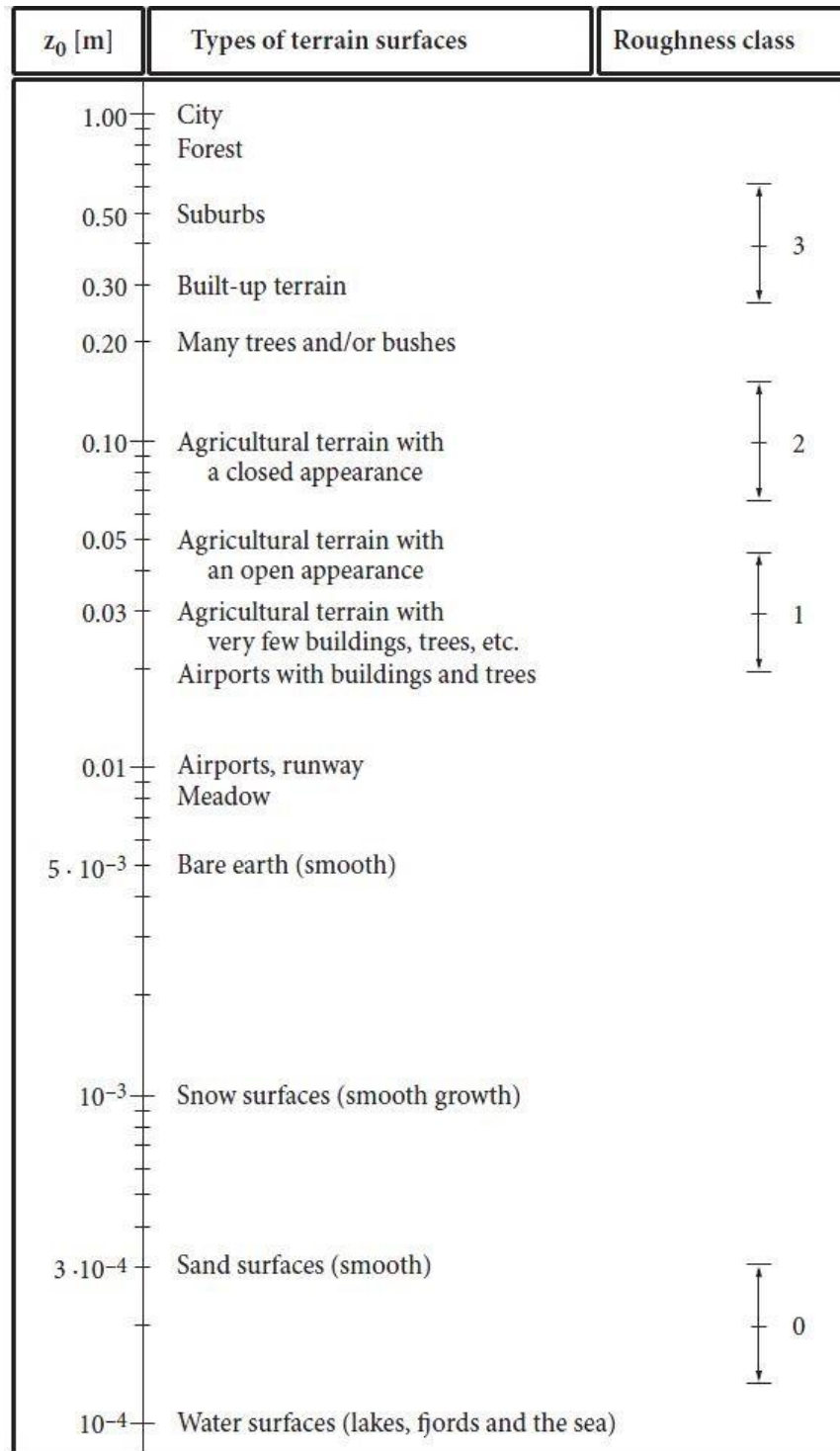


Figure 20: Roughness lengths and roughness classes according to terrain type.

Forman (2014) named basic windbreaks in urban areas as tree lines, walls and buildings. These elements behave as windbreaks for airflows and their qualities in that function basically depend on three variables. They are the positioning of the windbreak according to streamline airflow, the effective height and the windbreak porosity. A quiet zone occurs just beyond the windbreak and with lower wind speeds it extends to 8 times of windbreak height (8H). Similarly, occurred turbulence in the disturbed wind enters a wake zone between 15H and 25H distance from windbreak. Windbreak porosity directly affects the wind turbulence; most permeable structures create the fewer disturbances in the wind flow.

Table 22: Land use classes, functions, properties for urban parameterization (Brown, 1999).

Land use classes	Functions of land use	Properties of land use
Downtown / city center	f_{urban}	Urban albedo
Industrial / commercial	f_{roof}	Urban emissivity
Residential	f_{cyn}	Roof albedo
	h_c	Roof emissivity
	Bowen ratio	

Kanda, Inagaki, Miyamoto, & Gryschka (2013), employed five geometric parameters for their study with the purpose of aerodynamic parameterization for real urban surfaces. The research was based on two real cities, Tokyo and Nagoya, with sample zones of 1000 x 1000 m² areas. Although the aim was to develop an empirical, generic parameterization for real urban surfaces as simplified model geometries. To achieve this, they studied on three dimensional digital models of sample areas from a building data called MAPCUBE by Large Eddy Simulations of wind flow. Two aerodynamic values compared are roughness length and displacement height with more than one computational methods. As a classification, they defined three types of urban zones for their surfaces, as: Skyscrapers, business district and residential area. As a result,

they come up with five geometric parameters of urban surfaces with relatively higher sensitivity on wind flow characteristics as following:

- Average building height
- Maximum building height
- Standard deviation of building height
- Plane area index (ratio of building footprint area to total floor area)
- Frontal area index (ratio of windward surface areas of buildings to the total floor area)

(Kanda et al., 2013)

Table 23: Some constraint values and correlation functions for geometric parameters of urban surfaces deducted from wind flow simulations. Interpreted from (Kanda et al., 2013).

Parameter name	Constraint	Correlation
Plane area index	[Plane area index] >0,2 (values < 0,2 are classified as non-urban)	
Building height	[Building height] >3,5 m	[Maximum building height] = 12,51[building height]
Frontal area index	[Frontal area index] <2[plane area index]	Approximated as: $1,42[\text{plane area index}]^2 + 0,4[\text{plane area index}]$

It was claimed that frontal area ratio is the most important parameter for an estimation of pedestrian wind conditions in an urban environment (Abd Razak, Hagishima, Ikegaya, & Tanimoto, 2013).

With air flow measurement studies applied on simplified building arrays, it was observed that some morphological features of urban geometry has significant effect on flow fields over urban areas. According to Carpentieri & Robins (2015), these are:

- “Building height variability”
- “Building aspect ratio (or, conversely, “street canyon aspect ratio”)

- “The angle between street canyons and the incoming wind”
- Other local geometrical features such as: “the presence of much taller buildings immediately upwind of the studied area”

For the size of an experimental wind flow model for any urban site; Franke, (2006) argues that, an area with 300 m. radius should be modeled for wind tunnel experiments, while, especially for digital flow simulations, an outflow boundary of $15H$ can be proportioned by the height of the building object in question.

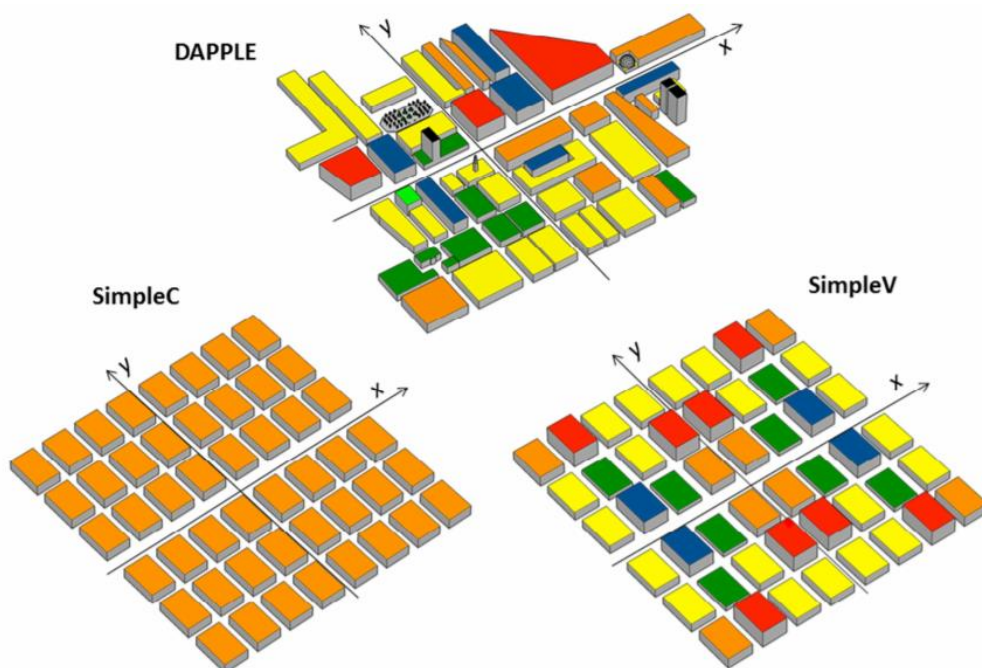


Figure 21: Building array models used in flow simulations from the study of Carpentieri & Robins (2015)

Carpentieri and Robins (2015) studied on building array models to construct flow and dispersion models. As seen from Figure 21, DAPPLE is a simplified model provided by a 3D digital construct of a real neighborhood, while SimpleV is an approximated version of a possible configuration and SimpleC is a comparison purposed simplest model with same building heights.

2.4 Examples of Algorithms for Producing Generic Forms

Tedeschi (2014), explains the basic difference between traditional practices and algorithm aided methods in architecture, based on the character of production process. Conventional methods like hand drawings and CAD routines are “additive processes”, whereas “algorithmic modelling” convert this definition to an “associative logic” by the contribution of parameters, according to his definition.

Algorithm aided tools in architectural practice might be associated with different kinds of purposes. These can be divided into two very broad categories based on their functions by a simplest taxonomy. Below, there are few example definitions:

I. Form finding, analytical design development.

- Algorithmic tools for “generative form finding processes” (Agkathidis, 2016)
- “Design exploration based on parametric logic” (Dino, 2012)

II. Analysis, simulation and optimization.

- “Parametric building simulation” and/or optimization tools (Nguyen, Reiter, & Rigo, 2014)
- “Procedural modeling of buildings” (Müller et al., 2006) and/or cities (Parish & Müller, 2001)

Janssen & Stouffs (2015), provide a classification for parametric modelling techniques in four broad categories as:

- Object modelling
- Associative modelling
- Dataflow modelling
- Procedural modelling

Following figures from their study, explains two different systems used in their production as “scene-based systems” and “feature-based-systems”

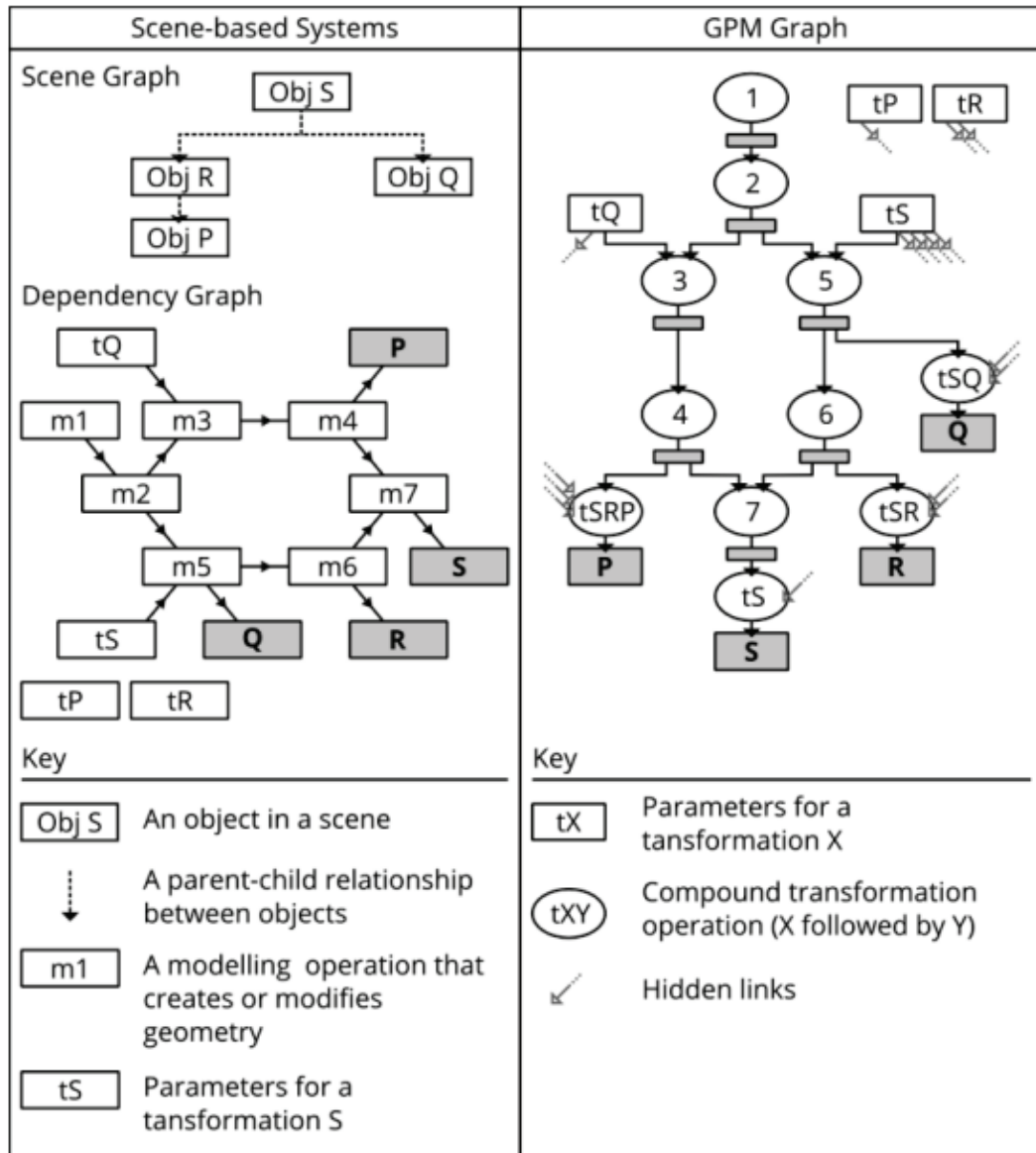


Figure 22: “An example model from a scene-based system” (P. Janssen & Stouffs, 2015)

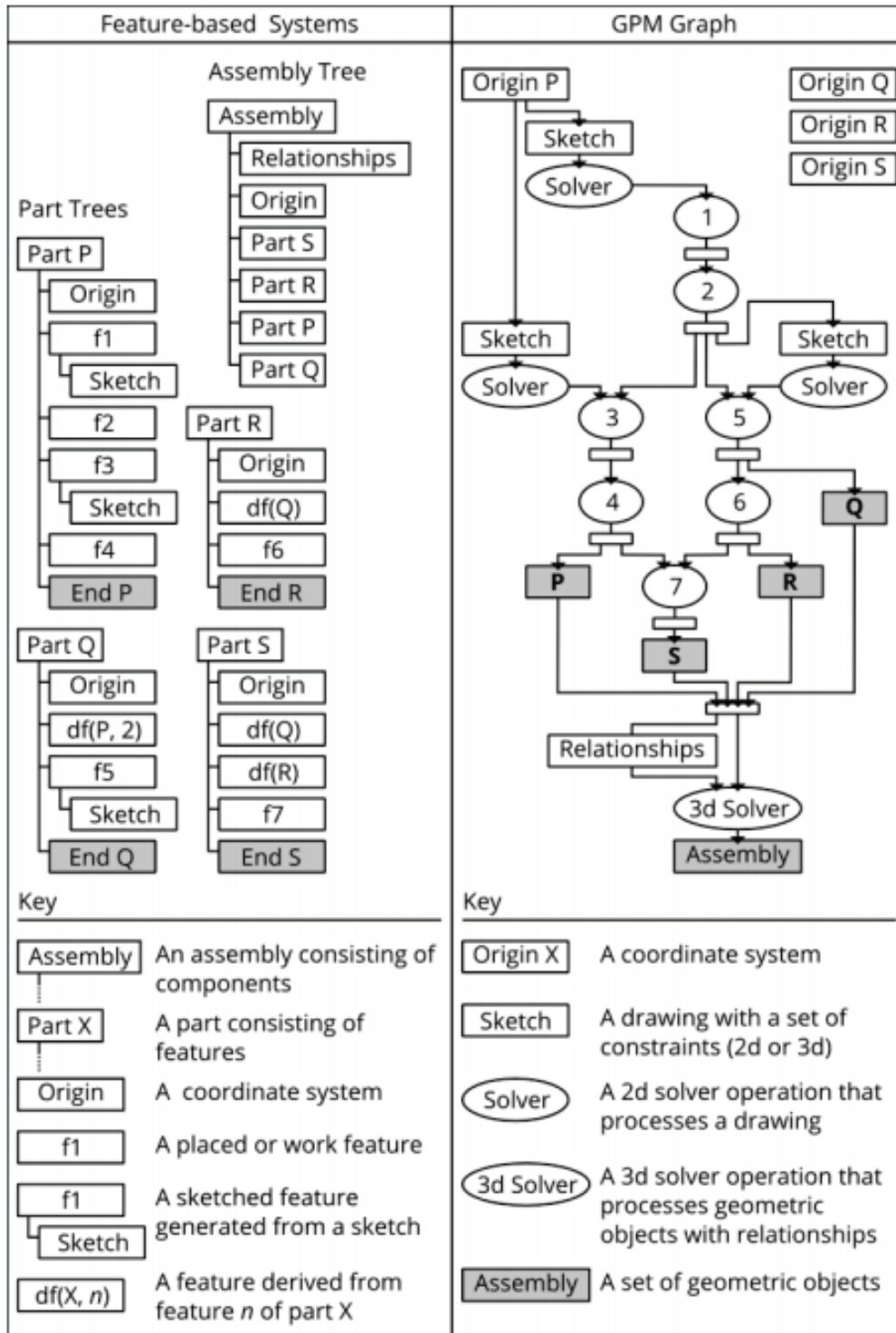


Figure 23: “An example model from a feature-based system” (P. Janssen & Stouffs, 2015)

Terzidis (2006) unwraps algorithms' capabilities to transform from each other. After comparing this potential with design process, he commented as:

Rather than using algorithms to copy, simulate, or replace manual methods of design (while perhaps desirable), instead they can be studied as methodologies that operate in ways similar, parallel, or complementary to that of the human mind. Second, along the lines of homo faber homo fabricatus (i.e. we make a tool and the tool makes us), algorithms can be seen as design tools that lead towards the production of novel concepts, ideas, or forms, which, in turn, have an effect in the way designers think thereafter.

(Terzidis, 2006)

Working with parameters brings the potential of expand the universe of possibilities for architectural forms as Kolarevic (2004) explains:

Parametrics can provide for a powerful conception of architectural form by describing a range of possibilities, replacing in the process stable with variable, singularity with multiplicity. Using parametrics, designers could create an infinite number of similar objects, geometric manifestations of a previously articulated schema of variable dimensional, relational or operative dependencies. When those variables are assigned specific values, particular instances are created from a potentially infinite range of possibilities.

(Kolarevic, 2004)

Biljecki, Ledoux, & Stoter (2016) introduced four level of details for generic building models in the simulation algorithm they presented named "Random3DCity". However, all building variations produced by this tool are based on projections of prismatic shapes.

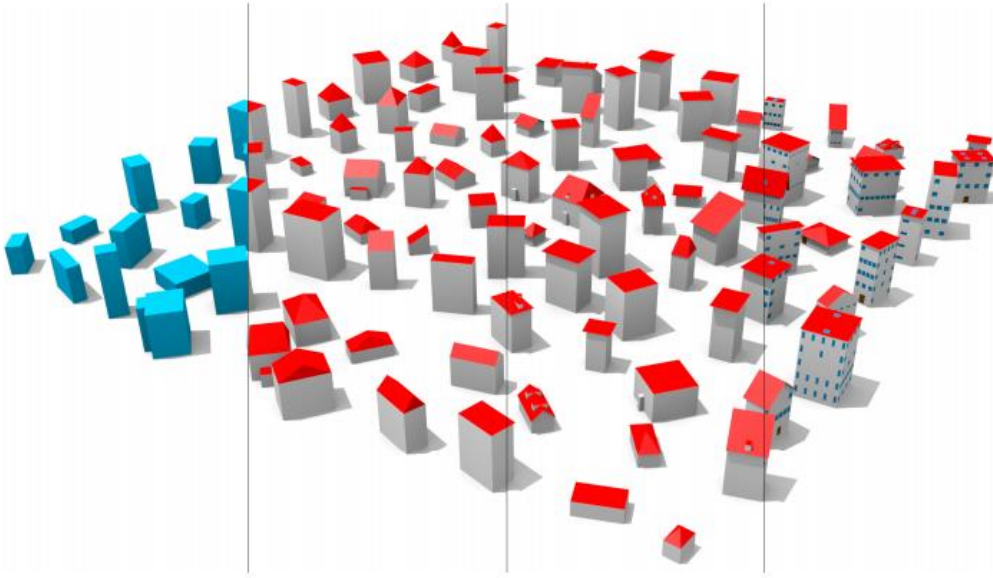


Figure 24: Randomly generated buildings by Random3DCity in four different level of details. (Biljecki et al., 2016)

Another, far more advanced tool for city simulations in commercial use is the “CityEngine” software by ESRI which was developed on CGA (Computer Generated Architecture) as a programming language based on shape grammars. The program basically simulates a digital model of a whole city in intended configuration on a scene based interface by procedural decisions.

Primary variables are a “Heightmap” input with isolines, categorical street graph selection from either generic pattern options or pre-defined representations of different real cities. (ESRI, date accessed: 06.06.2017) There are object parameters for each generated item.

In building level, the program runs on vertical extrusions of footprint shapes which can be user manipulated. There are selections and geometric control parameters for roof types. However, there is no option related to deformation of building’s primitive section. All building variants are forms produced by additive process of prismatic solids.



Figure 25: City model produced by ESRI CityEngine and an example control panel for object parameters of selected building. (Retrieved from <http://www.arcgis.com/apps/MapAndAppGallery/index.html> and <http://www.esri.com/software/cityengine/getting-started>; accessed date: 06.06.2017)

Dependency to post-optimization process in architectural design is decreasing by the effect of possible combinations between performance analysis tools and parametric modeling capabilities in the early stages. (Anton & Tănase, 2016)

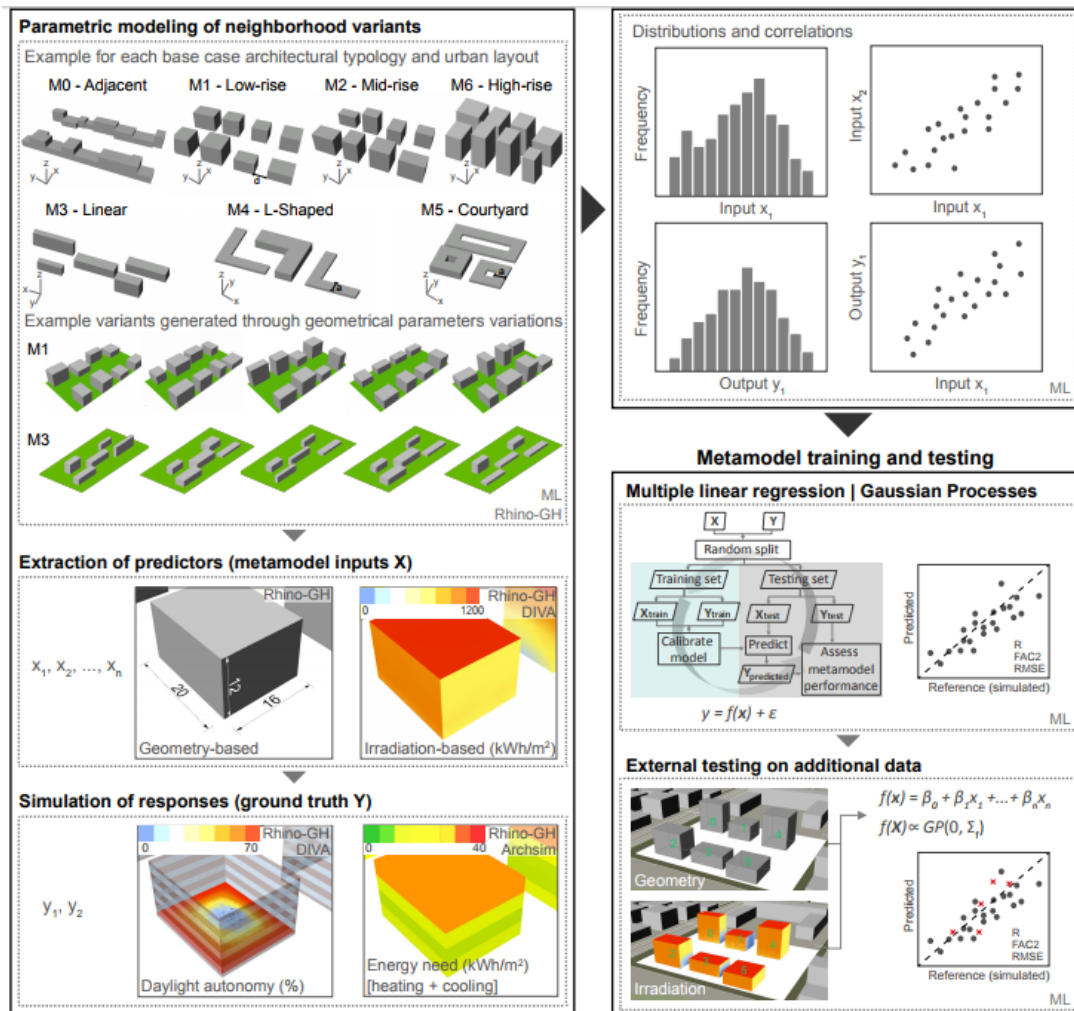


Figure 26: An example of a parametric model tested with sensitivity analysis for daylight qualities by multiple linear regression method. (Nault, Moonen, Rey, & Andersen, 2017)

Nault, Moonen, Rey, & Andersen (2017) used a parametric model to compare effects of eight urban form parameters on daylight qualities. They conducted the study in three steps as: Parametric modeling, daylight simulations, testing and comparing parameters effects by multiple linear regression. Parameters they have implemented in model are:

- Urban layout type
- Height
- Length
- Width
- Depth
- Distance between buildings
- Min plot ratio
- Min building footprint

Within same context, some analysis tools are developed with the ability to collaboratively operate with visual programming interfaces. As an example “Ladybug” provides climate analysis models in the form of parametric nodes within Rhino/Grasshopper interface. (Roudsari, Michelle Pak, Smith, 2013) In terms of wind, Ladybug has a node for visualizing annual wind profiles and wind rose diagrams.

Kelly & Wonka (2011) has presented a scene based interactive tool using footprint layouts and section outlines, which they call “profiles”, as user inputs to construct digital building models. This approach gives more variety in three dimension rather than other simplification methods used in the modelling of generic forms. There are three types of parameter sets in this tool: Parameters for footprint corners, parameters for offset events, parameters for anchor events

Visual programming interfaces like Grasshopper for Rhinoceros and Autodesk Dynamo Studio are in use for parametric modelling algorithms developed in architectural practices. One of the examples on the use of Autodesk Dynamo, is a model developed for determination the appropriate design alternatives for service cores in buildings. In this study, building footprint layouts are used as user inputs together with values of user defined variables like floor height and floor number to solve optimal solutions of service cores according to several regulations such as fire safety. (Das, Day, Dewberry, Toulkeridou, & Hauck, 2016) (See Figure 28)

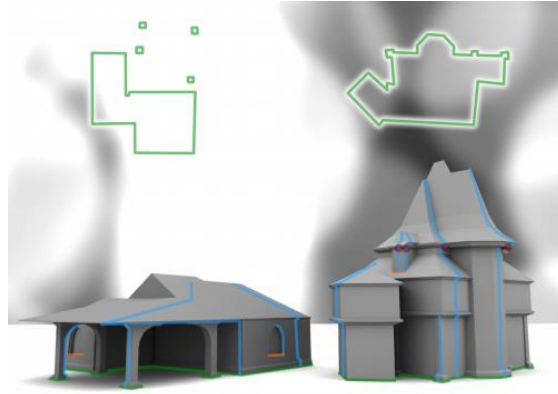


Figure 27: Plan and section profile inputs for constructing a building form with an algorithm. (Kelly & Wonka, 2011)

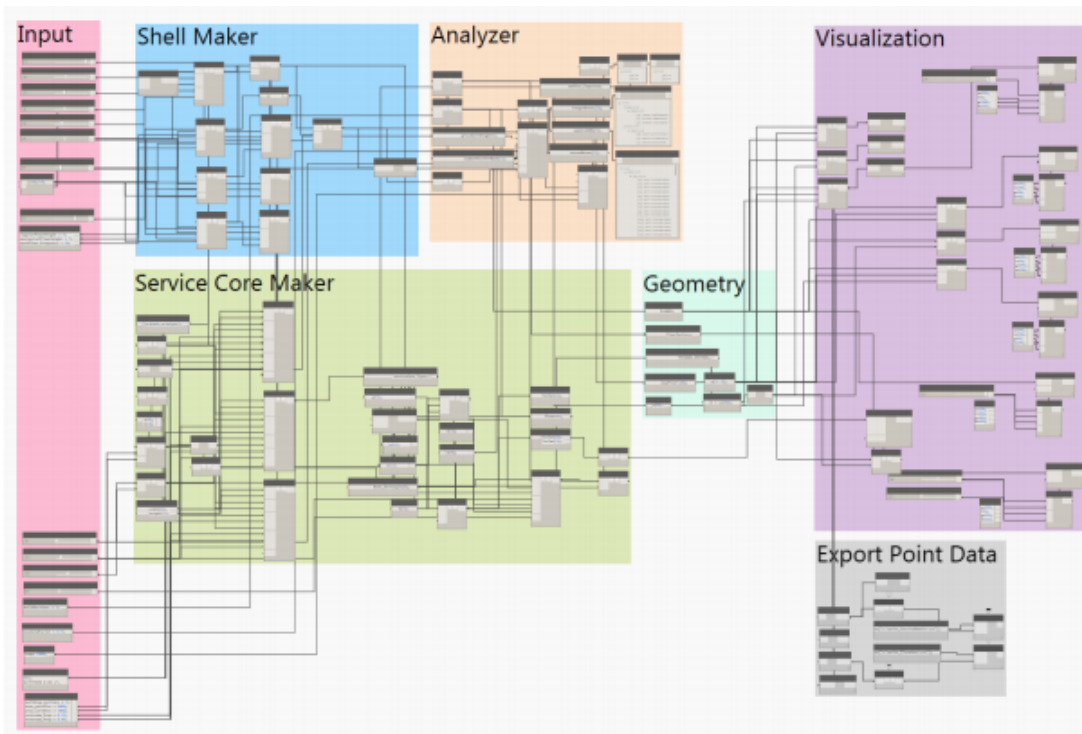


Figure 28: Automated service core generator algorithm produced in Autodesk Dynamo visual programming interface. (Das et al., 2016)

30 St Mary Axe in London is a building designed by Foster & Partners with the use of generative design methods to manage an environmentally – conscious design. The double gap facade system of the building both responds efficiently against wind loads and also makes the building benefit from natural ventilation and passive solar heating together with the floor shapes. (Giedrowicz, 2015) Individual Brezier curves were used to construct building's skin with parameters related to design concerns of structure, lighting, aerodynamic attributes and facade panel configuration. Figure 29 explains the design process by parametric model algorithm for this building.

There are other works which combines the design exploration process with the search for an optimized solution. Lin and Gerber (2014), provided one of the examples with a procedure which they called Evolutionary Energy Performance Feedback for Design (EEFPD) which can be implemented to different kind of design problems. In their study Lin and Gerber explored the use of the EEFPD on a workshop. A design problem was given to participants to address design objectives on a real site. Goals for the design were to maximize the spatial programming compliance score, to minimize energy use intensity and maximize net present value on a mixed use building. Following figure describes the parametric model formulated for this design problem.

Industry Foundation Classes (IFC) are data models which can be used in representing buildings and civil infrastructure in a digital format so that related information can be shared with models by many software applications. They can be used to define:

- Physical components of buildings,
- Manufactured products
- Mechanical/ electrical systems
- Structural analysis models
- Energy analysis models
- Cost breakdowns
- Work schedules

(www.buildingsmart-tech.org/ifc, accessed at 25.02.2018).

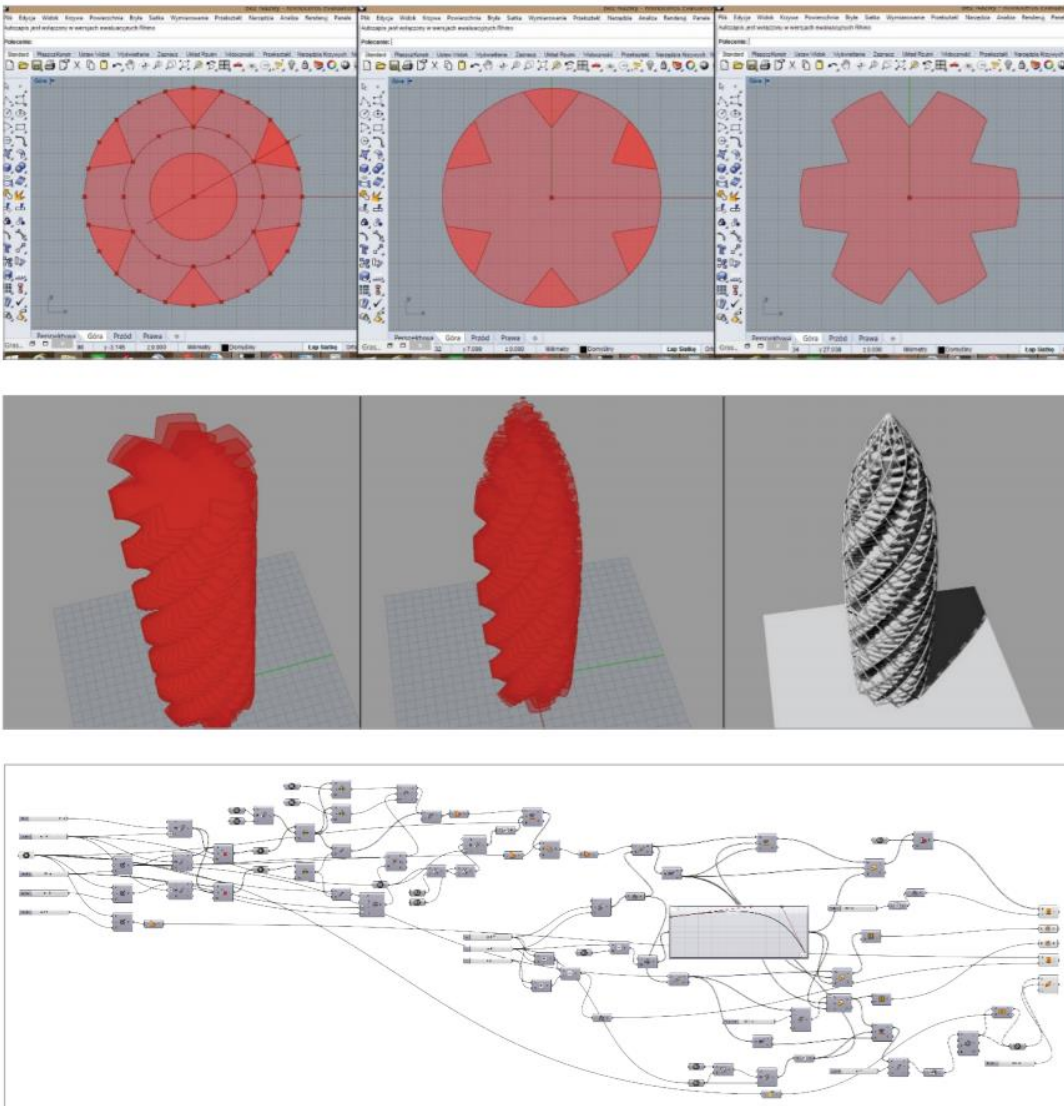


Figure 29: Explanation of the design of the St. Mary Axe with a parametric model. (Giedrowicz, 2015)

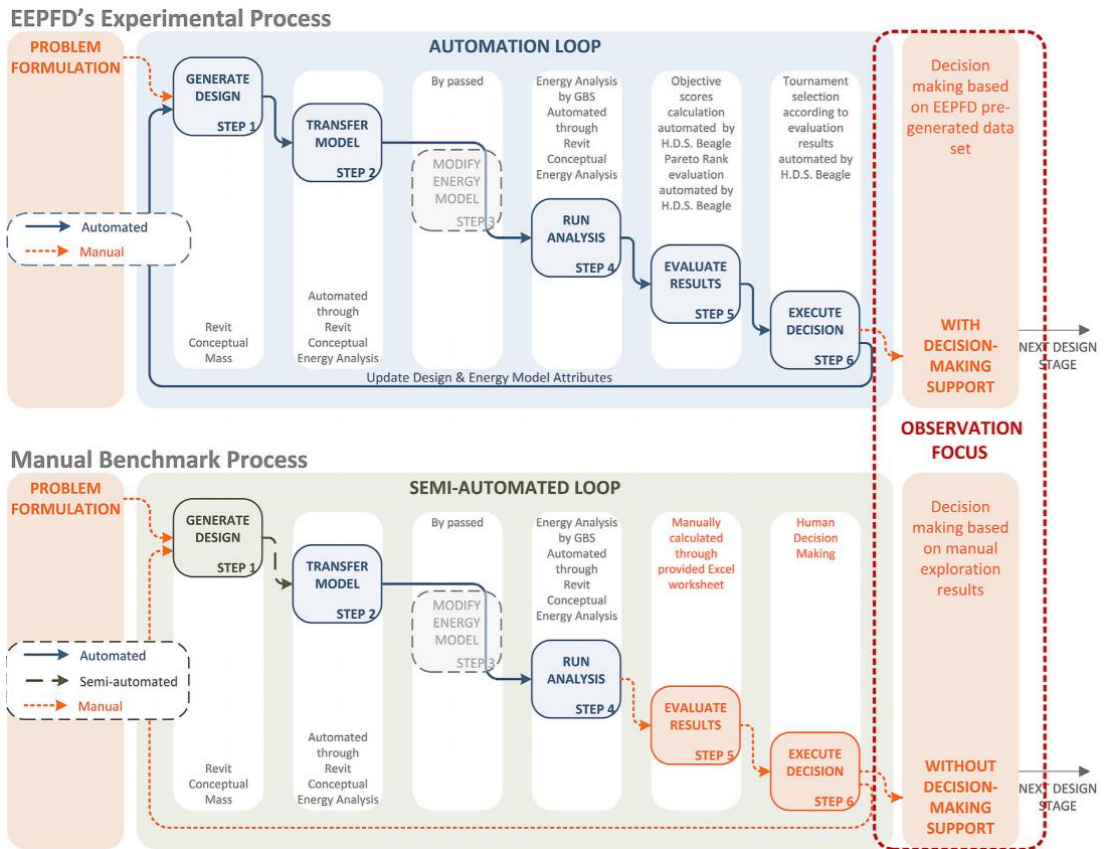


Figure 30: Explanation of the EEPFD's experimental process (Lin & Gerber, 2014).

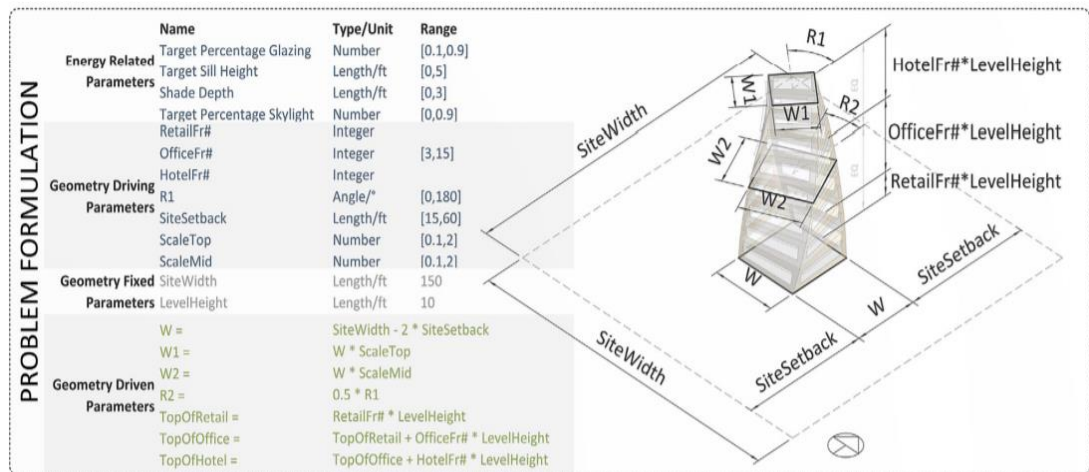


Figure 31: Problem formulation for a design process by EEPFD (Lin & Gerber, 2014).

2.5 Conclusions Deducted From Literature Review

Wind resource estimation practices referred in the literature are mostly concerning non-urban sites and configured for decision support on siting large scale wind turbines. About the character of wind resource in urban areas, doubts and challenges are given place together with some suggestions for research and development priorities for urban wind energy practices largely.

It is realized that for a proper wind resource assessment, especially for the determination of wind energy potential and feasibility of any potential initiation of wind energy conversion systems, modelling of the exact site in a proper level of detail and updated meteorology data is necessary. For estimations, however, there are some rule of thumb based on fluid dynamics, mathematical equations approximating the wind flow character and also knowledge based approaches which provide help for qualitative thinking. When urban areas considered for such purposes, there is room for improvement, as also mentioned in critical inferences in related literature. Some research topics discussed which are open for improvement are predominantly shaping around some key concerns:

- Improvement of the knowledge on wind flow characteristics in built environment.
- Improvements on analysis of the interaction between building form and wind flows for human comfort, ventilation and energy purposes.
- Improvements on evaluations of building stocks, if possible classifying them regarding to their potential to host wind energy.
- Improvements of the engineering and design of wind energy conversion systems to be implemented on buildings in terms of structure, acoustics and production efficiency.

After reviewing wind flow studies for urban areas investigating urban boundary layer and urban canopy layer, the first critical conclusion made was; research in this area is not communicative with some of other disciplines. Architects, designers, city planners, city administrators and other decision makers may not find their way easily while reviewing the literature, unless they have developed certain interest on the field,

enough to establish a connection with terminology, materials and methods used in fluid dynamics. Beneficial information extractable for design and renovation is limited with some broad suggestions. Very few sources like Wind Climate and Urban Geometry by Bottema (1993), provides specialized information for architects. This is caused by a couple of reasons as explained in following paragraphs.

Most wind flow studies conducted for building forms and urban areas include either case specific morphology or generic forms with a limited amount of parameters like binary comparisons. (See Appendix A) This scoping and disposition causes shortage of practical information. Within that context, designing a building for wind or deciding whether an innovative ventilation system or wind energy conversion system on existing building can be implemented become difficult; despite the existence of analytical tools in access for architects and designers by which they can provide inferences on the mass form decisions by simplified wind simulation engines.

Research on urban wind flows lack correlation to the architecture and urban morphology literature in terms of both terminology and range. There are classifications and definitions on form attributes for buildings and urban areas, while in most cases research on computational fluid dynamics does not refer to them while investigating architectural forms and urban formations. Besides, lesser number of different forms and formations are analyzed than the variety and scope of forms, by the classifications proposed in the literature. This is primarily because research questions are originated from engineering background and they influence the experimental setup to determine variables so as to find proper answers for their priorities.

The second critical conclusion is about the recognition of model making process for wind flow simulation studies. For all studies each model set-up is prepared separately, causing extra workload and time spent for each simulation.

Building forms and urban formations were analyzed and defined in studies from a wide range of field. Fields that have most interaction are: Architecture, building science, city planning and urban design, urban morphology, geo-information and photogrammetry. Although there are studies with the name or keyword of 'parameterization' for buildings and urban areas, the act of parameterization is usually

linked with the purpose of the study rather than an overall coverage of possible built forms, which is innately unfeasible and almost impossible. On the other hand, most of the form parameters can be excerpted from definitions in various studies. These definitions are originated from two different types of approaches. The essential difference is the methodology and type of data available.

Architects tend to provide classifications and attribute definitions based on qualitative judgment. Hence, resulted material for each study is highly subjective. Still, the possibility of aggregating these information by semantic relations is explored thoroughly and the potential it brings to this research is considered important.

Owing to the need for generalization and classification of built forms by computational practices in morphology, geo-information and photogrammetry studies; classes and attributes of forms defined by field research, satellite imagery or another similar quantitative method. From these studies it is possible to obtain significant form parameters in more objective approaches. Yet, there are two crucial quality of these studies to bear in mind: First, these studies are conducted for a well-defined specific area such as a shoreline, town, city or multiple settlements comparatively, and all conclusions they provide are valid for these region in each case. And secondly, form types, formations and attributes described in these studies have a behavior of covering most of the existing instances while ignoring exceptional occurrence, as they have no concern of giving place to future possibilities of geometric derivation.

Algorithms are becoming more and more involved to architectural practice as well as building science especially via visual programming tools. Despite that the literature providing introductory information to the algorithm aided architecture for a variety of purposes, practices mainly focuses on form finding possibilities and production support. Yet, algorithmic tools are also in use of the building simulation field. Almost each building simulation tool configured with different purposes such as energy efficiency, operates based on an algorithm. They are mostly procedural models, which enables user to make a set of selection in sequenced steps to get help in decisions or get an optimized result. Though, it is fair to say that these tools have the disadvantage of strict limitations and generalizations of form variability.

On the other hand, generative models are mainly proposed to produce forms via computational parameters to be used in design exploration or performative optimization with both sequential and non-sequential flows. Most of the not mentioned examples either attempting to generate extraordinary geometries, or develop solutions for innovative designs (e.g. non-uniform roof panels, façade joints or structural framing). Hence, it could be argued that current commercial practices of algorithmic models with form generation purpose have strong association with case specific design rather than analysis.

After sorting out these critical review segments, a group of final conclusions are established, supporting the motivation and aims of this study:

The communication between urban wind research and form & morphology research needs improvement. A generic classification and parameterization of built environment geometry could assist both fields. Since there is a need of variety and coverage in urban wind flow studies, that kind of an assistance can help decisions on experimental setups of wind tunnel studies, wind flow simulations and field measurement studies in future research. Then again, architects, urban designers and other decision makers may benefit from such a knowledge while it can behave as an intermediary transition medium between aerodynamic parameters and building forms.

An efficient method to provide generic built form classes and parameters to wind flow studies may be sustained by the use of parametric model algorithms. These algorithms should be capable of producing various 3D digital models of different building geometry and surrounding urban compositions, derived from each other by computational changes in form parameters. From the literature, it is decided that, form types and shape parameters should be based on geometric definitions rather than more indirect shape determiners like the use or function of a building or the dominant structural system. Since, parameters can be related to computational values and digital ranges more easily when the definitions are directly numerical values as geometric dependencies can be interpreted in.

To configure the algorithmic model, information on form parameters deducted from various fields should be synthesized. Since, parametric configuration of shape

attributes proposed should be inheritable from significant architectural aerodynamic parameters from literature. Besides, they also should cover the most of geometric attribute definitions specified either in wind studies or architecture literature.

After collecting and categorizing form classes and attributes, it is explored that qualitative form types can be related to each other by composition and inheritance. For example, it is possible that “segmental”, “spinal” and “radial” forms mentioned in literature as separated classes can be derived from “linear” form by definition. To be able to provide such transformations in an algorithm, extracted attributes from quantitative form definitions can be employed since they can be converted into computational form attributes within certain digital ranges.

CHAPTER 3

MATERIAL AND METHOD

The material and method implemented in the study is explained under two sections. Research process including the brief outline of this chapter is provided in the flowchart in Figure 36.

3.1 Material

This section includes information in three sub-headings for each material category involved in research process. In 3.1.1., parameters collected from literature are explained. 3.1.2 is related to software tools used in research. Lastly, sample configurations are mentioned in 3.1.3 which are gathered by random sampling in uniform distribution, and 3D model samples produced accordingly are presented in Results and Appendices

3.1.1 Categorized Parameters

A table of parameters extracted from literature, is filtered, combined (analyzed for overlaps, branches, ancestry, connections etc.) and categorized according to their type (class, inheritance, property, operation etc.) as the approach summarized in 2.2 suggests. After the critical review of literature, a four type categorization is proposed. The collected list for form parameters after aggregation is given in Table 25 in section 3.2.2 within the scope defined for the example model. Also a bibliographical table of form types and properties from wind flow studies is provided in the Appendix A.

Reference sources, which the data for parameters collected were sorted into two groups as explained in Chapter 2;

- Sources which include classification and categorization of building forms and urban formations.
- Sources from wind flow studies that include variables related with building forms or urban formations in their experimental setup.

3.1.2 Software Used

Four software tools are used in configuration and validation processes of the study.

I. Microsoft Visio:

Research process flowcharts as well as UML diagram models of algorithms were prepared by this software which includes substantial flowchart languages.

II. Autodesk Dynamo:

It is a visual programming interface providing algorithmic aid for architectural models, used by nodes (parameters and functions) to construct and transform geometry in relation to each other. The software is processing over a programming language called “DesignScript”. It is possible to interchange between code and node views for any selected part of model algorithm. With a single model algorithm, many different 3D data can be produced. Each can be used in intended purpose, which in this case is flow simulation. The software also has the ability to operate in coordination with Autodesk Revit, so it can be involved into Building Information Modeling (BIM) practices. Therefore, the primary advantage of using Dynamo for this research is that, it is one of proper tools to demonstrate the efficiency of algorithm aided architectural models in wind flow simulation studies.

III. IBM SPSS Statistics 24:

It is a statistical tool supporting research and data analysis. In addition to a variety of statistical tests like regression analysis and correlation plots the software is also capable of simulating data according to pre-defined distributions and correlations with Monte Carlo simulation and can provide sensitivity analysis on simulated data.

IV. Autodesk Flow Design:

For flow simulations, Autodesk Flow Design software was used. This is a simple flow design software with an easy to use interface and smaller calculation times specified for designers and architects by the definition of producer. Input values it can use are model geometry, basic type of flow and speed of flow. Output values it can provide

are wind speed at any location around model objects and surface pressures represented by flow lines or section planes.

3.1.3 3D Model Samples

A parametric model was produced for simulations and configured sample set was used for simulations.

Two model algorithms were developed initially on UML diagrams. And one of them is produced in Dynamo software to be analyzed. Considerations for the models, as well as their content and structure are explained in 3.2.1. Samples from the model are presented in Appendix C, with flow simulations on them. Whereas, Appendix B lists the parametric configuration of samples. Here, some examples are presented:

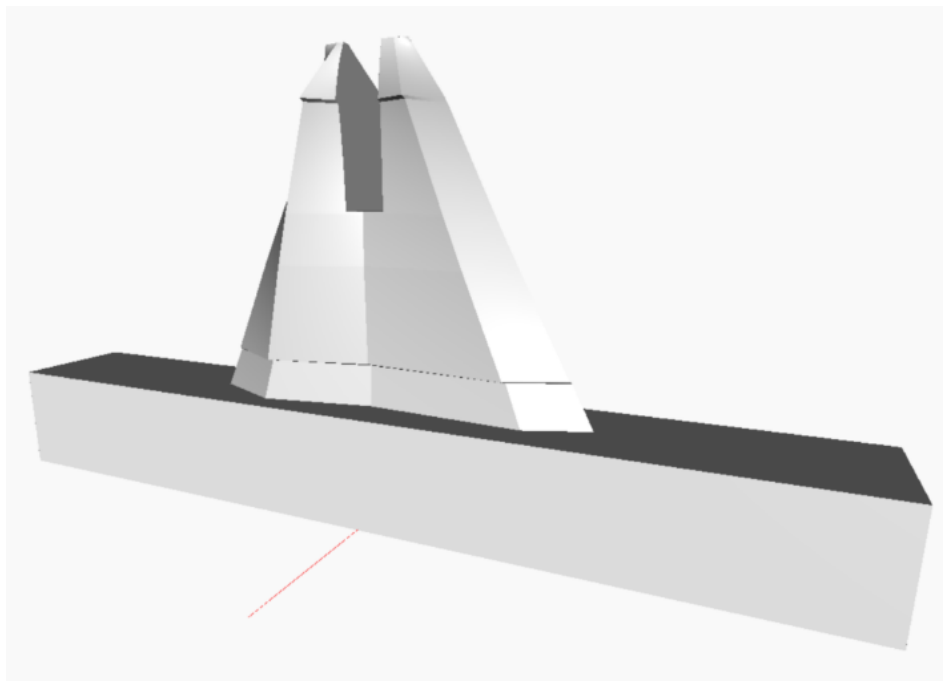


Figure 32: Model used as Sample 1

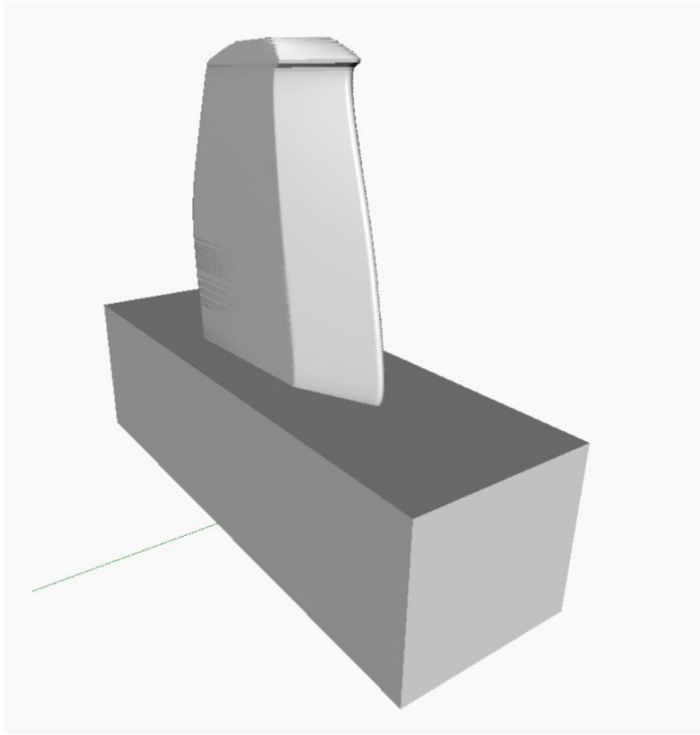


Figure 33: Model used as Sample 19.

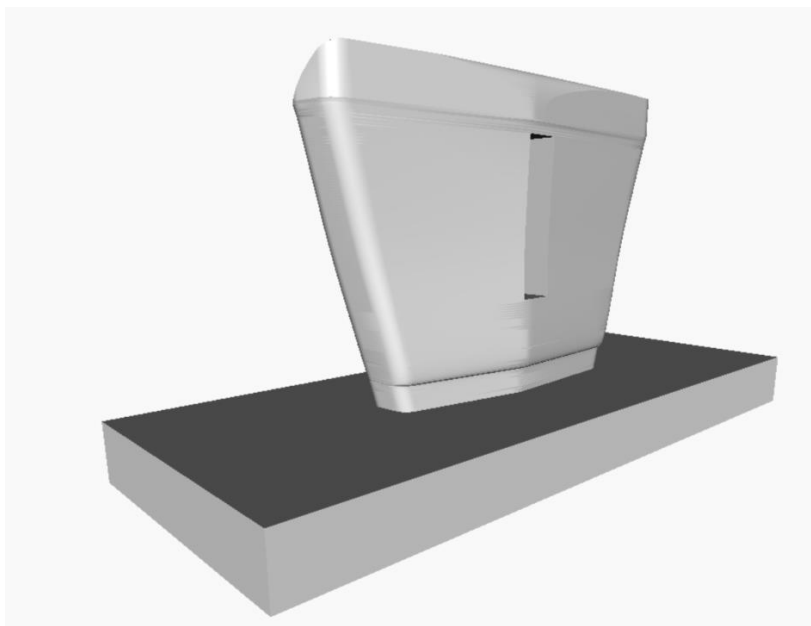


Figure 34: Model used as Sample 37

3.2 Method

In consideration of the conclusions deduced from literature review, a framework on parameterization of built environment for wind flow studies is proposed.

This framework is a matrix of three domain sizes and three steps which are expected to provide parametric interface(s) for different disciplines and related actions. Use of parametric model algorithms as an infrastructure is the essential core within that matrix. These models should provide base for generic form variations within the context of wind related parameters.

Table 24 and Figure 35 presents two definitions for the proposed scenario. The table explains the process in a matrix configuration, while the figure shows controls and mechanisms for each step. Last step is related to actions for which the parametric model algorithm will be used for. These actions can be related with design exploration by analyzing different generic forms which are generated based on different configurations of wind related form parameters. Research on built form – wind interactions by flow simulations can be conducted by the use of these models in sampling, since values of input parameters will be useful in computational methods as quantitative data with continuous or ordinal scales. Another possible area of use can be form optimization, as genetic algorithms or multi-objective decision making tools can be implemented onto the core parametric model.

The scope of this study is restricted to production of an example parametric model based on proposed framework only for Domain 1. Therefore, a parametric model algorithm is produced with the ability of generating generic building forms for wind related studies. This model is tested by statistical models on flow simulations to assess its relevancy with wind flow behaviors.

The research process is composed of three major parts and nine processes each supplies necessary inputs for the next stage(s). The first part is related to construction of parametric model algorithm, while other parts are intended for testing the convenience of the model and parameters.

Table 24: Definition of the proposed framework in a form of a matrix

	Step 1	Step 2	Step 3
	Parameter aggregation and algorithm design	Production of parametric model algorithms	Configuration and use of the model for intended action
Domain 1 Isolated Building	Input parameters for isolated building	Core parametric model for isolated building *	Action
Domain 2 Urban Block	Input parameters for urban block	Core parametric model for urban block	Action
Domain 3 Urban Area	Input parameters for urban area	Core parametric model for urban area	Action
* The position of the example model produced and analyzed within this study in the framework matrix.			

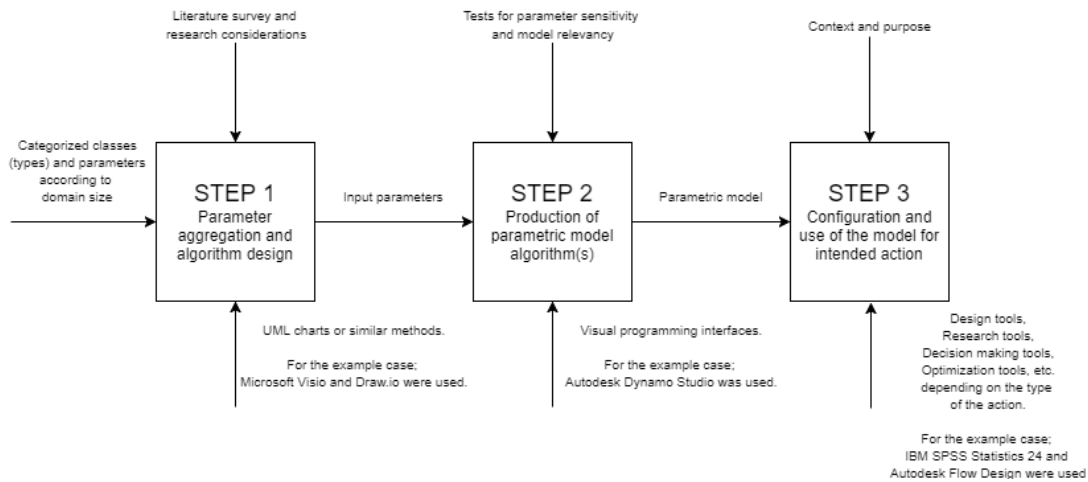


Figure 35: Definition of parameterization steps with IDEF0 diagram.

- Literature survey to explore form and morphology parameters related to urban wind flows (Process 1: Literature Review) followed by, parameter aggregation, analyzing architectural and urban form parameters deducted from literature in terms of their possible significance for aerodynamic parameters and wind flow characteristics. Initially structuring parametric relation diagrams for the model algorithm (Process 2: Parameter aggregation). The final step of this part is the construction of the model. (Process 3: Construction of parametric model algorithm) Production of an example parametric model, by structuring an algorithm between geometry defining attributes, operations and classes based on the UML diagrams prepared in previous processes. For this part, visual programming was implemented by Autodesk Dynamo interface.
- Second part is about preparing necessary configuration for the last part. Samples from parametric model are configured first, according to determined necessities of analysis that will be applied. (Process 4 Sample configuration) Then, sample models are generated using the parametric model, consistently with the configured values. (Process 5: Sample generation). Samples exported from the model went through flow simulations and specific output values are measured. (Process 6: Flow simulations)
- Parameter sensitivities are compared and their significant correlations with outputs are measured to determine the influences of selected parameters on basic wind flow characteristic around buildings. This process is applied on results gathered from wind flow simulations which are conducted in second part. This stage includes three sub-processes as (Process 7: Monte Carlo simulation), (Process 8: Statistical tests) and (Process 9: Discussion)

Three subsequent IDEF0 diagrams in the next page are presented in order to explain the research methodology visually. Each box represents a process (or function). Arrows from left are inputs, arrows from down are mechanisms used, whereas arrows from up represent controls. Arrows headed to the right side are outputs for each process.

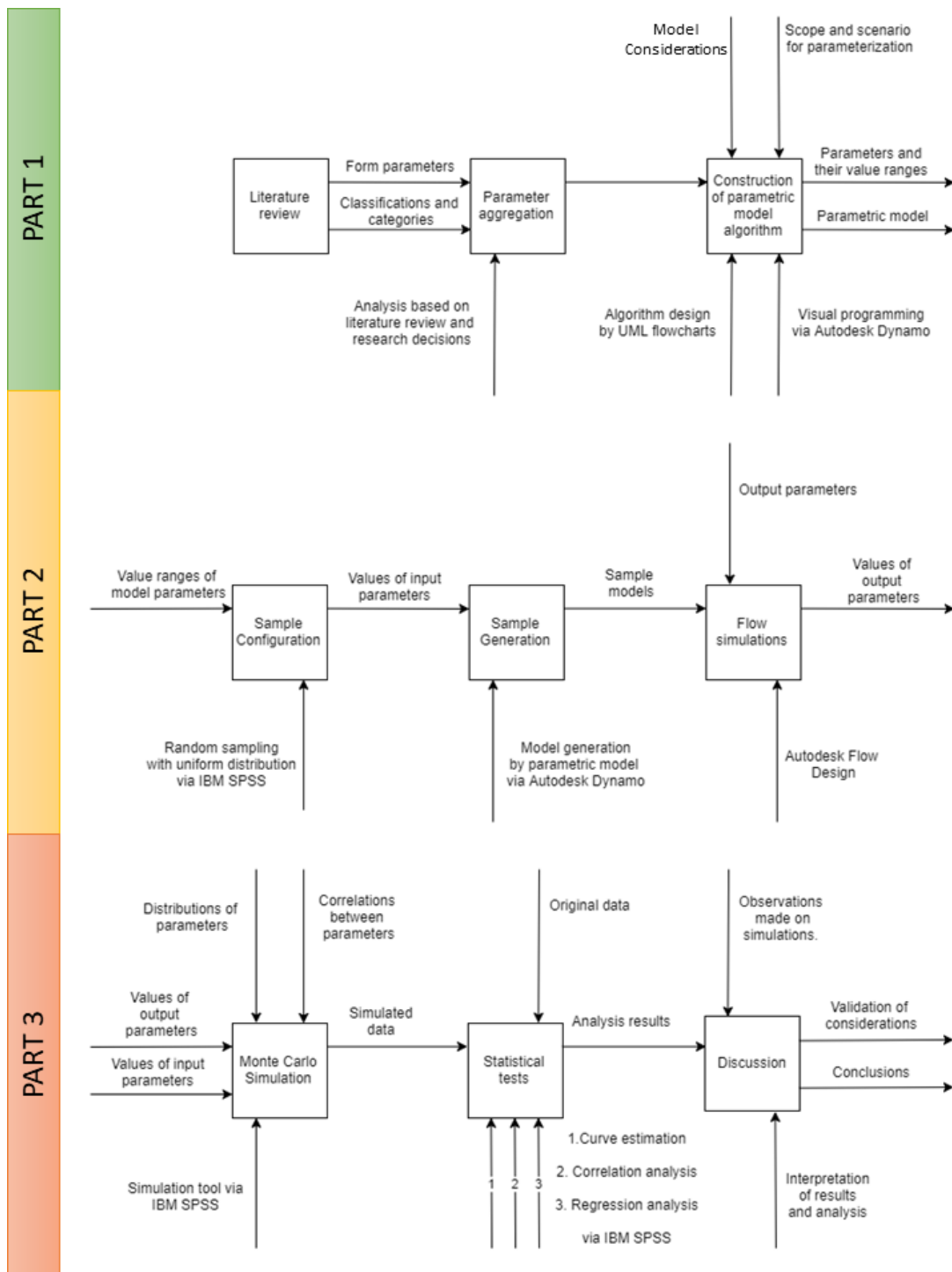


Figure 36: IDEF0 diagrams explaining three consequent stages with nine processes in total.

3.2.1 Parameter Aggregation and Constructing Parametric Model Algorithm

During the literature review process, form properties, operations and classes were grouped so as they can form an algorithmic flow.

- Form properties (or geometric properties) of buildings and urban areas, which are also related to aerodynamic parameters, in four categories. These categories are: building components, building, composition of buildings (clusters and blocks) and urban areas. (Then these properties are compared with parameters and samples of wind flow studies.)
- Formative operations derived from the literature related with form and morphology as well as parametric studies of architecture, which can be used in geometrical algorithm to affect values of form attributes
- Classes or object types which can be employed as primitive instances in parametric models.

Afterwards, the scenario proposed is implemented on a parametric model algorithm according to decided scope. Based on literature review, in terms of model sizes used, study methods and urban morphology definitions three domain sizes were determined as mentioned in the beginning of this chapter. These three domain sizes are:

- Isolated building (or/also building complex). The term “isolated” is used for studies based on single buildings due to its frequent use in literature of wind flow studies.
- Urban block (block and adjacent roads)
- Urban area (an urban zone with 300m radius)

According to this scenario related to domain size, a scope for an example application was determined for this study. A parametric model algorithm as an example for isolated building domain has been developed so as that two considerations are satisfied:

- **Consideration I.** Possibilities generated with algorithm should cover most of architectural types (or classes) mentioned in literature in a generic level of detail.

- ◆ Validation procedure: 3D Model geometry produced corresponding to typical definitions in classification for selected scope.
- **Consideration II.** Parameters employed in model should cover most of geometric attribute definitions specified either in wind studies or architecture literature. They are expected to have influence on wind flow simulation results.
 - ◆ Validation procedure: Testing and comparing parameters' effects using data simulation support (SPSS) and flow simulation (Autodesk Flow Design) software.

To assure these conditions, UML (Unified Modelling Language) system modelling is used through Microsoft Visio before constructing a model algorithm with Dynamo. Considering that the variables in model is to be tested by statistical models, the structure is configured by using quantitative (numerical) values for each parameter's variability range.

Two different strategies of constructing a parametric model algorithm are speculated from the review of the similar software tools or studies in literature:

Strategy I: From a library folder, several primitive instances - each representing a generic form type mentioned in the literature - can be used as stem models. Onto them variations on samples can be produced by using lesser amount of parameters.

The advantage of this strategy might be the speed, since each model of a separate type will operate in its own interface. Also a more concise flow of visual programming can provide intelligibility for researchers. However, while models will be constrained in a lower level of detail for generic solid types, there are already possible tools to produce these solids from primitive instances in CAD software like prisms, sphericals, conicals, and pyramidal. It is also considered that this approach may lack deriving a meaningful variation in forms due to the limitations of typical parameters which belong to essential solids with very definitive geometries.

Strategy II: Another scenario can be a parametric model running on a single interface with more parameters that can morph into solids, covering most of regular definitions but also more irregular forms which are harder to be categorized but possible to be

designed by architects. Also, it is predicted that, Consideration II might become focused on more accurately by that approach.

Therefore, it is aimed to generate generic geometry by an approach reducing primitive instancing and increasing form generating with computational tools so that the algorithm can produce different form types in literature, while originating from fewer primitive stems. In order to achieve this purpose, form types, from attributes and transformative operations deducted from literature collected in lists. Initially, the list of form attributes (shape attributes) is analyzed and merged by if necessary. Thus, a list of selected form attribute variables prepared for the algorithm. First, classes are clustered by analyzing them semantically and morphologically (See Table 25). Then, reduced items in list of form types are went through a second grouping (See Table 26) The possibility of employing form giving operations in this list as means of generating different types deriving from each other is aimed.

Biggest change occurred between first and second aggregations is the collapsing of List 1 into two items. The use of UML language for modeling the algorithm before visual programming helped discovering relations between types. Shape properties also decreased in number before they are inserted in visual programming due to a similar reason. They are also affected by each other, therefore they can be grouped by this relations. That process resulted with second aggregation in two proposed models consisting two primitive instances that can derivate into other types in a generic manner for isolated building simulation size. These are:

I. Central form: This primitive instance is used as a stem for creating single forms which are producible based on a polygonal footprint and two vertical sections. One of the section planes are parallel to windward direction (XZ plane in models and simulation setup) and the other one is normal to the wind flow (YZ plane in models and simulation setup) The model is composed of two primary components as vertical (named as tower) and horizontal (named as base) This model was constructed by Dynamo and analyzed by sensitivity analysis on wind flow simulations.

Table 25: Lists of architectural form types, form attributes and transformative operations after first aggregation from literature.

List 1: Form and Composition Types	List 2: Form Attributes	List 3: Transformative Operations
Cubic	Height	Dimensional transform
Spherical	Length	Subtraction
Cylindrical	Width	Addition
Pyramidal	Position	Bending
Conic	Orientation	Folding
Square based	Regularity	Breaking, cutting
Triangle based	Coverage (density)	Segmenting
Circle based	Enclosure	Accumulation
Polygonal	Smoothness	Superimposition
Central	Contiguity	Meshing
Clustered	Porosity	Interlacing
Gridal	Granularity	Distortion
Linear	Compactness	Combination
Axial	Squareness	Subdivision
Radial	Coordinates of Center	Assemblage
Network	Concavity	Overlapping
Superimposition	Elongation	Rotation
Labyrinth	Footprint area	Approximation
Fork-like	Surface area	Extrusion
Spinal	Perimeter length	Looping
Segmental	Size (Volume)	Algorithmic patterning
Branched	Roundness	Triangulation
Layered	Maximum height	
L footprint	Average height	
I footprint	Number of Vertices	
H footprint	Slimness	
A footprint	Number of storeys	
V footprint	Roof slope	
Tower and podium	Roof shape	
	Aspect ratio	
	Opening size	
	Projection size	

Table 26: Form types based on proposed origin algorithmic model after second aggregation.

Types derivate from central form algorithm	Types derivate from linear form algorithm
Cubic	Clustered
Spherical	Gridal
Cylindrical	Linear
Pyramidal	Axial
Conic	Radial
Square based	Network
Triangle based	Superimposition
Circle based	Labyrinth
Polygonal	Fork-like
Central	Spinal
Tower and podium	Segmental
	Branched
	Layered
	L footprint
	I footprint
	H footprint
	A footprint
	V footprint

II. Linear form: It might be programmed as the origin of most architectural compositions. By changing form attributes and transforming the primitive instance with change in their parameters, they can be modelled. The algorithm is expected to run on two components similar to the central form. Except, for this algorithm, these components are a core (central line) and branch(es). Together they can generate most of the types of compositions listed in first aggregation in a generic level of detail. This model is configured as UML scheme but it is not constructed by Dynamo and excluded from this study.



Figure 37: Initial sketches for central form (left) and linear form (right) layouts.

UML diagrams used prior to parameter aggregation are presented in Appendix A. They show scalar and categorical parameters derived from literature according to each model domain. Anticipated structure of model is presented with UML diagrams as used in pre-programming in figures 20 and 21. UML has seven basic types of connections. Among them two connections are used in models as:

- Composition: Meaning that the target type (arrowhead) include the source type (arrow tail).
- Dependence: Meaning that the existence of source type (arrow tail) depends on the data or value obtained from target type (arrowhead)

Data types of values that attributes can have are: Doubles and Integers as numeric, decimal or degree information.

During the actual construction period of the parametric model algorithm, decisions made on decreasing the complexity of the model by decreasing the amount of parameters, affording loses of sample variation and generative capability. This was due to the limitations of the study as skill, time and hardware. Three significant changes are:

The solid of tower part was planned to be generated by three components as footprint polygon, windward section curve and normal section curve. Alternatively, resulted model uses two components to make tower solid as footprint polygon and windward section only. Parameters related to normal section curve were excluded from model algorithm. Instead a single parameter named “S.NormalTapering” was added to the model as a modest replacement. So that, the capability of generating variants from normal section characteristics are significantly decreased while producing pyramid-like, sphere-like and conic-like forms together with the appropriate configuration of windward section parameters is still possible. Base part was simplified into a rectangular prism, which only have the variables of height, length and width dependently to the tower. A horizontal void is still possible to be produced with the model, since many wind flow studies include that type of voids in generic solids. However, the vertical void, representing a courtyard, was excluded from the algorithm.

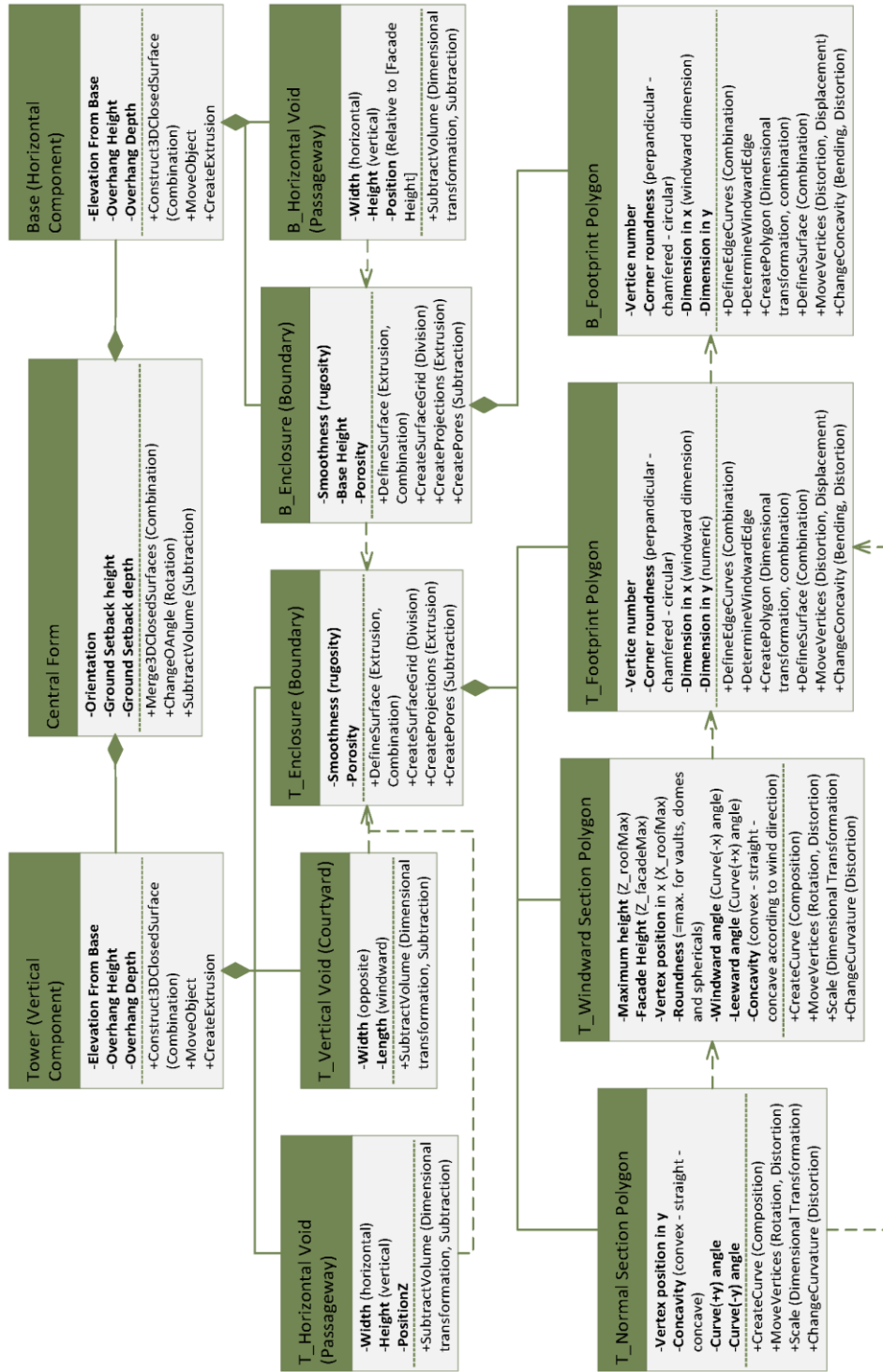


Figure 38: UML Flowchart of pre-configuration step for Central Form model algorithm. See Figure 40 for revised version.

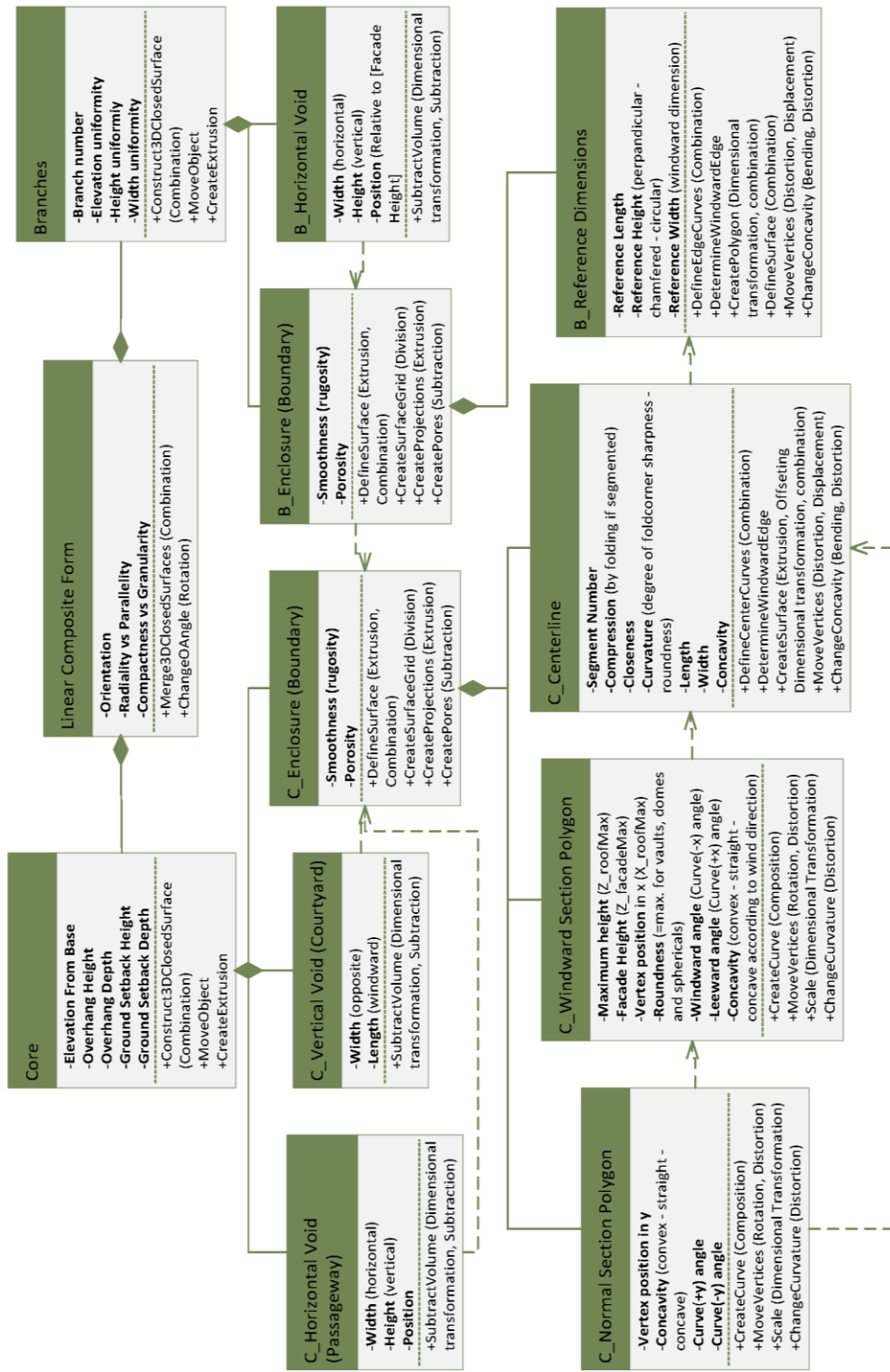


Figure 39: UML flowchart explaining pre-configured Linear Form model algorithm (not produced).

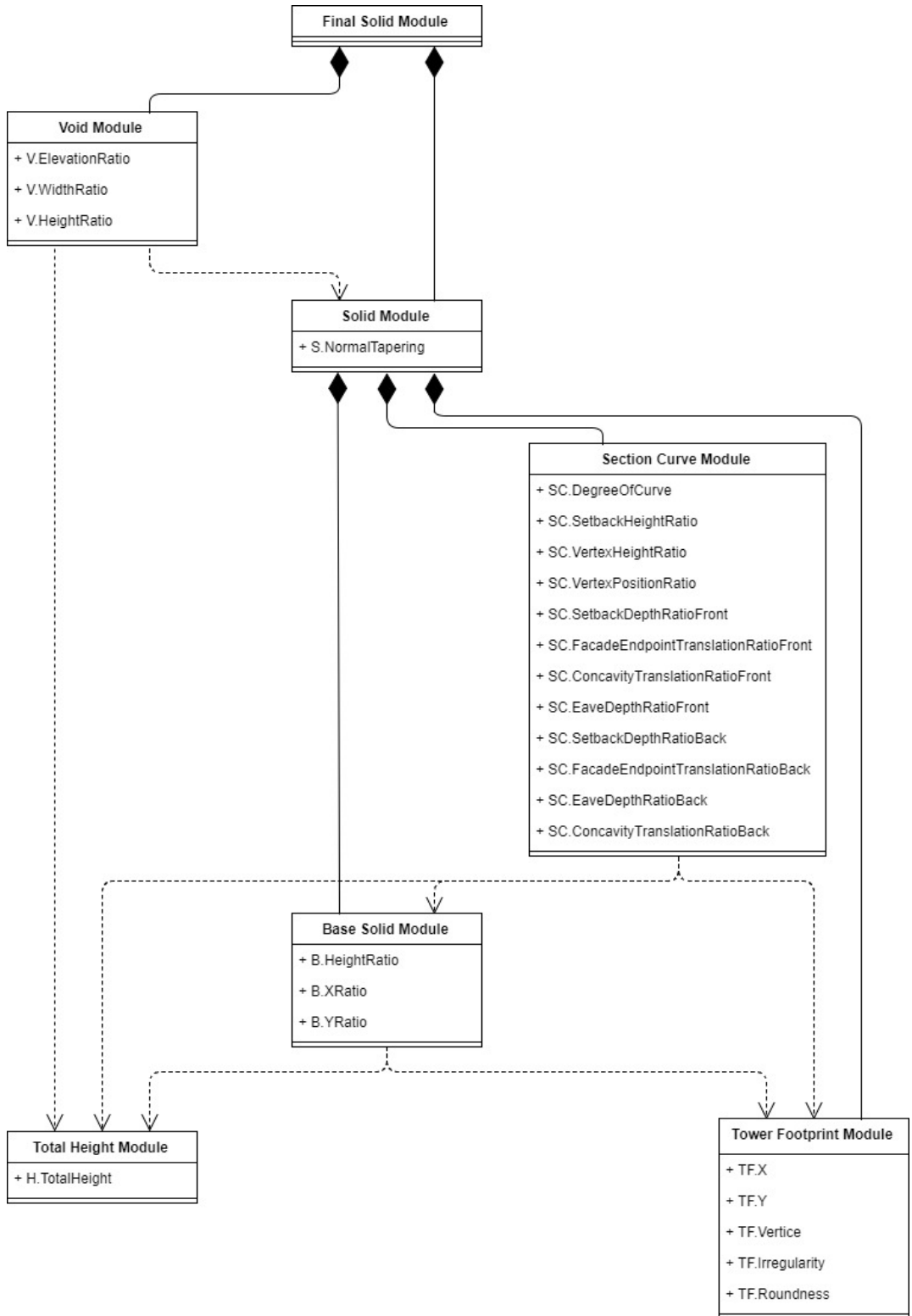


Figure 40: The UML diagram showing the structure of resulted parametric model algorithm.

Figures in previous pages are explaining the initial UML models for Central Form and Linear Form stems. The UML diagram explaining the resulted model is given in Figure 40. As described in that diagram, parameters of model are explained together with model construction steps which will be called as modules hereafter. Nodes in the visual programming interface of Dynamo are grouped into seven modules. Each module covers a procedural step in the algorithm and transmits information to other module(s).

- Tower Footprint Module:

This module is responsible of producing the footprint polycurve of the tower component. To generate the footprint, there are four procedural phases.

First, the model of a regular polygon with intended corner numbers is generated as inscribed in a circle. Then, according to user input, the size of polygon is adjusted by scaling it in two dimensions. Thus the origin polycurve of footprint is produced. Secondly, the parameter for varying the shape between regular and irregular forms acts as explained below in TowerFootprint.IrregularityRatio. Third phase determines the roundness of footprint corners by fillet, and the fourth phase is for a size calibration to restore original size if the original X and Y dimension are distorted after the fillet operation. Parameters in effect are explained below:

I. Tower Footprint. X (TF.X):

X dimension on XY plane which provides the scale amount for the escribed circle constructing a polygon. Defines the length of the bounding box for building footprint on the windward direction.

Data type: Integer. Range: 5 – 100 meters.

II. Tower Footprint. Y (TF.Y):

Y dimension on XY plane which provides the scale amount for the escribed circle constructing polygon. Defines the width of bounding box for building footprint on the normal direction to the wind.

Data type: Integer. Range: 5 – 100 meters.

III. Tower Footprint. Vertice (TF.V)

Number of footprint vertices. Circular or elliptic curves can be approximated by selecting the maximum value for TF.V as 8, together with increasing fillet radius.

Data Type: Integer. Range: 3 – 8.

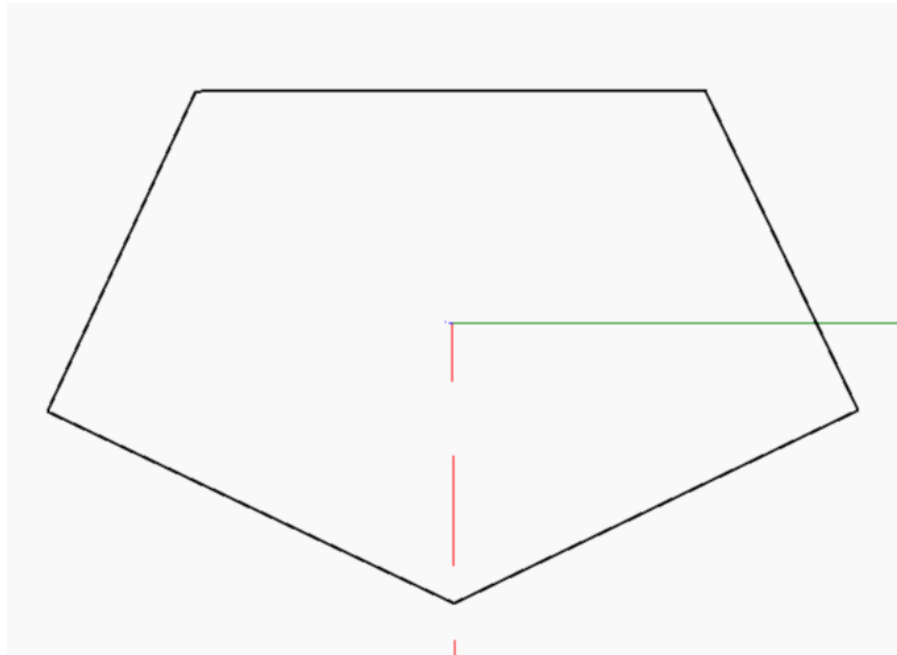


Figure 41: Polycurve of tower footprint produced by values as: TF.X = 41, TF.Y = 62, TF.VN = 5

IV. Tower Footprint. Roundness (TF.R)

This parameter acts as multiplier factor for controlling corner fillet radius which increases roundness of overall shape. Assigning independent values to the fillet radius of the corners cause unintended shape deformations with small sized polygons or insignificant effects on larger sized polygons. Therefore, to get relative fillet radius values with shape sizes, a mathematical product of the smaller dimension is used.

Data type: Double, Range: 0 – 0.20.

V. Tower Footprint. Irregularity (TF.IR)

To provide more irregular polygon shapes for footprint, an algorithmic module is constructed. Employing `Math.RandomList` function together with a series of `Remap` and `Range` functions of the Dynamo interface, x and y values for translation of vertices in XY plane is provided. Resulted values are the multiplication of shortest edge length from original polygon and TFIR. So that, for regular polygons, the TFIR value equals to 0.

Data type: Double . Range: 0 – 1.

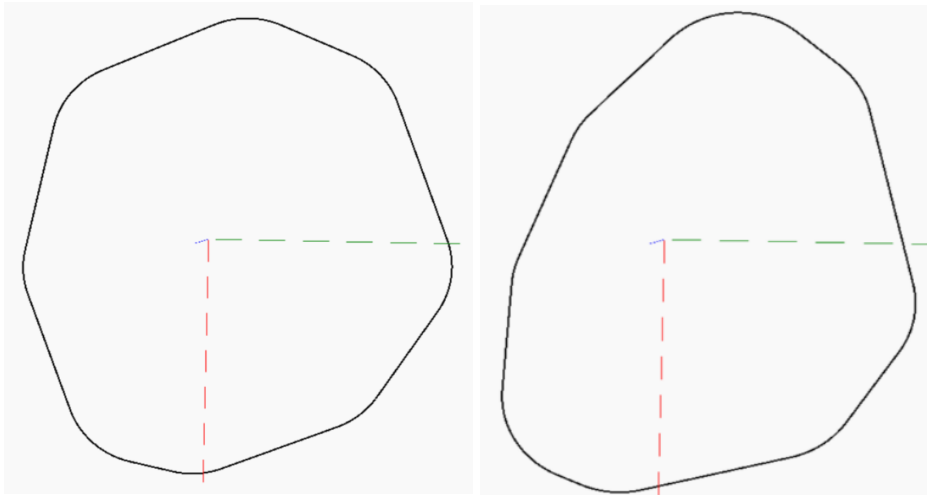


Figure 42: Two tower footprints with different irregularity conditions. On the left: Polycurve of tower footprint produced by values as: `TF.X = 40`, `TF.Y = 33`, `TF.VN = 8`, `TF.Roundness = 0.2`, `TF.Irregularity = 0.5`. On the right: Shape with same configuration but `TF.Irregularity = 0.9`

- Height Module:

The model is structured so as to total height value is constant and user input for that value cannot be affected by other parameters in model changes. This module is the smallest one in the model, purposed to get the height value and transmit it to other modules which operate dependently to generate base solid, section curve, building solid and void. The only parameter included is `H.TotalHeight`.

I. H. Total Height (H.TH)

It is the value of building height, all parts included like base and roof.

Data Type: Integer. Range: 3 - 100 meters

- **Base Solid Module:**

Base solid is produced here, by extrusion of a rectangular base relatively to the data from Total Height Module and Tower Footprint Module. There are three parameters which can be adjusted by user:

II. B. Height Ratio (B.HR)

This is a ratio of the base height to the total height of building. Therefore it also gives the value for tower height and transmits it to the Section Curve Module.

Base Height = H.TotalHeight x B.HR

Tower Height = H.TotalHeight – Base Height

Data Type: Double. Range: 0 – 0.4.

III. B. X Ratio (B.XR)

To determine the windward dimension of the base solid this ratio is multiplied by the TF.X value which is the X dimension of tower footprint.

Data Type: Double. Range: 1.5 – 5.

IV. B. Y Ratio (B.YR)

Similarly to the previous one this parameter is a ratio of the Y dimension of Base Solid (normal to the wind) to Y dimension of Tower Footprint.(TF.Y)

Data Type: Double . Range: 1,5 - 5

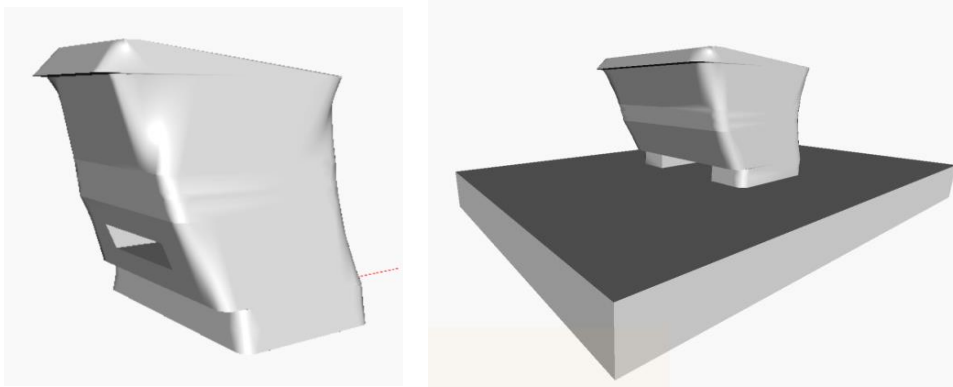


Figure 43: Different base - tower configurations. Total height does not change, tower height decreases relatively to increase of base height.

- **Section Curve Module:**

This module has the most parameters in the model. A section curve is produced by values of these parameters.

Both theoretical background of aerodynamics and wind flow studies suggests that the windward section character of a form has utmost importance. Yet, in most of research studies from wind flow studies and form generalization studies, prismatic solids which are direct extrusion of a footprint shape are used as samples of generic building forms. Hence, this study seeks to present an example with increased number of section profile variability.

The section curve is constructed by control points. Each of these points are located by computational means on the coordinate system by x,y,z values affected from related parameter values. Twelve parameters involved in this module are listed hereafter:

I. SC. Degree of Curve (SC.DOC)

Section curve is a NURBS curve. Degree of curvature of this type can be changed by the Dynamo. It can take values between 1 and 4. Bigger values increases the roundness of the section profile.

Data Type: Integer. Range: 1-4.

II. SC. Setback Height Ratio (SC.SHR)

Setback is the part of tower mass where it recesses on the ground level. This parameter is the ratio of the setback height (where the projected part of the façade start) to the total height. A constraint of 3 meters is assigned to the range in order to prevent unrealistic setback configurations. When the computed distance from the base is smaller than 3 meters, a setback is not produced in the section.

$$\text{Setback Height} = \text{SC.SHR} \times \text{H.TotalHeight}$$

Data Type: Double. Range: 0 – 0.2.

III. SC. Vertex Height Ratio (SC.VHR)

This parameter locates the Z value of the roof vertex point in coordinate system relatively to the total height as below:

$$\text{Vertex Height} = \text{SC.VHR} \times \text{H.TotalHeight}$$

For flat roofs this value equals to 0. Height of the façade is also dependent on this parameter, since the total height is constant:

$$\text{Facade Height} = \text{H.TotalHeight} - \text{VertexHeight} - \text{Setback Height} - \text{Base Height}$$

Data Type: Double

Range: 0 – 0.5

IV. SC. Vertex Position Ratio (SC.VPR)

While the previous one locates the Z component of the roof vertex point in section, this one determines the X component on coordinate axis. It helps positioning the vertex in a definite distance to front (windward) or back (leeward) facades. The length of the shortest line where the facade is ended is calculated by the algorithm. Then the value input for SC.VPR is multiplied by it to define the vertex position together with SC.VHR. as “VertexX = SC.VPR x Roof Base Length”

When the SC.VPR is 0, a vertex point aligned with the front façade can be obtained. Similarly, if it is set to 1, vertex point aligns with back façade. Thus, asymmetrical facade heights are possible to be produced with the model by changing this parameter.

Data Type: Double. Range: 0 – 1

V. SC. Setback Depth Ratio, Front (SC.SDRF)

This parameter determines the setback distance, if there is any, from the intersection of windward section curve and footprint edge. To be able to locate the point of setback line in section, TF.X called by the algorithm. Therefore, this parameter has dependence relation with the Tower Footprint Module.

$$\text{Setback Depth Front} = \text{SC.SDRF} \times (-\text{TF.X})$$

Data Type: Double. Range: 0 – 0.5.

VI. SC. Façade Endpoint Translation Ratio, Front (SC.FETRF)

To be able to produce buildings with different facade angles, this parameter is used. When the angle degree was used instead, model can produce unintentional section curves with self-intersection, causing unrealistic building forms. Thereby the angle of the façade line is defined by the translation of the facade endpoint in X, relatively to the Footprint edge.

$$\text{Façade Endpoint Translation} = \text{FETRF} \times (-\text{TF.X})$$

Data Type: Double. Range: (-1) – (1).

VII. SC. Concavity Translation Ratio, Front (SC.CTRF)

Buildings with concave or convex forms in plan layout are represented with some generic forms in some research studies on wind flows. However, during the literature review an example of generic forms with a vertical concavity property was not encountered. Yet, these type of building sections exists in architectural practice, especially in tall building designs. This parameter adds the model a variable on facade concavity with a presumption of significance for wind behaviors.

The working principle is simple, on the section curve, the midpoint of the distance between setback end and façade endpoint is located by the algorithm. Then this point translated in X by the value of SC.CTRF relatively to its aligned position with footprint.

Concavity Translation (Facade Midpoint Translation) = $SC.CTRF \times (-TF.X)$

Data Type: Double. Range: -0.25 – 0.25.

Positive values produce concave lines, while negative ones result in convex forms.

VIII. SC. Eave Depth Ratio, Front (SC.EDRF)

Eaves are also an important feature for the building aerodynamics according to literature. Therefore a parameter for eave size is added to the model. Similarly to the previous one, it locates the control point on section curve where the eave (if exists) ends relatively to the footprint edge.

Eave Depth = $SC.EDRF \times (-TF.X)$

Rest of the parameters in section module for the definition of control points of back (leeward) facade and listed below. They are not explained in detail since the working principle of them is the same with the parameters explained for front (windward) facade.

IX. SC. Setback Depth Ratio, Back (SC.SDRB)

X. SC. Facade Endpoint Translation Ratio, Back (SC.FETRB)

XI. SC. Eave Depth Ratio, Back (SC.EDRB)

XII. SC. Concavity Translation Ratio, Back (SC.CTRB)

Figure 44 is explaining building form properties which are controlled by Section Curve Module parameters.

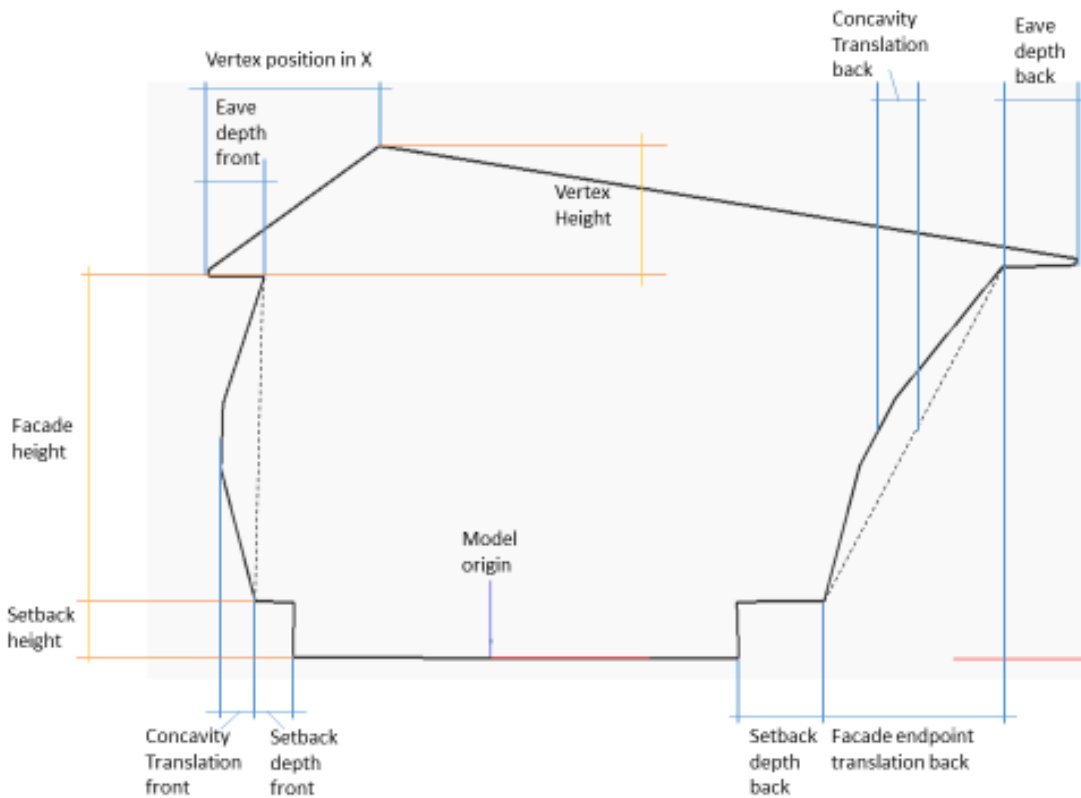


Figure 44: Form properties of building section except the roundness, each controlled by an independent parameter explained under Section Curve Module.

- Solid Module:

This module is purposed for the construction of tower solid and union of the base solid and tower solids. While it also includes a parameter for the tapering operation in normal section (in Y axis).

One of the biggest limitations faced in research is the very challenging use of 3D solid making operators in Dynamo. Ideally, the solid of the tower was intended to build by a sweep algorithm. However, after multiple trial and error in model making Loft tool is used for the construction. Footprint polycurve is translated in offset planes by Z components of section curve control points. Then a three step scale procedure is applied to each of them to intersect with the section curve. (There is no other align tool in Dynamo software) Finally, scaled curves are transmitted through a loft algorithm to end up with a solid with less possible geometry loss.

Only parameter in Solid Module is S.Normal Tapering, which is actually a modest replacement for the normal section curve parameters which was excluded from the model.

I. S.NormalTapering (S.NT)

This parameter scales the loft curves in a linear order to be able to generate tapered forms in normal section. Basically it is a ratio of roof base line in normal section to the ground line as intersected by section plane on footprint. Values closer to 0.1 acts as tapering while values after 1 results with reverse tapering

Data type: Double. Range: 0.1 – 2

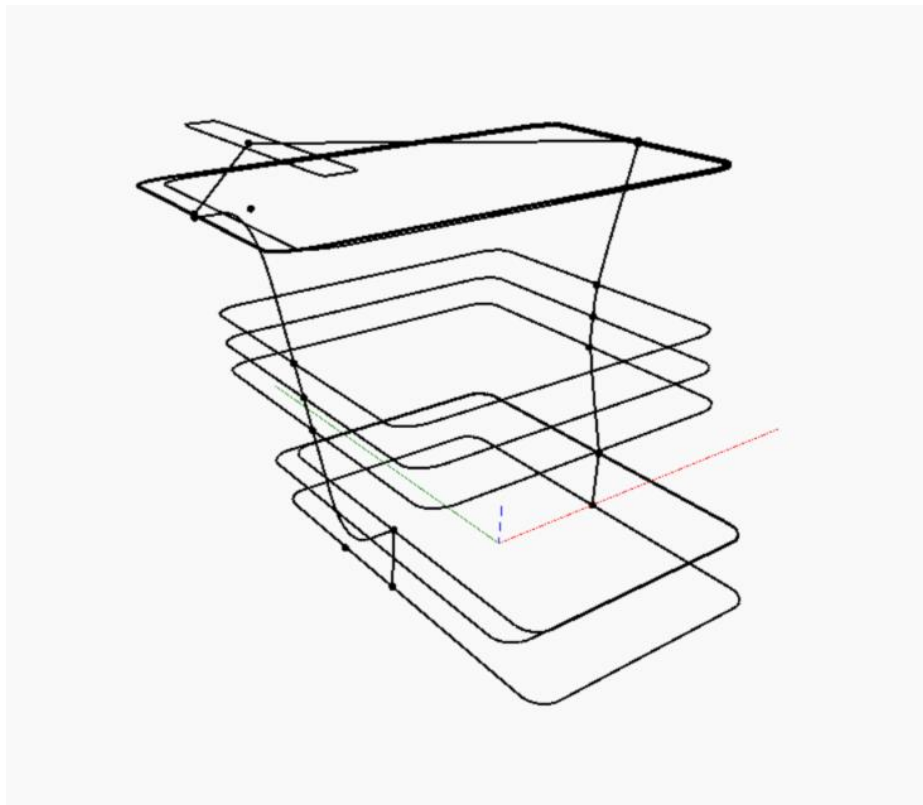


Figure 45: Section curve and loft curves to construct the building solid in a decreased amount. Original model has loft curves in every 0,5 meters of height.

- Void Module:

This module constructs a simplified horizontal void throughout the building solid that inherited from Solid Modeling Module. Basically, a rectangle is produced in the YZ plane and extruded. It includes three parameters as:

- I. V.ElevationRatio

It locates the center of the void's base rectangle relatively to the H.TotalHeight.

$$\text{Void elevation} = \text{H.TotalHeight} \times \text{V.ElevationRatio}$$

Data Type: Double. Range: 0 – 1.

- II. V.WidthRatio (V.WR)

It is a ratio of the Y dimension of the void to the width of building as Void Width equals to V.WR times building width (To evaluate it, an algorithm runs to determine the width of the building solid at a specific Z value of coordinate system which is defined by V.ElevationRatio.)

Data Type: Double. Range: 0 – 0.5.

- III. V.HeightRatio (V.HR)

This parameter is a ratio of void's height to the total height:

$$\text{Void Height} = \text{H.TotalHeight} \times \text{V.HR}$$

Data type: Double. Range: 0 – 0.5

- Final Solid Module:

This module contains the end product of model algorithm, the sample to be exported for wind flow simulations.

For purposes related to the experimental setup used in study, two more node groups were added to model, one is for gathering sample values from an excel file and the other one is for the exporting sample model files with .SAT extensions.

3.2.2 Sensitivity Analysis on Wind Flow Simulations

Six processes (from 4 to 9) are applied as explained in the beginning of this chapter to test the set of form parameters in terms of their effects on wind flow behaviors around the building form. Although they were initially explained under two parts, this section will describe them altogether for the sake of integrity between the experimental design and result analysis.

- Process 4. Random values with uniform distribution for each parameter generated for the production of sample models.
- Process 5. Sample models were generated using the parametric model algorithm according to values gathered from previous step.
- Process 6. Wind flow simulations were applied on sample models.
- Process 7. Based on input and output values of variables and results, Monte Carlo simulation was computed to generate a large dataset.
- Process 8. Both original data and simulated data tested with statistical models. Curve estimation on scatter plots, correlation analysis and standard linear model for regression analysis were applied.
- Process 9. Results are interpreted and discussed together with observations made during actual flow simulations. Additional simulations and analyses were made as a validation of the experimental setup.

The model has 25 parameters with different value ranges as explained in 3.2.1. The usual method for testing the influence of parameters would be to conduct statistical tests per each variable singularly. A specified number of samples should be taken for each parameter while other parameters are kept constant at their baseline or centerline values in order to assess parameter correlations with simulation output one by one.

This approach has some disadvantages for this study. First, the size of the variables would cause a very large number for samples to run simulations on. Say that a

minimum number of fixed values are selected for each parameter, there would be at least 5 values, which could lead to 125 samples in total. Yet, these samples would probably be statistically unreliable, as 5 dots in a scatter plot could give misleading results for curve estimations and correlations. A more reasonable number of values for each parameter could be 10, which would cause 250 samples, and still the dataset would be small for accuracy. Second disadvantage is the negligence of correlations between input variables. Form parameters in model are known and expected to have significant associations and dependencies to each other. Therefore, analyzing their effects singularly might lead misleading conclusions.

After considering possible shortcomings of testing the data per each variable independently, alternative methods are sought. For analysis of results with small number of cases and relatively large number of variables, statistical tests are usually applied on simulated data. Thus, simulated samples, based on definite or recognized character and relations of known samples can be produced to be able to get adequate numbers of cases for reliable predictive analyses such as linear regression. One of the prevalent methods for this approach is Monte Carlo Simulation. The procedure uses a pseudo-population which is generated by a computer algorithm. These computations uses original data as inputs to generate this pseudo-population, by analyzing the distributions of values (uniform, normal, triangular etc.) and correlations between them with probabilistic functions. (Mooney, 1993) (IBM Knowledge Center, retrieved in 2018) IBM SPSS can perform this simulation on given data.

The reason to get 50 samples is related with Monte Carlo procedure and explained in Step III. Random values of parameters for the 50 sample can be seen in Appendix B.

A node existing in Dynamo interface which imports values from an open Excel sheet is added to the model and linked to the values of parameters to get each sample with exact pre-defined values in a faster procedure. Solids constructed in model according to these configurations were exported from the Dynamo as .SAT files. SAT files contain Standard ACIS Texts which can be read by many solid modeling and simulation platforms. Parametric configuration of these samples are given in Appendix B.

Autodesk Flow Design is a “virtual wind tunnel” software. Hence, basic guidelines for wind tunnel setup also apply in its interface. (Autodesk Knowledge Network, accessed in 2018) The software automatically defines an ideal tunnel size depending on the input model dimensions. After that, user can change the dimensions if necessary. Below, an explanation of ideal tunnel sizes are provided with the graphics showing an automobile model as example from the website of Autodesk Knowledge Network explaining the use of program.

The program has two versions, one of them runs as an Add-On in Revit, but it does not exist for Revit platforms developed after 2014. The other version is the Stand-alone mode which has its own interface. There are three significant differences between these two versions. First, the Add-On version supports non-linear wind profiles as adjustable by the user while Stand-Alone version does not. And secondly, Add-On version can place probes on simulations to extract numeric values of wind speed, while Stand-Alone version cannot. On the other hand, Stand-Alone version is capable of analyzing the status of the flow, whether it is a transient flow or it is stabilized during simulation. Bearing in mind that two pros and one con, Autodesk Flow Design inside Revit was tried first to get more specific outputs in more realistic wind conditions. However, after first 5 samples it was realized that, some of the SAT files opened with Revit 2014 has missing information, also simulations run by Flow Design inside Revit interface took much more time than simulations run in Stand-Alone version.

Eventually, because of speed and accuracy concerns, Stand-Alone version is preferred for all 50 simulations. Thus, the opportunity of knowing the status of flow at any time, served the purpose also, while most of the outputs were able to be extracted during stabilized flow conditions. A time constraint applied for the simulations which did not turn into stabilized flow conditions. Their values are read if the flow is still transient after two hours. Models which are not labeled with a stabilized flow status are usually also showed stable values after one hour of simulation time. The wind speed in tunnel is set linear (as logarithmic wind profile option is not existed in program) at 10 m/s. Color options are kept at standard, but banding and contour lines are activated in order

to read speed and pressure values by comparing color legends. These options gave speed values as average between two contour lines.

All simulations are conducted in 3D option instead of 2D. Results are analyzed with 6 output images per sample.

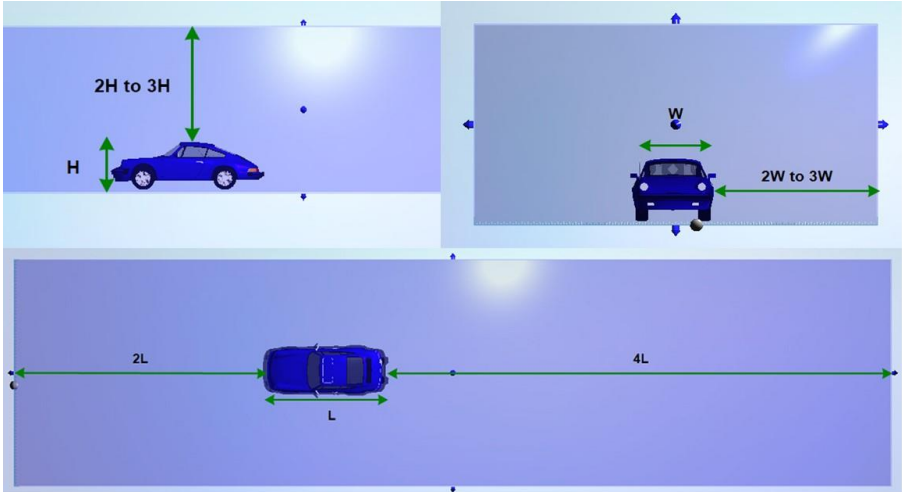


Figure 46: Explanation of the ideal tunnel sizes in Autodesk Flow Design. (Autodesk Knowledge Network, accessed in 2018)

Status:	Stabilized
Analysis:	3D
Wind Speed:	10.000 (m/s)
Length:	912.741 (m)
Width:	284.849 (m)
Height:	73.509 (m)
Voxel size:	3.063 (m)

Figure 47: Model status bar appears in the top-right corner of the simulation window, showing the flow condition.

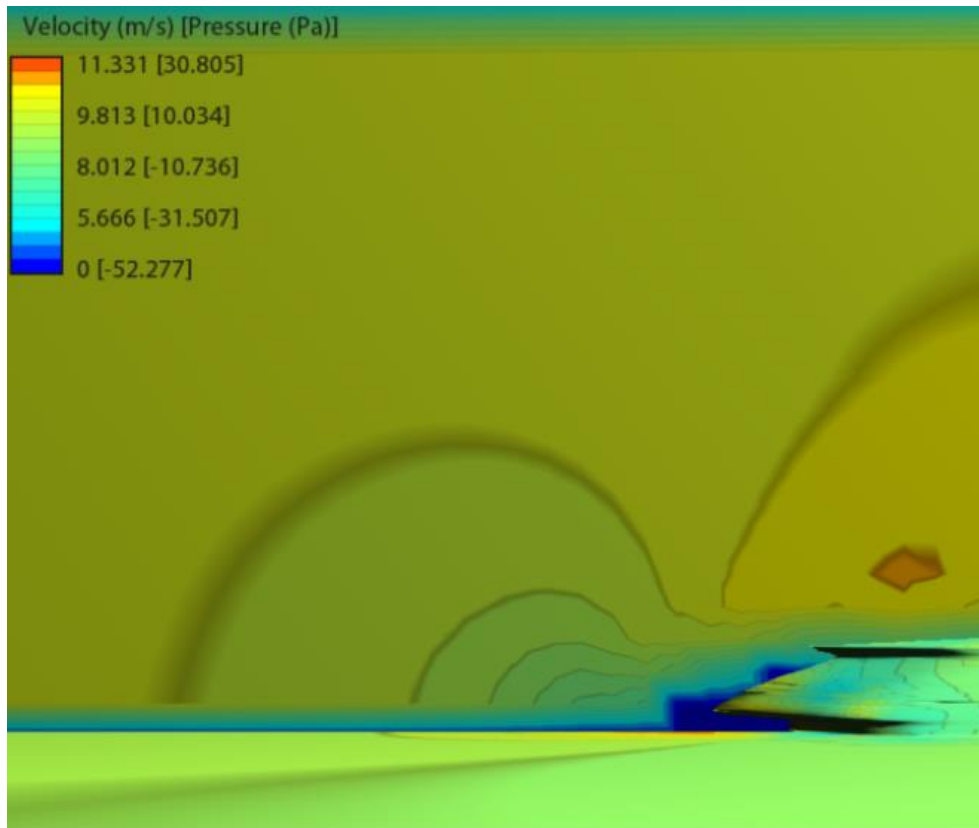


Figure 48: An example from simulation results showing the legend, color banding and contours.

Autodesk Flow Design provides two options of showing flow, planes and flow lines. 4 planes are placed in each simulation as:

- Windward section plane
- Normal section plane
- Pedestrian level plane (It is a plane crossing on the ground level of tower part instead of base part)
- Roof level plane (This plane is set in a high level according to top geometry of building solid and horizontal void)

These four planes explained by section lines are drawn on building elevation and plan views in Figures 49 and 50.

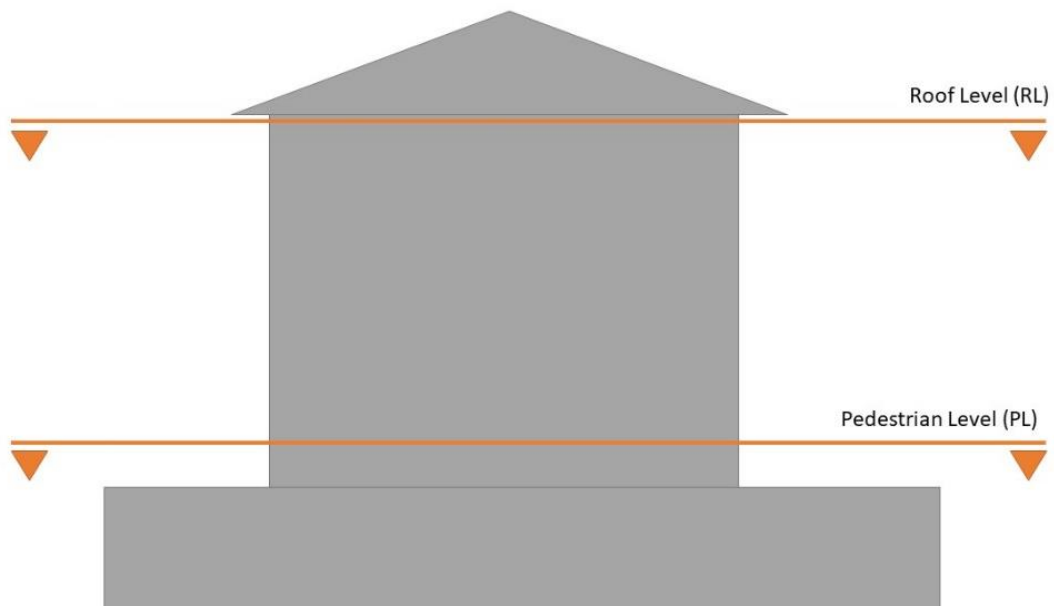


Figure 49: Horizontal planes used in simulations.

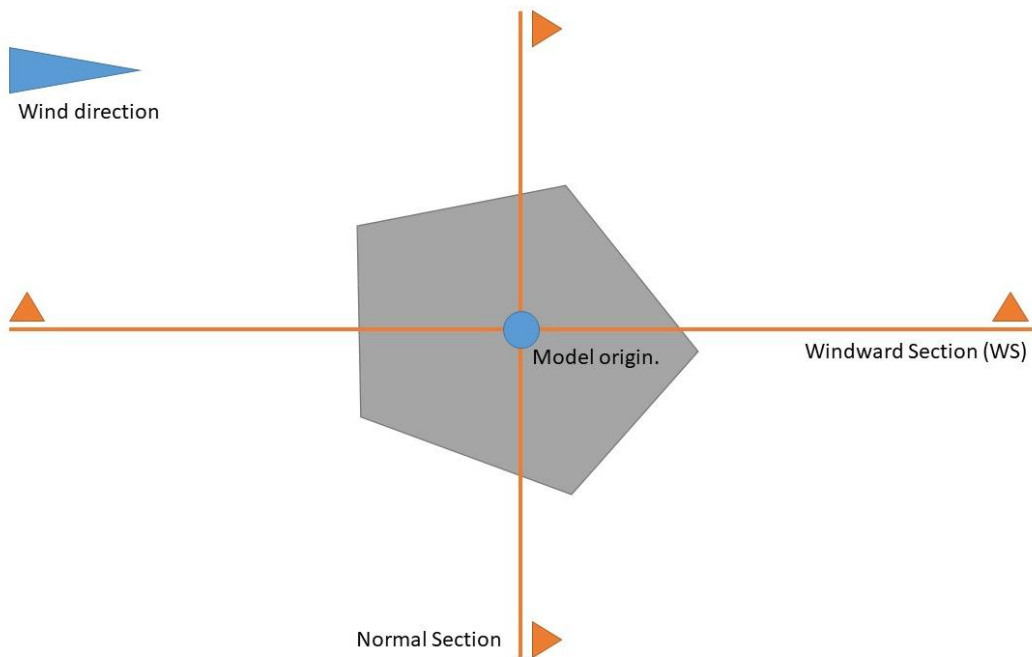


Figure 50: Vertical planes used in simulations.

Ten output parameters are defined to measure quantitative values from simulations:

- Average Drag Coefficient: A measure obtained from software as an index for resistance of an object in a fluid flow.
- WS Speed Up Regions: Number of regions showing relatively high wind speed concentration in windward section plane.
- WS Max Speed: Value of the highest wind speed measured on the windward section as explained previously.
- WS Max Location: Location of the maximum wind speed is categorized in a range between -3 and 3 as explained in Figure 52.
- NS Speed Up Regions: Number of regions showing relatively high wind speed concentration in normal section plane.
- NS Max Speed: Highest wind speed measured in normal section.
- RL Speed Up Regions: Number of regions showing relatively high wind speed concentration in roof level plane.
- RL Max Speed: Highest wind speed measured in roof level plane.
- PL Speed Up Regions: Number of regions showing relatively high wind speed concentration in pedestrian level plane.
- PL Max Speed: Highest wind speed measured in pedestrian level plane.

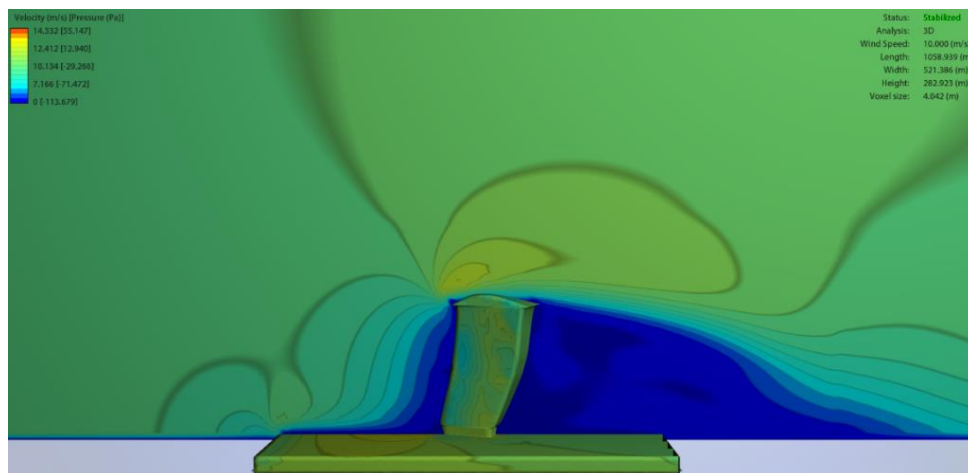


Figure 51: View of windward section plane from side view in sample 43, showing two speed up regions.

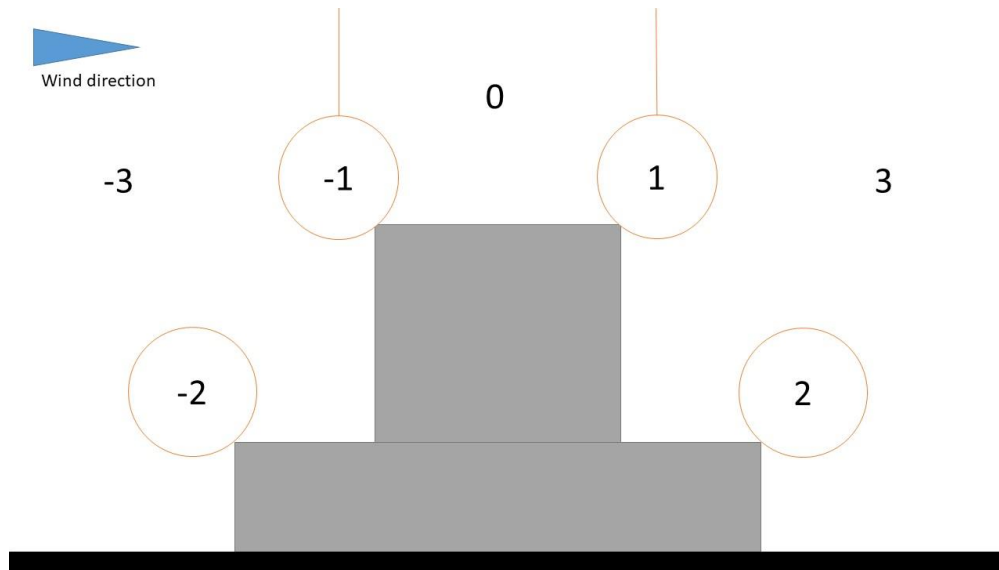


Figure 52: Location categories shown in windward section for WS_Max_Location.

If actual samples for inputs is produced by random values under uniform distribution, number of input samples needed is at least 1,5 times of variables to perform a reliable Monte Carlo Simulation. (EUJRC, 2008) Considering that limit, 50 samples as twice the parameter number were prepared by random values with uniform distribution. The random values for samples were also generated in SPSS. 10000 cases including 50 originals were generated by simulation. Over the data from these cases, analytical tests are applied to perform a sensitivity analysis. Results are compared with original samples and discussed in Chapter 4.

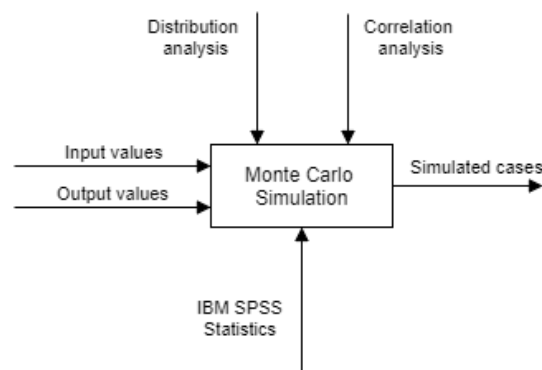


Figure 53: An IDEF0 scheme representing the flow of Monte Carlo process in this study.

Option I:

Comparison of importance factors for parameter sensitivity analysis is one of the methods used in assessment models. (Downing, Gardner, & Hoffman, 1985) There are many alternatives for quantifying relative importance. A regression analysis over simulation data with multiple predictors was preferred for this study. Regression analysis is one of the fundamental techniques which is applicable on sensitivity determination over simulation experiments. (Kleijnen & Kleijnen, 1992) Whole simulated dataset was used for multiple regression analysis based on output parameters. Input parameters are predictors and output parameters are targets. This option gives a direct influence scaling among input parameters by comparing the predictor importance. It is a scale between 0 and 100 which can be interpreted as percentages easily.

Three statistical methods including multiple regression analysis were applied over the simulated data.

Firstly, curve estimation was applied on all scatter plots as cross products of input variables and output variables (250 coupling by 25 inputs x 10 outputs) IBM SPSS provides a faster tool for this analysis, in which curve estimation tables are grouped under a pivot table for multiple dependents and one independent. This step delivered insight for the regression analysis by inspecting for any non-linear correlations between variables which could lead misleading interpretations in linear regression analysis. Then, linear regression analyses are run in SPSS interface by a function named “Automatic Linear Modelling” for each of 10 outputs as targets while all 25 input parameters were predictors. This function provide:

- Information criterion which is a measure of statistical model’s accuracy.
- Data preparation by trimming outliers.
- Predictor importance values.
- Studentized residuals histogram and P-P plot, which are measures of the data compliance for linear regression analysis.
- Positive and negative coefficients of predictors on target.

- Sum of Squares, Mean Square, F and Sig values which are used in analyzing the effect of an input parameter on outputs.

Correlation analysis are also computed by SPSS for both the simulated data and original data by Pearson's coefficients with two-tailed test of significance. Outcome of these charts are considered as a comparison / control group for predictor importance values from regression analysis.

Option II:

Another option is the use of sensitivity indices. (Hamby, 1994) A sensitivity index is the simplest measure of sensitivity comparison of parameters. These indices are found in two steps as:

Fixed values are determined in the range of each input parameter. Then, the data is simulated by user defined equations or one of the predictive methods applicable. Results of the simulations are compared and sensitivity indices are calculated with this equation below:

$$(\text{Output}_{\text{Max}} - \text{Output}_{\text{Min}}) / \text{Output}_{\text{Max}}$$

Here, $\text{Output}_{\text{Max}}$ and $\text{Output}_{\text{Min}}$ are maximum values of an output parameter from consecutive iterations based on values of the input parameter on which the sensitivity analysis was implemented.

This option was not preferred. Since, local sensitivity indices by iterated simulations provide indications for changes of output behaviors between discrete values of a single input parameter. Therefore, some local associations might appear, but these results should not be interpreted as the behavior of the overall pattern.

Results of these analysis are given and discussed in Chapter 4. Process 9, which covers the interpretation and discussion of results are also included in Chapter 4.

Expectation from the implementation of the selected method in terms of sensitivity analysis is:

- Regression models should give an overall smooth pattern of associations between multiple input parameters and an output parameter.

More complex sensitivity analysis methods which require either very long equation solving phases or use of emulators were not implemented.

Finally, as a validation step, four input parameters were selected to be analyzed by one-at-a-time process. Two of these parameters are the ones with the highest relative importance values according to initial regression analyses; whereas the other two are having least predictor importance values. Four flow simulations were made for each of these parameters as their values altered while rest of the input parameters were kept constant at either baseline or central values. Results of these 16 simulation were also analyzed by correlation matrices and observations during simulations.

CHAPTER 4

RESULTS AND DISCUSSION

Results from different stages of the study are presented and discussed under this chapter. 3D model examples of essential form types which were classified under central form algorithm previously, are presented in the first part, 4.1. Second part, 4.2., covers wind flow simulation results. Figures showing simulation results are given in Appendix C. Data analysis conducted on simulation results are presented in 4.3, with detailed information in Appendix D. Last part, 4.4., is about an overall discussion on results. Simulation results, statistical tests and observations logged were analyzed collectively to understand the efficiency of tested approach for parameterization and selected parameters' influence on wind conditions.

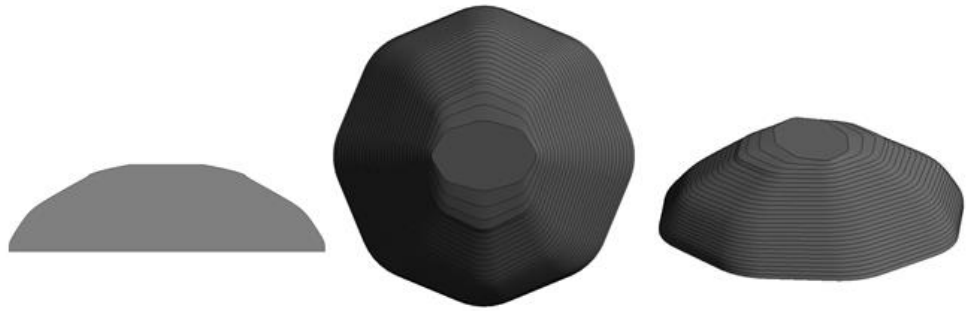
4.1 Samples Produced by the Model for Primary Form Types

Primary form types that were classified under central form category after aggregation (See 3.2.1) were produced by model to validate Consideration I, which is simply the ability of parametric model to produce essential types mentioned in literature within its scope. An example model from each type is presented with the parameter configuration produced it.

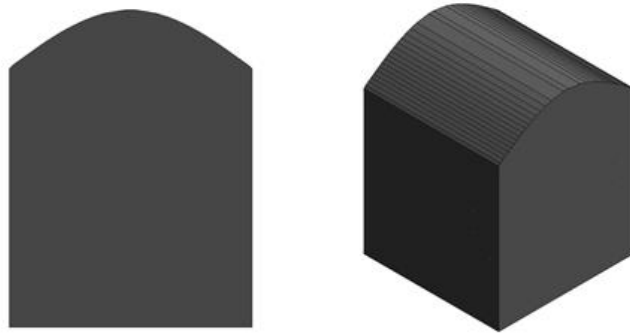
A combined table showing parameter values selected while producing each type is given in the next page. Images from each type's 3D model are presented in following pages. Lastly, some critical notes are discussed to analyze model's capability and limitations. Nine models representing essential types are produced. Type categories related with different polygons are not produced for each polygon (e.g. pentagon, hexagon, heptagon) since variations based of them already observable from other samples made for flow simulations.

Table 27: Examples of essential form types with their parametric configuration in model algorithm.

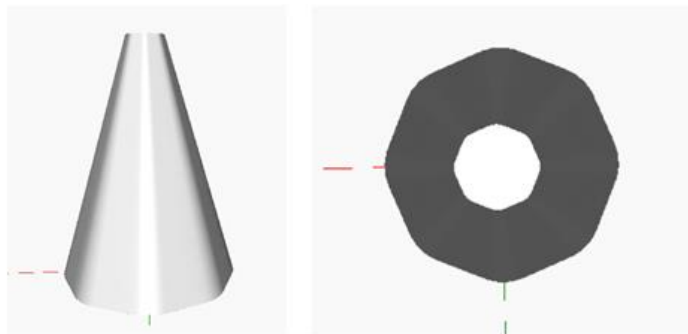
Model Parameters	spherical	vaulted	conic	pyramidal	cubic	square based	cylindrical	circular based	triangle based
TF X	50	50	50	50	60	60	30	30	40
TF Y	50	50	50	50	60	60	30	30	25
TF Vertice	8	4	8	4	4	4	8	8	3
TF Roundness	0,2	0	0,2	0	0	0	0,2	0,2	0
TF Irregularity	0	0	0	0	0	0	0	0	0
H Total Height	15	50	65	65	42	70	60	60	35
B Height Ratio	0	0	0	0	0	0,2	0	0,15	0
B X Ratio	1,5	1,5	1,5	1,5	1,5	1,5	1,5	3	1,5
B Y Ratio	1,5	1,5	1,5	1,5	1,5	1,5	1,5	1,5	1,5
SC Degree Of Curve	4	3	1	1	1	2	1	3	2
SC Setback Height Ratio	0,1	0,1	0	0	0	0,15	0	0	0
SC Vertex Height Ratio	0,2	0,25	0	0,2	0	0,4	0	0,25	0,1
SC Vertex Position Ratio	0,5	0,5	0,5	0,5	0	0,5	0,5	0,5	0,1
SC Setback Depth Ratio Front	0	0	0	0	0	0,15	0	0	0
SC Facade Endpoint Translation Ratio Front	-0,5	0	-0,8	-0,8	0	0	0	0	0
SC Concavity Ratio Front	-0,1	0	0	0	0	0	0	0,15	-0,25
SC Eave Depth Ratio Front	0	0	0	0	0	0,25	0	0	0,3
SC Setback Depth Ratio Back	0	0	0	0	0	0,15	0	0	0
SC Facade Endpoint Translation Ratio Back	-0,5	0	-0,8	-0,8	0	0,5	0	0	0
SC Eave Depth Ratio Back	0	0	0	0	0	0	0	0	0,3
SC Concavity Translation Ratio Back	0,1	0	0	0	0	0	0	0,15	0
S Normal Tapering	0,3	1	0,2	0,1	1	1	1	1	1
V Elevation Ratio	0	0	0	0	0	0,3	0	0	0,5
V Width Ratio	0	0	0	0	0	0,2	0	0	0,3
V Height Ratio	0	0	0	0	0	0,25	0	0	0,3



Spherical

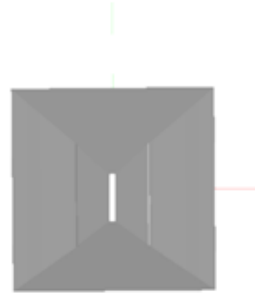
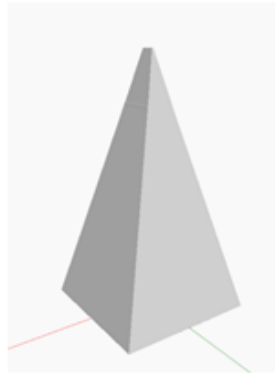


Vaulted

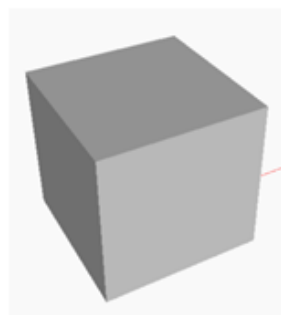


Conic

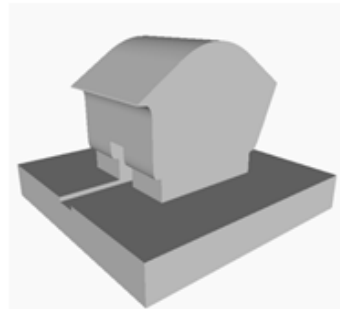
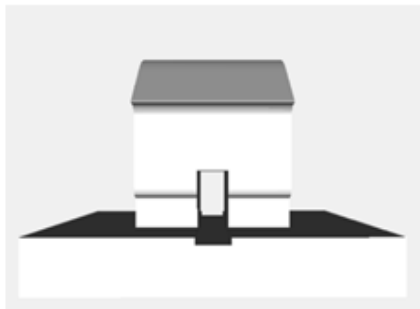
Figure 54: Spherical, vaulted and conic examples



Pyramidal

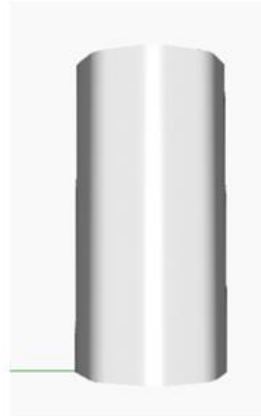
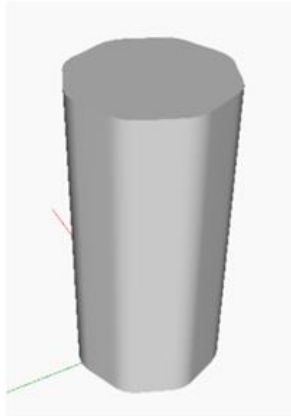


Cubic

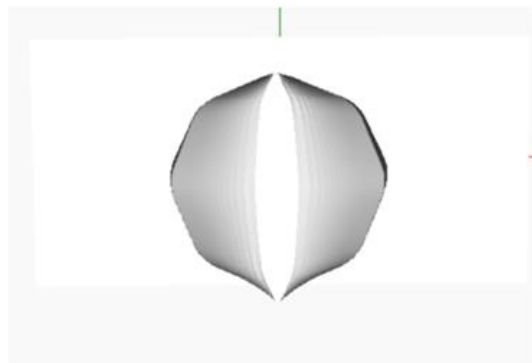
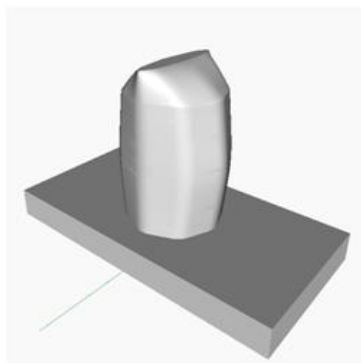


Square Based

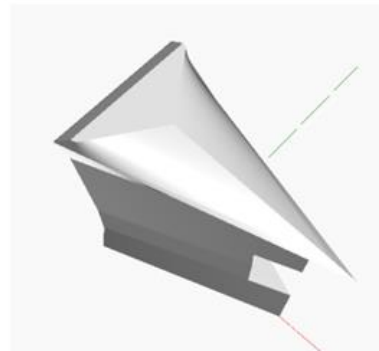
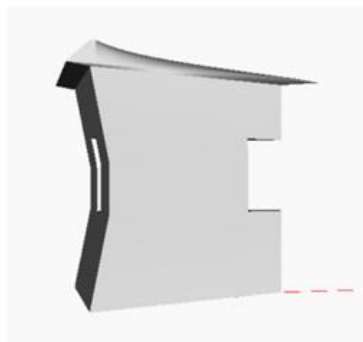
Figure 55: Pyramidal, cubic and square based examples.



Cylindrical



Circular based



Triangular based

Figure 56: Cylindrical, circular based and triangular based examples.

Some critical notes to mention are:

- For this study, TF.Vertice parameter (which decides the vertice number of tower unit's footprint polygon) is kept in a range between 3 and 8. To approximate circle based forms like cylinder or sphere, 8 is selected as maximum number, together with the maximum value of TF.Roundness (which decides the fillet ratio of footprint polygon corners). To get more realistic circular-like shapes, maximum constraint of vertice numbers can be set to a larger value like 12 or 24, based on case decisions in further studies.
- During the algorithm development process, normal section parameters were excluded from the model for simplicity and replaced with a single parameter S.NormalTapering (which decides the tapering ratio of building solid in Normal Section). This resulted with a lack of capability in producing perfect spherical or conical shapes, since the control points of the normal section curve are missing in final model.

Overall, the model has the ability to generate any kind of generic form which can derivate from central form stem in low level of detail without building components. There are limitations as expected in 3.2.2.

4.2 Results of Wind Flow Simulations

This part covers results of wind flow simulations. Numeric data is given in 4.2.1, whereas simulation visuals of each sample is presented in Appendix C. Other than quantitative results, taken notes are interpreted as logs per each sample and they are listed in 4.2.2.

4.2.1 Measured Values

Three tables are presented here, showing values for output parameters as defined in section 3.2.2, for each sample went through simulation. First two tables cover output values of first 50 simulation. Third table shows necessary information of both input and output values for samples 51-66, which are proceeded by one-at-a-time analyses on 4 parameters as explained in next section.

Table 28: Simulation outputs of samples 1 – 25.

	Average Drag Coefficient	Windward Section			Normal section		Roof level		Pedestrian level	
		WS_Speed_Up_Regions	WS_Max_Speed	WS_Max_Location	NS_Speed_Up_Regions	NS_Max_Speed	RL_Speed_Up_Regions	RL_Max_Speed	PL_Speed_Up_Regions	PL_Max_Speed
sample1	1,08	1	12,73	3	2	12,03	2	12,53	4	11,99
sample 2	0,44	1	11,79	-1	1	11,20	2	12,39	1	13,48
sample 3	0,49	2	11,91	-1	1	11,47	3	11,80	5	11,47
sample4	-0,03	2	10,95	-1	1	10,75	2	10,61	2	10,55
sample5	0,39	2	12,52	0	1	12,96	2	12,99	3	11,60
sample6	0,59	3	12,08	-2	2	11,64	3	12,66	4	12,41
sample7	0,42	3	10,72	0	1	11,78	2	11,24	5	11,32
sample8	0,08	1	12,32	-2	1	10,22	2	12,81	2	15,07
sample9	0,21	1	11,78	-1	1	11,59	2	11,70	6	11,06
sample10	0,42	2	11,10	-2	2	11,58	2	11,65	3	11,17
sample11	0,63	4	13,16	-1	2	11,24	4	13,18	3	11,34
sample12	0,11	3	11,21	-1	1	10,41	4	11,21	5	11,61
sample13	0,68	3	11,84	-1	4	11,30	3	11,47	6	11,44
sample14	0,48	1	11,45	3	1	11,41	5	13,26	4	11,29
sample 15	0,35	4	12,30	-2	0	9,85	0	9,55	2	10,87
sample16	0,61	2	12,42	0	3	12,41	3	12,40	3	12,40
sample17	0,26	2	12,50	-1	2	11,26	2	12,09	5	12,09
sample18	0,39	2	11,59	0	2	11,15	2	11,60	6	11,59
sample19	0,60	3	11,81	0	2	13,14	3	12,22	3	11,78
sample20	0,49	2	12,19	-1	3	11,64	3	12,18	6	12,19
sample21	0,99	2	12,34	3	1	12,21	3	12,46	3	11,59
sample22	0,63	1	12,58	-1	1	12,63	2	12,60	2	12,60
sample23	0,19	1	11,75	3	2	11,27	4	11,26	4	12,09
sample24	0,51	2	11,97	-1	1	11,49	2	11,50	2	11,09
sample25	1,24	2	12,66	3	3	12,11	3	12,55	3	12,53

Table 29: Simulation outputs of samples 25 – 50.

	Average Drag Coefficient	Windward Section			Normal section		Roof level		Pedestrian level	
		WSSpeedUpRegions	WSMaxSpeed	WSMaxLocation	NSSpeedUpRegions	NSMaxSpeed	RLSpeedUpRegions	RLMaxSpeed	PLSpeedUpRegions	PLMaxSpeed
sample26	0,73	2	11,26	3,00	2	11,78	2	11,78	4	12,22
sample27	0,59	2	12,57	0,00	2	11,93	2	12,49	7	11,91
sample28	0,55	3	11,89	3,00	3	11,75	2	11,83	2	11,73
sample29	0,59	2	12,86	-1,00	2	11,92	2	12,82	5	11,92
sample30	0,49	2	12,19	1,00	1	11,07	2	11,60	3	11,07
sample31	0,26	2	11,13	0,00	2	11,12	2	11,19	3	11,13
sample32	0,52	2	11,68	-1,00	2	11,68	2	11,67	2	11,67
sample33	0,65	3	11,43	3,00	3	12,73	2	11,84	5	11,33
sample34	0,68	2	11,20	0,00	2	11,22	2	11,20	3	12,16
sample35	0,34	4	12,36	0,00	2	11,90	2	11,90	4	11,90
sample36	0,47	2	11,57	0,00	1	11,56	2	11,98	5	11,56
sample37	1,16	2	12,26	3,00	3	11,70	2	12,43	2	12,58
sample38	0,83	2	11,63	3,00	2	11,61	2	12,12	5	11,64
sample39	0,04	2	10,19	1,00	1	10,20	4	10,19	6	10,19
sample40	0,95	3	12,18	3,00	3	12,16	3	12,17	2	12,15
sample41	0,61	3	11,79	-1,00	1	10,61	3	11,83	4	11,84
sample42	1,10	2	12,73	3,00	2	12,72	2	12,94	7	12,05
sample43	0,55	2	12,41	-1,00	1	12,43	4	11,21	3	11,21
sample44	0,60	2	11,78	3,00	4	11,76	3	12,09	4	10,46
sample45	0,46	1	12,68	-1,00	1	12,01	5	12,97	2	11,38
sample46	0,71	3	13,00	0,00	2	12,36	4	11,71	1	10,85
sample47	0,14	1	11,63	1,00	2	11,38	2	11,59	3	12,50
sample48	1,13	2	12,67	0,00	4	12,79	2	12,80	5	12,80
sample49	0,53	2	11,81	0,00	1	11,81	4	10,26	3	11,37
sample50	1,08	3	11,84	-2,00	1	12,42	5	12,39	5	12,48

Table 30: Values of parameters for samples 51-66

	Input parameters				Output parameters									
	TF.X	B.YR	SC.CTRB	V.HR	Average Drag Coefficient	WS SpeedUp Regions	WS Max Speed	WS Max Location	NS SpeedUp Regions	NS Max Speed	RL SpeedUp Regions	RL Max Speed	PL SpeedUp Regions	PL Max Speed
sample51	5	0	0	0	1,07	1	13,03	3	3	11,69	2	13,50	2	13,17
sample52	37	0	0	0	1,05	1	12,55	0	3	12,75	2	12,61	2	12,92
sample53	69	0	0	0	1,02	1	12,66	-1	2	12,13	2	12,23	4	13,00
sample54	100	0	0	0	0,99	1	11,98	-1	2	11,99	2	11,97	2	11,94
sample55	50	1,5	0	0	1,05	1	12,85	-1	1	12,19	4	12,65	4	12,15
sample56	50	2,7	0	0	0,81	2	12,26	-1	1	11,86	2	11,87	4	11,31
sample57	50	3,8	0	0	0,75	2	11,91	-1	1	11,86	2	11,39	4	10,86
sample58	50	1,5	0	0	0,89	1	11,77	-1	1	11,33	2	11,32	6	10,92
sample59	50	0	0,25	0	1,27	1	12,57	0	3	12,50	2	12,95	2	13,18
sample60	50	0	-0,1	0	1,31	1	12,82	0	3	12,64	2	12,60	2	13,15
sample61	50	0	0,1	0	1,24	1	12,58	3	2	12,67	2	12,78	2	13,65
sample62	50	0	0,25	0	1,25	1	12,33	3	3	12,40	2	12,63	4	12,93
sample63	50	0	0	0	1,19	1	12,18	3	3	12,25	2	13,17	2	13,31
sample64	50	0	0	0,15	1,18	2	13,26	3	2	12,15	3	13,18	3	15,01
sample65	50	0	0	0,35	1,19	2	12,69	0	2	12,41	2	12,35	2	12,71
sample66	50	0	0	0,5	1,19	2	12,42	0	2	12,07	2	12,21	2	13,08

Input and output parameters are shown together for 16 samples in Table 30. These are the samples in which a single input parameter has been altered while rest of the parameters kept constant at either their baseline or central values. Altered parameters per samples are: TF.X (Tower Footprint X) in Samples 51 – 54, B.YR (Base Y Ratio) in Samples 55 – 58, SC.CTRB (Section Curve Concavity Translation Ratio Back) in Samples 59 – 62, V.HR (Void Height Ratio) in Samples 63 – 66.

4.2.2 Observations Made During Simulations

The process of simulation setup and sample configuration was explained in previous chapter. Time passed during simulations were atypical for samples, it varied among 10 minutes to 2 hours with constraints as described before. Under this section, notes taken during the actual simulations and also while reading measurements over them are listed by sample number. Notes with high similarity due to the same conditions were briefly noted but not explained in detail for each sample. Repetition of the same information was avoided.

Sample 1:

- Highest speed of the wind flow in windward section is occurring relatively distant to building in leeward side (+Y), probably due to the slimness of building solid in that direction (TF.X / TF.Y) and the shape of the roof.
- In normal section a very significant pressure concentration is observable, while the concavity of the section curve is not too recognizable, the convexity in plan caused by TF.Irregularity parameter might have an impact in that concentration.

Sample 2:

- Horizontal and continuous back eave form lets the wind flow undisturbed in a linear streamline for a longer distance.
- Convex shape of building (SC.ConcavityTranslationRatioFront) lead to a concentrated high pressure zone on windward facade, perhaps together with the effect of a relatively small void opening.

Sample 3:

- Irregular shape of the footprint causes asymmetric and different wake zones and flow patterns on roof level and pedestrian level.
- Base edges are observed to behave similar to roof edges in terms of accelerating the wind flow.

Sample 4:

- Larger setback depth (SC.SetbackDepthRatioFront) on wind facing facade causes a high pressure zone on base surface.
- Front eave effects the location of highest wind speed in windward section, by causing a high wind spot just over itself.

Sample 5:

- Irregular footprint shape (TF.Irregularity) is clearly related with wind flow behaviors and wake zone regions in terms of symmetry.

Sample 6:

- Despite the very large void centered on building, more wind speed is observed over the roof. Probably this condition is somehow related to the resolution of simulation. This might point a limitation in study in terms of observing wind flow through voids.

Sample 7:

- No records logged.

Sample 8:

- A wide but low base solid causes significant increase on wind speed on its top edges as observable in pedestrian level plane. Probably, the B.XRatio parameter is also in effect for that condition. Since, the size of the base in windward direction is extremely larger than the tower size compared to other samples.

Sample 9:

- Observation made on wind section view supports the correlation between facade angle and max. speed region formation around facade endpoint in the absence of a significant eave depth.

Sample 10:

- 3 different stagnant zones are occurred behind the building. By comparison to a contrasting condition in Sample 3; probable causes are SC.Concavity, increased B.XRatio and smaller H.TotalHeight (or smaller height / length ratio of tower solid)
- The building form has narrower ends in plan layout in windward direction. Therefore, significant increase in wind speed occurred on sides in normal direction. Also, the wake zone is relatively narrow and shorter behind the building.

Sample 11:

- A base with a relatively big in height (B.HRatio) and width (B.YRatio) but smaller length (B.XRatio) is observed to cause two significantly different speed-up patterns on pedestrian level and roof level.
- Entrance of the flow into void is supported and accelerated by the channeling provided by front eave depth (SC.EaveDepthFront). Therefore a max. speed region is located in the void.

Sample 12:

- Front facade translation and eave depth together in effect to concentrate the flow speed over eave.

Sample 13:

- Narrow building form in windward dimension prevents wind flow to channel thorough the void. (See Normal Section view)

Sample 14:

- A very significant downwashing effect is observed in pressure distribution on base surface (See Normal Section) despite the absence of any observable wind flow movement on windward section.
- Void size seems too large to be able to channel the wind through.

Sample 15:

- Four almost identical speed up region patterns are observed in windward section plane, probably due to the low height (H.TotalHeight).
- Expressively larger eave depth on front facade (SC.EaveDepthTranslation Ratio) results with an almost bigger stagnant zone than leeward side.

Sample 16:

- No records logged.

Sample 17:

- Building form is narrowing towards to the top in normal section due to a smaller value in S.NormalTapering parameter. Therefore, the flow is divided to the sides on roof rather than centering on. (See Normal Section view)

Sample 18:

- Observations support the suggestions regarding on irregularity and small dimension in Y on other samples.

Sample 19:

- Very narrow end of the building on wind facing direction, creates a linear stagnant region on windward section while directing the flow to the sides as other similar examples.

Sample 20:

- A large and regular zone of identical flow speed is observed over the building until some distance to the leeward direction, probably thanks to flat ending of the building (as a flat roof)
- By comparing to similar and different samples, it is suggested that smaller values of TF.Roundness parameter creates concentrated speed up regions close to vertices. (See Roof Level plane view and Pedestrian Level plane view)

Sample 21:

- There are two significant vortexes observed on back facade resulting with a flow in reverse wind direction towards building. This condition is a result of very big building width / building length ratio. (TF.X / TF.Y)

Sample 22:

- It is possible with doubt that the concave shape of the leeward facade (SC.FacadeConcavityTranslationRatioBack) prevents the formation of speed up zones around vertical edges by deforming to edge from a linear shape to a curvilinear form. (See Pedestrian Level view with Windward Section view)

Sample 23:

- More speed up regions occurred over base edges than tower envelope due to the very large B.YRatio value and small sizes of tower. (See Roof Level view)

Sample 24:

- No record logged.

Sample 25:

- Higher position of the roof vertex (SC.VertexHeightRatio) generates a high speed zone behind the building in windward direction.

- Contrary to many other samples void size and positioning is able to produce a very significant flow through. Probably, other parameters of building form are supporting that condition like the small ratio of TF.X / TF.Y.

Sample 26:

- Opposing to previous sample (25), no significant flow is observed through the void. Smaller void width (V.WidthRatio) is probably responsible from that condition.

Sample 27:

- Flow is centered over the building apparently because of a vaulted shape of roof (effected by SC.DegreeOfCurve)

Sample 28:

No records logged.

Sample 29:

- It is noticed that the speed of the flow is increased around building corners in plan layout by analyzing the view on horizontal plane views (PL and RL). This condition is tend to occur in samples with more vertices in footprint polygon (TF.Vertice)
- Slanted front facade (SC.FacadeTranslationRatioFront) together with an eave (SC.EaveDepthRatio) causing a pressure concentration on windward facade, and also a max. speed zone just over the facade edge, like many other samples.

Sample 30:

- It is noticed that when the absence of significant eave depths, a pointed roof vertex controls the max. speed location over building single-handedly.
- Facade endpoint translation (SC.FacadeEndpointTranslationRatioFront) towards the leeward direction (+X) is also speeding the wind up to over building.

- A very small width of building form (small TF.Y) together with the linearity and rectangular shape of wind facing facade; a very significant linear pressure zone occurs at facade, where wind power could be transformed to energy with vertical configurations from ground to top.

Sample 31:

- A high vertex position near to windward facade (SC.Vertex.Height, SC.VertexPosition) lets the flow continue downwards at back facade together with the effect of the overall angle occur in building form at that side (SC.FacadeEndpointTranslationRatioBack) If the eave depth was smaller, there could have been an even more significant flow pattern towards ground line . (SC.EaveDepthRatioBack)

Sample 32:

- Width of the base in normal axis (Y) is so huge relatively to the tower dimensions that the base hosts most of the max. speed zones occur around building on its edges which are not shadowed by tower solid.
- Without the guidance of enough surface area on facade, the void cannot host much wind flow (see Normal Section view)

Sample 33:

- Due to the small value of V.ElevationRatio parameter, a void as a passage on ground level is generated by model. This is reflected in simulation by a thin layer of high speed region on pedestrian level (observable in Wind Section view)

Sample 34:

- A very similar condition with Sample 33 is observed related the void.

Sample 35:

- By comparing this sample with similar and different examples from previous ones, it is suggested that when a void is generated in the middle of tower solid with

approximately half of the height and width (V.ElevationRatio, V.HeightRatio, V.WidthRatio), a more significant flow passage is occurring.

Sample 36:

- At roof level, irregular shape of the solid deflects wind flow asymmetrically to the sides. The side which faces the wind slightly less, hosts more significant wind flow increase around building corner. (See Roof Level plane view)

Sample 37:

- Comparing to the Sample 26, it is observed that an increase in void width (V.WidthRatio), increased wind flow inside with other dimensions determined by Void Module parameters were relatively similar (V.Height Ratio, V.ElevationRatio)
- This time, the effect of a slim building body on max. speed location clearly observed also in horizontal planes (See Pedestrian Level plane view). Similarly to the conditions in windward section, max. speed regions occurred distantly behind the building.

Sample 38:

- Large frontal facade surface areas both in base and tower leads to larger pressure zones, where wind effects should be considered in design or resource estimation.

Sample 39:

- Despite the TF.X is not small as other examples with similar conditions, the location of maximum speed zone in windward section is observed behind the building again. The suggested reason is the effect of low height of building (H.TotalHeight) together with back-slanted front facade (SC.Facade TranslationRatioFront)

Sample 40:

- Three distinctively separated max. wind speed zones are observed in windward section while none of them is effected by base solid. This is rather a rare condition between samples.

Sample 41:

- The condition of channeled wind flow on the leeward facade towards ground level in Sample 2, is observable in this sample more clearly. The probable reason is the narrower angle that back facade makes with the base (SC.FacadeTranslation RatioBack) , and smaller eave depth (SC.EaveDepth RatioBack).
- There are two almost identical locations of Max. speed which are observed in wind section. One of them is caused by the vertex position while the other one is a result of relatively larger dimension of the base in windward axis (B.XRatio)

Sample 42:

- Despite not having a convex facade facing wind, there is a significant pointwise concentrated wind pressure.
- There are two identical regions of increased wind speed on base, both sides of tower in normal axis (Y). They look promising in terms of wind power harnessing.

Sample 43:

No records logged.

Sample 44:

Observations support suggestions in Sample 1 and Sample 25 regarding on the form parameters' effects on slimness of building and location of max. wind speed regions accordingly.

Sample 45:

- A void open on top, together with an increased Y dimension of tower roof (due to S.NormalTapering) creates a canyon effect over building. The flow crossing over

the building seems to be slightly pushed down by that effect. (See Normal Section view)

Sample 46:

- Front facade translation towards the wind direction (SC.FacadeEndpoint TranslationRatioFront) produces a significant high pressure zone on base with a downwashing effect.
- It is observed that the flow speed is higher around the entrance of void, rather than its end as a rare condition between samples.

Sample 47:

- Exactly same effect is observed in front facade with previous sample (46) despite different dimensions. This time the cause is setback depth (SC.SetbackDepth RatioFront), which is relatively very large compared to other building dimensions.

Sample 48:

- No records logged.

Sample 49:

- The condition of the void acting as a canyon is similar to the Sample 45; whereas observed more clearly thanks to larger value of V.HeightRatio.

Sample50:

- The dimension of the base in windward axis (X) is extremely larger than the sizes of tower. That condition results with the highest wind speed in windward section is occurring over base edge rather than tower edges.

Further discussion on these observations are made on section 4.4 where deductions from this phase is compared by data analysis results and also results of additional 16 simulations.

4.3 Results of Statistical Tests

There are two motives for the analyses presented in this part. First and the primary reason is to test if the second consideration for the parametric model algorithm is satisfied or not. In short; measuring the significance of parameters selected for model by analyzing results of wind flow simulations conducted with 50 samples.

Secondary reason is to acquire an influence assessment of parameters on some wind flow characteristics around isolated buildings within the context of this study by analyzing associations between values of input and output variables.

Methodology for the sampling, simulations and statistical tests are explained under section 3.2.2 but also briefly described here.

4.3.1 Curve Estimations

Curve estimations were applied to determine possible non-linear associations between input parameters and output parameters, as explained in 3.2.2. At first, 250 tables on the simulated data are computed and reviewed by comparing R^2 values of non-linear equation types with the linear one. No significant non-linear association is found. Then, original data is also tested in the same way. Only five of the charts are considered as referring possible non-linearity are presented here.

Each of the R Square values pointing possible curve fittings with non-linear equations are below 0,2 in tables presented. Therefore, they are not suggesting strong matches. Other 245 estimates were found insignificant due to three types of conditions:

- None of the R Square values are over 0,1.
- R Square value of the linear equation is significant (between 0,1 to 0,9), while others not.
- Multiple R Square values are over 0,1 but there is no significant difference between them and R Square value of the linear equation.

Table 31: Curve estimation results for output parameter WS.SpeedUpRegions vs. input parameter SC.DegreeOf Curve

Equation	Model Summary					Parameter Estimates			
	R Square	F	df1	df2	Sig.	Constant	b1	b2	b3
Linear	0,044	2,223	1	48	0,142	1,922	0,221		
Logarithmic	0,075	3,887	1	48	0,054	1,994	0,580		
Inverse	0,100	5,349	1	48	0,025	3,008	-1,130		
Quadratic	0,123	3,284	2	47	0,046	0,557	1,544	-0,283	
Cubic	0,129	2,270	3	46	0,093	-0,374	3,034	-0,980	0,098
Compound	0,078	4,038	1	48	0,050	1,654	1,150		
Power	0,114	6,189	1	48	0,016	1,762	0,342		
S	0,140	7,798	1	48	0,007	1,149	-0,638		
Growth	0,078	4,038	1	48	0,050	0,503	0,140		
Exponential	0,078	4,038	1	48	0,050	1,654	0,140		

Table 32: Curve estimation results for output parameter WS.MaxSpeed vs. input parameter SC.EaveDepthRatioFront

Equation	Model Summary					Parameter Estimates			
	R Square	F	df1	df2	Sig.	Constant	b1	b2	b3
Linear	0,078	4,088	1	48	0,049	0,535	-0,033		
Logarithmic	0,085	4,431	1	48	0,041	1,142	-0,404		
Inverse	0,091	4,785	1	48	0,034	-0,272	4,913		
Quadratic	0,166	4,664	2	47	0,014	6,331	-1,015	0,042	
Cubic	0,166	4,664	2	47	0,014	6,331	-1,015	0,042	0,000

Table 33: Curve estimation results for output parameter WS.MaxLocation vs. input parameter H.TotalHeight

Equation	Model Summary					Parameter Estimates			
	R Square	F	df1	df2	Sig.	Constant	b1	b2	b3
Linear	0,020	0,963	1	48	0,331	50,777	2,260		
Logarithmic									
Inverse									
Quadratic	0,116	3,083	2	47	0,055	60,710	8,557	-3,830	
Cubic	0,154	2,794	3	46	0,051	59,462	-3,710	-6,890	2,470
Compound	0,032	1,581	1	48	0,215	40,076	1,081		
Power									
S									
Growth	0,032	1,581	1	48	0,215	3,691	0,078		
Exponential	0,032	1,581	1	48	0,215	40,076	0,078		

Table 34: Curve estimation results for output parameter WS.MaxLocation vs input parameter SC.VertexPositionRatio

Equation	Model Summary					Parameter Estimates			
	R Square	F	df1	df2	Sig.	Constant	b1	b2	b3
Linear	0,004	0,182	1	48	0,672	0,431	0,010		
Logarithmic									
Inverse									
Quadratic	0,114	3,011	2	47	0,059	0,541	0,080	-0,043	
Cubic	0,155	2,807	3	46	0,050	0,555	0,213	-0,009	-0,027
Compound									
Power									
S									
Growth									
Exponential									

Table 35: Curve estimation results for output parameter RL.MaxSpeed vs V.ElevationRatio

Equation	Model Summary					Parameter Estimates			
	R Square	F	df1	df2	Sig.	Constant	b1	b2	b3
Linear	R Square	F	df1	df2	Sig.	Constant	b1	b2	b3
Logarithmic	0,001	0,031	1,000	48,000	0,861	0,486	0,009		
Inverse	0,000	0,002	1,000	48,000	0,963	0,526	0,028		
Quadratic	0,000	0,008	1,000	48,000	0,931	0,544	0,592		
Cubic	0,140	3,812	2,000	47,000	0,029	16,209	-2,704	0,116	
Compound	0,140	3,831	2,000	47,000	0,029	5,958	0,000	-0,120	0,007
Power									
S									
Growth									
Exponential									

Based on these results, it is decided that there should be no inconveniency to continue with analysis methods based on linear associations like linear correlation and linear regression models.

4.3.2 Assessment of Parameters' Effects by Relative Importance Values

Regression analysis were made on simulated data by Forward Stepwise method to evaluate and compare the sensitivities of model parameters used in the study. A brief evaluation of their results are discussed within this section, whereas more information can be followed on Appendix D.

A statistical model is exported from SPSS by “Automatic Linear Modeling” function under regression category per each of the 10 output parameters. These parameters are called as “targets” in regression analysis, whereas input parameters are called as “predictors”.

A cumulative table, which is prepared by combining all results of predictor importance values from 10 regression analysis results, is presented under this section. Predictor importance values for 25 input parameters are listed according to their targets (output parameters) within a single table to easily compare the results.

The sum and the average of all importance values are calculated and added to the table as last two columns. Input parameters are ranked according to them. Comparison of average values can give a perception for the overall influences of model parameters on wind flow characteristics which were quantitatively measurable by simulation design.

Results indicate that 20 of the 25 parameters has average predictor importance values over 5 %. Four of them is over 10 %, including one parameter (TF.X) which has an average value over 0,20.

Importance values over 10 % are highlighted with yellow color in the Table 36. Six of the parameters has at least two values as such, while 15 parameters have at least one.

Out of ten regression analyses, five of them were identified with accuracy ratios over 65% according to information criterion as shown in Appendix D. Rest of the five analysis should be treated cautiously. These are:

- Regression Model 3, Target: WS Max Speed, accuracy: 61,9%
- Regression Model 6;Target: NS Max Speed, accuracy: 63,5%

- Regression Model 8, Target: RL Max Speed, accuracy: 49,3% *
- Regression Model 9, Target: PL Speed Up Regions, accuracy: 55,7%
- Regression Model 10, Target: PL Max Speed, accuracy: 57,0%

The most conspicuous one among these as the lowest one (below 50%) is the accuracy of Regression Model 8, which was implemented on the output parameter RL_Max_Speed.

Four from the five low accuracy levels are belong to analyses on output parameters related with wind speed. This condition is considered as an obvious pattern. Thus, results suggests that this analysis method was more reliable on estimating variance among speed up regions in terms of number and location, while less reliable for wind speed variance. Three causes were considered as possibly responsible for this pattern.

Autodesk Flow Design can be judged as a rather qualitative decision support tool with respect to its limited measurement options. The simulation interface has no logarithmic wind profile option. Height depended acceleration of wind was not observed as resembling atmospheric conditions. Therefore, variance in wind speed values might have been relatively insignificant for regression analysis. In addition, speed values were measured with the help of contour lines and color legend as explained in 3.2.2. Regional average values were read by this method on banded colors instead of point-precise values.

Secondly, Monte Carlo simulations over the measurement data could have adapted to wind speed values below expectation at that uncertainty level.

Third possible cause is the possibility of a missed non-linear correlation of speed-related output parameters with input parameters during curve estimations (explained in 4.2.1). More sensitive methods or qualitative reviews might point any significant non-linearity on scatter plots.

Table 36: Table showing predictor importance values of model parameters for each simulation output as targets. Parameters are ranked according to their average importance over all targets. Yellow filled cells are over 10%.

	Average Drag Coefficient	WSSpeedUpRegions	WSMaxSpeed	WSMaxLocation	NSSpeedUpRegions	NSMaxSpeed	RLSpeedUpRegions	RLMaxSpeed	PLSpeedUpRegions	PLMaxSpeed	Total Importance	Average Importance
TF.X	0,29	0,01	0,01	0,56	0,15	0,23	0,00	0,04	0,02	0,01	1,34	0,24
B.YRatio	0,21	0,00	0,09	0,01	0,04	0,15	0,00	0,11	0,01	0,09	0,71	0,13
H.TotalHeight	0,06	0,07	0,02	0,03	0,22	0,17	0,03	0,01	0,00	0,07	0,68	0,12
SC.CTRF	0,00	0,20	0,00	0,04	0,03	0,00	0,00	0,11	0,06	0,21	0,65	0,12
SC.EDRF	0,02	0,00	0,25	0,03	0,03	0,00	0,04	0,01	0,01	0,13	0,52	0,09
TF.Y	0,00	0,10	0,02	0,02	0,01	0,02	0,10	0,16	0,02	0,01	0,44	0,08
SC.SDRB	0,01	0,08	0,00	0,00	0,19	0,00	0,07	0,01	0,00	0,08	0,44	0,08
SC.SDRF	0,01	0,05	0,00	0,06	0,04	0,00	0,06	0,03	0,17	0,00	0,42	0,08
SC.DOC	0,02	0,00	0,02	0,00	0,00	0,09	0,02	0,03	0,23	0,00	0,41	0,08
S.NTapering	0,01	0,00	0,01	0,00	0,05	0,00	0,24	0,01	0,03	0,03	0,38	0,07
SC.FETRF	0,00	0,01	0,13	0,02	0,07	0,03	0,06	0,03	0,01	0,01	0,38	0,07
SC.VPR	0,05	0,16	0,01	0,00	0,02	0,04	0,00	0,03	0,04	0,01	0,36	0,07
SC.SHR	0,02	0,03	0,01	0,02	0,00	0,00	0,03	0,16	0,05	0,02	0,35	0,06
SC.EDRB	0,09	0,06	0,06	0,01	0,02	0,03	0,00	0,00	0,07	0,01	0,35	0,06
B:HeightRatio	0,00	0,02	0,03	0,02	0,02	0,02	0,06	0,04	0,05	0,04	0,29	0,05
B.XRatio	0,00	0,04	0,10	0,00	0,00	0,08	0,03	0,00	0,01	0,01	0,28	0,05
SC.VHR	0,02	0,00	0,01	0,06	0,00	0,00	0,05	0,03	0,05	0,06	0,27	0,05
V.WidthRatio	0,03	0,05	0,01	0,00	0,00	0,01	0,15	0,01	0,01	0,00	0,27	0,05
TF.Vertice	0,01	0,00	0,02	0,00	0,06	0,05	0,02	0,09	0,01	0,01	0,27	0,05
SC.FETRB	0,00	0,07	0,08	0,04	0,00	0,04	0,00	0,01	0,01	0,00	0,25	0,05
T.Irregularity	0,02	0,00	0,01	0,03	0,01	0,00	0,00	0,05	0,08	0,05	0,24	0,04
V.ElevationRatio	0,04	0,00	0,01	0,03	0,00	0,00	0,01	0,00	0,00	0,10	0,20	0,04
TF.Roundness	0,03	0,01	0,03	0,00	0,03	0,02	0,00	0,00	0,00	0,04	0,16	0,03
V.HeightRatio	0,03	0,00	0,07	0,01	0,00	0,00	0,00	0,03	0,01	0,01	0,16	0,03
SC.CTRB	0,03	0,05	0,00	0,02	0,00	0,00	0,01	0,00	0,03	0,00	0,16	0,03

TF: Tower Footprint, B: Base, H: Height, SC: Section Curve, S: Solid, V:Void
 CTRF: Concavity translation ratio front VPR: Vertex positioning ratio
 EDRF: Eave depth ratio front SHR: Setback height ratio
 SDRB: Setback depth ratio back EDRB: Eave depth ratio back
 DOC: Degree of curve VHR: Vertex height ratio
 NTapering: Normal Tapering FETRB: Facade endpoint translation ratio
 FETRF: Facade endpoint translation ratio front back
 CTRB: Concavity translation ratio back

Following illustrations show the top ten significant predictors, as suggested by regression models, by their relative importance based on each target.

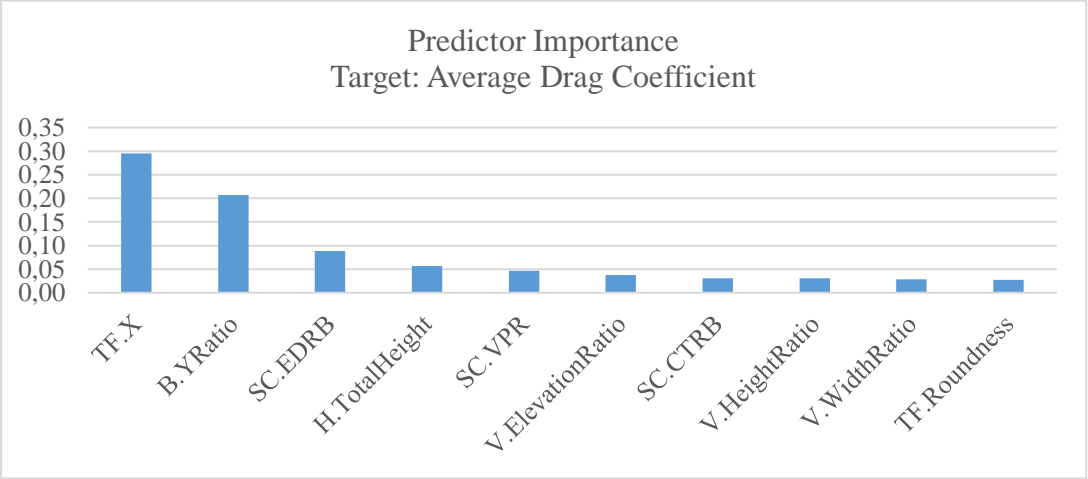


Figure 57: Predictor Importance comparison for Average Drag coefficient, among top ten standardized effects.

Regression Model 1, on Average Drag Coefficient, suggests that two of the input parameters are relatively more significant in terms of their association with the target. These are TF.X (Tower Footprint X) and B.YRatio (Base Y ratio). Coefficient values indicate negative correlation between both of the two values and the target.

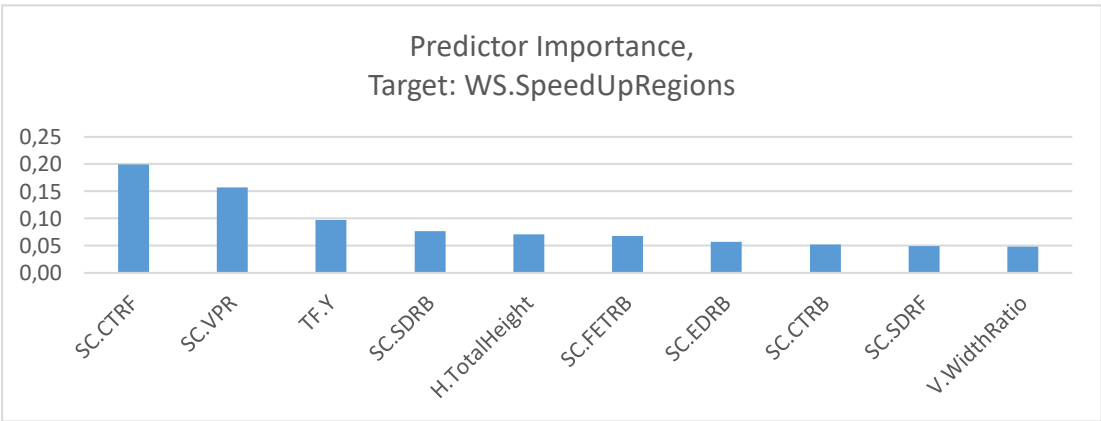


Figure 58: Predictor Importance comparison for WS.SpeedUpRegions among top ten standardized effects.

When the Regression Model 2 is analyzed, two of the parameters are distinguishable by their relative importance in predictive analysis: SC.CTRF (Section Curve. Concavity Translation Ratio Front) and SC.VPR (Section Curve. Vertex Positioning Ratio). Based on their coefficients given in Appendix D, it is comprehended that the model suggests SC.CTRF has a positive correlation with the number of speed up regions in windward section. Hence, concave forms possibly increases the amount of observable high-speed spots. On the other hand, SC.VPR has a negative coefficient, which means; analysis suggests that vertex positions closer to the wind facing facade (the front facade) has a decreasing effect on the number of high-speed regions.

According to Regression Model 3, which is about WS.MaxSpeed output parameter, two parameters which correspond to more than 10% predictor importance in linear regression model are, SC.EDRF (Section Curve. Eave Depth Ratio Front) and SC.FETRF (Section Curve. Facade Endpoint Translation Ratio Front) Eave Depth seems negatively related with the maximum speed measured in flow simulations with the sample cases. Whereas, the SC.FETRF; therefore the inclination of facade towards windward side, seems positively related.

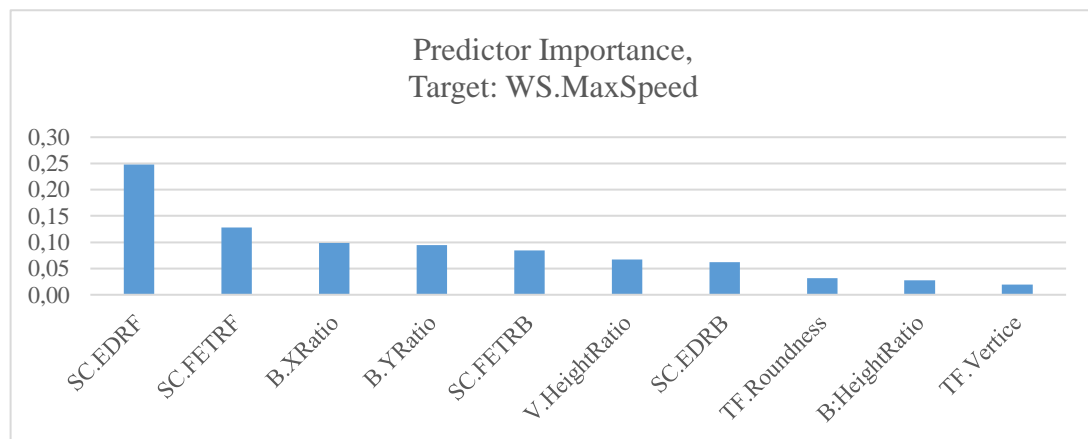


Figure 59: Predictor Importance comparison for WS.MaxSpeed among top ten standardized effects.

The accuracy level for Regression Model 3 was a smaller one as mentioned before. Thus, these inferences for two most significant parameters were compared by correlation matrices on both datasets.

SC.EDRF has a negative correlation with Pearson Correlation; -0,310, in the simulated dataset. Original dataset has the almost same value as: -0,280. These values justify the consideration made upon regression analysis, while showing nearly moderate correlations.

SC.FETRF shows a significant but weak positive correlation with WS.MaxSpeed for simulated dataset. The Pearson Correlation coefficient equals to 0,185, and similarly 0,200 in the correlation matrix of original dataset. These values indicate the same tendency with regression analysis.

WS.MaxLocation was a parameter defined for the determination of the highest wind speed occur in Windward Section plane as explained in Figure 52; in 3.2.2. The very significant effect of building’s shorter length in wind direction on this output was already observed in simulations frequently. (See 4.2.2)

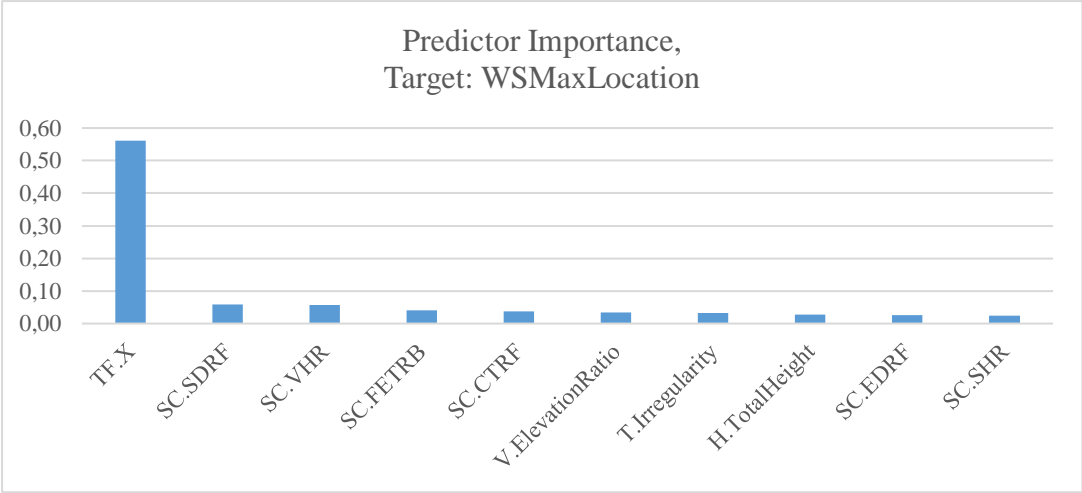


Figure 60: Predictor Importance comparison for WS.MaxLocation among top ten standardized effects.

As expected, TF.X parameter which is related with that form dimension is found highly effective on Regression Model 4 applied on WS.MaxLocation as target. The reason for relatively insignificant importance values is thought to be this dominance of TF.X on that output.

Three parameters have importance values over 10% in Regression Model 5. H.TotalHeight seems as the most important parameter on target NS.SpeedUp Regions and it is marked by a positive value as coefficient. Therefore, results suggest that there is a positive correlation with the number of higher speed regions observed in Normal Section plane with H.TotalHeight parameter which controls the height of the sample. This condition is probably related with the downwashing effects on wind flows by taller buildings as mentioned in the literature.

SC.SDRB (Section Curve.Setback Depth Ratio Back) seems positively related also (Coefficient: 3.397, Importance: 0,192). While, TF.X (Tower Footprint X) has a negative association (Coefficient: -0,014, importance: 0,153)

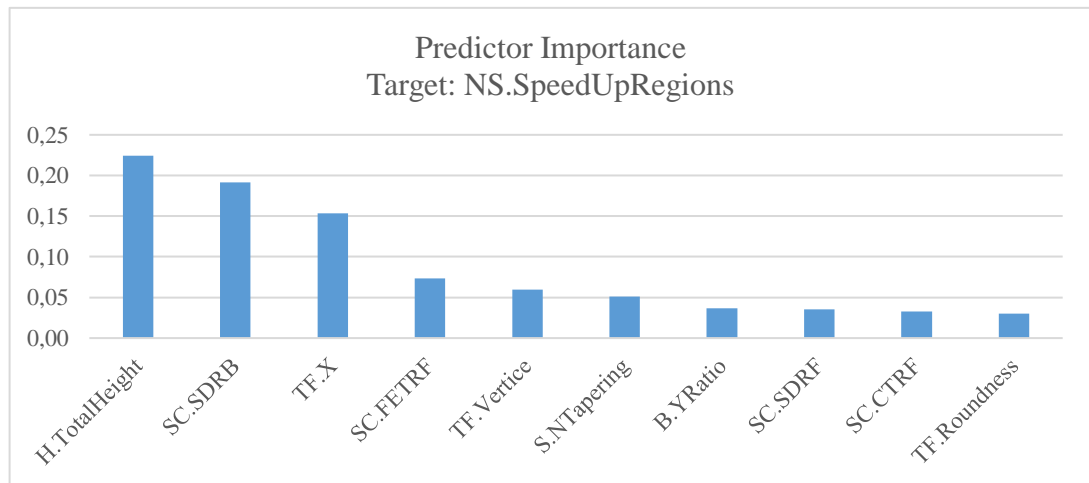


Figure 61: Predictor Importance comparison for NS.SpeedUpRegions among top ten standardized effects.

Regression Model 6 on Target NS.MaxSpeed was one of the models with a lower accuracy value. Therefore, results were compared with correlation matrices as a control step. Three parameters with highest importance values were checked.

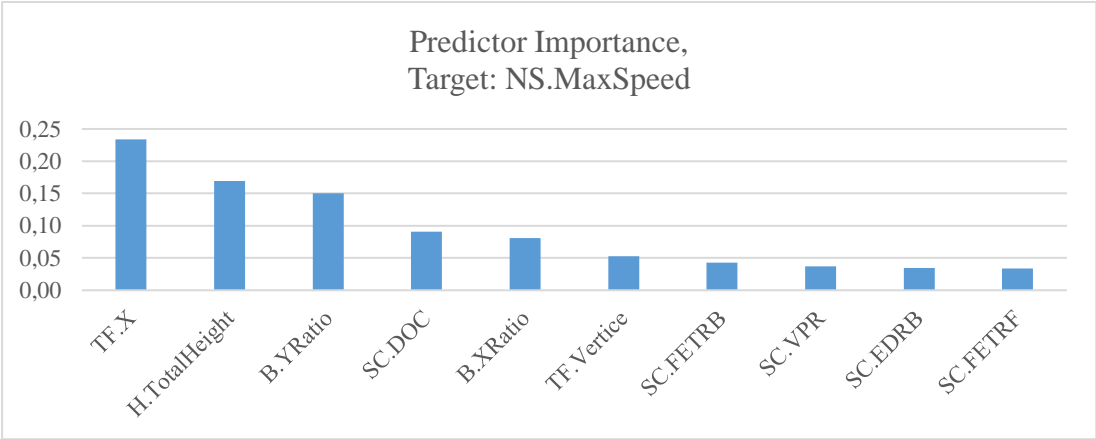


Figure 62: Predictor Importance comparison for NS.MaxSpeed among top ten standardized effects

TF.X shows highest importance with a negative coefficient in regression analysis. Correlation matrix of simulated data shares the same tendency with a moderate level negative Pearson Correlation as -0,418. Then again -0,479 is read from the correlations of original dataset. Hence, it is safe to consider TF.X and the highest speed in normal section has a negative correlation.

H.TotalHeight seems to be positively correlated with NS.MaxSpeed in all of three charts. Regression analysis gives 0,016 as coefficient by 0,169 importance. Correlation matrices shows Pearson Correlation as 0,316 for original data and the same for simulated data. Again, results are consistent with each other.

Lastly, B.YRatio has a negative coefficient in regression analysis (-0,250) with an importance value of 0,151. The Pearson Correlation values for this parameter with NS.MaxSpeed are -0,374 in simulated dataset and -0,380 in original dataset.

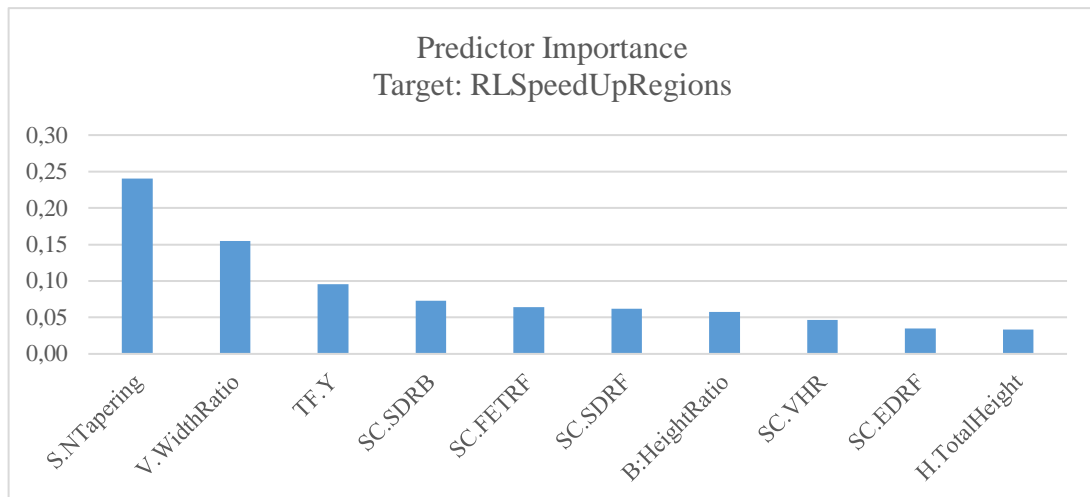


Figure 63: Predictor Importance comparison for RLSpeedUpRegions among top ten standardized effects

Seventh result to be discussed here is the regression model on RLSpeedUp Regions. There are two significant parameters by their importance values. S.NTapering, which determines the tapering ratio of building solid in normal section as explained in 3.2.2, is the first one. The second one is V.WidthRatio which is the ratio of void's width to the building width. They both have positive correlations with the amount of higher speed regions observed in Roof Level plane according to regression coefficients and Pearson Correlations.

Regression Model 8; which has the lowest accuracy value calculated as 49.3%, has the output RL.MaxSpeed as target.

Two most significant parameters with more than 15% importance were cross-checked by Pearson's Correlation, regression coefficient and importance values.

SC.SHR (Section Curve. Setback Height Ratio) is negatively related with RL.MaxSpeed by regression coefficient -4.439; Sum of Squares 3816.477 and importance 0.16. Its Pearson Correlation values are -0.185 for original data and -0,204 for simulated data. The suggestion of negative correlation looks acceptable.

Regression analysis indicates that TF.Y (Tower Footprint. Y) is positively correlated with RL.MaxSpeed based on values; regression coefficient = 0.011, Sum of Squares

= 3688,492 corresponding to 0,159 relative importance. Pearson Correlation values are again pointing the same tendency with 0.262 for original data and 0.242 for simulated data.

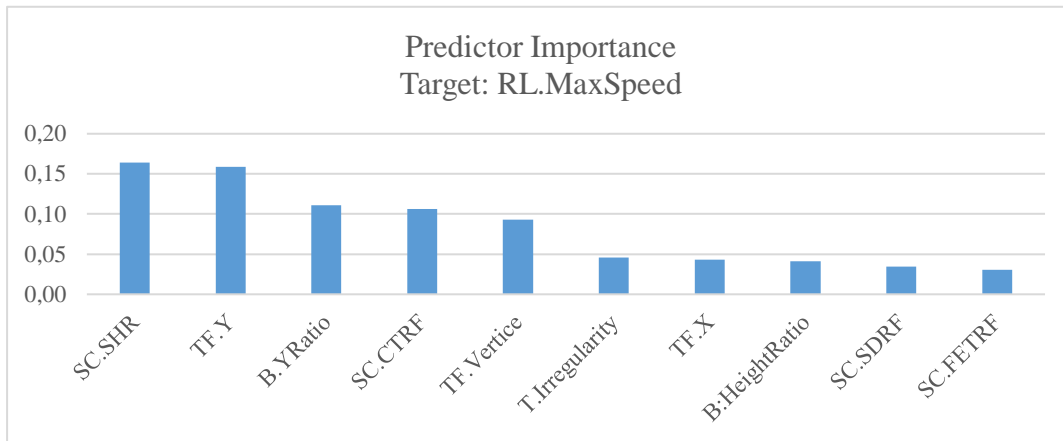


Figure 64: Predictor Importance comparison for RL.MaxSpeed

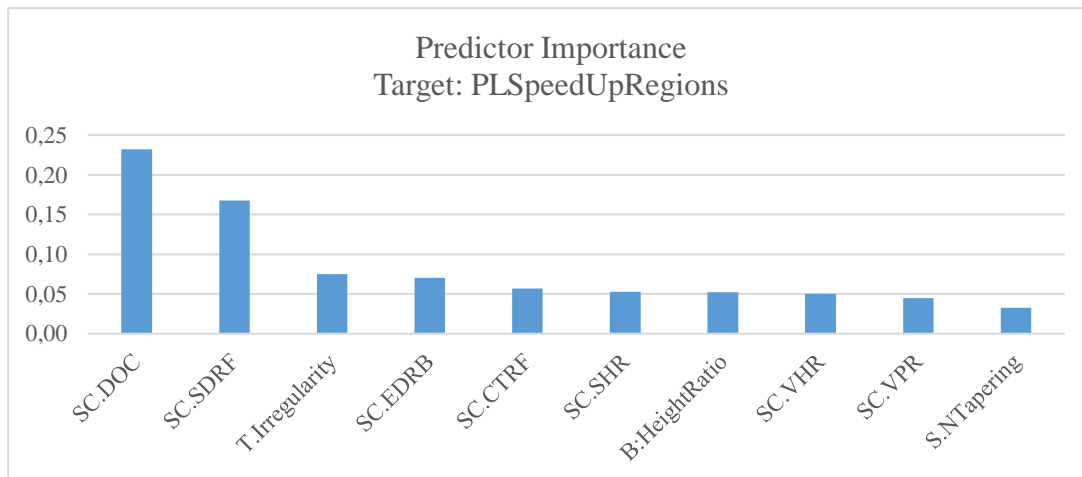


Figure 65: Predictor Importance comparison for PL.SpeedUpRegions among top ten standardized effects.

Two of the most significant parameters based on their association with high speed regions in pedestrian level plane (PL) are SC.DOC and SC.SDRF according to Regression Model 9. Results suggest that SC.DOC (Section Curve. Degree Of

Curvature) has a positive correlation with PL.SpeedUpRegions, while SC.SDRF (Section Curve. Setback Depth Ratio Front) has a negative correlation.

The last regression model has the PL.MaxSpeed output parameter as target which is the measured value of maximum speed at Pedestrian Level plane view. This model has one of the accuracy levels below 65% according to Information Criterion. Therefore, its results were compared with Pearson’s Correlation values like similar others. Two parameters with highest predictor importance values are SC.CTRF (Section Curve. Concavity Translation Ratio Front and SC.EDRF (Section Curve. Eave Depth Ratio Front).

Regression analysis indicates that SC.CTRF has a negative correlation with PL.MaxSpeed with regression coefficient -2,350. Simulated data has a Pearson Correlation of -0,253 and for original dataset it is similar: -0,123. Therefore the negative correlation is acceptable. SC.EDRF also has a negative correlation with PL.MaxSpeed according to all of three analyses: Regression coefficient: -3,646; Pearson Correlation in original dataset: -0,295 and in simulated dataset: -0,240

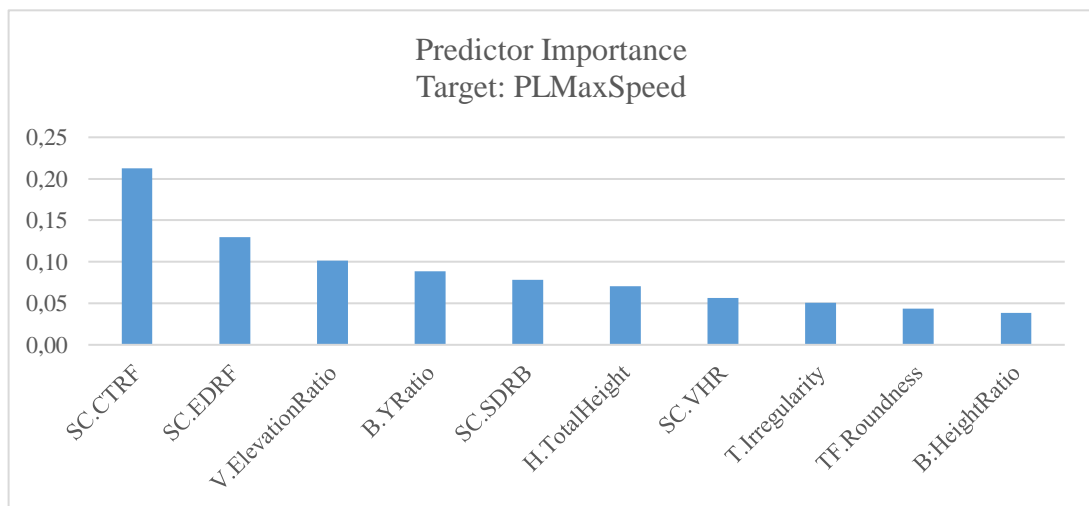


Figure 66: Predictor Importance comparison for PL.MaxSpeed among top ten standardized effects.

Initial findings suggested that TF.X (Tower Footprint X) and B.YR (Base Y Ratio) are parameters with most influence on wind flow behaviors while SC.CTRB (Section Curve Concavity Translation Ratio Back) and V.HR (Void Height Ratio) are matched with least predictor importance values according to ten regression models mentioned above. (See Table 36). Hence, additional simulations on these four parameters by one-at-a-time approach were performed to explore a possible validation procedure for the research process. For each of them, four values are defined within constraints and ranges of the parametric model by uniform distribution. Output values of those simulations were presented in 4.2.1. Then, correlation analyses were done on the data for each input parameter and results were considered collectively with observations during simulations. Correlation matrices are given in Appendix D together with data belonging to previous analyses.

According to the findings from samples 51 - 54; T.FX seems more significantly correlated with 5 parameters Average Drag Coefficient, WS Max Speed, WS Max Location, NS SpeedUp Regions and RL Max Speed.

For B.Y Ratio, results from samples 55 – 58 indicate possible correlations with 4 parameters as WS Max Speed, NS Max Speed, RL Max Speed and PL Max Speed. Negative correlations for all of those four maximum speed values suggests that higher Y dimensions (perpendicular to wind direction) of base decreases the speed of wind flow over building mass.

Void Height Ratio has been altered in Samples 63 – 66 and simulation results indicate that three possible correlations exists with output parameters. There is a weak correlation with WS Speed Up Regions, meaning that it is possible that bigger values of void height may be responded with an increase in the number of regions with relatively higher wind speed in windward section. Although that correlation should be more obvious according to the literature, the reason it was found weaker in simulations is probably related with the limitations of the study. Especially with the lack of output parameters which can measure effects of void configurations and also the resolution of wind flow in simulation setup. Other two parameters possibly correlated with V.Height Ratio are WS.Max Location and PL Max Speed. In terms of the location of

maximum wind speed measured in windward section the situation is quite similar to the WS Speed Up Regions as explained above. On the other hand, output values for PL Max Speed might suggest a non-linear correlation with V.Height Ratio, which can be considered contradictory to the curve estimations previously performed on simulated data.

Lastly, judging by results from samples 59 – 62, Two output parameters that SC.CTRB (Section Curve Concavity Translation Ratio Back) has possible correlation with are PL.Max Speed and WS.Max Location. Similarly to the results gathered from regression analyses on simulated dataset, these results also suggest that SC.CTRB is a parameter with relatively non-significant sensitivity on wind behaviours according to the experimental setup used in this study. While the concavity is considered as a significant attribute of building form in terms of wind interactions according to literature, in the parametric configuration there were two parameters affecting it on building section. The parameter related to the concavity of wind facing facade (SC.CTRF) has already higher importance values than the parameter related to the concavity of leeward facade (SC.CTRB). Therefore, within the scope of this study it is understandable that the overall shape of the leeward building surfaces has less effect on output data.

4.4 Inferences from Analysis of Results

This section includes two headings. First one 4.4.1 is a critical review of the proposed parameterization framework based on the specific model developed and tested in this study. Second heading, 4.4.2 consists of some inferences observed by simulations and data analysis on building form – wind flow interactions and insights for wind energy potential around isolated buildings referring to speed up zones and their locations.

4.4.1 A Critical Review of Proposed Method

As explained in Chapter 3, a framework matrix on parameterization of built forms for wind related studies was proposed. In this regard, the key mechanism was the production of core parametric models with visual programming interfaces as algorithm

aided tools. Based on the example model configured and analyzed within this study, some critical considerations and suggestions are discussed in this part.

Overall, results suggested that considerations determined for the production of parametric model were partially satisfied.

In 4.1, essential generic form types which are expected to derivate from the “central form” stem were presented with the parametric configuration that used to generate them from the model. As discussed on that section, these types were generated in a level of approximation with some limitations. Consideration I was that the model should be able to produce essential generic form types mentioned in literature was satisfied within that context.

Consideration II was related to the relevancy of parametric model with wind behaviors. This concern was tested with wind flow simulations as explained in 3.2.2 and data analysis over their results. According to observations made during simulations and results of multiple linear regression models; all of the parameters used in model have significant effects on simulation outputs in different parameter sensitivity levels.

The parameterization procedure consists of three consequent steps. First step was the parameter aggregation based on literature survey. Although results indicate that selected parameters has significant correlations for intended use; more sophisticated methods for determination of parameter sets can be applied. An intelligent database comparing various urban morphology studies and wind flow studies would be ideal. Furthermore, research methods including multiple participants from all of the concerned disciplines as joint research groups would be more reliable as a decision mechanism. Yet, as long as the model relevancy can be tested with quantitative statistical models, it is safe to suggest that proposed model(s) is practicable and research decisions can be validated.

Step 2 was related to construction of parametric model algorithm. Some inferences was made on the process and results within the context of example applied for that study.

The pre-configuration of parameter relations with UML diagrams was efficient in this example. Though, a more compact process includes that configuration embedded within the visual programming procedure is also applicable since visual programming languages also have the capability of behaving as flow diagrams.

One of the most significant challenges was the determination of parameter constraints. Some logical functions like If Statements was applied, after seeing bugs occurred while the generation of sample models. The dependency of model parameters within themselves by the use of ratios are consistent with the terminology preferred for urban morphology as well as architectural aerodynamics in literature. However, this type of a structure requires a systematic approach to assure the algorithm is performing faultlessly for all combinations of parameter values defined in different ranges.

After literature review, it was suggested that the use of section properties of building form in windward direction should be crucial for generic building forms to be used in wind flow research. Despite there seems a gap in literature as most of wind flow studies does not include section related variables and most generic form definitions basically depend on the vertical extrusion of building footprints also in classification of forms on urban morphology studies. In order to examine this suggestion, the model used for this study was structured on the combination of parameters belong to building footprints and section curves to form building solids. Both observation logs (4.2.2, Appendix C) and regression analysis (4.3.2, Appendix D) supports this approach. Section curve parameters are effective on simulation outputs as much as other model parameters. The ideal condition would be the construction of solid forms based on three reference curves as footprint, windward section and normal section. Whereas, a simplified model can be constructed with at least the footprint layout and windward section is acceptable for analysis of wind interactions. A parameter for tapering the solid on reference loft curves was explained in 3.2.2 as a modest replacement for normal section properties.

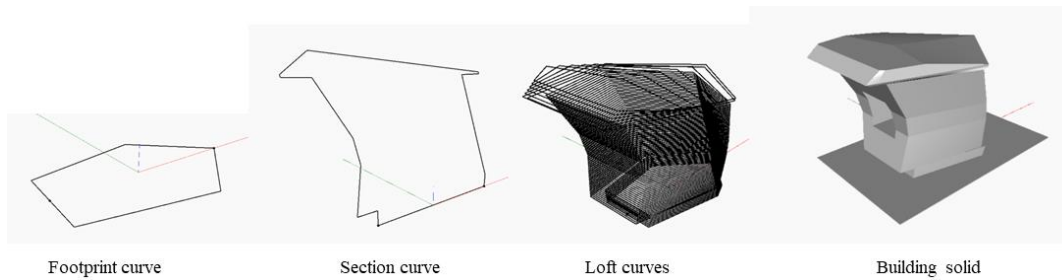


Figure 67: Building solid as a cross product of footprint layout and section curve, after reverse tapered with S.NormalTapering parameter and void opened.

The third step involves possible actions by the use of the core model. These actions can vary from design exploration, wind flow research or form optimization as discussed in Chapter 3. For this study, wind flow simulations can be considered as this step while also being part of the test mechanism for the model relevancy. The essential contribution of the parametric model was the capability to produce samples in a fast way as the sampling method required. Any intended value set for input parameters within model ranges can be constructed for any intended number of model samples. This is both relatively a much faster way than making digital models one by one, also supports reliability of experimental setup by the identical quantitative structure of variables which is shared among all models.

4.4.2 Inferences on Interactions Between Building Form and Wind Flows

As a secondary outcome of research, some inferences on the association of form parameters with wind resource around buildings are discussed within this part as they can be measured with the specific experimental setup used. It is vital to state that these findings are restricted with the limitations of simple simulation setup and output parameters in question as explained in 3.2.2. Therefore, it is important not to consider these suggestions as facts in terms of building aerodynamics, since very crucial behaviors of urban wind flows were out of the scope (e.g. turbulent characteristics of flow, logarithmic wind profile, vortex formations on surface edges.)

These inferences will be discussed on four group of parameters as they were used in model structure.

I. Tower Footprint parameters.

Results suggest that for most of the output parameters, effects of TF.X and TF.Y should be handled as a ratio of them to each other. (TF.X / TF.Y)

One of the most repetitive observable patterns in simulations was the correlation of TF.X/TF.Y with the region of max. wind speed occurred in Windward Section plane (WS.MaxLocation) As also suggested in literature, building slimness is a significant factor in wind – building interactions. A small value of TF.X (dimension of building in X) vs. a relatively larger value of TF.Y (dimension of building in Y) resulted with a max. speed location behind the building mass in many samples. (See samples 1,25,26,44) This pattern was also confirmed with the results of regression analysis. (See Regression Model 4) and Pearson Correlation values between TF.X and TF.Y and WS.MaxLocation. A similar condition is observed in Pedestrian Level view (PL) also (see sample 37), while there is no output parameter for measuring the maximum wind speed location in that measurement plane.

Measured values of average drag coefficient indicate that buildings with a smaller TF.X / TF.Y ratio has more resistance against wind flows by having more surface area in wind facing direction. (See samples 1,21,37, Regression Model 1). Although not measured with a quantitative output parameter, differences in wake zones are observed through simulations on many samples (See 4.2.2, Appendix C) TF.X / TF.Y ratio has also an effect on that differences. A building with a small dimension in X axis, while having a bigger dimension in Y axis tends to cause bigger wake zones. (See Sample 21) For a contradictory example see Sample 19.

As expected, irregular forms; formed by higher values of TF.Irregularity parameter, caused asymmetrical patterns for speed up regions and wake zones. (e.g. sample 5) Furthermore, Pearson Correlation values and regression models (3, 10) suggests a weak negative correlation of TF.Irregularity on maximum wind speed observed in windward section and pedestrian level section. (See appendix D)

Similarly, rounded forms derivate from higher values in TF.Roundness parameter shows decreased resistance against flow as expected. This is deductible from the

average drag coefficient values (See Regression Model 1). Besides, observations suggest that possible flow speed acceleration on side edges and front vertices of building forms might be prevented by round forms.

TF.Vertice parameter seems positively correlated with WS.Max Location, meaning that the maximum wind speed occurred in windward section is observed closer to the leeward side on samples with more corners in footprint. Although, there is no explanation attached to this correlation based on observation logs for now. Sample 29 shows a possible association with wind flows and TF.Vertice parameter judging by locations of max. speed regions in Roof Level plane (RL) and Pedestrian Level plane (PL)

II. Base Solid parameters

Observations suggest that when the X dimension of base solid (B.XRatio) is relatively much larger than tower dimensions with a significant base height (B.HeightRatio); maximum speed regions occurred in windward section (WS) are located closer to windward side. (e.g. sample 32) Regression Model 4 and Pearson Correlation values support this suggestion while showing significant but weak correlations values.

Higher values of B.YRatio (dimension of base solid in Y/ TF.Y) causes lower values of wind speed measured in all planes (WS, NS, PL, RL) (see regression models 3,6,8,10) According to observations, the possible reason for this behavior is the increased building surface area in wind facing direction, as it also provide distributed zones of high surface pressure which can be another wind energy potential by the development of surface based conversion systems. It is also observed that more speed up regions occurred over base edges when the B.YRatio is bigger. (See Sample 23)

III. Section Curve parameters

SC.DegreeOfCurve parameter which controls the roundness of section curve seems as the most important predictor on multiple regression for PLSpeedUp Regions (See Regression Model 9). This result suggests a positive correlation between rounded section profiles and the amount of higher speed regions occurred in pedestrian level.

A possible explanation of this behavior might be that rounded forms increase the downwashing effects caused by eaves, concave facade forms and ground floor setbacks by channeling the air movement more smoothly towards ground. Sample 27 is one of the examples which gives the idea that this parameter also has an effect on the location of maximum wind speed with a tendency of centering this location over the building form when TF.X is not too small.

Setback height and depth observed as effective on preventing some portion of wind flow towards up. (See samples 4, 47). A supportive deduction for this observation comes from Regression Model 8, where the SC.SetbackHeightRatio is the most important predictor with a negative correlation on RL.MaxSpeed (Maximum speed measured at roof level plane) The flow is splitted into two streams by the setback projection on facade, therefore speed on roof level measured in lower values. SC.SetbackDepthRatioFront and SC.Setback DepthRatioBack are also among top ten effects and both have negative correlations.

Similarly to setback formations, concavity on facade seems to have the same effect of channeling the wind flow partially towards ground, by splitting it into two on windward section. Log recorded for Sample 46 includes an observation of this behavior while Regression Model 8 also confirms that pattern by showing a negative correlation between SCConcavityRatioFront and RLMaxSpeed among top ten effects. On the other hand, convex forms are observed to concentrate wind pressure on facade in point-wise shapes.(e.g. Sample 2) This tendency can be taken advantage on, while placing wind energy conversion systems on building facades.

Either concavity, setback depth or eave depth (SC.EaveDepthRatio) can form stagnant areas on windward facades. (e.g. sample 15) As known from the literature they are already used as design strategies to increase pedestrian comfort. Regression Model 10 and Pearson Correlation values also support this inference by indicating negative correlations between each of these parameters and maximum wind speed measured in Pedestrian Level plane (PL.MaxSpeed) However, this condition should be considered together with the wind facing facade angle which is controlled by (SC.FETRF) parameter. Observations in Sample 29 and Sample 46 show a slanted facade might

cause high wind pressure on ground, in front of the building, by channeling the wind towards that direction together with an eave.

Translation of the facade endpoint is also effective on the resistance of building form against wind. (See Regression Model 1) Forms slanted towards windward side tend to have higher resistances judging by the average drag coefficient values from simulation results. Whereas, a translation on the leeward facade endpoint (SC.FETRB) together with a significant eave depth on that side (SC.EaveDepth RatioBack) might provide undisturbed flow streams and regular wake zone patterns. (See Sample 2) Similar pattern is also observable with flat roofs, which are resulted in model when the V.HRatio (Vertex height ratio) is equals or closer to 0.

Sample 12 is an example of front facade translation and eave depth acting together to center a high speed zone over the eave closer to the roof. This condition is supported by lower values of SC.DegreeOfCurve as a pattern observed in many simulations.

Vertex position and vertex height (controlled by SC.VPR and SC.VHR parameters) are detected to have decisive effects on the location of max. wind speed in windward section. (e.g. samples 25, 30, 31)

IV. Solid and Void parameters

SNormalTapering has a moderate positive correlation with the amount of speed up regions observed in roof level according to Regression Model 7 and Pearson Correlation values. Same type of an association is also a case in point for width of the void.

VWidthRatio (void width / solid width) effects the number of high speed regions on roof level plane positively. Regression Model 7 suggest so, as a comparison of samples 45, 46, 47 may also support.

Significant effects of void height and void elevation are not displayed in statistical tests with precise suggestions, probably due to a lack of specific output type. However, observation logs on samples 6, 11, 13, 14, 25, 32, 34, 35, 45, 46, 49 have suggestions on effects of void dimensions and positioning, combined with other form parameters.

.CHAPTER 5

CONCLUSION

This chapter is laid out in five sections as summary, main outcomes, limitations and recommendations for future research.

5.1 Summary of the Research

The motivation of the study can be summed with one sentence as: Parameterization of built environment by visual programming to be used in possible actions including design exploration, wind flow studies, optimization and feasibility studies. The expected contribution is to point the potential of algorithm aided design tools in improving interdisciplinary research between concerned fields.

A framework matrix proposed for this purpose, as a cross product of three domain sizes and three consequent steps as parameter aggregation, construction of parametric model algorithm and the use this core model as an infrastructure for intended actions.

Although, three domain sizes for wind flow studies by parametric models are proposed as isolated building, urban block and urban area; only an example model for isolated building scale is modelled and tested by simulations. The other two scales are recommended for further studies with suggestions.

Research process is composed of nine sub-process steps which may be grouped under three stages as:

- Parameter extraction and aggregation
- Algorithm design and construction of core parametric models for generic forms and formations
- Sensitivity analysis of form parameters on wind flow simulations.

Essential findings of the research are outlined in next section, main outcomes. As an inclusive judgment, it can be claimed that the study has showed the potential of

algorithm aided modeling tools to be implemented in wind flow studies as expected and promises a connection among terminology and technicalities of different disciplines related to urban wind resource.

5.2 Main Outcomes

Parameter aggregation process helped discovering potential relations between significant wind flow characteristics and shape attributes, some of them were not mentioned by name in reviewed wind flow studies. This deduction may also help to architects and planners who may not be familiar with computational definitions of wind flow behaviors.

A comprehensive collection of architectural form definitions and urban pattern attributes was compiled. (Chapter 2) Despite not being a primary concern of this study, it is conceived as a considerable contribution to the literature. Wind flow studies are also reviewed for form parameters included (Appendix A)

An example parametric model algorithm as a pilot for proposed framework was constructed. The process of model construction as well as tests on model's relevancy with flow simulations and statistical tests resulted with a critical review of the procedure. (4.4.1) Simulations and data analysis showed that the model is relevant to the purpose according to pre-determined considerations in 3.2.2. Therefore, some of the suggested parameters for building scale may be used in future studies as they were compared and analyzed in terms of their effects on wind flow as a secondary motivation of study. (4.3; 4.4)

Some inferences from research process which were also mentioned in previous chapters can be summarized as following:

The basic principle of grouping generic forms into lesser amount of primitive instances according to generative possibilities among them might be feasible for producing parametric models for wind related studies. However, case based enquiries will possibly require case-specific implementations. The approach used in this study for parametric model configuration might be more beneficial in wind-related research

rather than pre-design and design processes where the analysis on wind behaviors can be made on actual form that have been developed. Yet, with additional procedures on core parametric models, tools for design exploration and form optimization can also be developed.

Results suggested that parameters selected after aggregation for the algorithmic configuration have significant effects on wind flow behaviours. However, a need for a simpler setup to be used as parametric core with lesser amount of variables and more specifically defined constraints was also stated. Nevertheless, it is suggested that form parameters related with building section should always be considered for wind flow studies rather than procedures extruding building forms directly from footprints.

Some examples of the most significant patterns observed on interactions of building form parameters and wind flows within the scope of this study are:

The dimension of the building footprint on wind direction has an effect on the location of the region with highest wind speed occurring in windward section. Narrower buildings in wind direction tend to cause wind flow accelerations behind the building form, whereas when the dimension is bigger, wind flow speeds up in wind facing edge.

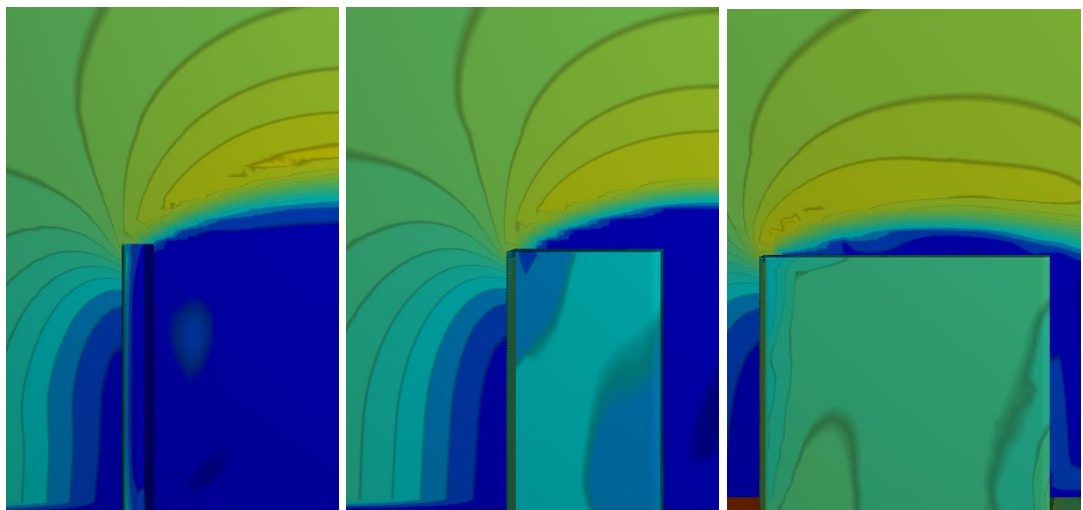


Figure 68: Change of the maximum speed region in windward section, depending on the building dimension.

Base solids relatively larger in wind facing direction, create multiple areas with higher wind speed in pedestrian level. That might cause possibly uncomfortable conditions, but also can be considered as a potential for wind energy conversion.

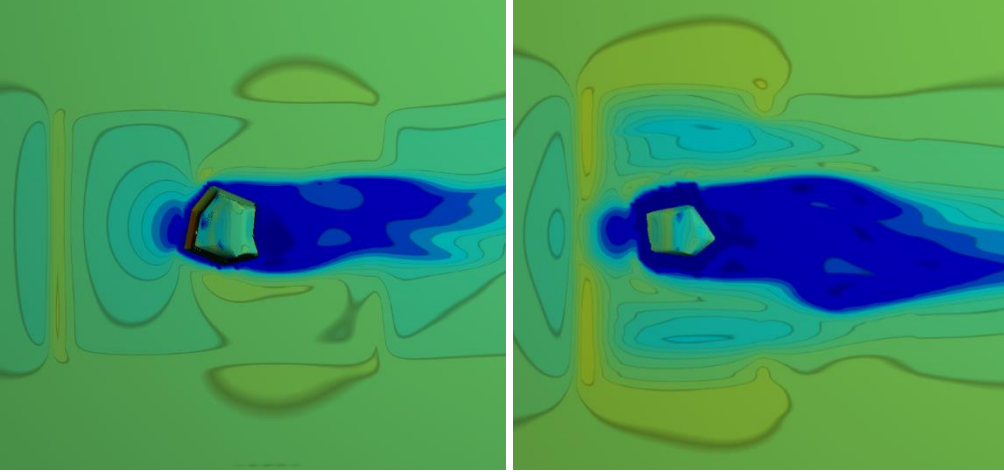


Figure 69: Examples of wind flow patterns over the building base.

Pointed regions in section curve such as a roof vertex or eave have a tendency to accelerate wind flow around them. Similarly concave surfaces center wind induced pressure on their focal regions as expected.

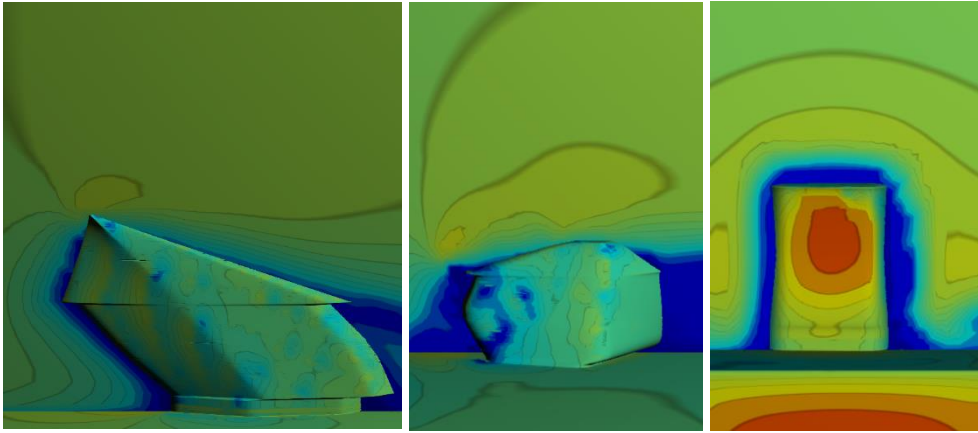


Figure 70: Three different concentrator effects of building forms.

5.3 Limitations of the Study

The study has four primary limitations as listed and explained below:

When possible form properties and classes were extracted from literature review a systematical process was implemented as explained in the second chapter. As the scope and the motivation of the study implies, references with only direct geometrical inferences were selected for aggregation. Yet again, a specific elimination method was inevitably used since it is almost impossible to include every bibliographical source which are related to architectural form and urban formation. Overall, the study is limited with the literature which can be surveyed within its context in terms of parameter aggregation.

A parametric model algorithm was produced so as it can generate simplified and generalized building models as both wind and morphology studies suggested. However, only generic building masses were produced, while most building components are excluded in that level of detail. Parametric configuration was simplified due to challenges in modelling and testing as explained in Chapter 3. Some possibly significant parameters were also left out of the scope like surface porosity. Topography of urban areas is one of the most influencing parameters on wind flows occurring in urban environments according to literature. However, it was ignored in experimental setup of parametric models and wind simulations conducted in this research. Reasons for that decision are to sustain stable conditions for simulations by keeping the ground surface variables constant and the possibility of importing approximated earth surface models to any 3D model environment by simple processes. Still, it is a significant limitation of the study.

With the intention of analyzing geometric attributes and types in many numbers as can be derived from source parametric model; flow simulations kept rather simple. Autodesk Flow Design software is a tool which specifically addressed to architects and designers to have a broad insight on form - flow interactions during early design stages. Although it is a proficient tool for evaluating early mass models of architectural designs, it is not an overall CFD engine. It is called as a virtual wind tunnel by the

producer company. Limitations regarding simulation setup was explained in 3.2.2 and 4.4.1 with more detail.

Considering 25 input parameters and 10 output parameters, an experimental setup based on 50 samples was decided as explained in Chapter 3 and Chapter 4. Monte Carlo simulations and multiple linear regression models are applied on data within the context of parameter sensitivity analysis, in order to keep sample number in a smaller amount. The use of predictive methods instead of producing minimum sample amount required for each parameter's single-handedly exploration also can be considered as a limitation of study. Yet, this approach may have helped discovering associations between parameters and measuring combined and/or compared effects.

5.4 Recommendations for Further Research

Based on the outcomes of this study, there are possible stems to build up on by further research.

First and most important, more sophisticated ways of parameter aggregation might be developed as research process for the Step 1 which is defined in proposed framework. A more explanatory suggestion is provided in fourth section of Chapter 4.

Secondly, the example model developed for the study covers a primitive instance in the isolated building domain size. This model has a generative scope for central forms (See 3.2.2). Other core parametric models either in same domain or other domains can be produced and diversified; notably the linear form algorithm for which the pre-configuration was already discussed in this study by an UML diagram. (See Figure 39)

With respect to the research limitations faced with during the validation of model considerations; a study which will link the parameterization framework with CFD guidelines or similar practice conventions, while still keeping the method efficient and feasible, should be very beneficial.

Third step of the proposed framework is the action to be implemented on constructed parametric models. This step is generously open for addition by new studies. Interactive applications, BIM plug-ins, genetic algorithms or other evolutionary tools,

optimization schemes, extensions for simulation interfaces are only some of the possible tracks. It is also possible to use the example model and its parameters as an outcome product for wind flow studies to measure their effects in different experimental configurations.

REFERENCES

- Abd Razak, A., Hagishima, A., Ikegaya, N., & Tanimoto, J. (2013). Analysis of airflow over building arrays for assessment of urban wind environment. *Building and Environment*, 59, 56-65.
- Achten, H. (2012, December). Typical design without the use of types. In CAAD futures 1997: Proceedings of the 7th International Conference on Computer Aided Architectural Design Futures held in Munich, Germany, 4–6 August 1997 (p. 117). Springer Science & Business Media
- Adolphe, L. (2001). A simplified model of urban morphology: application to an analysis of the environmental performance of cities. *Environment and planning B: planning and design*, 28(2), 183-200.
- Agkathidis, A. (2016). *Generative Design: Form-finding Techniques in Architecture*. Laurence King Publishing.
- Ahrens, C. D. (2012). *Meteorology today: an introduction to weather, climate, and the environment*. Cengage Learning.
- Ai, Z. T., & Mak, C. M. (2017). CFD simulation of flow in a long street canyon under a perpendicular wind direction: Evaluation of three computational settings. *Building and Environment*, 114, 293-306.
- Aihara, A., Uzunoglu, B., & Goude, A. (2016). Wind Flow Resource Analysis Of Urban Structures: A Validation Study. In *12th EAWE PhD Seminar on Wind Energy in Europe. 25-27 May 2016 DTU Lyngby, Denmark*.
- Aliaga, D. G., Vanegas, C., Lei, M., & Niyogi, D. (2013). Visualization-based decision tool for urban meteorological modeling. *Environment and Planning B: Planning and Design*, 40(2), 271-288.
- Allardyce, S. (2011). *Small Scale Wind Power Case Study: North Walls Community School*.

- Anderson, S. R. (1992). *A-morphous morphology* (Vol. 62). Cambridge University Press.
- Anton, I., & Tănase, D. (2016). Informed geometries. Parametric modelling and energy analysis in early stages of design. *Energy Procedia*, 85, 9-16.
- Autodesk Knowledge Network. (2018). Wind Tunnel Flow Design. Retrieved January 8, 2018, from <https://knowledge.autodesk.com/support/flow-design/learn>
- Babsail, M. O. (2011). Toward Net Zero Energy: The correlation between architectural forms of tall buildings and wind power production. Illinois Institute of Technology.
- Badger, J., Badger, M., Kelly, M., & Guo Larsén, X. (2016). Global Wind Atlas. Retrieved June 21, 2017, from <http://globalwindatlas.com/datasets.html>
- Bady, M., Kato, S., Takahashi, T., & Huang, H. (2011). An experimental investigation of the wind environment and air quality within a densely populated urban street canyon. *Journal of Wind Engineering and Industrial Aerodynamics*, 99(8), 857-867.
- Baniotopoulos, C., Borri, C., & Stathopoulos, T. (Eds.). (2011). *Environmental wind engineering and design of wind energy structures* (Vol. 531). Springer Science & Business Media.
- Bard, S. (2004). Quality assessment of cartographic generalisation. *Transactions in GIS*, 8(1), 63-81.
- Baskaran, S., Davis, B., Long, J., & Steiner, M. (2009). Building-Integrated Small Wind Energy.
- Belgiu, M., Tomljenovic, I., Lampoltshammer, T. J., Blaschke, T., & Höfle, B. (2014). Ontology-based classification of building types detected from airborne laser scanning data. *Remote Sensing*, 6(2), 1347-1366.
- Biljecki, F., Ledoux, H., & Stoter, J. (2016). Generation of multi-LOD 3D city models

- in CityGML with the procedural modelling engine Random3Dcity. *ISPRS Annals of the Photogrammetry, Remote Sensing and Spatial Information Sciences*, 4, 51.
- Blocken, B., Janssen, W. D., & van Hooff, T. (2012). CFD simulation for pedestrian wind comfort and wind safety in urban areas: General decision framework and case study for the Eindhoven University campus. *Environmental Modelling & Software*, 30, 15-34.
- Blocken, B., Stathopoulos, T., & Van Beeck, J. P. A. J. (2016). Pedestrian-level wind conditions around buildings: Review of wind-tunnel and CFD techniques and their accuracy for wind comfort assessment. *Building and Environment*, 100, 50-81.
- Bobrova, D. (2015). Building-integrated wind turbines in the aspect of architectural shaping. *Procedia engineering*, 117, 404-410
- Bottema, M. (1993). Wind climate and urban geometry.
- Brady, R. H. (1994). Pattern description, process explanation, and the history of morphological sciences. L. Grand, and O. Rieppel. *Interpreting the Hierarchy of Nature: Transystemic Patterns to Evolutionary Process Theories*. Academic Press. San Diego. California, USA, 7-31.
- BuildingSMART. (n.d). About IFC. Retrieved Retrieved January 07, 2018, from <http://www.buildingsmart-tech.org/ifc/>
- Staffell, I., Brett, D. J., Brandon, N. P., & Hawkes, A. D. (Eds.). (2015). *Domestic microgeneration: renewable and distributed energy technologies, policies and economics*. Routledge.
- Brown, M. J. (2000). Urban parameterizations for mesoscale meteorological models. *Mesoscale atmospheric dispersion*, 193-255.
- Burian, S. J., Brown, M. J., & Linger, S. P. (2002). Morphological analyses using 3D building databases: Los Angeles, California. *Rep. LA-UR-02*, 781.

- Burian, S. J., Brown, M. J., & Velugubantla, S. P. (2002). *Building Height-Characteristics in Three US Cities* (No. LA-UR-02-1089). Los Alamos National Laboratory.
- Bussel, G. J. W., & Mertens, S. M. (2005, July). Small wind turbines for the built environment. In *Proceedings of the 4th European and African conference on wind engineering*.
- Cai, Y., Zhao, F., & Liu, S. (2015). Wind Field CFD Analysis on the Flat Roof of the Building. In *Proceedings of International Conference on Information Sciences, Machinery, Materials and Energy* (Vol. 2015, pp. 591–594).
- Campbell, N., Stankovic & S., Graham (2001). Wind energy for the built environment (Project Web). *A report for Joule III Contract No JOR3-CT98-01270..*
- Carmona, M., Marshall, S., & Stevens, Q. (2006). Design codes: their use and potential. *Progress in Planning*, 65(4), 209-289.
- Carpentieri, M., & Robins, A. G. (2015). Influence of urban morphology on air flow over building arrays. *Journal of Wind Engineering and Industrial Aerodynamics*, 145, 61-74.
- Casini, M. (2016). Small vertical axis wind turbines for energy efficiency of buildings. *Journal of Clean Energy Technologies*, 4(1), 56-65.
- Chaudhry, H. N., Calautit, J. K., & Hughes, B. R. (2015). Computational analysis to factor wind into the design of an architectural environment. *Modelling and Simulation in Engineering*, 2015, 5.
- Chaudhry, H. N., Calautit, J. K. S., & Hughes, B. R. (2014). The influence of structural morphology on the efficiency of Building Integrated Wind Turbines (BIWT). *Aims Energy*, 2(3), 219-236.
- Chen, B., Li, T., Feng, C., Zhang, T., & Zhang, D. (2009, April). Concentration for wind power in the built environment. In *Sustainable Power Generation and Supply, 2009. SUPERGEN'09.*(pp. 1-6). IEEE.

- Chen, Q. Y. (2004). Using computational tools to factor wind into architectural environment design. *Energy and buildings*, 36(12), 1197-1209.
- Ching, F. D. (2014). *Architecture: Form, space, and order*. John Wiley & Sons.
- Cóstola, D., Blocken, B., Ohba, M., & Hensen, J. L. M. (2010). Uncertainty in airflow rate calculations due to the use of surface-averaged pressure coefficients. *Energy and Buildings*, 42(6), 881-888.
- Çalışkan, O. (2013). Pattern formation in urbanism: A critical reflection on urban morphology, planning and design. (Doctoral dissertation, TU Delft). Retrieved February 10, 2017, from <https://repository.tudelft.nl/islandora/object/uuid:9a0f4d24-bc77-469e-9f56-e6c14eda252a?collection=research>
- Dallman, A., Di Sabatino, S., & Fernando, H. J. S. (2013). Flow and turbulence in an industrial/suburban roughness canopy. *Environmental fluid mechanics*, 13(3), 279-307.
- Das, S., Day, C., Dewberry, M., Toulkeridou, V., & Hauck, A. (2016). Automated Service Core Generator in Autodesk Dynamo. eCAADe 2016.
- Deru, M., Field, K., Studer, D., Benne, K., Griffith, B., Torcellini, P., ... & Yazdanian, M. (2011). US Department of Energy commercial reference building models of the national building stock.
- Dimoudi, A., Kantzioura, A., Zoras, S., Pallas, C., & Kosmopoulos, P. (2013). Investigation of urban microclimate parameters in an urban center. *Energy and Buildings*, 64, 1-9.
- Dino, I. (2012). Creative design exploration by parametric generative systems in architecture. *METU Journal of Faculty of Architecture*, 29(1), 207-224.
- Djairam, D., Hubacz, A. N., Morshuis, P. H. F., Marijnisen, J. C. M., & Smit, J. J. (2005, November). The development of an electrostatic wind energy converter (EWICON). In *Future Power Systems, 2005 International Conference on* (pp. 4-pp). IEEE.

- Downing, D. J., Gardner, R. H., & Hoffman, F. O. (1985). An examination of response-surface methodologies for uncertainty analysis in assessment models. *Technometrics*, 27(2), 151-163.
- Drew, D. R., Barlow, J. F., & Lane, S. E. (2013). Observations of wind speed profiles over Greater London, UK, using a Doppler lidar. *Journal of Wind Engineering and Industrial Aerodynamics*, 121(C), 98–105.
- Dutton, A. G., Halliday, J. A., & Blanch, M. J. (2005). The feasibility of building-mounted/integrated wind turbines (BUWTs): Achieving their potential for carbon emission reductions. *Energy Research Unit, CCLRC*, 77-83.
- Eckler, J. F. (2012). *Language of Space and Form: Generative Terms for Architecture*. John Wiley & Sons.
- ESRI. (n.d.). Esri CityEngine: Getting Started. Retrieved January 13, 2018, from <http://www.esri.com/software/cityengine/getting-started>
- EUJRC. (2008). SimLab 2.2 Reference Manual. Retrieved June 15, 2017, from <https://ec.europa.eu/jrc/en/samo/simlab>
- European Energy Agency. (2007). EEA project Wind - Energy potential in Europe.
- EWEA. (2009). *The Economics of Wind Energy*. European Wind Energy Association
- Foley, A. M., Leahy, P. G., Marvuglia, A., & McKeogh, E. J. (2012). Current methods and advances in forecasting of wind power generation. *Renewable Energy*, 37(1), 1-8.
- Forman, R. T. (2014). *Urban ecology: science of cities*. Cambridge University Press.
- Franke, J. (2006, July). Recommendations of the COST action C14 on the use of CFD in predicting pedestrian wind environment. In *The fourth international symposium on computational wind engineering, Yokohama, Japan* (pp. 529-532).
- Fletcher, J. A., & Mills, G. (2013). The role of urban form as an energy management parameter. *Energy Policy*, 53, 218-228.

- Gaffuri, J., & Trévisan, J. (2004, August). Role of urban patterns for building generalisation: An application of AGENT. In *The 7th ICA workshop on generalization and multiple representation*.
- Gan, Y., & Chen, H. (2016). Discussion on the Applicability of Urban Morphology Index System for Block Natural Ventilation Research. *Procedia Engineering*, 169, 240-247.
- Gao, Y., Yao, R., Li, B., Turkbeyler, E., Luo, Q., & Short, A. (2012). Field studies on the effect of built forms on urban wind environments. *Renewable energy*, 46, 148-154.
- Giedrowicz, M. M. (2015). Parametric Design for Ecological Purposes—Case Studies and Algorithm Examples. *Journal of Sustainable Architecture and Civil Engineering*, 12(3), 75-85.
- Grayson, M., & Garcia, E. (2014, November). Urban Wind: Effects of Structural Geometry. In *ASME 2014 International Mechanical Engineering Congress and Exposition*. American Society of Mechanical Engineers.
- Grieser, B., Sunak, Y., & Madlener, R. (2015). Economics of small wind turbines in urban settings: An empirical investigation for Germany. *Renewable Energy*, 78, 334-350.
- Grimmond, C. S. B., & Oke, T. R. (1999). Aerodynamic properties of urban areas derived from analysis of surface form. *Journal of applied meteorology*, 38(9), 1262-1292.
- Gsänger, S., & Pitteloud, J. (2014). Small Wind World Report 2014, WWEA.
- Günel, M. H., & Ilgin, H. E. (2014). Tall Buildings: Structural Systems and Aerodynamic Form. Routledge.
- Günel, M. H., Ilgin, H. E., & Sorguç, A. G. (2007). *Rüzgar Enerjisi ve Bina Tasarımı*. ODTÜ Mimarlık Fakültesi

- Hajra, B. (2015). Modelling of Buoyancy Driven Flows along a Building Wall in an Urban Environment. *International Journal*, 3(1), 1-15.
- Hamaina, R., Leduc, T., & Moreau, G. (2012). Towards urban fabrics characterization based on buildings footprints. In *Bridging the Geographic Information Sciences* (pp. 327-346). Springer Berlin Heidelberg.
- Hamby, D. M. (1994). A review of techniques for parameter sensitivity analysis of environmental models. *Environmental monitoring and assessment*, 32(2), 135-154.
- Hang, J., Luo, Z., Sandberg, M., & Gong, J. (2013). Natural ventilation assessment in typical open and semi-open urban environments under various wind directions. *Building and environment*, 70, 318-333.
- Hanlon, D. (2009). *Compositions in architecture*. John Wiley & Sons.
- Hau, E. (2013). *Wind turbines: fundamentals, technologies, application, economics*. Springer.
- Hemsath, T. L., & Bandhosseini, K. A. (2015). Sensitivity analysis evaluating basic building geometry's effect on energy use. *Renewable Energy*, 76, 526-538.
- Henn, A., Römer, C., Gröger, G., & Plümer, L. (2012). Automatic classification of building types in 3D city models. *GeoInformatica*, 16(2), 281-306.
- Hils, D. D. (1992). Visual languages and computing survey: Data flow visual programming languages. *Journal of Visual Languages & Computing*, 3(1), 69-101.
- Ho, Y. K., & Liu, C. H. (2017). A wind tunnel study of flows over idealised urban surfaces with roughness sublayer corrections. *Theoretical and Applied Climatology*, 130(1-2), 305-320.
- Ho, Y. K., Liu, C. H., & Wong, M. S. (2015). Preliminary study of the parameterisation of street-level ventilation in idealised two-dimensional simulations. *Building and*

Environment, 89, 345-355.

- Houda, S., Zemmouri, N., Athmani, R., & Belarbi, R. (2011). Effect of urban morphology on wind flow distribution in dense urban areas. *Revue des Energies Renouvelables*, 14(1), 85-94.
- Huang, Y., Hu, X., & Zeng, N. (2009). Impact of wedge-shaped roofs on airflow and pollutant dispersion inside urban street canyons. *Building and Environment*, 44(12), 2335-2347.
- IBM Knowledge Center. (n.d.). Simulation. Retrieved January 8, 2018, from https://www.ibm.com/support/knowledgecenter/en/SSLVMB_22.0.0/com.ibm.spss.statistics.help/spss/base/simulation.htm
- Iqbal, Q. M. Z., & Chan, A. L. S. (2016). Pedestrian level wind environment assessment around group of high-rise cross-shaped buildings: Effect of building shape, separation and orientation. *Building and Environment*, 101, 45-63.
- Irwin, P., Kilpatrick, J., Robinson, J., & Frisque, A. (2008). Wind and tall buildings: negatives and positives. *The structural design of tall and special buildings*, 17(5), 915-928.
- Ishugah, T. F., Li, Y., Wang, R. Z., & Kiplagat, J. K. (2014). Advances in wind energy resource exploitation in urban environment: A review. *Renewable and sustainable energy reviews*, 37, 613-626.
- Janssen, P. A. T. R. I. C. K., & Stouffs, R. U. D. I. (2015). Types of parametric modelling. In *Proc. 20th Int. Conf. Computer-Aided Architectural Design Research in Asia (CAADRRIA 2015)* (pp. 157-166).
- Janssen, W. D., Blocken, B., & van Hooff, T. (2013). Pedestrian wind comfort around buildings: Comparison of wind comfort criteria based on whole-flow field data for a complex case study. *Building and Environment*, 59, 547-562.
- Jesson, M., Sterling, M., Letchford, C., & Baker, C. (2015). Aerodynamic forces on the roofs of low-, mid-and high-rise buildings subject to transient winds. *Journal*

- of Wind Engineering and Industrial Aerodynamics*, 143, 42-49.
- Kaldellis, J. K., Zafirakis, D., Kondili, E., & Papapostolou, C. (2012). Trends, prospects and R&D directions of the global wind energy sector. *Proceedings of EWEA 2012 Annual Event*.
- Kanda, M., Inagaki, A., Miyamoto, T., Gryscha, M., & Raasch, S. (2013). A new aerodynamic parametrization for real urban surfaces. *Boundary-layer meteorology*, 148(2), 357-377.
- Karava, P., & Stathopoulos, T. (2011). Wind-induced internal pressures in buildings with large façade openings. *Journal of Engineering Mechanics*, 138(4), 358-370.
- Kelly, T., & Wonka, P. (2011). Interactive architectural modeling with procedural extrusions. *ACM Transactions on Graphics (TOG)*, 30(2), 14.
- Kleijnen, J. P. (1992). Sensitivity analysis of simulation experiments: regression analysis and statistical design. *Mathematics and Computers in Simulation*, 34(3-4), 297-315.
- Kolarevic, B. (2004). Digital Morphogenesis. In B. Kolarevic (Ed.), *Architecture in the digital age: design and manufacturing*. Taylor & Francis.
- Kosutova, K., van Hooff, T., Blocken, B., & Hensen, J. L. M. (2015, May). CFD analysis of ventilative cooling in a generic isolated building equipped with ventilation louvers. In *Proceedings of Healthy Buildings 2015 Europe* (pp. 1-8).
- Krier, R., & Vorreiter, G. (1988). *Architectural composition* (Vol. 10). New York: Rizzoli.
- Kropf, K. (2009). Aspects of urban form. *Urban Morphology*, 13(2), 105.
- Kunze, A., Dyllong, J., Halatsch, J., Waddell, P., & Schmitt, G. (2012). Parametric building typologies for San Francisco Bay Area: A conceptual framework for the implementation of design code building typologies towards a parametric procedural city model, in *Digital Physicality - 30th eCAADe Conference*.

- Kwon, D. K., Kijewski-Correa, T., & Kareem, A. (2008). e-Analysis of high-rise buildings subjected to wind loads. *Journal of Structural Engineering*, 134(7), 1139-1153.
- Ledo, L., Kosasih, P. B., & Cooper, P. (2011). Roof mounting site analysis for micro-wind turbines. *Renewable Energy*, 36(5), 1379-1391.
- Li, B., Liu, J., & Gao, J. (2015). Surface wind pressure tests on buildings with various non-uniformity morphological parameters. *Journal of Wind Engineering and Industrial Aerodynamics*, 137, 14-24.
- Li, B., Liu, J., & Li, M. (2013). Wind tunnel study on the morphological parameterization of building non-uniformity. *Journal of Wind Engineering and Industrial Aerodynamics*, 121, 60-69.
- Li, B., Luo, Z., Sandberg, M., & Liu, J. (2015). Revisiting the 'venturi effect' in passage ventilation between two non-parallel buildings. *Building and Environment*, 94, 714-722.
- Lin, M., Hang, J., Li, Y., Luo, Z., & Sandberg, M. (2014). Quantitative ventilation assessments of idealized urban canopy layers with various urban layouts and the same building packing density. *Building and Environment*, 79, 152-167.
- Lin, S. H., & Gerber, D. J. (2014). Evolutionary energy performance feedback for design: Multidisciplinary design optimization and performance boundaries for design decision support. *Energy and Buildings*, 84, 426-441.
- Liu, C. H., Ng, C. T., & Wong, C. C. (2015). A theory of ventilation estimate over hypothetical urban areas. *Journal of hazardous materials*, 296, 9-16.
- Local Wind Resource Assessment and Energy Analysis. (n.d.). Retrieved June 21, 2017, from <https://www.wind-energy-the-facts.org/introduction-2.html>
- Marshall, S., & Çalişkan, O. (2011). A joint framework for urban morphology and design. *Built Environment*, 37(4), 409-426.

- Mathew, S. (2006). *Wind energy: fundamentals, resource analysis and economics* (Vol. 1). Heidelberg: Springer.
- Mertens, S. (2002). Wind energy in urban areas: Concentrator effects for wind turbines close to buildings. *Refocus*, 3(2), 22-24.
- Mertens, S. (2005). Wind energy in the built environment. In keynote on the 1st SWH International Conference, Segovia (Spain).
- Mertens, S. (2006). Wind Energy in the Built Environment. *Wind Engineering*, 26(3), 125–143.
- Millward-Hopkins, J. T., Tomlin, A. S., Ma, L., Ingham, D. B., & Pourkashanian, M. (2013). Assessing the potential of urban wind energy in a major UK city using an analytical model. *Renewable Energy*, 60, 701-710.
- Millward-Hopkins, J. T., Tomlin, A. S., Ma, L., Ingham, D., & Pourkashanian, M. (2011). Estimating aerodynamic parameters of urban-like surfaces with heterogeneous building heights. *Boundary-layer meteorology*, 141(3), 443-465.
- Montazeri, H., & Blocken, B. (2013). CFD simulation of wind-induced pressure coefficients on buildings with and without balconies: validation and sensitivity analysis. *Building and Environment*, 60, 137-149.
- Mooney, C. Z. (1993). Monte Carlo Simulation. *Computers in Physics* (Vol. 7).
- Moriarty, M. (2010). *Feasibility of small-scale urban wind energy generation* (Doctoral dissertation, University of Pittsburgh).
- Moussavi, F., & Lopez, D. (2009). *The function of form*. Actar.
- Müller, P., Wonka, P., Haegler, S., Ulmer, A., & Van Gool, L. (2006). Procedural modeling of buildings. In *Acm Transactions On Graphics (Tog)* (Vol. 25, No. 3, pp. 614-623). ACM.
- Myers, B. A. (1986). Visual programming, programming by example, and program visualization: a taxonomy. In *ACM SIGCHI Bulletin* (Vol. 17, No. 4, pp. 59-66).

ACM.

- Nault, E., Moonen, P., Rey, E., & Andersen, M. (2017). Predictive models for assessing the passive solar and daylight potential of neighborhood designs: A comparative proof-of-concept study. *Building and Environment*, *116*, 1-16.
- Ng, E., Yuan, C., Chen, L., Ren, C., & Fung, J. C. (2011). Improving the wind environment in high-density cities by understanding urban morphology and surface roughness: a study in Hong Kong. *Landscape and Urban planning*, *101*(1), 59-74.
- Nguyen, A. T., Reiter, S., & Rigo, P. (2014). A review on simulation-based optimization methods applied to building performance analysis. *Applied Energy*, *113*, 1043-1058.
- Nyhart, L. K. (1995). *Biology takes form: Animal morphology and the German universities, 1800-1900*. University of Chicago Press.
- Ozmen, Y., Baydar, E., & Van Beeck, J. P. A. J. (2016). Wind flow over the low-rise building models with gabled roofs having different pitch angles. *Building and Environment*, *95*, 63-74.
- Özdemir, B., & Önal, F. (2016). Sequential Form Formation Diagrams in Architectural Design. *MEGARON*, *11*(2), 230–240.
- Parish, Y. I., & Müller, P. (2001, August). Procedural modeling of cities. In *Proceedings of the 28th annual conference on Computer graphics and interactive techniques* (pp. 301-308). ACM.
- Perén, J. I., van Hooff, T., Leite, B. C. C., & Blocken, B. (2015). CFD analysis of cross-ventilation of a generic isolated building with asymmetric opening positions: Impact of roof angle and opening location. *Building and Environment*, *85*, 263–276.
- Peren, J. I., van Hooff, T., Ramponi, R., Blocken, B., & Leite, B. C. C. (2015). Impact of roof geometry of an isolated leeward sawtooth roof building on cross-

ventilation: Straight, concave, hybrid or convex? *Journal of Wind Engineering and Industrial Aerodynamics*, 145, 102–114.

Pisello, A. L., Taylor, J. E., & Cotana, F. (2013, December). Simulating the effect of urban morphology on indoor thermal behavior: an Italian case study. In *Proceedings of the 2013 Winter Simulation Conference: Simulation: Making Decisions in a Complex World* (pp. 2008-2019). IEEE Press.

Ramponi, R., & Blocken, B. (2012). CFD simulation of cross-ventilation flow for different isolated building configurations: validation with wind tunnel measurements and analysis of physical and numerical diffusion effects. *Journal of Wind Engineering and Industrial Aerodynamics*, 104, 408-418.

Ramponi, R., Blocken, B., Laura, B., & Janssen, W. D. (2015). CFD simulation of outdoor ventilation of generic urban configurations with different urban densities and equal and unequal street widths. *Building and Environment*, 92, 152-166.

Requicha, A. A. (1980). Representations of rigid solid objects. In *Computer Aided Design Modelling, Systems Engineering, CAD-Systems* (pp. 1-78). Springer, Berlin, Heidelberg.

Richards, R. J. (2008). *The tragic sense of life: Ernst Haeckel and the struggle over evolutionary thought*. University of Chicago Press.

Roudsari, M. S., Pak, M., & Smith, A. (2013, August). Ladybug: a parametric environmental plugin for grasshopper to help designers create an environmentally-conscious design. In *Proceedings of the 13th international IBPSA conference held in Lyon, France Aug.*

Sari, D. P. (2015). Measurement of the Influence of Roof Pitch to Increasing Wind Power Density. *Energy Procedia*, 65, 42–47.

Sari, D. P., & Cho, K. P. (2014). CFD and Wind Tunnel Analysis for Mounted-Wind Turbine in a Tall Building for Power Generation. *Journal of Mechatronics, Electrical Power, and Vehicular Technology*, 5(1), 45-50.

- Schroth, O., & Ju, Q. (2016, June). Modelling microclimates in the smart city: A campus case study on natural ventilation. In *Proceedings of 21st International Conference on Urban Planning, Regional Development and Information Society* (pp. 473-479).
- Shetabivash, H. (2015). Investigation of opening position and shape on the natural cross ventilation. *Energy and Buildings*, 93, 1-15.
- Shu, N. C. (1988, January). A visual programming language designed for automatic programming. In *System Sciences, 1988. Vol. II. Software Track, Proceedings of the Twenty-First Annual Hawaii International Conference on* (Vol. 2, pp. 662-671). IEEE.
- Smith, J., Forsyth, T., Sinclair, K., & Oteri, F. (2012). *Built-environment wind turbine roadmap* (No. NREL/TP-5000-50499). National Renewable Energy Lab. (NREL), Golden, CO (United States).
- Stankovic, S., Campbell, N., & Harries, A. (2009). *Urban wind energy*. Routledge.
- Stathopoulos, T. (2007). *Wind Effects on Buildings and Structures. Nature (Vol. 199)*. Springer
- Stathopoulos, T. (1985). Wind environmental conditions around tall buildings with chamfered corners. *Journal of Wind Engineering and Industrial Aerodynamics*, 21(1), 71-87.
- Stathopoulos, T., & Blocken, B. (2016). Pedestrian wind environment around tall buildings. In *Advanced Environmental Wind Engineering* (pp. 101-127). Springer, Tokyo.
- Stathopoulos, T., Zisis, I., & Wang, K. Terrain classification and exposure factor in the 2005 National Building Code of Canada.
- Steadman, J. P. (1994). Built forms and building types: some speculations. *Environment and Planning B: Planning and Design*, 21(7), S7-S30.

- Steadman, P. (2014). *Building types and built forms*. Troubador Publishing Ltd.
- Steadman, P., Bruhns, H. R., Holtier, S., Gakovic, B., Rickaby, P. A., & Brown, F. E. (2000). A classification of built forms. *Environment and Planning B: Planning and Design*, 27(1), 73–91
- Steiniger, S., Lange, T., Burghardt, D., & Weibel, R. (2008). An approach for the classification of urban building structures based on discriminant analysis techniques. *Transactions in GIS*, 12(1), 31-59.
- Stewart, S. W., Haupt, S. E., & Cole, J. A. (2011, January). Assessing Wind Resource Potential in the Built Environment. In *ASME 2011 5th International Conference on Energy Sustainability* (pp. 2223-2235). American Society of Mechanical Engineers.
- Stiny, G. (1980). Introduction to shape and shape grammars. *Environment and planning B: planning and design*, 7(3), 343-351..
- Summerfield, M. A. (2014). *Global geomorphology*. Routledge.
- Szalay, Z. (2008). Modelling building stock geometry for energy, emission and mass calculations. *Building Research & Information*, 36(6), 557-567.
- Tablada, A., De Troyer, F., Blocken, B., Carmeliet, J., & Verschure, H. (2009). On natural ventilation and thermal comfort in compact urban environments—the Old Havana case. *Building and Environment*, 44(9), 1943-1958.
- Taleghani, M., Kleerekoper, L., Tenpierik, M., & van den Dobbelen, A. (2015). Outdoor thermal comfort within five different urban forms in the Netherlands. *Building and environment*, 83, 65-78.
- Tamura, Y., Xu, X., Tanaka, H., Kim, Y. C., Yoshida, A., & Yang, Q. (2017). Aerodynamic and Pedestrian-Level Wind Characteristics of Super-Tall Buildings with Various Configurations. *Procedia Engineering*, 199, 28-37.
- Tedeschi, A., (2014). AAD, Algorithms-aided Design: Parametric Strategies Using

Grasshopper. Le penseur.

Terzidis, K. (2006). *Algorithmic architecture*. Routledge

Toja-Silva, F., Colmenar-Santos, A., & Castro-Gil, M. (2013). Urban wind energy exploitation systems: Behaviour under multidirectional flow conditions— Opportunities and challenges. *Renewable and Sustainable Energy Reviews*, 24, 364-378.

Tominaga, Y., Akabayashi, S. I., Kitahara, T., & Arinami, Y. (2015). Air flow around isolated gable-roof buildings with different roof pitches: Wind tunnel experiments and CFD simulations. *Building and Environment*, 84, 204-213.

Tominaga, Y., & Blocken, B. (2016). Wind tunnel analysis of flow and dispersion in cross-ventilated isolated buildings: Impact of opening positions. *Journal of Wind Engineering and Industrial Aerodynamics*, 155, 74-88.

Tominaga, Y., & Stathopoulos, T. (2010). Numerical simulation of dispersion around an isolated cubic building: model evaluation of RANS and LES. *Building and Environment*, 45(10), 2231–2239.

Tooke, T. R., Van der Laan, M., Coops, N., Christen, A., & Kellett, R. (2011). Classification of residential building architectural typologies using LiDAR. In *2011 Joint Urban Remote Sensing Event, JURSE 2011 - Proceedings* (pp. 221–224). IEEE.

Tulloch, D. (2017). Toward a working taxonomy of geodesign practice. *Transactions in GIS*, 21(4), 635-646.

Turan, S., Peacock, A. D., & Newborough, M. (2007). Micro and small wind turbine applications in the built environment. *ISESCO Science and Technology Vision*, 3(3), 106-110.

UN Commission on Sustainable Development. (2007). Climate Change, Statement by Brian Williams, Chief Energy and Transport Section. Retrieved from https://sustainabledevelopment.un.org/content/documents/habitat_2may_cc.pdf

- van Hooff, T., & Blocken, B. (2010). Coupled urban wind flow and indoor natural ventilation modelling on a high-resolution grid: A case study for the Amsterdam ArenA stadium. *Environmental Modelling & Software*, 25(1), 51–65.
- van Hooff, T., Blocken, B., Aanen, L., & Bronsema, B. (2012). Numerical analysis of the performance of a venturi-shaped roof for natural ventilation: influence of building width. *Journal of Wind Engineering and Industrial Aerodynamics*, 104, 419–427.
- van Hooff, T., Blocken, B., & Tominaga, Y. (2017). On the accuracy of CFD simulations of cross-ventilation flows for a generic isolated building: comparison of RANS, LES and experiments. *Building and Environment*, 114, 148-165.
- Varapaev, V. N., & Doroshenko, A. V. (2014). Methodology for the prediction and the assessment of pedestrian wind environment around buildings. *Procedia Engineering*, 91, 200-203.
- Wen, C. Y., Juan, Y. H., & Yang, A. S. (2017). Enhancement of city breathability with half open spaces in ideal urban street canyons. *Building and Environment*, 112, 322-336.
- Wheeler, S. M. (2008). The evolution of built landscapes in metropolitan regions. *Journal of Planning Education and Research*, 27(4), 400–416.
- Wurm, M., Schmitt, A., & Taubenböck, H. (2016). Building types' classification using shape-based features and linear discriminant functions. *IEEE Journal of Selected Topics in Applied Earth Observations and Remote Sensing*, 9(5), 1901-1912.
- Yuan, C., & Ng, E. (2012). Building porosity for better urban ventilation in high-density cities—A computational parametric study. *Building and Environment*, 50, 176-189.
- Zhang, W., Lv, X. C., & Zhang, D. X. (2012). Numerical Study of Wind Flow around Two High-Rise Buildings in Tandem Arrangement Using Lattice Boltzmann Method. In *Applied Mechanics and Materials* (Vol. 174, pp. 3069-3073). Trans

Tech Publications.

- Zhang, W., Zhang, Y., Li, Z., Zheng, Z., Zhang, R., & Chen, J. (2017). A rapid evaluation method of existing building applied photovoltaic (BAPV) potential. *Energy and Buildings*, 135, 39-49
- Zhang, Y., Gu, Z., Wang, Z., Cheng, Y., & Lee, F. S. (2013). Advances in the fine scale simulation of urban wind environment. *Indoor and Built Environment*, 22(1), 332-336.
- Zheng, S., Xiong, X., Vause, J., & Liu, J. (2013). Real-time measurement of wind environment comfort in urban areas by Environmental Internet of Things. *International Journal of Sustainable Development & World Ecology*, 20(3), 254-260.
- Zhi, L. H., Fang, M. X., & Li, Q. S. (2017). Estimation of wind loads on a tall building by an inverse method. *Structural Control and Health Monitoring*, 24(4).
- Zisis, I., & Stathopoulos, T. (2012). Wind load transfer mechanisms on a low wood building using full-scale load data. *Journal of Wind Engineering and Industrial Aerodynamics*, 104, 65-75.

APPENDIX A

PARAMETERS FROM LITERATURE SURVEY

A.1 Survey of Parameters in Wind Flow Studies

Table 37: Parameters from wind flow studies based on reference source.

Reference source	Number of samples	Definition of samples	Method of study	Parameters (Variables)
(Zhi, Fang, & Li, 2017)	1 form	Square shaped tall building	CFD equations	Height
(Ai & Mak, 2017)	6 formations	Parallel arrangements of longitudinal low-rise blocks in differing lengths	CFD simulations	Length of blocks Number of blocks
(Zahid Iqbal & Chan, 2016)	4 formations	cross-shaped high-rise building models in decreased level of detail from real case	Wind tunnel tests	incident angle passage width building separations Number of buildings
(Tamura et al., 2017)	40 forms	Super-tall building models resulted from combinations of form type classes	Wind tunnel tests	Form category
			Wind induced response analysis	Form type
(Tominaga & Blocken, 2016)	5 forms	five generic isolated single-zone buildings with different opening positions	Wind tunnel tests	Opening position (as inlet and outlet)
(Ozmen et al., 2016)	3 forms	Three models with different roof angles	Wind tunnel tests	Roof angle
(T. van Hooff, Blocken, & Tominaga, 2016)	1 form	Generic cubic form with an opening	CFD simulations	Simulation method
			Wind tunnel tests	
(Aihara, Uzunoglu, & Goude, 2016)	2 forms	Case buildings and their digital models	CFD simulations	None
			Field measurements	
(Cóstola, Blocken, Ohba, & Hensen, 2010)	10 forms	Same building with 10 different inflow opening types	CFD simulations	Opening (window) types
			Wind tunnel tests	

Table 37 (continued)

Reference source	Number of samples	Definition of samples	Method of study	Parameters (Variables)
(Blocken, Stathopoulos, & van Beeck, 2016)	9 forms	Same building modified with 8 design features, also with a case study	Knowledge based definitions	Positioning of opening through
			Wind tunnel tests	Ground floor setback
			CFD simulations	Podium size
Height				
(Hajra, 2015)	3 formations	Same building tested in different arrangements and orientations	Wind tunnel tests	Orientation
				Number of buildings
				Adjacency
(Peren, van Hooff, Ramponi, Blocken, & Leite, 2015)	3 forms	Same building with 3 different saw tooth roof geometry	CFD simulations	Roof concavity
(Ledo et al., 2011)	3 forms	3 roof types arranged in same formation on 12 identical low rise buildings	CFD simulations	Roof type
(Cai, Zhao, & Liu, 2015)	1 form	Digital 3D Model of a real building in a moderate level of detail	CFD simulations	Distance above roof
(Shetabivash, 2015)	8 forms	Digital model of a generic single floor building with opening variations	CFD simulations	Opening position
				Opening shape
(Jesson, Sterling, Letchford, & Baker, 2015)	11 forms	11 combinations of 3 generic form parameters	Wind tunnel tests	Footprint size (L/W ratio)
				Building height
				Roof ridge height
(Taleghani, Kleerekoper, Tenpierik, & Dobbelsteen, 2015)	3 forms, 10 formations	3 types of prismatic solids in 10 different formations	Flow simulations	Footprint size
				Building number
				Formation type
				Orientation
(Sari, 2015)	4 forms	4 models derived from altering the roof surface angle of a generic cubic building model	CFD simulations	Roof slope
(Chaudhry, Calautit, & Hughes, 2015)	1 form	Model of a real building with a mesh approximation	CFD simulations	None
(Perén, van Hooff, Leite, & Blocken, 2015)	3 forms	Surface Model of a generic single volume building with altering position of inlet, outlet and roof slope	CFD simulations	Position of window openings
			Wind tunnel tests	Roof slope

Table 37 (continued)

Reference source	Number of samples	Definition of samples	Method of study	Parameters (Variables)
(Kosutova, Hooff, Blocken, & Hensen, 2015)	4 forms	Same generic building solid model with 4 different versions of window louvers	CFD simulations	Window louver angle
(Tominaga, Akabayashi, Kitahara, & Arinami, 2015).	3 forms	Solid model with 3 different roof slopes	CFD simulations	Roof pitch
(Biao Li, Luo, Sandberg, & Liu, 2015)).	14 formations	14 formations by changing the orientation of a couple longitudinal buildings	CFD simulations	Orientation
(Biao Li, Liu, et al., 2015)	5 formations	Various formations of 2 different generic forms extruded on 2 footprint types	Wind tunnel tests	Building footprint type
			CFD simulations	Pattern density Pattern regularity
(Sari & Cho, 2014)	3 forms	3 solid models of the same tall building with differing roof geometries	Wind tunnel tests	Roof edge roundness
(Varapaev & Doroshenko, 2014)	1 formation	A real city with surroundings and its digital model with low level of detail	CFD simulations	None
			Wind tunnel tests	
			Field measurements	
(Kanda et al., 2013)	3 formations	3D models of real urban areas of 1000x1000m boundary, in 2m resolution	CFD simulations	Average building height
				Frontal area index
				Plane area index
(Pisello, Taylor, & Cotana, 2013)	3 forms	Digital models of 3 existing buildings	CFD simulations	Surrounding urban density
				Average building height
(W. D. Janssen, Blocken, & van Hooff, 2013)	3 forms	Real building and its digital model with 3 different canopy size	Field measurements	Canopy size
			CFD simulations	Canopy height
(Montazeri & Blocken, 2013)	2 forms	A prismatic solid with and without surface projections shaped like balcony	CFD simulations	Facade projections
(Hang, Luo, Sandberg, & Gong, 2013)	3 formations	40 generic models with various combinations of street covers	Wind tunnel tests	Eave size (Street cover ratio)
Janssen, W. D., Blocken, B., & van Hooff, T. (2013).	1 formation	1 digital solid model in low detail of a selected case of building complex	CFD simulations	None

Table 37 (continued)

Reference source	Number of samples	Definition of samples	Method of study	Parameters (Variables)
(B Li, Liu, & Li, 2013)	2 forms, 5 formations	5 models of generic urban areas with two types of solids in differing arrangements	Wind tunnel tests	Footprint shape
				Regularity
				Compactness
(R. Ramponi & Blocken, 2012)	4 forms	2 cube solids with different opening sizes and locations	CFD simulations	Opening size
			Wind tunnel tests	Opening location
(W Zhang et al., 2012)	1 form	1 digital model of a building with two tall parts	CFD simulations	None
(Zisis & Stathopoulos, 2012)	1 form	Real building	Field measurements	None
(Twan van Hooff, Blocken, Aanen, & Bronsema, 2012)	5 forms	Generic solid building model with a "Venturi shaped" roof design	CFD simulations	Building width (windward dimension)
(Gao et al., 2012)	6 forms	6 real buildings representing generic types	Field measurements	Building layout types
(Yuan & Ng, 2012).	9 forms	9 generic street models with building solids defined by parameters based on a real city	CFD simulations	Street grid orientation
				Mean building height
				Site coverage ratio
(Karava & Stathopoulos, 2011)	8 forms	Hollow cube models with different opening conditions	Wind tunnel tests	Wall porosity
				Inlet / outlet ratio
				Opening positions
(Babsail, 2011)	16 forms	Digital and physical solid models of 16 real tall buildings	Wind tunnel tests	Footprint shape
			CFD simulations	Height
				Tower number
(Millward-Hopkins et al., 2011)	18 formations	18 physical models with different size and arrangement of prismatic solids	Wind tunnel tests	Surface area density
				Building height variability
(T Van Hooff & Blocken, 2010)	1 form	Digital model of a real building	CFD simulations	None
(Tominaga & Stathopoulos, 2010)	1 form	Digital model of a solid cube	CFD simulations	None
(B. Chen, Li, Feng, Zhang, & Zhang, 2009)	4 forms	4 digital models of solids	CFD simulations	Type of footprint shape
				Concavity of footprint
(Huang et al., 2009)	2 forms, 16 formations	16 digital models including linear arrangements of 2 solids types	CFD simulations	Roof type
			Wind tunnel tests	Sequence of buildings

Table 37 (continued)

Reference source	Number of samples	Definition of samples	Method of study	Parameters (Variables)
(Kwon, Kijewski-Correa, & Kareem, 2008)	N.A.	A tool for producing structural calculations based on user inputs	Load analysis	Environment type (urban - rural)
				Footprint shape
				Building height
(Irwin et al., 2008)	5 forms	5 physical solid models of real buildings representing generic types	Wind tunnel tests	Corner roundness
				Tapering
				Porosity
				Projections
(Tablada, De Troyer, Blocken, Carmeliet, & Verschure, 2009)	3 forms	3 digital models of clusters with different arrangements of a rectangular solid	CFD simulations	Compactness
				Orientation
(Wen, Juan, & Yang, 2017)	17 formations	17 digital model of generic street sections	CFD simulations	Building height
				Canyon width
				Height of arcade
				Width of arcade
(Schroth & Ju, 2016)	1 formation	Digital model of an university campus in moderate level of detail	Flow simulations	None
(Ho & Liu, 2016)	3 formations	Surface mounted strips to satisfy roughness differences. 3 types in same test.	Wind tunnel tests	Compactness (Proximity)
(Gan & Chen, 2016)	14 formations	2 types of prismatic solids with 5 shape parameters sequenced in grid.	CFD simulations	Footprint shape (as type)
				Spacing differences
				Comprehensive porosity
				Relative rugosity
				Ventilation obstruction
(Carpentieri & Robins, 2015)	3 formations	1 digital model of an existing case compared to 2 modified versions composed of cuboids	Wind tunnel tests	Height variability
			CFD simulations	Building aspect ratio
				Orientation
(Rubina Ramponi, Blocken, Laura, & Janssen, 2015)	3 formations	3 digital models composed of cubic solids in different arrays	CFD simulations	Density
				Street width equality
(Liu, Ng, & Wong, 2015)	18 formations	18 digital models composed of 2 solids from 8 generic types in a grid array	CFD simulations	Building aspect ratio
				Number of street canyons
				Height of roof vertex

Table 37 (continued)

(Ho, Liu, & Wong, 2015)	8 formations	Idealised roughness models by infinite extrusion from data of 8 real city sections.	CFD simulations	Average building height
				Height variation
			Wind tunnel tests	Proximity
				Number of street canyons
	Average building aspect ratio			
(Lin, Hang, Li, Luo, & Sandberg, 2014)	14 formations	Various grid based placement of cubic solids with different heights	CFD simulations	Number or building rows
				Total windward length of built area
				Building heights
				Orientation
				Array type
(Dimoudi, Kantzioura, Zoras, Pallas, & Kosmopoulos, 2013)	2 formations	Two streets in a real city.	Field measurements	Case based morphology
(Abd Razak et al., 2013)	6 formations	6 formations of square prism solids in different heights and different arrays	CFD simulations	Height uniformity (variety)
				Compactness of array
				Type of array
(Zheng, Xiong, Vause, & Liu, 2013)	1 formation	1 district from real city	Field measurements	Case based morphology
(Drew, Barlow, & Lane, 2013)	1 formation	LIDAR imagery for 1 city	Satellite imagery	Case based morphology
			LIDAR data	
(Dallman, Sabatino, & Fernando, 2013)	2 formations	Average values gathered from morphometric analysis of real building data.	Data Analysis	Case based morphology
			Field measurements	
(Y. Zhang, Gu, Wang, Cheng, & Lee, 2013)	N.A.	Form analysis based on relevant literature	Literature review	Height of street canyon
				Width of street canyon
				Type of urban layout
				Level of detail
(Houda et al., 2011)	1 formation	Simplified digital solid model of a real city based on building footprints	CFD simulations	Case based morphology
(Ng, Yuan, Chen, Ren, & Fung, 2011)	1 formation	Both digital and physical models of a real city and some generic digital models	CFD simulations	Ground coverage ratio
				Podium height
			Wind tunnel tests	Building height
				Urban canopy height

A.2 UML Diagrams of Reviewed Form Parameters

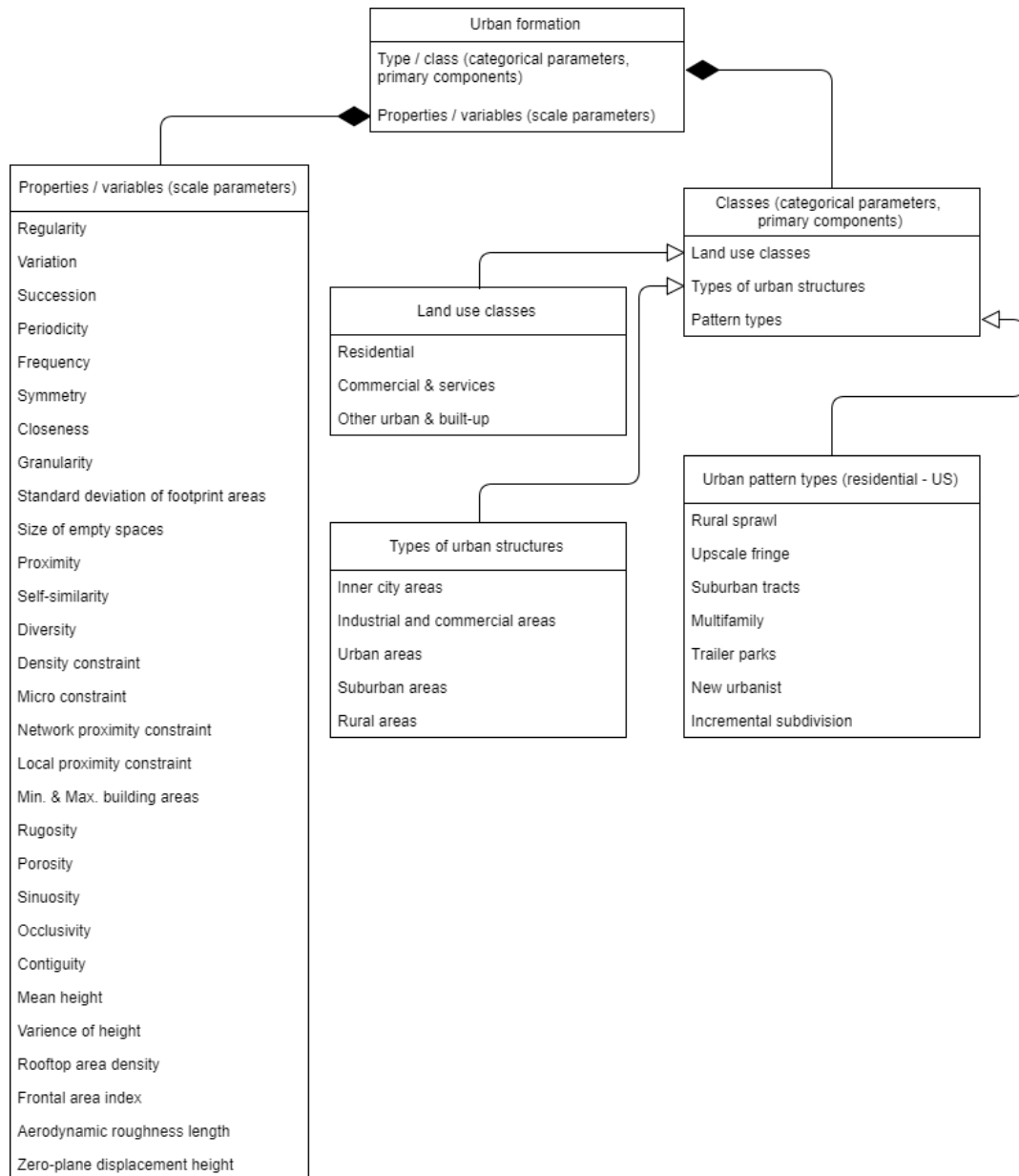


Figure 71: UML diagram showing parameters derived from literature for urban area formation.

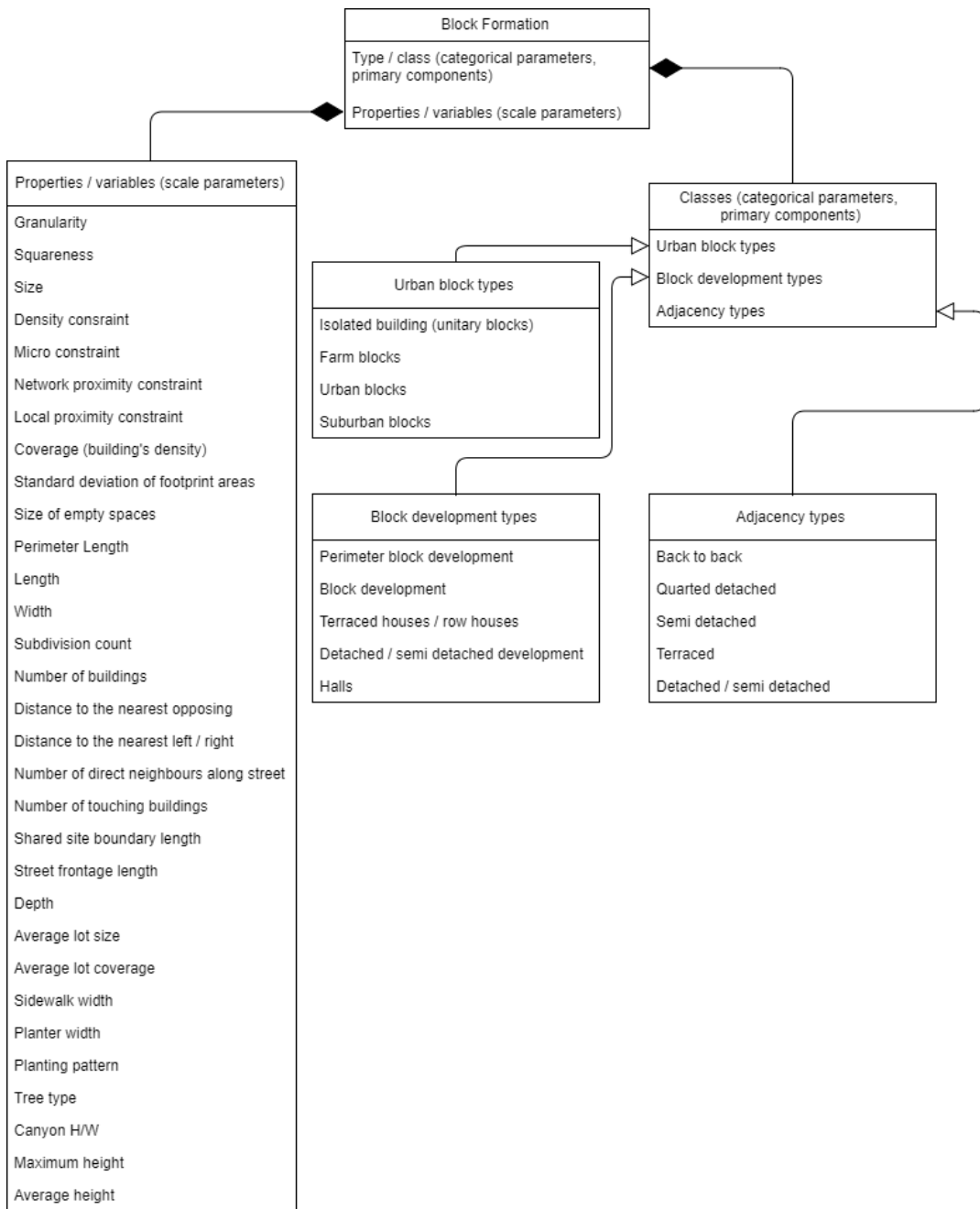


Figure 72: UML diagram showing parameters derived from literature for block formation.

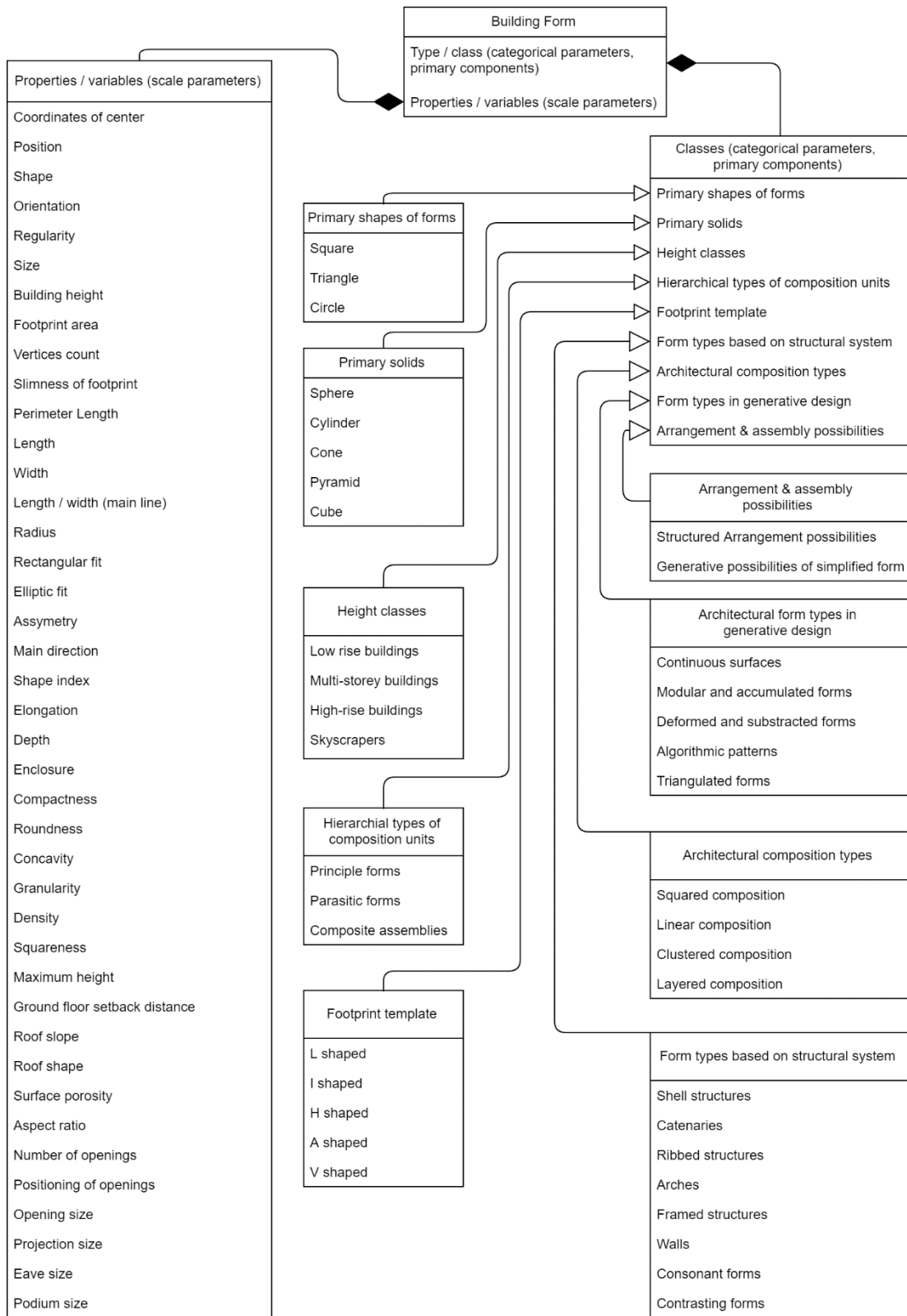


Figure 73: UML diagram showing form parameters derived from literature for building form.

APPENDIX B

PARAMETRIC CONFIGURATION OF SAMPLE MODELS

Table 38: Parametric configuration of sample models for samples 1-10.

Model Parameters	Sample1	Sample2	Sample3	Sample4	Sample5	Sample6	Sample7	Sample8	Sample9	Sample10
TF.X	14	88	57	71	75	68	49	69	19	76
TF.Y	84	81	66	48	93	66	10	35	87	10
TF.Vertice	8	6	5	6	7	4	7	6	6	8
TF.Roundness	0	0,15	0,1	0,2	0,05	0,15	0,05	0,1	0,2	0,1
TF.Irregularity	0,5	0,1	0,3	0,5	0,7	0,4	0,5	0,5	0,5	0,7
H.TotalHeight	96	86	42	11	71	59	43	6	18	36
B.HeightRatio	0,25	0	0,25	0,05	0,1	0,4	0,2	0,4	0,15	0,25
B.X.Ratio	2	2	2	4,9	4,5	3,3	4,1	4,5	2,5	2,8
B.Y.Ratio	2,3	1,6	2,7	4,8	2,6	1,6	1,8	2,9	3,1	3,6
SC.DOC	1	2	2	2	2	2	2	1	3	4
SC.SHR	0,13	0,15	0,03	0,12	0,14	0,09	0,1	0,05	0,08	0,12
SC.VHR	0,15	0,1	0,35	0,25	0,2	0,25	0,15	0,25	0,2	0,25
SC.VPR	1	0	0,7	0,6	0,8	0,5	0,5	0,1	0,5	0,5
SC.SDRF	0,05	0,1	0,05	0,3	0,4	0,2	0,1	0,05	0,15	0,35
SC.FETRF	0,8	0,2	0,1	-0,5	-0,9	-0,5	0,4	-0,6	0	-0,4
SC.CTRF	-0,2	-0,2	0,25	0,05	-0,3	0,05	-0,1	-0,2	-0,1	0,25
SC.EDRF	0,15	0,05	0,2	0,2	0	0,05	0,3	0,05	0,05	0,2
SC.SDRB	0,35	0,1	0,35	0,35	0	0,3	0,3	0,15	0,35	0,1
SC.FETRB	0,6	-0,1	0,1	0,4	0,3	0,5	0,5	-0,7	0,5	-0,9
SC.EDRB	0,15	0,2	0,05	0,3	0,1	0,3	0,15	0,1	0,25	0,15
SC.CTRB	0,25	0,05	0	0,05	0,2	0,2	0,3	0,25	0,1	0,2
S.NormalTapering	0,2	0,9	0,4	0,6	0,6	0,4	1,2	1,8	0,6	0,6
V.Elevation.Ratio	0,9	0,3	0,1	0,3	0,6	0,4	0,7	1,0	0,6	0,5
V.WidthRatio	0,35	0,15	0,20	0,10	0,05	0,35	0,10	0,10	0,15	0,20
V.HeightRatio	0,45	0,05	0,10	0,15	0,10	0,50	0,05	0,45	0,30	0,15

Table 38 (continued)

Model Parameters	Sample11	Sample12	Sample13	Sample14	Sample15	Sample16	Sample17	Sample18	Sample19	Sample20
TF.X	100	89	31	32	98	72	44	76	54	69
TF.Y	46	48	16	81	11	86	82	32	15	36
TF.Vertice	7	6	5	4	5	5	6	5	6	6
TF.Roundness	0,15	0,15	0,15	0,1	0,15	0,1	0,1	0,05	0,05	0,05
TF.Irregularity	0	0,6	0,7	0,5	0,5	0,7	0,4	0,7	0,6	0,7
H.TotalHeight	71	14	91	27	10	72	26	97	84	51
B.HeightRatio	0,35	0,35	0,05	0,05	0,25	0,15	0,1	0,1	0,35	0,15
B.X.Ratio	2,2	2,9	1,9	4,3	2,2	3,6	5	2,1	1,9	1,8
B.Y.Ratio	3,4	4	4,4	4,3	2,4	2,1	3,1	2,3	2,2	4,2
SC.DOC	2	3	3	1	2	3	1	3	3	4
SC.SHR	0,01	0,08	0,08	0,01	0,18	0,04	0,02	0,06	0	0,07
SC.VHR	0,25	0,25	0,15	0,2	0,05	0,35	0,05	0,25	0,1	0
SC.VPR	0,1	0,1	0,1	0,3	0	0,1	0,9	1	0,4	0,4
SC.SDRF	0	0,25	0,15	0,1	0,35	0,4	0	0,35	0,1	0,2
SC.FETRF	0,3	0,6	-0,9	0,1	0,1	0,9	-0,7	-0,4	-0,5	0,1
SC.CTRF	0,1	0,2	-0,3	-0,1	0	0,15	-0,1	-0,2	0,05	-0,2
SC.EDRF	0,1	0,25	0,1	0,25	0,25	0,15	0,05	0,15	0,15	0,15
SC.SDRB	0,35	0,25	0,15	0,25	0,1	0,3	0,3	0,3	0	0,4
SC.FETRB	0,6	-0,9	0,8	-0,6	-0,1	-0,6	0,5	0,9	-0,4	-0,4
SC.EDRB	0,05	0,25	0,25	0,1	0,15	0,1	0,05	0,2	0	0,2
SC.CTRB	0,05	0,2	0,2	0,15	0,2	0,15	0,15	0,25	0,25	0,15
S.NormalTapering	0,8	0,8	1,6	1,6	1,4	1,6	0,2	0,4	1	1,8
V.Elevation.Ratio	0,8	0,5	0,7	0,8	1,0	0,1	0,9	0,3	1,0	0,1
V.WidthRatio	0,20	0,45	0,45	0,50	0,40	0,25	0,45	0,25	0,20	0,20
V.HeightRatio	0,30	0,20	0,50	0,40	0,35	0,20	0,10	0,00	0,40	0,15
TF: Tower Footprint H : Height B: Base V: Void S: Solid SC.DOC : Section Curve. Degree Of Curve SC.SHR: Section Curve. Setback Height Ratio SC.VHR: Section Curve. Vertex Height Ratio SC.VPR: Section Curve. Vertex Positioning Ratio SC.SDRF: Section Curve. Setback Depth Ratio Front SC.FETRF: Section Curve. Facade Endpoint Translation Ratio Front SC.CTRF: Section Curve. Concavity Translation Ratio Front SC.EDRF: Section Curve. Eave Depth Ratio Front SC.SDRB: Section Curve. Setback Depth Ratio Back SC.FETRB: Section Curve. Facade Endpoint Translation Ratio Back SC.EDRB: Section Curve. Eave Depth Ratio Back SC.CTRB: Section Curve. Concavity Translation Ratio Back										

Table 38 (continued)

Model Parameters	Sample21	Sample22	Sample23	Sample24	Sample25	Sample26	Sample27	Sample28	Sample29	Sample30
TF.X	13	40	7	61	14	10	53	33	44	41
TF.Y	90	32	88	36	90	42	26	22	69	8
TF.Vertice	6	5	7	5	8	4	6	7	8	4
TF.Roundness	0,05	0,1	0,15	0,15	0,05	0,05	0	0,05	0,2	0,05
TF.Irregularity	0,7	0,1	0,3	0,4	0,7	0,4	0,4	0	0,1	0,5
H.TotalHeight	35	54	9	43	54	25	60	95	87	71
B.HeightRatio	0,1	0,35	0,3	0,25	0,05	0,35	0,35	0,05	0,4	0,05
B.X.Ratio	1,9	1,6	2,9	2,3	2,3	3,6	1,6	3,1	4,1	1,7
B.Y.Ratio	1,8	2,8	4,3	3,4	1,9	3,1	2,3	4,4	2,6	2,5
SC.DOC	3	3	1	3	1	3	3	2	2	3
SC.SHR	0,19	0,09	0,07	0,08	0,13	0,03	0,1	0,14	0,16	0,1
SC.VHR	0,35	0,2	0,3	0,1	0,4	0,1	0,45	0,4	0,1	0,25
SC.VPR	0,3	0,9	0,7	0,2	0,4	0,5	0,5	0,4	0,1	1
SC.SDRF	0,25	0,25	0,05	0,15	0,3	0,35	0,25	0,25	0,15	0,1
SC.FETRF	0,2	-0,1	0	0	0,5	-0,5	0,8	-0,1	0,9	-0,7
SC.CTRF	-0,1	-0,2	0,15	-0,2	0,2	-0,2	-0,1	-0,2	-0,2	-0,1
SC.EDRF	0,3	0,15	0,15	0,1	0,2	0,1	0,1	0,05	0,25	0,05
SC.SDRB	0,1	0,1	0,2	0,4	0,25	0,25	0,25	0,2	0,15	0,15
SC.FETRB	-0,2	0,2	-0,7	-0,3	-0,5	-0,4	-0,2	0,1	0,2	0,6
SC.EDRB	0,1	0,2	0,05	0,05	0,3	0,15	0,1	0,1	0,25	0,15
SC.CTRB	0,15	0,3	0,3	0,1	0	0,2	0,05	0,3	0,15	0,3
S.NormalTapering	2	2	1,6	0,4	1,8	0,2	1,4	1,2	0,8	1
V.Elevation.Ratio	0,9	0,4	0,7	0,6	0,5	0,6	0,7	0,7	0,3	0,4
V.WidthRatio	0,35	0,10	0,40	0,25	0,30	0,05	0,05	0,35	0,00	0,15
V.HeightRatio	0,05	0,35	0,30	0,20	0,20	0,45	0,00	0,15	0,35	0,00
<p>TF: Tower Footprint H : Height B: Base V: Void S: Solid SC.DOC : Section Curve. Degree Of Curve SC.SHR: Section Curve. Setback Height Ratio SC.VHR: Section Curve. Vertex Height Ratio SC.VPR: Section Curve. Vertex Positioning Ratio SC.SDRF: Section Curve. Setback Depth Ratio Front SC.FETRF: Section Curve. Facade Endpoint Translation Ratio Front SC.CTRF: Section Curve. Concavity Translation Ratio Front SC.EDRF: Section Curve. Eave Depth Ratio Front SC.SDRB: Section Curve. Setback Depth Ratio Back SC.FETRB: Section Curve. Facade Endpoint Translation Ratio Back SC.EDRB: Section Curve. Eave Depth Ratio Back SC.CTRB: Section Curve. Concavity Translation Ratio Back</p>										

Table 38 (continued)

Model Parameters	Sample31	Sample32	Sample33	Sample34	Sample35	Sample36	Sample37	Sample38	Sample39	Sample40
TF.X	83	16	31	60	58	72	22	23	50	25
TF.Y	32	46	19	56	37	41	75	73	92	89
TF.Vertice	7	4	6	5	6	5	6	7	5	7
TF.Roundness	0,2	0,05	0,2	0,1	0,15	0,05	0,15	0,05	0,05	0
TF.Irregularity	0,5	0,5	0,9	0,1	0,3	0,5	0,5	0,5	0,4	0,3
H.TotalHeight	80	16	38	86	54	59	84	48	15	79
B.HeightRatio	0,05	0,25	0,2	0,15	0,15	0,1	0,15	0,35	0,25	0,3
B.X.Ratio	4,6	2,5	3,3	4,1	3,7	4,1	2,9	3,2	3,9	2,4
B.Y.Ratio	2,5	4,4	1,9	4,4	4,7	5	2,1	2,4	4,5	3,1
SC.DOC	1	2	3	2	3	3	3	2	3	2
SC.SHR	0,08	0,19	0,07	0,04	0,11	0,08	0,08	0,04	0,14	0,08
SC.VHR	0,45	0,1	0,3	0,25	0,4	0,35	0,2	0,1	0,2	0,5
SC.VPR	0,1	0,7	0,3	0,9	0,7	0,2	0	0,2	0,7	0,1
SC.SDRF	0	0,25	0,1	0,2	0,1	0,1	0,3	0,1	0,2	0,35
SC.FETRF	1	-0,8	-0,7	0,5	0,4	-0,7	0	0	-0,9	0,1
SC.CTRF	0,05	-0,2	0,25	0,2	0,2	-0,1	-0,1	0,15	0,15	0,1
SC.EDRF	0,15	0,1	0,1	0,2	0,15	0,1	0,05	0,1	0,25	0,15
SC.SDRB	0,35	0,35	0,1	0,1	0,1	0,1	0,1	0,15	0,3	0,4
SC.FETRB	-0,6	-0,4	-0,8	0,9	0,8	-0,2	-0,1	-0,7	0,5	0
SC.EDRB	0,25	0,1	0,1	0,15	0,15	0,15	0,1	0,25	0,25	0,25
SC.CTRB	0,1	0,05	0,1	0,05	0,3	0,05	0,15	0,3	0,05	0,3
S.NormalTapering	0,4	0,2	1,8	1,6	1,4	0,4	1,6	0,4	1,8	0,6
V.Elevation.Ratio	0,8	0,7	0,1	0,0	0,4	1,0	0,6	0,3	0,8	0,7
V.WidthRatio	0,05	0,40	0,10	0,20	0,25	0,15	0,10	0,15	0,10	0,30
V.HeightRatio	0,40	0,30	0,30	0,25	0,15	0,05	0,40	0,30	0,20	0,35
TF: Tower Footprint H : Height B: Base V: Void S: Solid SC.DOC : Section Curve. Degree Of Curve SC.SHR: Section Curve. Setback Height Ratio SC.VHR: Section Curve. Vertex Height Ratio SC.VPR: Section Curve. Vertex Positioning Ratio SC.SDRF: Section Curve. Setback Depth Ratio Front SC.FETRF: Section Curve. Facade Endpoint Translation Ratio Front SC.CTRF: Section Curve. Concavity Translation Ratio Front SC.EDRF: Section Curve. Eave Depth Ratio Front SC.SDRB: Section Curve. Setback Depth Ratio Back SC.FETRB: Section Curve. Facade Endpoint Translation Ratio Back SC.EDRB: Section Curve. Eave Depth Ratio Back SC.CTRB: Section Curve. Concavity Translation Ratio Back										

Table 38 (continued)

Model Parameters	Sample41	Sample42	Sample43	Sample44	Sample45	Sample46	Sample47	Sample48	Sample49	Sample50
TF.X	94	5	44	18	22	43	71	32	74	56
TF.Y	35	28	66	36	61	40	41	38	33	31
TF.Vertice	4	8	5	8	7	4	7	3	6	7
TF.Roundness	0	0,1	0	0,1	0,05	0,1	0,1	0,15	0,15	0,15
TF.Irregularity	0,3	0,3	0,6	0,6	0,7	0,3	0,5	0,1	0,8	0,3
H.TotalHeight	59	35	90	70	15	52	10	62	69	10
B.HeightRatio	0,25	0,3	0,1	0,05	0,3	0,1	0,05	0,4	0,3	0,4
B.X.Ratio	4,4	2,6	4,9	1,7	1,6	4,3	2,4	2	3,4	4,5
B.Y.Ratio	3,2	2,6	2	4,9	2,3	3	3,3	1,7	3,8	1,8
SC.DOC	3	4	2	2	2	2	2	4	2	3
SC.SHR	0,15	0,14	0,06	0,04	0,08	0,19	0,17	0,12	0,12	0,16
SC.VHR	0,45	0,35	0,1	0,35	0,1	0,3	0,45	0,1	0,5	0,4
SC.VPR	0,1	0,3	0,3	0,5	0,5	0,2	0,8	0,6	0,6	0,3
SC.SDRF	0,05	0,3	0,05	0,1	0,05	0,1	0,25	0,1	0,4	0
SC.FETRF	-0,3	-0,3	-0,6	-0,6	-0,7	0,2	-1	0	0,9	-0,2
SC.CTRF	-0,1	0,1	-0,1	0	0,1	0,05	0,15	-0,2	-0,2	-0,1
SC.EDRF	0,15	0,15	0,2	0,1	0,2	0,05	0,05	0,1	0,15	0,2
SC.SDRB	0,15	0	0,15	0,15	0,05	0,3	0,05	0,4	0,15	0,25
SC.FETRB	0,8	0,9	0,9	0,5	1	-0,6	0,3	0,8	-0,7	0,2
SC.EDRB	0,05	0,15	0,25	0,15	0,15	0,1	0,15	0,05	0,1	0,05
SC.CTRB	0,25	0,05	0,25	0,25	0,15	0,1	0,1	0,1	0	0,1
S.NormalTapering	1	0,2	1,6	0,6	2	2	1,6	1	1,2	1,8
V.Elevation.Ratio	0,6	1,0	0,7	0,6	0,9	0,8	0,4	0,9	0,8	0,2
V.WidthRatio	0,10	0,30	0,10	0,40	0,30	0,40	0,40	0,00	0,45	0,40
V.HeightRatio	0,20	0,25	0,40	0,20	0,20	0,25	0,10	0,10	0,25	0,15
<p>TF: Tower Footprint H : Height B: Base V: Void S: Solid SC.DOC : Section Curve. Degree Of Curve SC.SHR: Section Curve. Setback Height Ratio SC.VHR: Section Curve. Vertex Height Ratio SC.VPR: Section Curve. Vertex Positioning Ratio SC.SDRF: Section Curve. Setback Depth Ratio Front SC.FETRF: Section Curve. Facade Endpoint Translation Ratio Front SC.CTRF: Section Curve. Concavity Translation Ratio Front SC.EDRF: Section Curve. Eave Depth Ratio Front SC.SDRB: Section Curve. Setback Depth Ratio Back SC.FETRB: Section Curve. Facade Endpoint Translation Ratio Back SC.EDRB: Section Curve. Eave Depth Ratio Back SC.CTRB: Section Curve. Concavity Translation Ratio Back</p>										

APPENDIX C

SIMULATION RESULTS

Table 39: Screenshots of first 50 simulations used in sensitivity analysis.

Sample 1	Windward Sect. view (WS)	<p>Station: SkyBoard Analysis: 30 Wind Speed: 10.000 (m/s) Length: 750.000 (mm) Width: 571.422 (mm) Height: 206.422 (mm) Voxel size: 4.362 (mm)</p>
	Normal Section view (NS)	<p>Station: SkyBoard Analysis: 30 Wind Speed: 10.000 (m/s) Length: 750.000 (mm) Width: 571.422 (mm) Height: 206.422 (mm) Voxel size: 4.362 (mm)</p>
	Roof Level view (RL)	<p>Station: SkyBoard Analysis: 30 Wind Speed: 10.000 (m/s) Length: 750.000 (mm) Width: 571.422 (mm) Height: 206.422 (mm) Voxel size: 4.362 (mm)</p>
	Pedestrian Level view (PL)	<p>Station: SkyBoard Analysis: 30 Wind Speed: 10.000 (m/s) Length: 750.000 (mm) Width: 571.422 (mm) Height: 206.422 (mm) Voxel size: 4.362 (mm)</p>

Table 39 (continued)

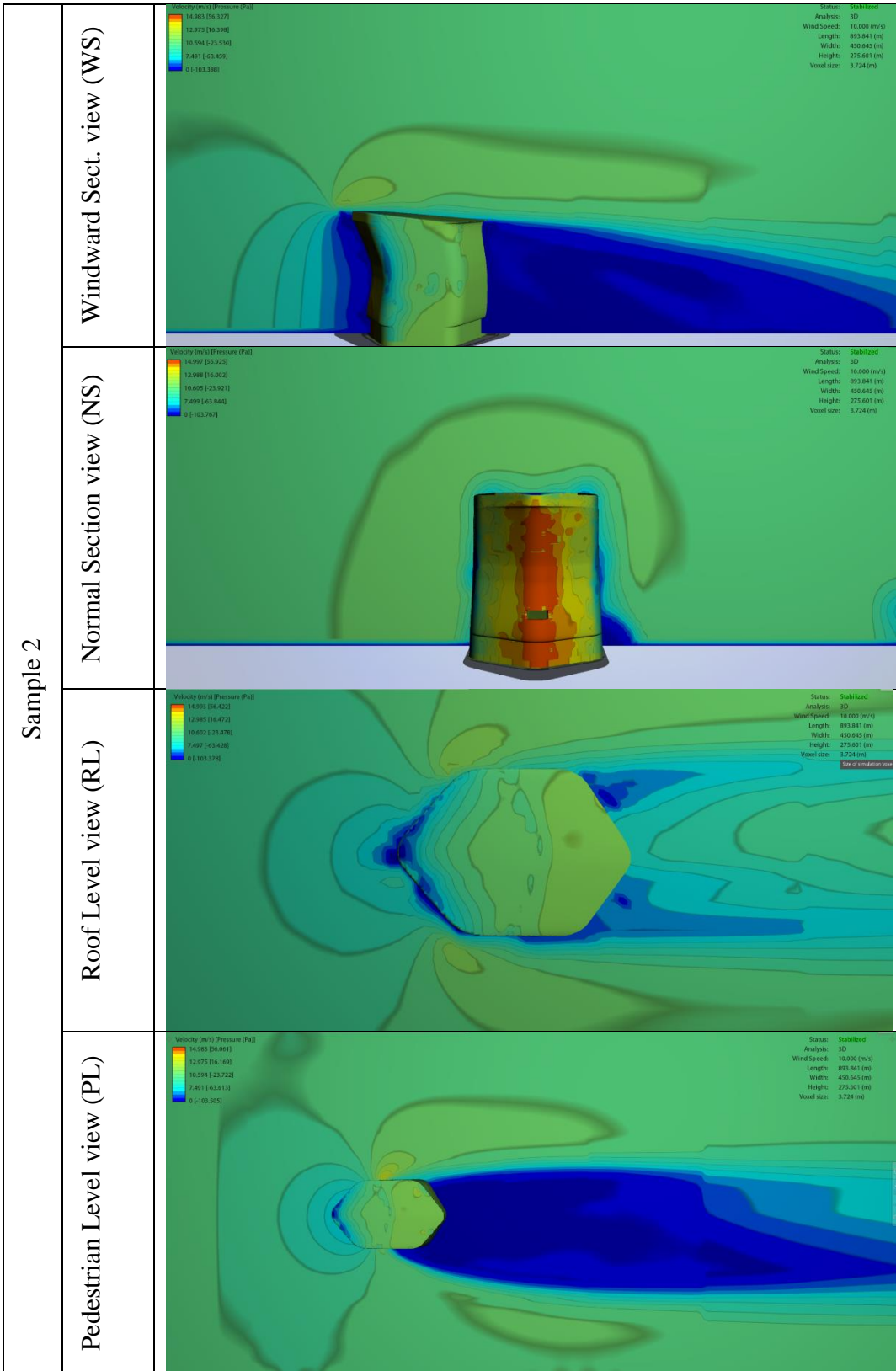


Table 39 (continued)

Sample 3	Windward Sect. view (WS)	<p>Velocity (m/s) (Pressure (Pa))</p> <ul style="list-style-type: none"> 13.245 [50.034] 11.471 [22.324] 9.366 [5.386] 6.619 [-33.096] 0 [-60.882] <p>Status: Stabilized Analysis: 3D Wind Speed: 10.000 (m/s) Length: 907.026 (m) Width: 393.700 (m) Height: 151.599 (m) Voxel size: 2.569 (m)</p>
	Normal Section view (NS)	<p>Velocity (m/s) (Pressure (Pa))</p> <ul style="list-style-type: none"> 13.245 [50.034] 11.465 [22.322] 9.361 [5.390] 6.619 [-33.090] 0 [-60.631] <p>Status: Stabilized Analysis: 3D Wind Speed: 10.000 (m/s) Length: 907.026 (m) Width: 393.700 (m) Height: 151.599 (m) Voxel size: 2.569 (m)</p>
	Roof Level view (RL)	<p>Velocity (m/s) (Pressure (Pa))</p> <ul style="list-style-type: none"> 13.245 [50.034] 11.465 [22.322] 9.379 [5.491] 6.602 [-34.775] 0 [-60.687] <p>Status: Stabilized Analysis: 3D Wind Speed: 10.000 (m/s) Length: 740.110 (m) Width: 398.521 (m) Height: 152.680 (m) Voxel size: 2.588 (m)</p>
	Pedestrian Level view (PL)	<p>Velocity (m/s) (Pressure (Pa))</p> <ul style="list-style-type: none"> 13.239 [49.896] 11.465 [22.234] 9.361 [-5.428] 6.619 [-33.090] 0 [-60.752]

Table 39 (continued)

Sample 4	Windward Sect. view (WS)	<p>Velocity (m/s) (Pressure (Pa))</p> <p>11.331 (10.809) 9.813 (10.046) 8.012 (11.736) 5.664 (11.507) 0 (1.52277)</p> <p>Status: Stabilized Analysis: 3D Wind Speed: 10.000 (m/s) Length: 912.741 (m) Width: 284.849 (m) Height: 73.509 (m) Voxel size: 3.063 (m)</p>
	Normal Section view (NS)	<p>Velocity (m/s) (Pressure (Pa))</p> <p>11.333 (10.927) 9.815 (11.188) 8.014 (11.511) 5.664 (11.290) 0 (1.52209)</p> <p>Status: Stabilized Analysis: 3D Wind Speed: 10.000 (m/s) Length: 912.741 (m) Width: 284.849 (m) Height: 73.509 (m) Voxel size: 3.063 (m)</p>
	Roof Level view (RL)	<p>Velocity (m/s) (Pressure (Pa))</p> <p>11.333 (10.429) 9.813 (9.676) 8.014 (11.077) 5.664 (11.810) 0 (1.52383)</p> <p>Status: Stabilized Analysis: 3D Wind Speed: 10.000 (m/s) Length: 912.741 (m) Width: 284.849 (m) Height: 73.509 (m) Voxel size: 3.063 (m)</p>
	Pedestrian Level view (PL)	<p>Velocity (m/s) (Pressure (Pa))</p> <p>11.327 (10.486) 9.810 (9.779) 8.010 (11.929) 5.664 (11.634) 0 (1.52344)</p> <p>Status: Stabilized Analysis: 3D Wind Speed: 10.000 (m/s) Length: 912.741 (m) Width: 284.849 (m) Height: 73.509 (m) Voxel size: 3.063 (m)</p>

Table 39 (continued)

Sample 5	Windward Sect. view (WS)	<p>Velocity (m/s) [Pressure (Pa)]</p> <ul style="list-style-type: none"> 13.919 [47.457] 12.054 [14.522] 9.842 [18.413] 6.960 [51.348] 0 [84.282] <p>Status: Stabilized Analysis: 3D Wind Speed: 10.000 (m/s) Length: 1525.796 (m) Width: 557.575 (m) Height: 229.811 (m) Voxel size: 3.767 (m)</p>
	Normal Section view (NS)	<p>Velocity (m/s) [Pressure (Pa)]</p> <ul style="list-style-type: none"> 13.894 [47.085] 12.032 [14.183] 9.824 [18.718] 6.947 [51.619] 0 [84.520] <p>Status: Stabilized Analysis: 3D Wind Speed: 10.000 (m/s) Length: 1525.796 (m) Width: 557.575 (m) Height: 229.811 (m) Voxel size: 3.767 (m)</p>
	Roof Level view (RL)	<p>Velocity (m/s) [Pressure (Pa)]</p> <ul style="list-style-type: none"> 13.926 [47.339] 12.060 [14.395] 9.847 [18.549] 6.963 [51.494] 0 [84.438] <p>Status: Stabilized Analysis: 3D Wind Speed: 10.000 (m/s) Length: 1525.796 (m) Width: 557.575 (m) Height: 229.811 (m) Voxel size: 3.767 (m)</p>
	Pedestrian Level view (PL)	<p>Velocity (m/s) [Pressure (Pa)]</p> <ul style="list-style-type: none"> 13.941 [46.877] 12.073 [13.879] 9.858 [19.118] 6.970 [52.116] 0 [85.113] <p>Status: Stabilized Analysis: 3D Wind Speed: 10.000 (m/s) Length: 1525.796 (m) Width: 557.575 (m) Height: 229.811 (m) Voxel size: 3.767 (m)</p>

Table 39 (continued)

Sample 6	Windward Sect. view (WS)	<p>Velocity (m/s) [Pressure (Pa)]</p> <ul style="list-style-type: none"> 13.949 [56.447] 12.080 [20.180] 9.863 [-16.088] 6.974 [-52.356] 0 [-88.623]
	Normal Section view (NS)	<p>Velocity (m/s) [Pressure (Pa)]</p> <ul style="list-style-type: none"> 14.092 [56.372] 12.204 [19.433] 9.964 [-17.507] 7.046 [-54.446] 0 [-91.386]
	Roof Level view (RL)	<p>Velocity (m/s) [Pressure (Pa)]</p> <ul style="list-style-type: none"> 14.615 [57.711] 12.657 [18.141] 10.334 [-21.430] 7.307 [-61.000] 0 [-100.570] <p>Status: Stabilized</p> <p>Analysis: 3D</p> <p>Wind Speed: 10.000 (m/s)</p> <p>Length: 1034.498 (m)</p> <p>Width: 300.497 (m)</p> <p>Height: 179.806 (m)</p> <p>Voxel size: 2.463 (m)</p>
	Pedestrian Level view (PL)	<p>Velocity (m/s) [Pressure (Pa)]</p> <ul style="list-style-type: none"> 14.333 [55.303] 12.413 [16.544] 10.135 [-22.216] 7.167 [-60.975] 0 [-99.734] <p>Status: Stabilized</p> <p>Analysis: 3D</p> <p>Wind Speed: 10.000 (m/s)</p> <p>Length: 1034.498 (m)</p> <p>Width: 300.497 (m)</p> <p>Height: 179.806 (m)</p> <p>Voxel size: 2.463 (m)</p>

Table 39 (continued)

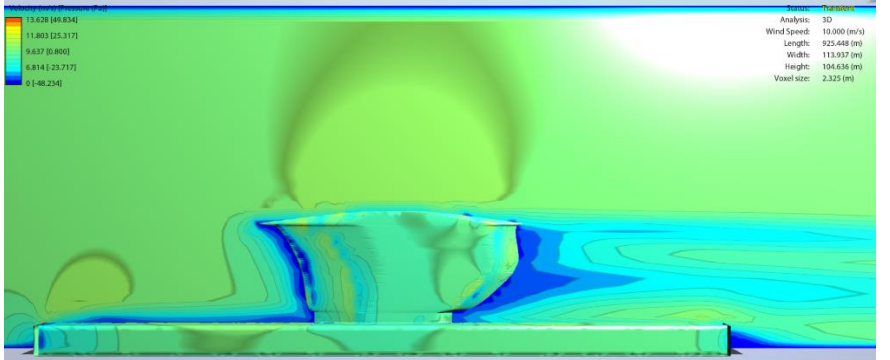
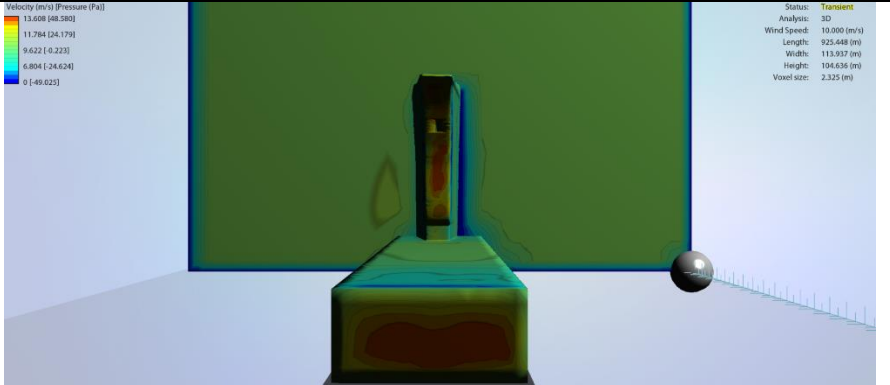
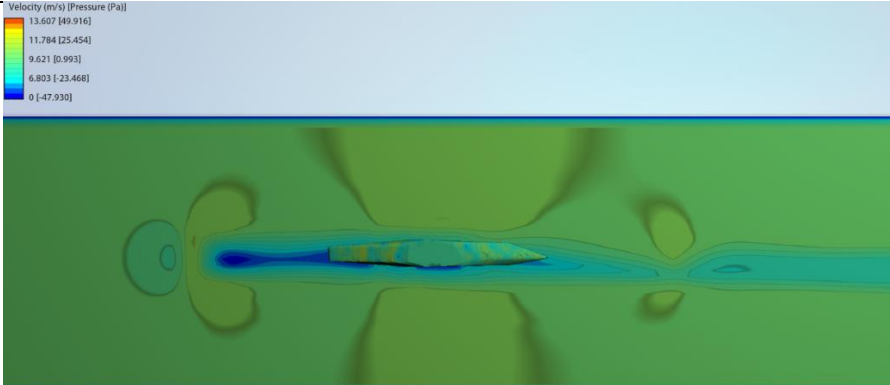
Sample 7	Windward Sect. view (WS)	
	Normal Section view (NS)	
	Roof Level view (RL)	
	Pedestrian Level view (PL)	

Table 39 (continued)

Sample 8	Windward Sect. view (WS)	<p>Velocity (m/s) [Pressure (Pa)]</p> <p>15.662 [36.408] 13.563 [15.666] 11.074 [5.036] 7.831 [-25.758] 0 [-46.479]</p> <p>Status: Transient Analysis: 3D Wind Speed: 10.000 (m/s) Length: 1425.170 (m) Width: 180.062 (m) Height: 45.973 (m) Voxel size: 1.916 (m)</p>
	Normal Section view (NS)	<p>Velocity (m/s) [Pressure (Pa)]</p> <p>15.601 [35.575] 13.511 [14.668] 11.032 [-4.239] 7.800 [-27.145] 0 [-46.052]</p> <p>Status: Transient Analysis: 3D Wind Speed: 10.000 (m/s) Length: 1425.170 (m) Width: 180.062 (m) Height: 45.973 (m) Voxel size: 1.916 (m)</p>
	Roof Level view (RL)	<p>Velocity (m/s) [Pressure (Pa)]</p> <p>15.506 [36.850] 13.429 [16.422] 10.964 [-4.007] 7.753 [-24.436] 0 [-44.865]</p> <p>Status: Transient Analysis: 3D Wind Speed: 10.000 (m/s) Length: 1425.170 (m) Width: 180.062 (m) Height: 45.973 (m) Voxel size: 1.916 (m)</p>
	Pedestrian Level view (PL)	<p>Velocity (m/s) [Pressure (Pa)]</p> <p>15.378 [36.296] 13.491 [14.586] 11.015 [-7.124] 7.789 [-28.834] 0 [-50.544]</p> <p>Status: Transient Analysis: 3D Wind Speed: 10.000 (m/s) Length: 1425.170 (m) Width: 180.062 (m) Height: 45.973 (m) Voxel size: 1.916 (m)</p>

Table 39 (continued)

Sample 9	Windward Sect. view (WS)	<p>Velocity (m/s) [Pressure (Pa)]</p> <ul style="list-style-type: none"> 16.663 [45.387] 14.433 [7.363] 11.794 [-30.662] 8.333 [-68.687] 0 [-105.712] <p>Status: Stabilized Analysis: 3D Wind Speed: 10.000 (m/s) Length: 1016.183 (m) Width: 398.946 (m) Height: 79.036 (m) Voxel size: 3.764 (m)</p>
	Normal Section view (NS)	<p>Velocity (m/s) [Pressure (Pa)]</p> <ul style="list-style-type: none"> 16.387 [45.447] 14.192 [7.819] 11.587 [-30.209] 8.193 [-68.037] 0 [-105.864] <p>Status: Stabilized Analysis: 3D Wind Speed: 10.000 (m/s) Length: 1016.183 (m) Width: 398.946 (m) Height: 79.036 (m) Voxel size: 3.764 (m)</p>
	Roof Level view (RL)	<p>Velocity (m/s) [Pressure (Pa)]</p> <ul style="list-style-type: none"> 16.542 [45.540] 14.326 [7.534] 11.697 [-30.273] 8.271 [-68.080] 0 [-105.880] <p>Status: Stabilized Analysis: 3D Wind Speed: 10.000 (m/s) Length: 1016.183 (m) Width: 398.946 (m) Height: 79.036 (m) Voxel size: 3.764 (m)</p>
	Pedestrian Level view (PL)	<p>Velocity (m/s) [Pressure (Pa)]</p> <ul style="list-style-type: none"> 16.886 [45.230] 14.624 [7.540] 11.940 [-30.150] 8.443 [-67.839] 0 [-105.529] <p>Status: Stabilized Analysis: 3D Wind Speed: 10.000 (m/s) Length: 1016.183 (m) Width: 398.946 (m) Height: 79.036 (m) Voxel size: 3.764 (m)</p>

Table 39 (continued)

Sample 10	Windward Sect. view (WS)	<p>Velocity (m/s) [Pressure (Pa)]</p> <ul style="list-style-type: none"> 11.892 [32.393] 10.299 [10.971] 8.409 [-10.451] 5.946 [-31.873] 0 [-53.295] <p>Status: Transient</p> <p>Analysis: 3D</p> <p>Wind Speed: 10.000 (m/s)</p> <p>Length: 988.149 (m)</p> <p>Width: 147.958 (m)</p> <p>Height: 105.684 (m)</p> <p>Voxel size: 2.642 (m)</p>
	Normal Section view (NS)	<p>Velocity (m/s) [Pressure (Pa)]</p> <ul style="list-style-type: none"> 11.979 [33.376] 10.374 [11.554] 8.470 [10.267] 5.989 [-32.088] 0 [-53.909] <p>Status: Transient</p> <p>Analysis: 3D</p> <p>Wind Speed: 10.000 (m/s)</p> <p>Length: 988.149 (m)</p> <p>Width: 147.958 (m)</p> <p>Height: 105.684 (m)</p> <p>Voxel size: 2.642 (m)</p>
	Roof Level view (RL)	<p>Velocity (m/s) [Pressure (Pa)]</p> <ul style="list-style-type: none"> 11.913 [32.949] 10.317 [10.556] 8.424 [-11.837] 5.956 [-34.230] 0 [-56.623] <p>Status: Transient</p> <p>Analysis: 3D</p> <p>Wind Speed: 10.000 (m/s)</p> <p>Length: 988.149 (m)</p> <p>Width: 147.958 (m)</p> <p>Height: 105.684 (m)</p> <p>Voxel size: 2.642 (m)</p>
	Pedestrian Level view (PL)	<p>Velocity (m/s) [Pressure (Pa)]</p> <ul style="list-style-type: none"> 11.947 [34.187] 10.346 [11.957] 8.448 [-10.272] 5.973 [-32.501] 0 [-54.730] <p>Status: Transient</p> <p>Analysis: 3D</p> <p>Wind Speed: 10.000 (m/s)</p> <p>Length: 988.149 (m)</p> <p>Width: 147.958 (m)</p> <p>Height: 105.684 (m)</p> <p>Voxel size: 2.642 (m)</p>

Table 39 (continued)

Sample 11	Windward Sect. view (WS)	<p>Velocity (m/s) (Pressure (Pa))</p> <ul style="list-style-type: none"> 18.613 [37.476] 16.119 [10.098] 13.161 [-17.280] 9.306 [-44.658] 0 [-72.036] <p>Status: Stabilized Analysis: 3D Wind Speed: 10.000 (m/s) Length: 1014.271 (m) Width: 494.132 (m) Height: 260.069 (m) Voxel size: 3.251 (m)</p>
	Normal Section view (NS)	<p>Velocity (m/s) (Pressure (Pa))</p> <ul style="list-style-type: none"> 18.618 [37.524] 16.124 [10.061] 13.165 [-17.403] 9.309 [-44.867] 0 [-72.331] <p>Status: Stabilized Analysis: 3D Wind Speed: 10.000 (m/s) Length: 1014.271 (m) Width: 494.132 (m) Height: 260.069 (m) Voxel size: 3.251 (m)</p>
	Roof Level view (RL)	<p>Velocity (m/s) (Pressure (Pa))</p> <ul style="list-style-type: none"> 16.642 [37.529] 16.144 [9.730] 13.182 [-18.070] 9.321 [-45.869] 0 [-73.669] <p>Status: Stabilized Analysis: 3D Wind Speed: 10.000 (m/s) Length: 1014.271 (m) Width: 494.132 (m) Height: 260.069 (m) Voxel size: 3.251 (m)</p>
	Pedestrian Level view (PL)	<p>Velocity (m/s) (Pressure (Pa))</p> <ul style="list-style-type: none"> 18.782 [38.348] 16.265 [10.711] 13.281 [-16.926] 9.391 [-44.564] 0 [-72.201] <p>Status: Stabilized Analysis: 3D Wind Speed: 10.000 (m/s) Length: 1014.271 (m) Width: 494.132 (m) Height: 260.069 (m) Voxel size: 3.251 (m)</p>

Table 39 (continued)

Sample 12	Windward Sect. view (WS)		<p>Status: Transient Analysis: 3D Wind Speed: 10.000 (m/s) Length: 1205.379 (m) Width: 323.230 (m) Height: 77.441 (m) Voxel size: 3.367 (m)</p>
	Normal Section view (NS)		<p>Status: Transient Analysis: 3D Wind Speed: 10.000 (m/s) Length: 1205.379 (m) Width: 323.230 (m) Height: 77.441 (m) Voxel size: 3.367 (m)</p>
	Roof Level view (RL)		<p>Status: Transient Analysis: 3D Wind Speed: 10.000 (m/s) Length: 1205.379 (m) Width: 323.230 (m) Height: 77.441 (m) Voxel size: 3.367 (m)</p>
	Pedestrian Level view (PL)		<p>Status: Transient Analysis: 3D Wind Speed: 10.000 (m/s) Length: 1205.379 (m) Width: 323.230 (m) Height: 77.441 (m) Voxel size: 3.367 (m)</p>

Table 39 (continued)

Sample 13	Windward Sect. view (WS)	<p>Velocity (m/s) [Pressure (Pa)]</p> <ul style="list-style-type: none"> 12.689 [55.493] 10.989 [27.423] 8.973 [-0.248] 6.345 [28.119] 0 [-55.989] <p>Status: Stabilized Analysis: 3D Wind Speed: 10.000 (m/s) Length: 367.594 (m) Width: 192.027 (m) Height: 155.450 (m) Voxel size: 1.829 (m)</p>
	Normal Section view (NS)	<p>Velocity (m/s) [Pressure (Pa)]</p> <ul style="list-style-type: none"> 12.558 [56.818] 10.876 [28.839] 8.880 [1.149] 6.279 [26.318] 0 [-54.197] <p>Status: Stabilized Analysis: 3D Wind Speed: 10.000 (m/s) Length: 367.594 (m) Width: 192.027 (m) Height: 155.450 (m) Voxel size: 1.829 (m)</p>
	Roof Level view (RL)	<p>Velocity (m/s) [Pressure (Pa)]</p> <ul style="list-style-type: none"> 12.296 [56.363] 10.649 [29.856] 8.695 [3.349] 6.148 [-23.157] 0 [-49.664] <p>Status: Stabilized Analysis: 3D Wind Speed: 10.000 (m/s) Length: 367.594 (m) Width: 192.027 (m) Height: 155.450 (m) Voxel size: 1.829 (m)</p>
	Pedestrian Level view (PL)	<p>Velocity (m/s) [Pressure (Pa)]</p> <ul style="list-style-type: none"> 12.278 [56.247] 10.633 [29.605] 8.682 [2.963] 6.139 [-23.679] 0 [-50.321] <p>Status: Stabilized Analysis: 3D Wind Speed: 10.000 (m/s) Length: 367.594 (m) Width: 192.027 (m) Height: 155.450 (m) Voxel size: 1.829 (m)</p>

Table 39 (continued)

Sample 14	Windward Sect. view (WS)	<p>Velocity (m/s) [Pressure (Pa)]</p> <ul style="list-style-type: none"> 15.327 [54.490] 13.274 [18.922] 10.838 [16.646] 7.664 [52.215] 0 [-87.783] <p>Status: Transient</p> <p>Analysis: 3D</p> <p>Wind Speed: 10.000 (m/s)</p> <p>Length: 1378.664 (m)</p> <p>Width: 470.972 (m)</p> <p>Height: 85.631 (m)</p> <p>Voxel size: 4.282 (m)</p>
	Normal Section view (NS)	<p>Velocity (m/s) [Pressure (Pa)]</p> <ul style="list-style-type: none"> 15.312 [54.576] 13.261 [18.938] 10.828 [16.701] 7.656 [52.339] 0 [-87.978] <p>Status: Steady-state</p> <p>Analysis: 3D</p> <p>Wind Speed: 10.000 (m/s)</p> <p>Length: 1378.664 (m)</p> <p>Width: 470.972 (m)</p> <p>Height: 85.631 (m)</p> <p>Voxel size: 4.282 (m)</p>
	Roof Level view (RL)	<p>Velocity (m/s) [Pressure (Pa)]</p> <ul style="list-style-type: none"> 15.307 [54.642] 13.256 [19.003] 10.824 [16.637] 7.654 [52.276] 0 [-87.916] <p>Status: Transient</p> <p>Analysis: 3D</p> <p>Wind Speed: 10.000 (m/s)</p> <p>Length: 1378.664 (m)</p> <p>Width: 470.972 (m)</p> <p>Height: 85.631 (m)</p> <p>Voxel size: 4.282 (m)</p>
	Pedestrian Level view (PL)	<p>Velocity (m/s) [Pressure (Pa)]</p> <ul style="list-style-type: none"> 15.305 [54.741] 13.255 [19.089] 10.822 [16.562] 7.653 [52.214] 0 [-87.865] <p>Status: Transient</p> <p>Analysis: 3D</p> <p>Wind Speed: 10.000 (m/s)</p> <p>Length: 1378.664 (m)</p> <p>Width: 470.972 (m)</p> <p>Height: 85.631 (m)</p> <p>Voxel size: 4.282 (m)</p>

Table 39 (continued)

Sample 15	Windward Sect. view (WS)	<p>Velocity (m/s) (Pressure (Pa))</p> <p>20.384 [29.340] 17.653 [14.898] 14.414 [0.456] 10.192 [-13.987] 0 [-28.429]</p> <p>Status: Transient Analysis: 3D Wind Speed: 10.000 (m/s) Length: 995.110 (m) Width: 83.127 (m) Height: 38.551 (m) Voxel size: 1.205 (m)</p>
	Normal Section view (NS)	<p>Velocity (m/s) (Pressure (Pa))</p> <p>19.700 [28.004] 17.061 [13.243] 13.930 [-1.518] 9.850 [-16.279] 0 [-31.040]</p> <p>Status: Transient Analysis: 3D Wind Speed: 10.000 (m/s) Length: 995.110 (m) Width: 83.127 (m) Height: 38.551 (m) Voxel size: 1.205 (m)</p>
	Roof Level view (RL)	<p>Velocity (m/s) (Pressure (Pa))</p> <p>19.104 [27.047] 16.545 [11.956] 13.509 [-3.136] 9.552 [-18.227] 0 [-33.319]</p> <p>Status: Transient Analysis: 3D Wind Speed: 10.000 (m/s) Length: 995.110 (m) Width: 83.127 (m) Height: 38.551 (m) Voxel size: 1.205 (m)</p>
	Pedestrian Level view (PL)	<p>Velocity (m/s) (Pressure (Pa))</p> <p>19.495 [27.184] 16.884 [12.281] 13.785 [-2.622] 9.748 [-17.525] 0 [-32.428]</p> <p>Status: Transient Analysis: 3D Wind Speed: 10.000 (m/s) Length: 995.110 (m) Width: 83.127 (m) Height: 38.551 (m) Voxel size: 1.205 (m)</p>

Table 39 (continued)

Sample 16	Windward Sect. view (WS)	<p>Velocity (m/s) [Pressure (Pa)]</p> <ul style="list-style-type: none"> 14.340 [50.515] 12.419 [14.176] 10.140 [-22.162] 7.170 [-58.500] 0 [-94.838] <p>Status: Stabilized Analysis: 3D Wind Speed: 10.000 (m/s) Length: 1182.067 (m) Width: 562.102 (m) Height: 272.785 (m) Voxel size: 4.133 (m)</p>
	Normal Section view (NS)	<p>Velocity (m/s) [Pressure (Pa)]</p> <ul style="list-style-type: none"> 14.324 [50.139] 12.405 [14.041] 10.129 [-22.058] 7.162 [-58.156] 0 [-94.254] <p>Status: Stabilized Analysis: 3D Wind Speed: 10.000 (m/s) Length: 1182.067 (m) Width: 562.102 (m) Height: 272.785 (m) Voxel size: 4.133 (m)</p>
	Roof Level view (RL)	<p>Velocity (m/s) [Pressure (Pa)]</p> <ul style="list-style-type: none"> 14.316 [50.325] 12.398 [14.265] 10.123 [-21.795] 7.158 [-57.854] 0 [-93.914] <p>Status: Stabilized Analysis: 3D Wind Speed: 10.000 (m/s) Length: 1182.067 (m) Width: 562.102 (m) Height: 272.785 (m) Voxel size: 4.133 (m)</p>
	Pedestrian Level view (PL)	<p>Velocity (m/s) [Pressure (Pa)]</p> <ul style="list-style-type: none"> 14.309 [50.337] 12.392 [14.447] 10.118 [-21.444] 7.155 [-57.334] 0 [-93.225] <p>Status: Stabilized Analysis: 3D Wind Speed: 10.000 (m/s) Length: 1182.067 (m) Width: 562.102 (m) Height: 272.785 (m) Voxel size: 4.133 (m)</p>

Table 39 (continued)

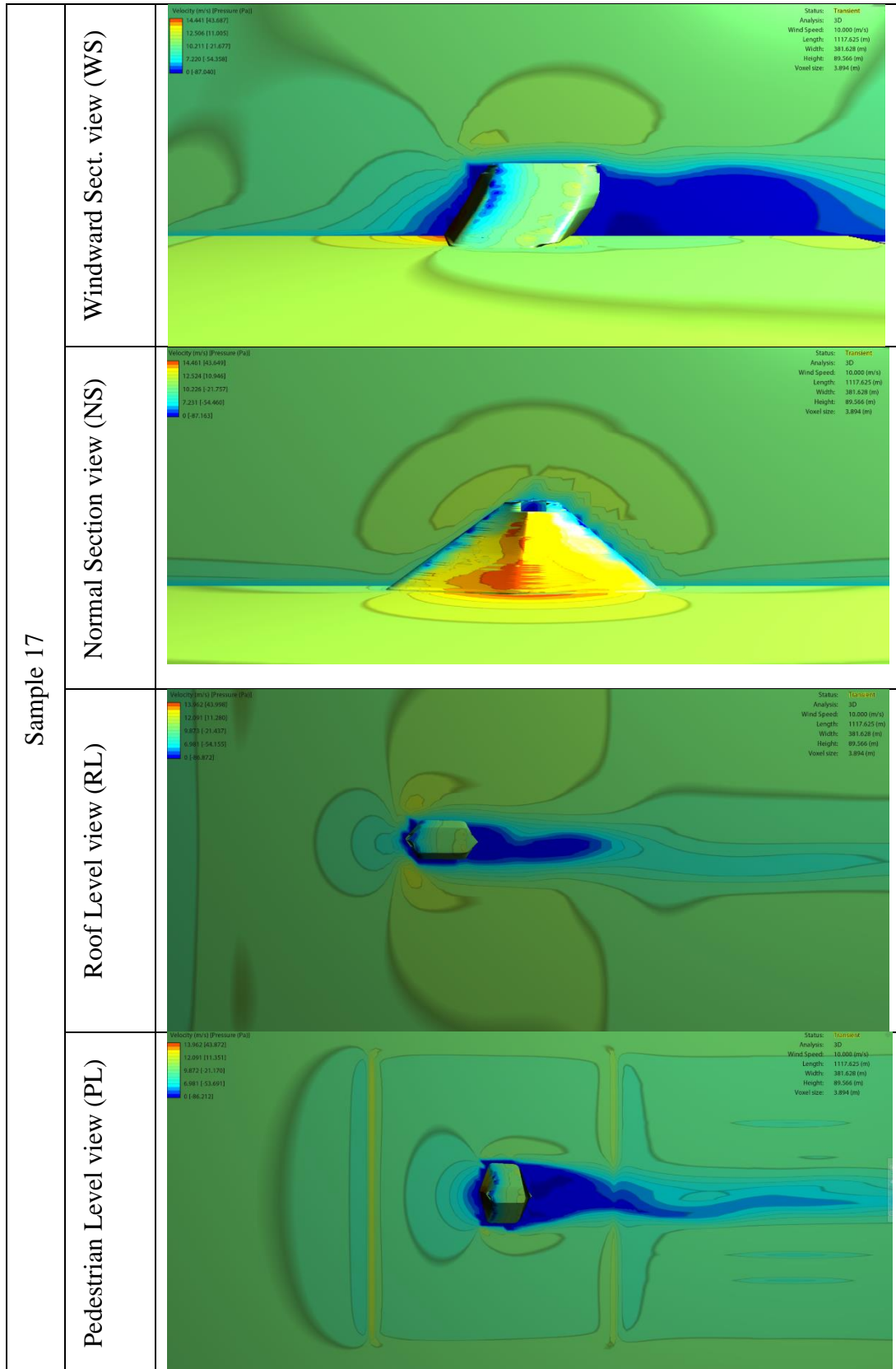


Table 39 (continued)

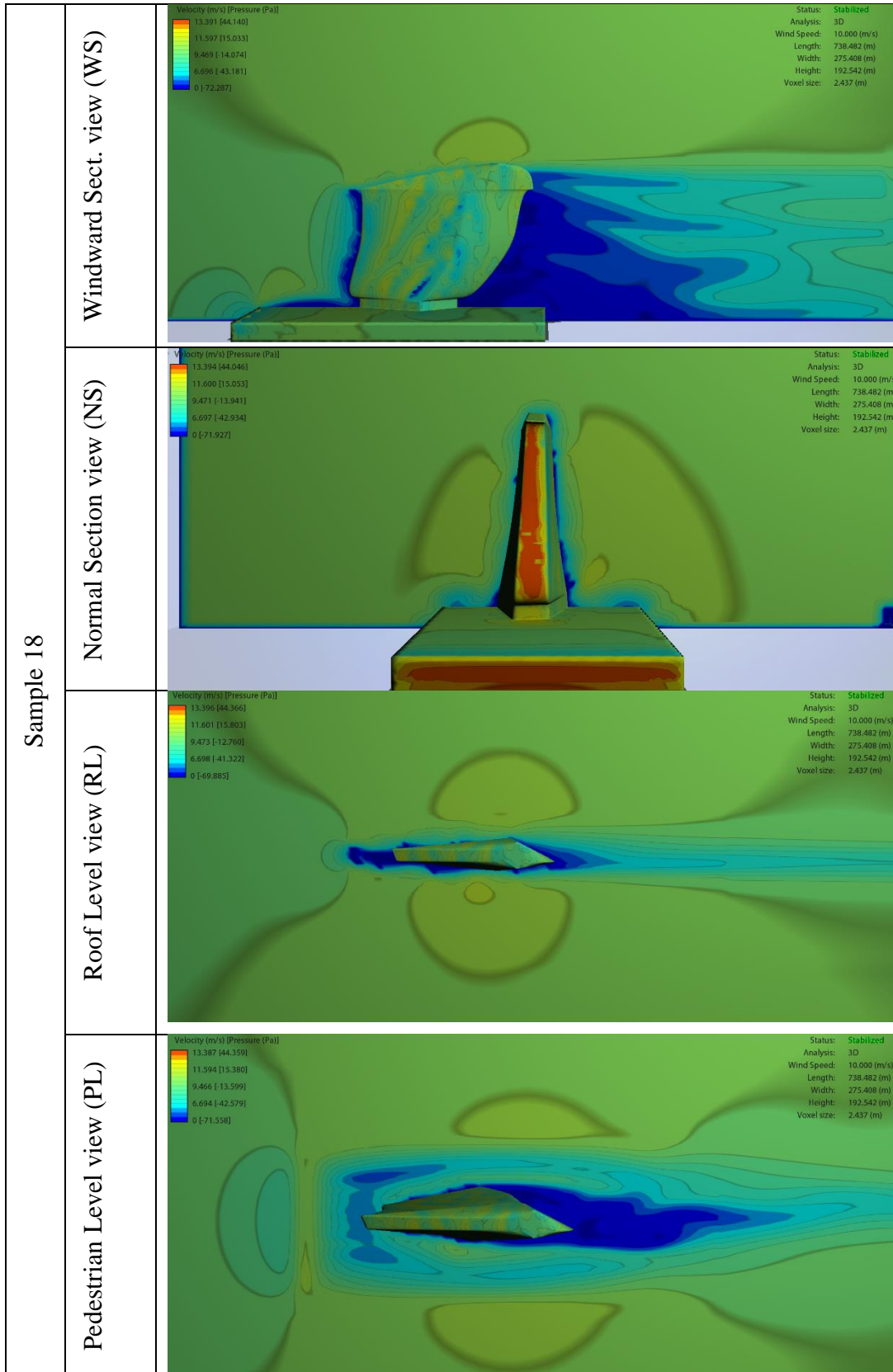


Table 39 (continued)

Sample 19	Windward Sect. view (WS)		<p>Status: Stabilized Analysis: 3D Wind Speed: 10.000 (m/s) Length: 514.459 (m) Width: 216.159 (m) Height: 194.543 (m) Voxel size: 2.162 (m)</p>
	Normal Section view (NS)		<p>Status: Stabilized Analysis: 3D Wind Speed: 10.000 (m/s) Length: 514.459 (m) Width: 216.159 (m) Height: 194.543 (m) Voxel size: 2.162 (m)</p>
	Roof Level view (RL)		<p>Status: Stabilized Analysis: 3D Wind Speed: 10.000 (m/s) Length: 514.459 (m) Width: 216.159 (m) Height: 194.543 (m) Voxel size: 2.162 (m)</p>
	Pedestrian Level view (PL)		<p>Status: Stabilized Analysis: 3D Wind Speed: 10.000 (m/s) Length: 514.459 (m) Width: 216.159 (m) Height: 194.543 (m) Voxel size: 2.162 (m)</p>

Table 39 (continued)

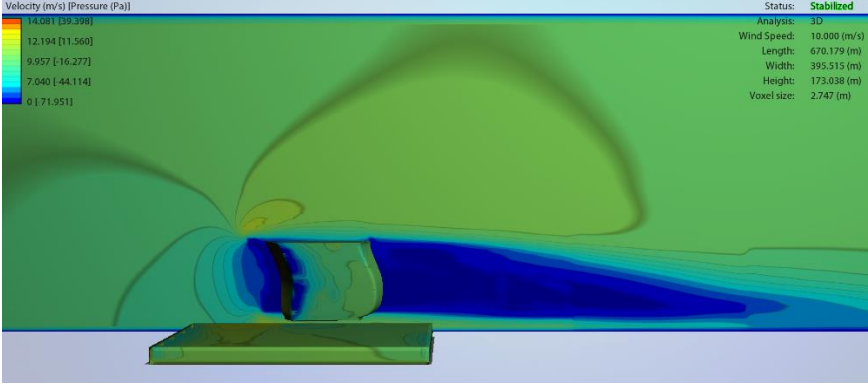
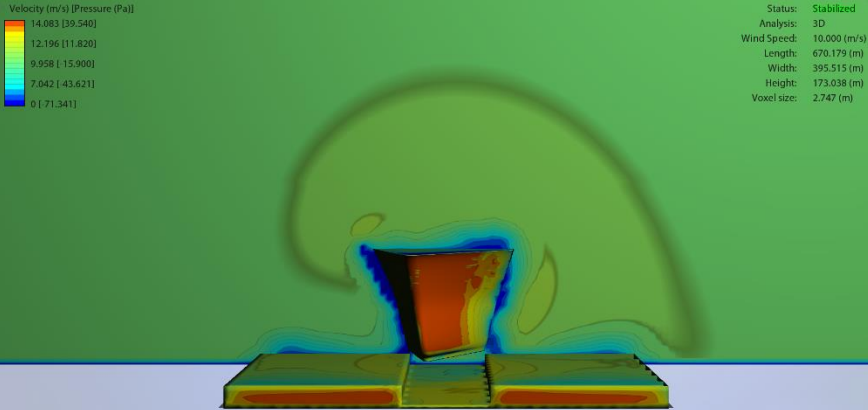
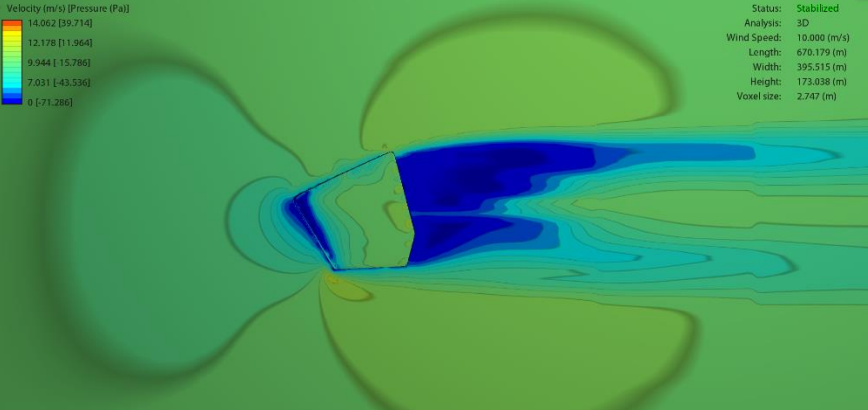
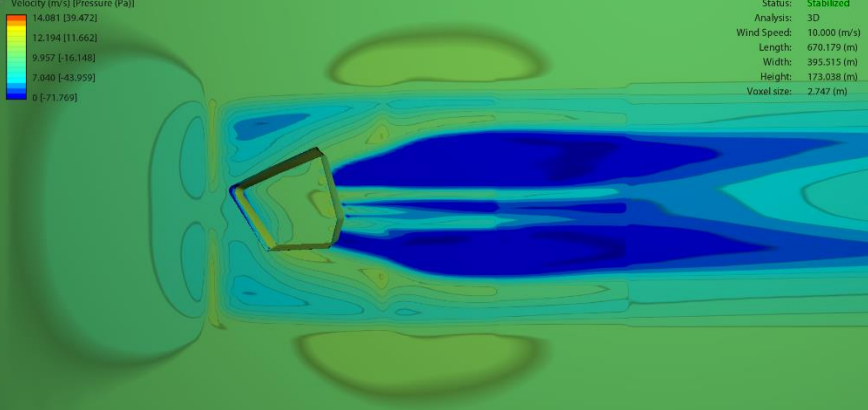
Sample 20	Windward Sect. view (WS)	
	Normal Section view (NS)	
	Roof Level view (RL)	
	Pedestrian Level view (PL)	

Table 39 (continued)

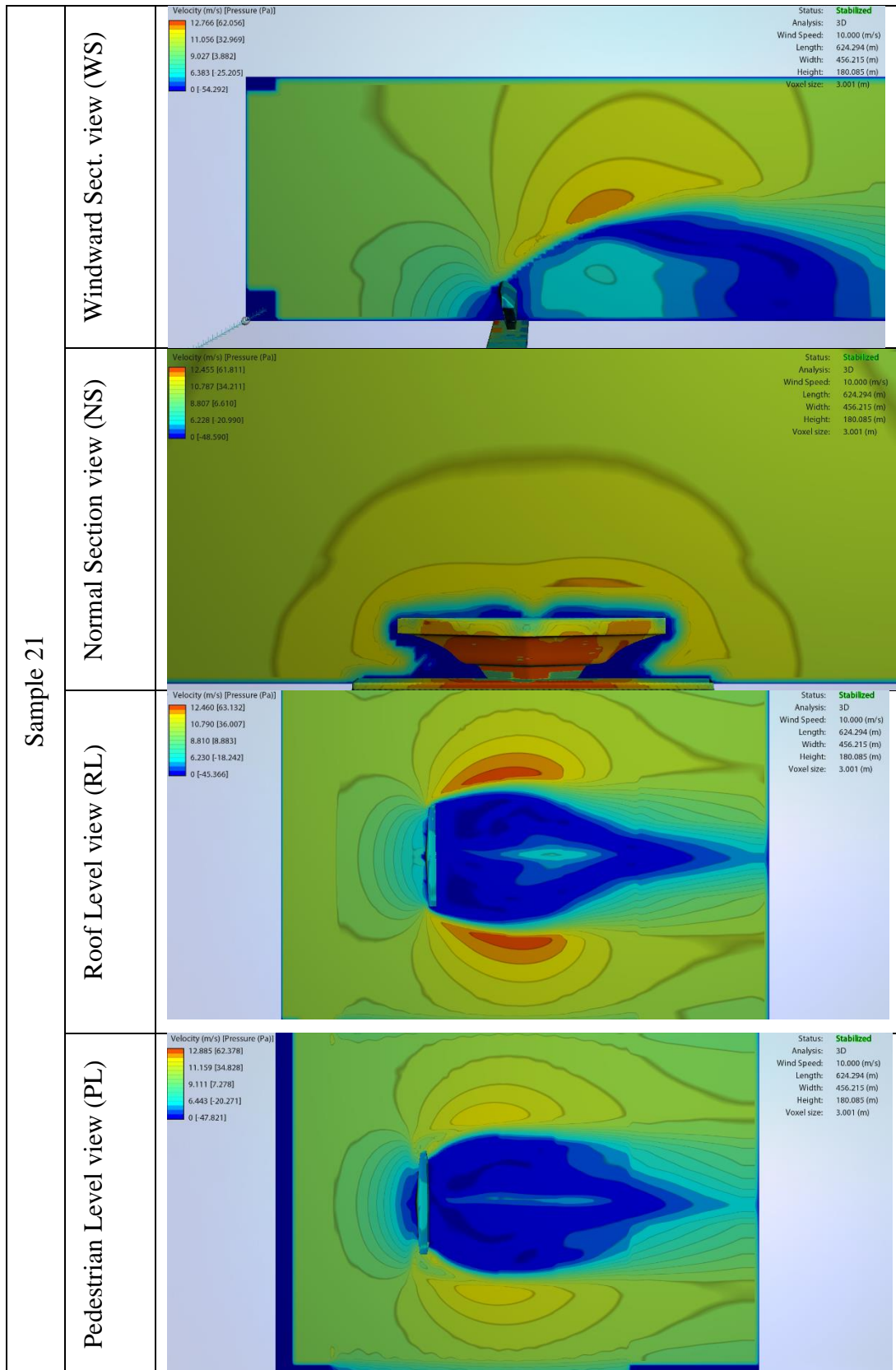


Table 39 (continued)

Sample 22	Windward Sect. view (WS)		<p>Status: Stabilized</p> <p>Analysis: 3D</p> <p>Wind Speed: 10.000 (m/s)</p> <p>Length: 405.112 (m)</p> <p>Width: 350.367 (m)</p> <p>Height: 194.344 (m)</p> <p>Voxel size: 2.737 (m)</p>
	Normal Section view (NS)		<p>Status: Stabilized</p> <p>Analysis: 3D</p> <p>Wind Speed: 10.000 (m/s)</p> <p>Length: 405.112 (m)</p> <p>Width: 350.367 (m)</p> <p>Height: 194.344 (m)</p> <p>Voxel size: 2.737 (m)</p>
	Roof Level view (RL)		<p>Status: Stabilized</p> <p>Analysis: 3D</p> <p>Wind Speed: 10.000 (m/s)</p> <p>Length: 405.112 (m)</p> <p>Width: 350.367 (m)</p> <p>Height: 194.344 (m)</p> <p>Voxel size: 2.737 (m)</p>
	Pedestrian Level view (PL)		<p>Status: Stabilized</p> <p>Analysis: 3D</p> <p>Wind Speed: 10.000 (m/s)</p> <p>Length: 405.112 (m)</p> <p>Width: 350.367 (m)</p> <p>Height: 194.344 (m)</p> <p>Voxel size: 2.737 (m)</p>

Table 39 (continued)

Sample 23	Windward Sect. view (WS)	<p>Velocity (m/s) [Pressure (Pa)]</p> <p>13.060 [47.154] 11.310 [21.715] 9.235 [3.724] 6.530 [-29.163] 0 [-54.602]</p> <p>Status: Transient Analysis: 3D Wind Speed: 10.000 (m/s) Length: 1371.488 (m) Width: 493.119 (m) Height: 65.492 (m) Voxel size: 3.852 (m)</p>
	Normal Section view (NS)	<p>Velocity (m/s) [Pressure (Pa)]</p> <p>13.011 [47.065] 11.268 [21.697] 9.200 [3.670] 6.506 [-29.037] 0 [-54.405]</p> <p>Status: Transient Analysis: 3D Wind Speed: 10.000 (m/s) Length: 1371.488 (m) Width: 493.119 (m) Height: 65.492 (m) Voxel size: 3.852 (m)</p>
	Roof Level view (RL)	<p>Velocity (m/s) [Pressure (Pa)]</p> <p>13.005 [47.090] 11.262 [21.743] 9.196 [-3.605] 6.502 [-28.953] 0 [-54.301]</p> <p>Status: Transient Analysis: 3D Wind Speed: 10.000 (m/s) Length: 1371.488 (m) Width: 493.119 (m) Height: 65.492 (m) Voxel size: 3.852 (m)</p>
	Pedestrian Level view (PL)	<p>Velocity (m/s) [Pressure (Pa)]</p> <p>12.964 [46.637] 11.227 [21.435] 9.167 [-3.768] 6.482 [-28.971] 0 [-54.174]</p> <p>Status: Transient Analysis: 3D Wind Speed: 10.000 (m/s) Length: 1371.488 (m) Width: 493.119 (m) Height: 65.492 (m) Voxel size: 3.852 (m)</p>

Table 39 (continued)

Sample 24	Windward Sect. view (WS)		<p>Status: Stabilized Analysis: 3D Wind Speed: 10.000 (m/s) Length: 649.230 (m) Width: 313.794 (m) Height: 134.174 (m) Voxel size: 2.164 (m)</p>
	Normal Section view (NS)		<p>Status: Stabilized Analysis: 3D Wind Speed: 10.000 (m/s) Length: 649.230 (m) Width: 313.794 (m) Height: 134.174 (m) Voxel size: 2.164 (m)</p>
	Roof Level view (RL)		<p>Status: Stabilized Analysis: 3D Wind Speed: 10.000 (m/s) Length: 649.230 (m) Width: 313.794 (m) Height: 134.174 (m) Voxel size: 2.164 (m)</p>
	Pedestrian Level view (PL)		<p>Status: Stabilized Analysis: 3D Wind Speed: 10.000 (m/s) Length: 649.230 (m) Width: 313.794 (m) Height: 134.174 (m) Voxel size: 2.164 (m)</p>

Table 39 (continued)

Sample 25	Windward Sect. view (WS)	<p>Velocity (m/s) [Pressure (Pa)]</p> <ul style="list-style-type: none"> 12.650 [73.098] 10.955 [40.468] 8.945 [7.837] 6.325 [-24.793] 0 [-57.423] <p>Status: Stabilized Analysis: 3D Wind Speed: 10.000 (m/s) Length: 657.900 (m) Width: 540.418 (m) Height: 254.545 (m) Voxel size: 3.916 (m)</p>
	Normal Section view (NS)	<p>Velocity (m/s) [Pressure (Pa)]</p> <ul style="list-style-type: none"> 12.529 [74.984] 10.851 [43.733] 8.860 [12.481] 6.265 [-18.771] 0 [-50.023] <p>Status: Stabilized Analysis: 3D Wind Speed: 10.000 (m/s) Length: 657.900 (m) Width: 540.418 (m) Height: 254.545 (m) Voxel size: 3.916 (m)</p>
	Roof Level view (RL)	<p>Velocity (m/s) [Pressure (Pa)]</p> <ul style="list-style-type: none"> 12.549 [76.194] 10.868 [45.125] 8.874 [14.057] 6.275 [-17.012] 0 [-48.080] <p>Status: Stabilized Analysis: 3D Wind Speed: 10.000 (m/s) Length: 657.900 (m) Width: 540.418 (m) Height: 254.545 (m) Voxel size: 3.916 (m)</p>
	Pedestrian Level view (PL)	<p>Velocity (m/s) [Pressure (Pa)]</p> <ul style="list-style-type: none"> 12.523 [75.418] 10.845 [44.114] 8.855 [12.810] 6.262 [-18.494] 0 [-49.798] <p>Status: Stabilized Analysis: 3D Wind Speed: 10.000 (m/s) Length: 657.900 (m) Width: 540.418 (m) Height: 254.545 (m) Voxel size: 3.916 (m)</p>

Table 39 (continued)

Sample 26	Windward Sect. view (WS)	<p>Velocity (m/s) (Pressure (Pa))</p> <p>13.862 (14.480) 13.834 (15.300) 9.814 (13.986) 0 (96.871)</p> <p>Status: Stabilized Analysis: 3D Wind Speed: 10.000 (m/s) Length: 499.847 (m) Width: 282.256 (m) Height: 101.755 (m) Voxel size: 1.785 (m)</p>
	Normal Section view (NS)	<p>Velocity (m/s) (Pressure (Pa))</p> <p>13.629 (14.341) 11.782 (14.624) 9.620 (10.094) 6.862 (5.281) 0 (96.529)</p> <p>Status: Stabilized Analysis: 3D Wind Speed: 10.000 (m/s) Length: 499.847 (m) Width: 282.256 (m) Height: 101.755 (m) Voxel size: 1.785 (m)</p>
	Roof Level view (RL)	<p>Velocity (m/s) (Pressure (Pa))</p> <p>13.607 (14.310) 11.784 (14.386) 9.621 (10.538) 6.863 (5.442) 0 (97.387)</p> <p>Status: Stabilized Analysis: 3D Wind Speed: 10.000 (m/s) Length: 499.847 (m) Width: 282.256 (m) Height: 101.755 (m) Voxel size: 1.785 (m)</p>
	Pedestrian Level view (PL)	<p>Velocity (m/s) (Pressure (Pa))</p> <p>13.589 (14.742) 11.787 (15.152) 9.608 (18.431) 6.794 (5.218) 0 (85.004)</p> <p>Status: Stabilized Analysis: 3D Wind Speed: 10.000 (m/s) Length: 499.847 (m) Width: 282.256 (m) Height: 101.755 (m) Voxel size: 1.785 (m)</p>

Table 39 (continued)

Sample 27	Windward Sect. view (WS)	<p>Velocity (m/s) (Pressure (Pa))</p> <ul style="list-style-type: none"> 15.215 [60.810] 13.176 [15.941] 10.739 [-28.928] 7.607 [-73.798] 0 [-118.667] <p>Status: Stabilized</p> <p>Analysis: 3D</p> <p>Wind Speed: 10.000 (m/s)</p> <p>Length: 441.193 (m)</p> <p>Width: 273.766 (m)</p> <p>Height: 167.427 (m)</p> <p>Voxel size: 2.263 (m)</p>
	Normal Section view (NS)	<p>Velocity (m/s) (Pressure (Pa))</p> <ul style="list-style-type: none"> 15.166 [60.661] 13.134 [16.017] 10.724 [-28.627] 7.583 [-73.271] 0 [-117.915] <p>Status: Stabilized</p> <p>Analysis: 3D</p> <p>Wind Speed: 10.000 (m/s)</p> <p>Length: 441.193 (m)</p> <p>Width: 273.766 (m)</p> <p>Height: 167.427 (m)</p> <p>Voxel size: 2.263 (m)</p>
	Roof Level view (RL)	<p>Velocity (m/s) (Pressure (Pa))</p> <ul style="list-style-type: none"> 15.113 [61.150] 13.088 [16.509] 10.686 [-28.131] 7.556 [-72.772] 0 [-117.412] <p>Status: Stabilized</p> <p>Analysis: 3D</p> <p>Wind Speed: 10.000 (m/s)</p> <p>Length: 441.193 (m)</p> <p>Width: 273.766 (m)</p> <p>Height: 167.427 (m)</p> <p>Voxel size: 2.263 (m)</p>
	Pedestrian Level view (PL)	<p>Velocity (m/s) (Pressure (Pa))</p> <ul style="list-style-type: none"> 15.140 [60.838] 13.112 [16.329] 10.706 [-28.180] 7.570 [-72.689] 0 [-117.198] <p>Status: Stabilized</p> <p>Analysis: 3D</p> <p>Wind Speed: 10.000 (m/s)</p> <p>Length: 441.193 (m)</p> <p>Width: 273.766 (m)</p> <p>Height: 167.427 (m)</p> <p>Voxel size: 2.263 (m)</p>

Table 39 (continued)

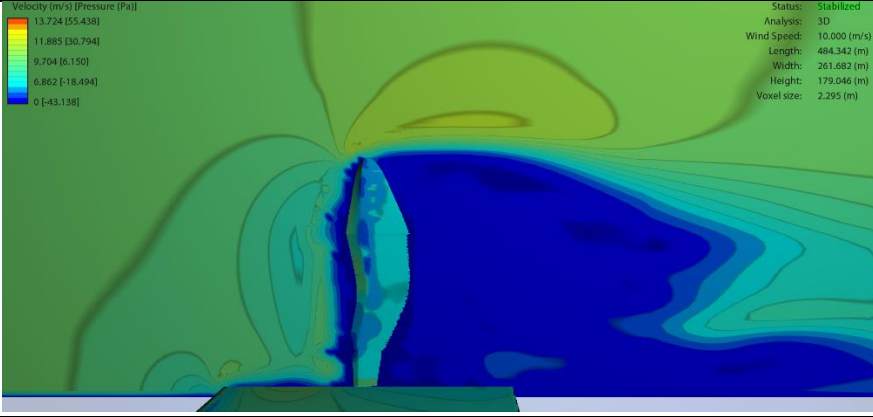
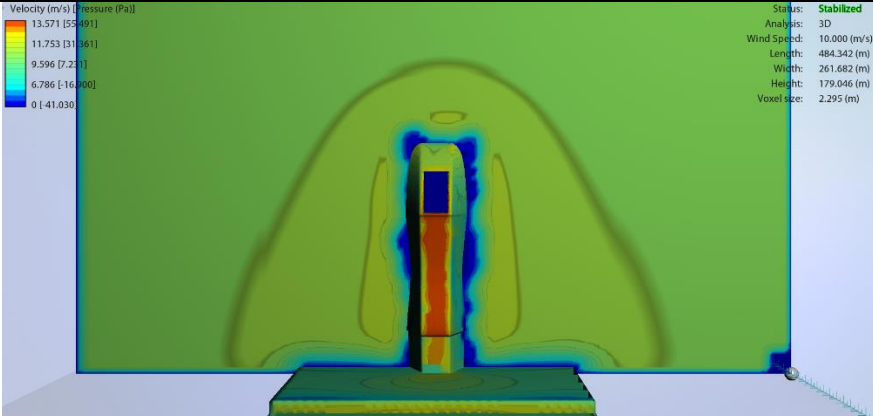
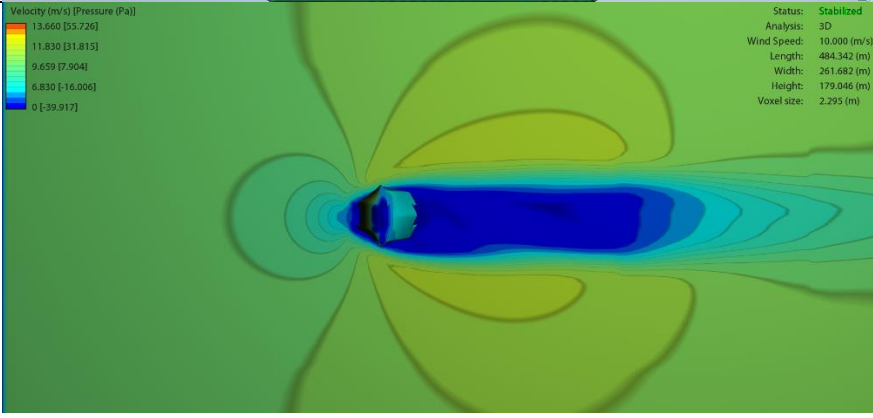
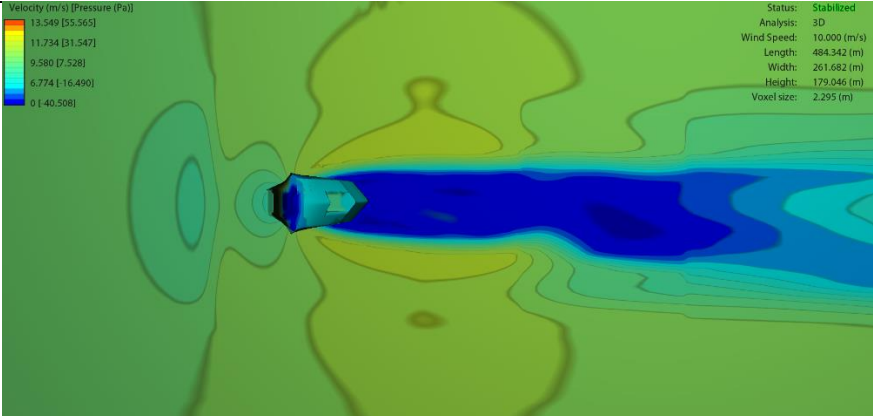
Sample 28	Windward Sect. view (WS)	 <p>Velocity (m/s) [Pressure (Pa)] 13.724 [55.438] 11.885 [30.794] 9.704 [6.150] 6.862 [-18.494] 0 [-43.138]</p> <p>Status: Stabilized Analysis: 3D Wind Speed: 10.000 (m/s) Length: 484.342 (m) Width: 261.682 (m) Height: 179.046 (m) Voxel size: 2.295 (m)</p>
	Normal Section view (NS)	 <p>Velocity (m/s) [Pressure (Pa)] 13.571 [55.691] 11.753 [31.361] 9.596 [7.251] 6.786 [-16.960] 0 [41.030]</p> <p>Status: Stabilized Analysis: 3D Wind Speed: 10.000 (m/s) Length: 484.342 (m) Width: 261.682 (m) Height: 179.046 (m) Voxel size: 2.295 (m)</p>
	Roof Level view (RL)	 <p>Velocity (m/s) [Pressure (Pa)] 13.660 [55.726] 11.830 [31.815] 9.659 [7.504] 6.830 [-16.006] 0 [-39.917]</p> <p>Status: Stabilized Analysis: 3D Wind Speed: 10.000 (m/s) Length: 484.342 (m) Width: 261.682 (m) Height: 179.046 (m) Voxel size: 2.295 (m)</p>
	Pedestrian Level view (PL)	 <p>Velocity (m/s) [Pressure (Pa)] 13.549 [55.565] 11.734 [31.547] 9.580 [7.528] 6.774 [-16.450] 0 [40.508]</p> <p>Status: Stabilized Analysis: 3D Wind Speed: 10.000 (m/s) Length: 484.342 (m) Width: 261.682 (m) Height: 179.046 (m) Voxel size: 2.295 (m)</p>

Table 39 (continued)

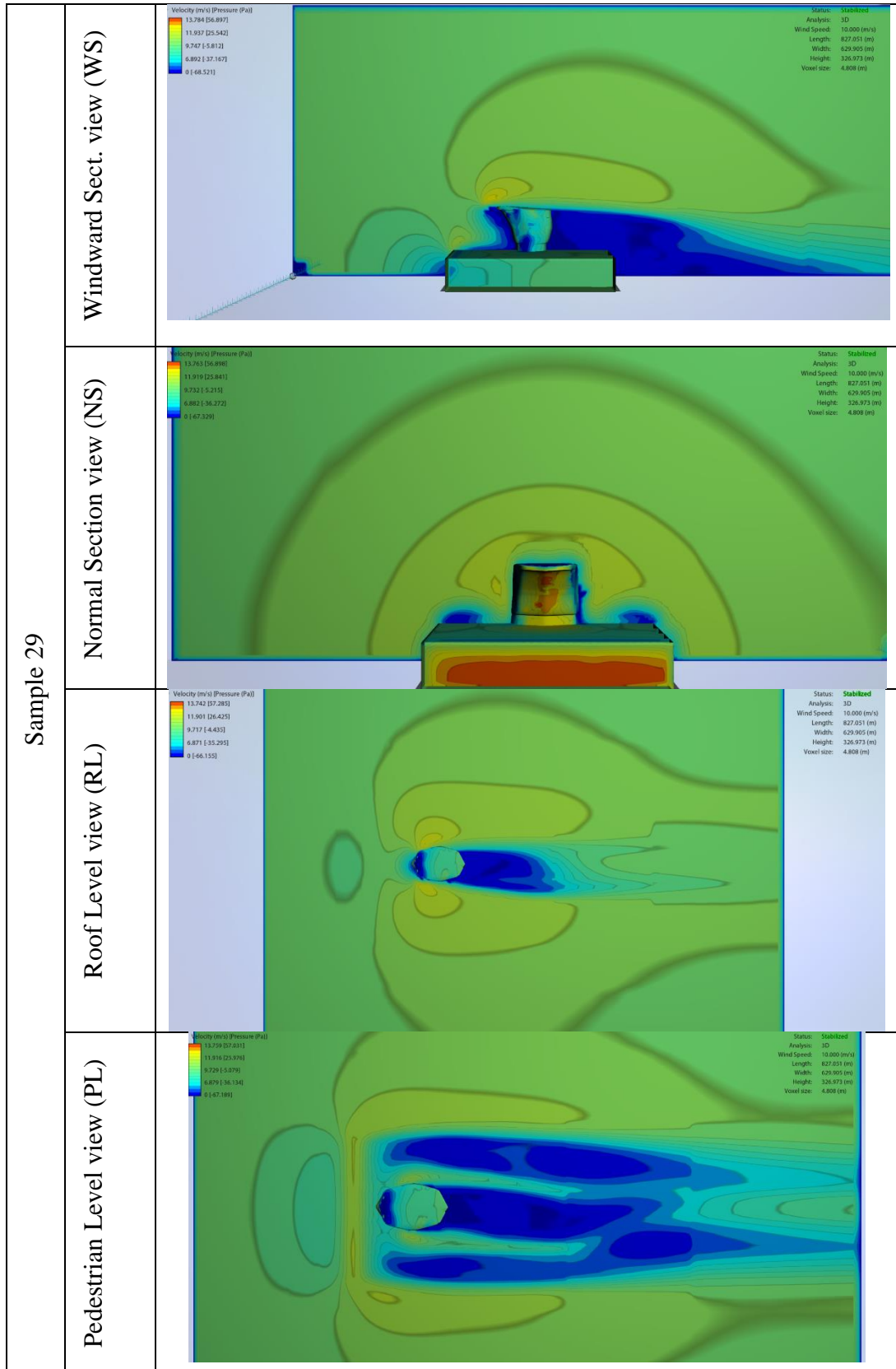


Table 39 (continued)

Sample 30	Windward Sect. view (WS)	<p>Velocity (m/s) [Pressure (Pa)] 13.554 [46.767] 11.738 [19.273] 9.584 [8.221] 6.777 [35.715] 0 [-63.209]</p> <p>Status: Stabilized Analysis: 3D Wind Speed: 10.000 (m/s) Length: 324.063 (m) Width: 92.146 (m) Height: 104.570 (m) Voxel size: 1.035 (m)</p>
	Normal Section view (NS)	<p>Velocity (m/s) [Pressure (Pa)] 13.399 [47.004] 11.604 [19.518] 9.474 [7.968] 6.699 [35.454] 0 [-62.940]</p> <p>Status: Stabilized Analysis: 3D Wind Speed: 10.000 (m/s) Length: 324.063 (m) Width: 92.146 (m) Height: 104.570 (m) Voxel size: 1.035 (m)</p>
	Roof Level view (RL)	<p>Velocity (m/s) [Pressure (Pa)] 13.389 [46.963] 11.595 [19.528] 9.467 [7.906] 6.694 [35.341] 0 [-62.775]</p> <p>Status: Stabilized Analysis: 3D Wind Speed: 10.000 (m/s) Length: 324.063 (m) Width: 92.146 (m) Height: 104.570 (m) Voxel size: 1.035 (m)</p>
	Pedestrian Level view (PL)	<p>Velocity (m/s) [Pressure (Pa)] 13.397 [47.062] 11.602 [19.576] 9.473 [7.918] 6.698 [35.396] 0 [-62.882]</p> <p>Status: Stabilized Analysis: 3D Wind Speed: 10.000 (m/s) Length: 324.063 (m) Width: 92.146 (m) Height: 104.570 (m) Voxel size: 1.035 (m)</p>

Table 39 (continued)

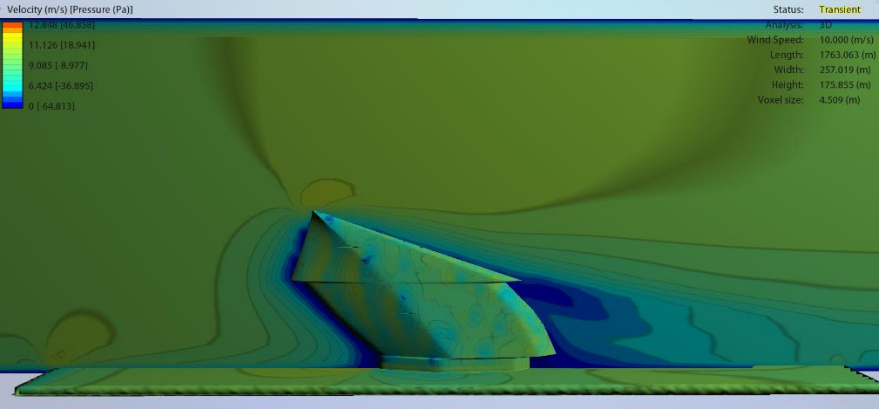
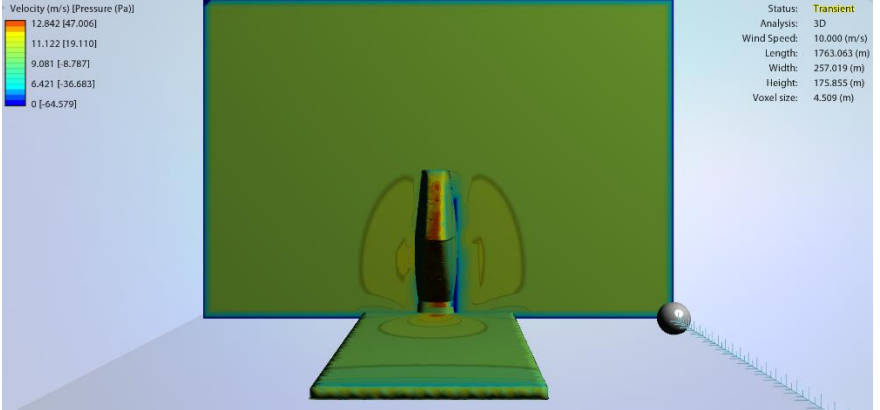
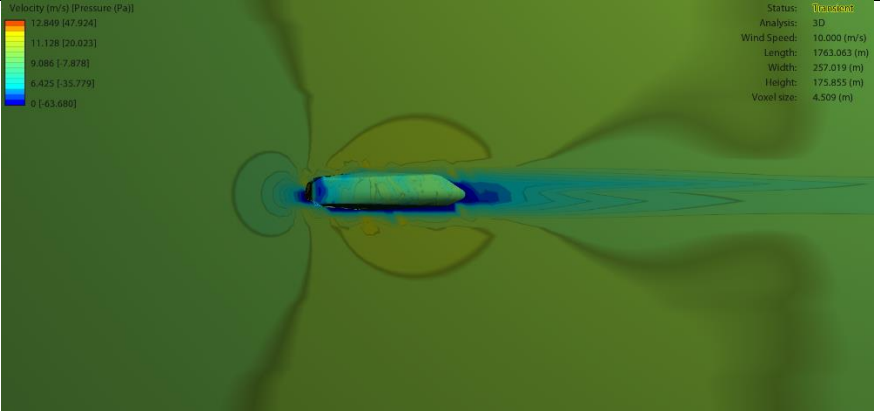
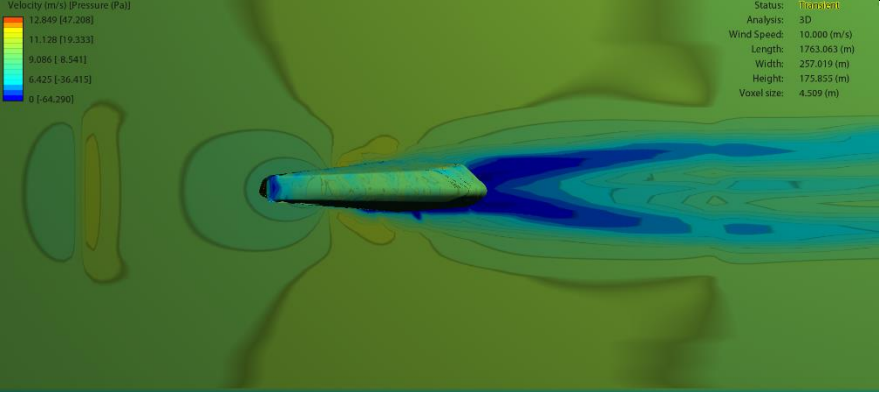
Sample 31	Windward Sect. view (WS)	 <p>Velocity (m/s) (Pressure (Pa))</p> <p>12.849 [47.924] 11.126 [18.941] 9.085 [8.977] 6.424 [-36.895] 0 [-64.813]</p> <p>Status: Transient Analysis: 3D Wind Speed: 10.000 (m/s) Length: 1763.063 (m) Width: 257.019 (m) Height: 175.855 (m) Voxel size: 4.509 (m)</p>
	Normal Section view (NS)	 <p>Velocity (m/s) (Pressure (Pa))</p> <p>12.842 [47.006] 11.122 [19.110] 9.081 [8.787] 6.421 [-36.683] 0 [-64.579]</p> <p>Status: Transient Analysis: 3D Wind Speed: 10.000 (m/s) Length: 1763.063 (m) Width: 257.019 (m) Height: 175.855 (m) Voxel size: 4.509 (m)</p>
	Roof Level view (RL)	 <p>Velocity (m/s) (Pressure (Pa))</p> <p>12.849 [47.924] 11.128 [20.023] 9.086 [7.878] 6.425 [-35.779] 0 [-63.680]</p> <p>Status: Transient Analysis: 3D Wind Speed: 10.000 (m/s) Length: 1763.063 (m) Width: 257.019 (m) Height: 175.855 (m) Voxel size: 4.509 (m)</p>
	Pedestrian Level view (PL)	 <p>Velocity (m/s) (Pressure (Pa))</p> <p>12.849 [47.208] 11.128 [19.333] 9.086 [8.541] 6.425 [-36.415] 0 [-64.290]</p> <p>Status: Transient Analysis: 3D Wind Speed: 10.000 (m/s) Length: 1763.063 (m) Width: 257.019 (m) Height: 175.855 (m) Voxel size: 4.509 (m)</p>

Table 39 (continued)

Sample 32	Windward Sect. view (WS)	<p>Velocity (m/s) Pressure (Pa)</p> <p>13.481 (38.542) 11.674 (11.337) 9.522 (11.468) 6.740 (42.274) 0 (1.69.000)</p> <p>Status: Simulated Analysis: 3D Wind Speed: 10.000 (m/s) Length: 752.063 (m) Width: 305.818 (m) Height: 71.774 (m) Voxel size: 3.121 (m)</p>
	Normal Section view (NS)	<p>Velocity (m/s) Pressure (Pa)</p> <p>13.480 (38.520) 11.674 (11.281) 9.522 (11.337) 6.740 (42.396) 0 (1.69.251)</p> <p>Status: Simulated Analysis: 3D Wind Speed: 10.000 (m/s) Length: 752.063 (m) Width: 305.818 (m) Height: 71.774 (m) Voxel size: 3.121 (m)</p>
	Roof Level view (RL)	<p>Velocity (m/s) Pressure (Pa)</p> <p>13.480 (38.542) 11.664 (11.372) 9.522 (11.417) 6.734 (42.307) 0 (1.68.997)</p> <p>Status: Simulated Analysis: 3D Wind Speed: 10.000 (m/s) Length: 752.063 (m) Width: 305.818 (m) Height: 71.774 (m) Voxel size: 3.121 (m)</p>
	Pedestrian Level view (PL)	<p>Velocity (m/s) Pressure (Pa)</p> <p>13.465 (38.396) 11.661 (11.562) 9.522 (11.272) 6.733 (42.106) 0 (1.68.941)</p> <p>Status: Simulated Analysis: 3D Wind Speed: 10.000 (m/s) Length: 752.063 (m) Width: 305.818 (m) Height: 71.774 (m) Voxel size: 3.121 (m)</p>

Table 39 (continued)

Sample 33	Windward Sect. view (WS)	<p>Velocity (m/s) [Pressure (Pa)] 13.188 [50.311] 11.421 [15.748] 9.325 [-18.815] 6.594 [-53.378] 0 [-87.941]</p> <p>Status: Stabilized Analysis: 3D Wind Speed: 10.000 (m/s) Length: 471.504 (m) Width: 167.895 (m) Height: 106.333 (m) Voxel size: 1.399 (m)</p>
	Normal Section view (NS)	<p>Velocity (m/s) [Pressure (Pa)] 13.170 [51.248] 11.405 [16.397] 9.312 [-18.454] 6.585 [-53.300] 0 [-86.157]</p> <p>Status: Stabilized Analysis: 3D Wind Speed: 10.000 (m/s) Length: 471.504 (m) Width: 167.895 (m) Height: 106.333 (m) Voxel size: 1.399 (m)</p>
	Roof Level view (RL)	<p>Velocity (m/s) [Pressure (Pa)] 13.162 [50.189] 11.399 [15.913] 9.307 [-18.362] 6.581 [-52.638] 0 [-86.913]</p> <p>Status: Stabilized Analysis: 3D Wind Speed: 10.000 (m/s) Length: 471.504 (m) Width: 167.895 (m) Height: 106.333 (m) Voxel size: 1.399 (m)</p>
	Pedestrian Level view (PL)	<p>Velocity (m/s) [Pressure (Pa)] 13.088 [50.679] 11.334 [16.266] 9.254 [-18.148] 6.544 [-52.551] 0 [-86.974]</p> <p>Status: Stabilized Analysis: 3D Wind Speed: 10.000 (m/s) Length: 471.504 (m) Width: 167.895 (m) Height: 106.333 (m) Voxel size: 1.399 (m)</p>

Table 39 (continued)

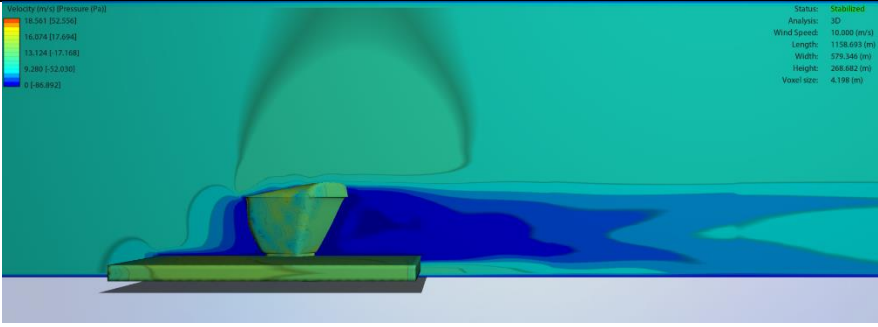
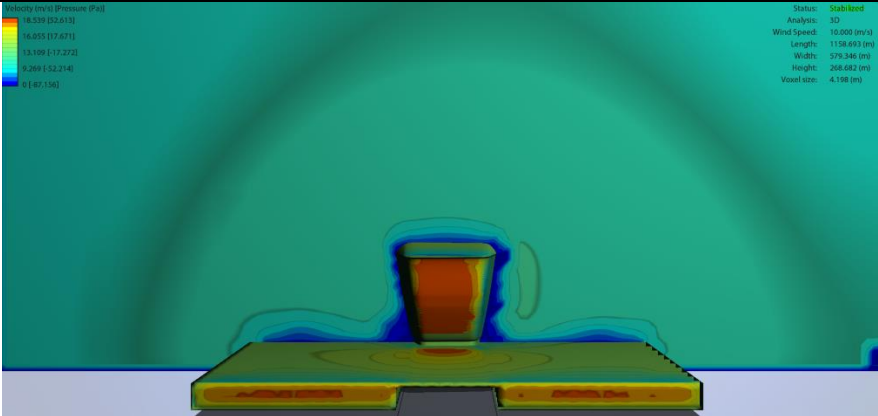
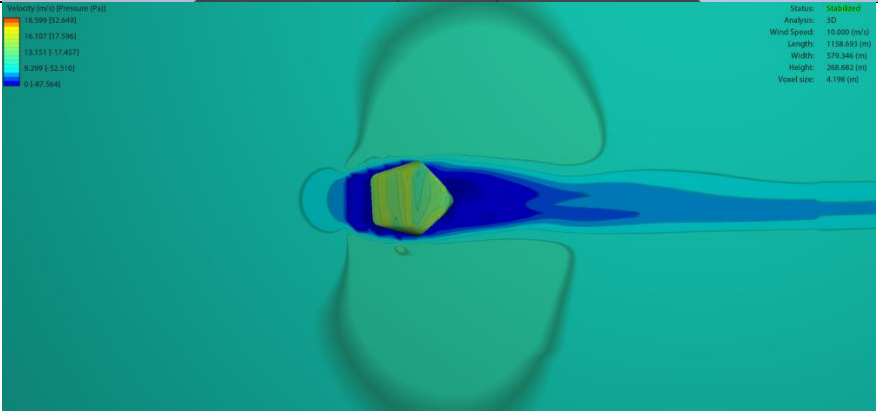
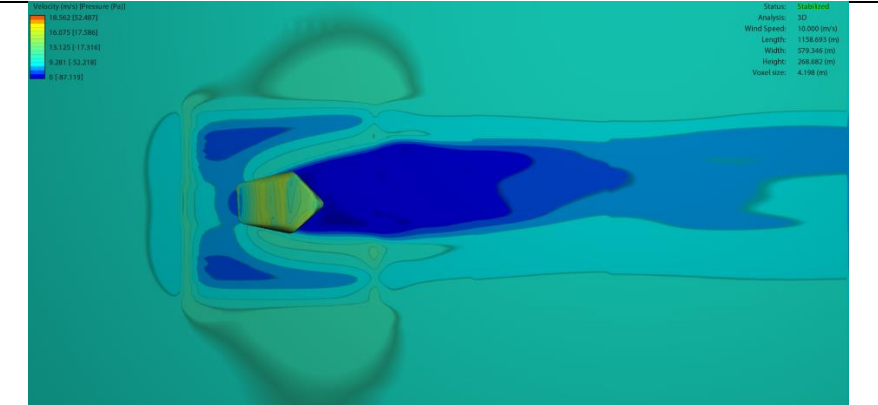
Sample 34	Windward Sect. view (WS)	
	Normal Section view (NS)	
	Roof Level view (RL)	
	Pedestrian Level view (PL)	

Table 39 (continued)

Sample 35	Windward Sect. view (WS)	
	Normal Section view (NS)	
	Roof Level view (RL)	
	Pedestrian Level view (PL)	

Table 39 (continued)

Sample 36	Windward Sect. view (WS)	<p>Velocity (m/s) (Pressure (Pa))</p> <ul style="list-style-type: none"> 12.396 [27.983] 10.735 [13.358] 8.765 [11.267] 6.198 [35.892] 0.160 [317] <p>Status: Transient Analysis: 3D Wind Speed: 10.000 (m/s) Length: 1359.726 (m) Width: 373.446 (m) Height: 134.058 (m) Voxel Size: 4.788 (m)</p>
	Normal Section view (NS)	<p>Velocity (m/s) (Pressure (Pa))</p> <ul style="list-style-type: none"> 12.589 [27.965] 10.730 [13.246] 8.761 [11.468] 6.193 [36.183] 0.160 (890) <p>Status: Transient Analysis: 3D Wind Speed: 10.000 (m/s) Length: 1359.726 (m) Width: 373.446 (m) Height: 134.058 (m) Voxel Size: 4.788 (m)</p>
	Roof Level view (RL)	<p>Velocity (m/s) (Pressure (Pa))</p> <ul style="list-style-type: none"> 13.292 [27.226] 10.732 [12.507] 8.762 [12.212] 6.196 [36.931] 0.161 (650) <p>Status: Transient Analysis: 3D Wind Speed: 10.000 (m/s) Length: 1359.726 (m) Width: 373.446 (m) Height: 134.058 (m) Voxel Size: 4.788 (m)</p>
	Pedestrian Level view (PL)	<p>Velocity (m/s) (Pressure (Pa))</p> <ul style="list-style-type: none"> 12.389 [38.029] 10.729 [13.228] 8.760 [11.573] 6.194 [36.374] 0.161 (170) <p>Status: Transient Analysis: 3D Wind Speed: 10.000 (m/s) Length: 1359.726 (m) Width: 373.446 (m) Height: 134.058 (m) Voxel Size: 4.788 (m)</p>

Table 39 (continued)

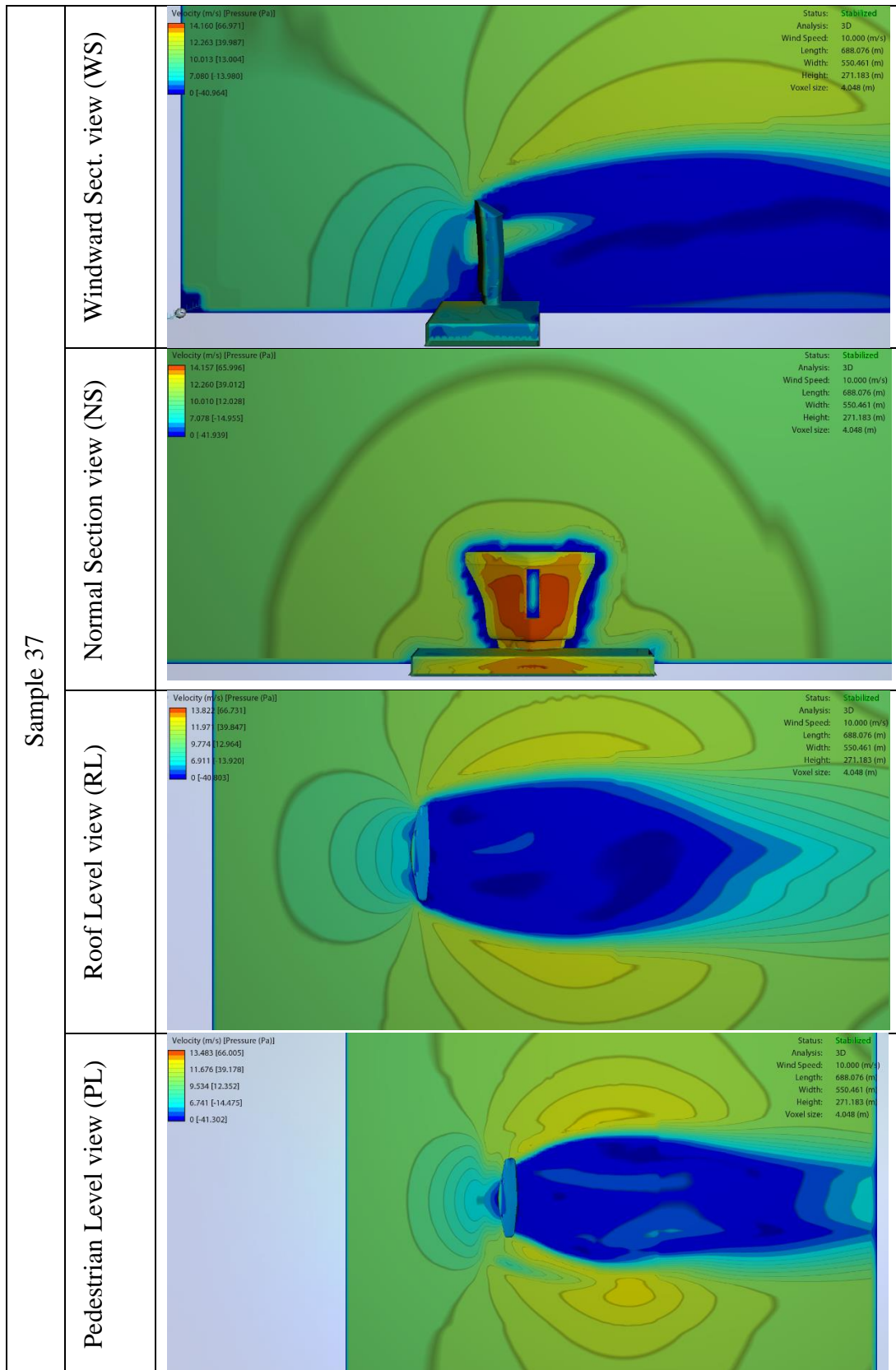


Table 39 (continued)

Sample 38	Windward Sect. view (WS)	<p>Velocity (m/s) [Pressure (Pa)]</p> <ul style="list-style-type: none"> 14.069 [54.113] 12.184 [24.171] 9.948 [-5.772] 7.034 [-35.715] 0 [-65.657] <p>Status: Stabilized Analysis: 3D Wind Speed: 10.000 (m/s) Length: 722.902 (m) Width: 462.657 (m) Height: 202.413 (m) Voxel size: 3.213 (m)</p>
	Normal Section view (NS)	<p>Velocity (m/s) [Pressure (Pa)]</p> <ul style="list-style-type: none"> 14.031 [54.292] 12.152 [24.581] 9.922 [-5.130] 7.016 [-34.841] 0 [-64.552] <p>Status: Stabilized Analysis: 3D Wind Speed: 10.000 (m/s) Length: 722.902 (m) Width: 462.657 (m) Height: 202.413 (m) Voxel size: 3.213 (m)</p>
	Roof Level view (RL)	<p>Velocity (m/s) [Pressure (Pa)]</p> <ul style="list-style-type: none"> 13.992 [54.243] 12.118 [24.673] 9.894 [-4.897] 6.996 [-34.467] 0 [-64.037] <p>Status: Stabilized Analysis: 3D Wind Speed: 10.000 (m/s) Length: 722.902 (m) Width: 462.657 (m) Height: 202.413 (m) Voxel size: 3.213 (m)</p>
	Pedestrian Level view (PL)	<p>Velocity (m/s) [Pressure (Pa)]</p> <ul style="list-style-type: none"> 13.950 [54.757] 12.081 [25.477] 9.864 [-3.804] 6.975 [-33.084] 0 [-62.365] <p>Status: Stabilized Analysis: 3D Wind Speed: 10.000 (m/s) Length: 722.902 (m) Width: 462.657 (m) Height: 202.413 (m) Voxel size: 3.213 (m)</p>

Table 39 (continued)

Sample 39	Windward Sect. view (WS)	<p>Velocity (m/s) [Pressure (Pa)]</p> <ul style="list-style-type: none"> 11.263 [31.959] 10.187 [8.601] 8.318 [-14.757] 5.865 [-37.115] 0 [-61.473] <p>Status: Transient Analysis: 3D Wind Speed: 10.000 (m/s) Length: 1669.407 (m) Width: 586.124 (m) Height: 104.665 (m) Voxel size: 5.233 (m)</p>
	Normal Section view (NS)	<p>Velocity (m/s) [Pressure (Pa)]</p> <ul style="list-style-type: none"> 11.729 [31.924] 10.158 [8.763] 8.294 [-14.595] 5.865 [-37.560] 0 [-60.722] <p>Status: Transient Analysis: 3D Wind Speed: 10.000 (m/s) Length: 1669.407 (m) Width: 586.124 (m) Height: 104.665 (m) Voxel size: 5.233 (m)</p>
	Roof Level view (RL)	<p>Velocity (m/s) [Pressure (Pa)]</p> <ul style="list-style-type: none"> 11.724 [31.966] 10.153 [8.757] 8.290 [-14.452] 5.862 [-37.661] 0 [-60.869] <p>Status: Transient Analysis: 3D Wind Speed: 10.000 (m/s) Length: 1669.407 (m) Width: 586.124 (m) Height: 104.665 (m) Voxel size: 5.233 (m)</p>
	Pedestrian Level view (PL)	<p>Velocity (m/s) [Pressure (Pa)]</p> <ul style="list-style-type: none"> 11.716 [31.941] 10.146 [8.751] 8.284 [-14.439] 5.858 [-37.629] 0 [-60.819] <p>Status: Transient Analysis: 3D Wind Speed: 10.000 (m/s) Length: 1669.407 (m) Width: 586.124 (m) Height: 104.665 (m) Voxel size: 5.233 (m)</p>

Table 39 (continued)

Sample 40	Windward Sect. view (WS)	<p>Velocity (m/s) [Pressure (Pa)] 12.597 [55.271] 10.910 [24.759] 8.908 [-5.753] 6.299 [-36.265] 0 [-66.776]</p> <p>Status: Stabilized Analysis: 3D Wind Speed: 10.000 (m/s) Length: 1026.228 (m) Width: 718.833 (m) Height: 283.750 (m) Voxel size: 4.729 (m)</p>
	Normal Section view (NS)	<p>Velocity (m/s) [Pressure (Pa)] 12.527 [56.448] 10.849 [26.255] 8.838 [-3.938] 6.264 [-34.131] 0 [-64.324]</p> <p>Status: Stabilized Analysis: 3D Wind Speed: 10.000 (m/s) Length: 1026.228 (m) Width: 718.833 (m) Height: 283.750 (m) Voxel size: 4.729 (m)</p>
	Roof Level view (RL)	<p>Velocity (m/s) [Pressure (Pa)] 12.514 [56.238] 10.837 [25.976] 8.848 [-4.285] 6.257 [-34.546] 0 [-64.807]</p> <p>Status: Stabilized Analysis: 3D Wind Speed: 10.000 (m/s) Length: 1026.228 (m) Width: 718.833 (m) Height: 283.750 (m) Voxel size: 4.729 (m)</p>
	Pedestrian Level view (PL)	<p>Velocity (m/s) [Pressure (Pa)] 12.508 [56.332] 10.832 [26.107] 8.845 [-4.119] 6.254 [-34.344] 0 [-64.569]</p> <p>Status: Stabilized Analysis: 3D Wind Speed: 10.000 (m/s) Length: 1026.228 (m) Width: 718.833 (m) Height: 283.750 (m) Voxel size: 4.729 (m)</p>

Table 39 (continued)

Sample 41	Windward Sect. view (WS)	<p>Velocity (m/s) [Pressure (Pa)]</p> <ul style="list-style-type: none"> 14.995 [52.357] 12.986 [22.306] 10.603 [7.746] 7.488 [-37.767] 0 [-67.849] <p>Status: Transient Analysis: 3D Wind Speed: 10.000 (m/s) Length: 1897.425 (m) Width: 328.308 (m) Height: 159.326 (m) Voxel size: 4.828 (m)</p>
	Normal Section view (NS)	<p>Velocity (m/s) [Pressure (Pa)]</p> <ul style="list-style-type: none"> 15.006 [50.894] 12.996 [20.398] 10.611 [-9.589] 7.503 [-40.095] 0 [-70.102] <p>Status: Transient Analysis: 3D Wind Speed: 10.000 (m/s) Length: 1897.425 (m) Width: 328.308 (m) Height: 159.326 (m) Voxel size: 4.828 (m)</p>
	Roof Level view (RL)	<p>Velocity (m/s) [Pressure (Pa)]</p> <ul style="list-style-type: none"> 15.036 [50.614] 13.022 [20.412] 10.632 [-9.790] 7.518 [-39.992] 0 [-70.199] <p>Status: Transient Analysis: 3D Wind Speed: 10.000 (m/s) Length: 1897.425 (m) Width: 328.308 (m) Height: 159.326 (m) Voxel size: 4.828 (m)</p>
	Pedestrian Level view (PL)	<p>Velocity (m/s) [Pressure (Pa)]</p> <ul style="list-style-type: none"> 15.049 [51.251] 13.033 [21.196] 10.641 [-8.860] 7.524 [-38.915] 0 [-68.970] <p>Status: Transient Analysis: 3D Wind Speed: 10.000 (m/s) Length: 1897.425 (m) Width: 328.308 (m) Height: 159.326 (m) Voxel size: 4.828 (m)</p>

Table 39 (continued)

Sample 42	Windward Sect. view (WS)		<p>Status: Stabilized</p> <p>Analysis: 3D</p> <p>Wind Speed: 10.000 (m/s)</p> <p>Length: 270.564 (m)</p> <p>Width: 222.917 (m)</p> <p>Height: 115.713 (m)</p> <p>Voxel size: 1.702 (m)</p>
	Normal Section view (NS)		<p>Status: Stabilized</p> <p>Analysis: 3D</p> <p>Wind Speed: 10.000 (m/s)</p> <p>Length: 270.564 (m)</p> <p>Width: 222.917 (m)</p> <p>Height: 115.713 (m)</p> <p>Voxel size: 1.702 (m)</p>
	Roof Level view (RL)		<p>Status: Stabilized</p> <p>Analysis: 3D</p> <p>Wind Speed: 10.000 (m/s)</p> <p>Length: 270.564 (m)</p> <p>Width: 222.917 (m)</p> <p>Height: 115.713 (m)</p> <p>Voxel size: 1.702 (m)</p>
	Pedestrian Level view (PL)		<p>Status: Stabilized</p> <p>Analysis: 3D</p> <p>Wind Speed: 10.000 (m/s)</p> <p>Length: 270.564 (m)</p> <p>Width: 222.917 (m)</p> <p>Height: 115.713 (m)</p> <p>Voxel size: 1.702 (m)</p>

Table 39 (continued)

Sample 43	Windward Sect. view (WS)	<p>Velocity (m/s) (Pressure (Pa))</p> <p>14,332 (25,147) 12,412 (17,940) 10,134 (19,266) 7,166 (17,142) 0 (113,679)</p> <p>Status: Stabilized Analysis: 3D Wind Speed: 10,000 (m/s) Length: 1058.939 (m) Width: 521.386 (m) Height: 282.923 (m) Voxel size: 4.042 (m)</p>
	Normal Section view (NS)	<p>Velocity (m/s) (Pressure (Pa))</p> <p>14,333 (25,072) 12,430 (17,915) 10,149 (19,243) 7,176 (17,160) 0 (113,557)</p> <p>Status: Stabilized Analysis: 3D Wind Speed: 10,000 (m/s) Length: 1058.939 (m) Width: 521.386 (m) Height: 282.923 (m) Voxel size: 4.042 (m)</p>
	Roof Level view (RL)	<p>Velocity (m/s) (Pressure (Pa))</p> <p>14,240 (24,878) 12,339 (17,868) 10,075 (19,252) 7,124 (17,131) 0 (113,401)</p> <p>Status: Stabilized Analysis: 3D Wind Speed: 10,000 (m/s) Length: 1058.939 (m) Width: 521.386 (m) Height: 282.923 (m) Voxel size: 4.042 (m)</p>
	Pedestrian Level view (PL)	<p>Velocity (m/s) (Pressure (Pa))</p> <p>14,290 (24,975) 12,375 (17,898) 10,104 (19,179) 7,145 (17,125) 0 (113,334)</p> <p>Status: Stabilized Analysis: 3D Wind Speed: 10,000 (m/s) Length: 1058.939 (m) Width: 521.386 (m) Height: 282.923 (m) Voxel size: 4.042 (m)</p>

Table 39 (continued)

Sample 44	Windward Sect. view (WS)	<p>Velocity (m/s) [Pressure (Pa)]</p> <ul style="list-style-type: none"> 12.191 [50.540] 10.558 [27.197] 8.621 [3.853] 6.096 [-19.491] 0 [-42.834] <p>Status: Stabilized Analysis: 3D Wind Speed: 10.000 (m/s) Length: 666.337 (m) Width: 337.894 (m) Height: 151.225 (m) Voxel size: 2.363 (m)</p>
	Normal Section view (NS)	<p>Velocity (m/s) [Pressure (Pa)]</p> <ul style="list-style-type: none"> 12.057 [50.880] 10.442 [27.579] 8.526 [4.277] 6.029 [-19.025] 0 [-42.327] <p>Status: Stabilized Analysis: 3D Wind Speed: 10.000 (m/s) Length: 666.337 (m) Width: 337.894 (m) Height: 151.225 (m) Voxel size: 2.363 (m)</p>
	Roof Level view (RL)	<p>Velocity (m/s) [Pressure (Pa)]</p> <ul style="list-style-type: none"> 12.094 [50.560] 10.474 [27.275] 8.552 [3.989] 6.047 [-19.296] 0 [-42.582] <p>Status: Stabilized Analysis: 3D Wind Speed: 10.000 (m/s) Length: 666.337 (m) Width: 337.894 (m) Height: 151.225 (m) Voxel size: 2.363 (m)</p>
	Pedestrian Level view (PL)	<p>Velocity (m/s) [Pressure (Pa)]</p> <ul style="list-style-type: none"> 12.076 [50.794] 10.458 [27.524] 8.539 [4.254] 6.038 [-19.016] 0 [-42.286] <p>Status: Stabilized Analysis: 3D Wind Speed: 10.000 (m/s) Length: 666.337 (m) Width: 337.894 (m) Height: 151.225 (m) Voxel size: 2.363 (m)</p>

Table 39 (continued)

Sample 45	Windward Sect. view (WS)	<p>Velocity (m/s) (Pressure (Pa))</p> <p>16.316 (41.626) 11.996 (30.468) 11.295 (23.847) 8.048 (15.500) 0 (0.000)</p> <p>Status: Stable Analysis: 3D Wind Speed: 10.000 (m/s) Length: 333.940 (m) Width: 313.643 (m) Height: 100.814 (m) Voxel size: 1.867 (m)</p>
	Normal Section view (NS)	<p>Velocity (m/s) (Pressure (Pa))</p> <p>11.932 (30.329) 11.375 (22.811) 9.044 (15.493) 0 (0.000)</p> <p>Status: Stable Analysis: 3D Wind Speed: 10.000 (m/s) Length: 333.940 (m) Width: 313.643 (m) Height: 100.814 (m) Voxel size: 1.867 (m)</p>
	Roof Level view (RL)	<p>Velocity (m/s) (Pressure (Pa))</p> <p>14.422 (31.543) 12.490 (29.354) 10.198 (22.438) 7.211 (15.450) 0 (0.000)</p> <p>Status: Stable Analysis: 3D Wind Speed: 10.000 (m/s) Length: 333.940 (m) Width: 313.643 (m) Height: 100.814 (m) Voxel size: 1.867 (m)</p>
	Pedestrian Level view (PL)	<p>Velocity (m/s) (Pressure (Pa))</p> <p>16.097 (41.361) 13.940 (33.373) 11.382 (22.816) 8.048 (15.500) 0 (0.000)</p> <p>Status: Stable Analysis: 3D Wind Speed: 10.000 (m/s) Length: 333.940 (m) Width: 313.643 (m) Height: 100.814 (m) Voxel size: 1.867 (m)</p>

Table 39 (continued)

Sample 46	Windward Sect. view (WS)	<p>Velocity (m/s) [Pressure (Pa)]</p> <ul style="list-style-type: none"> 16.531 [53.547] 14.316 [18.037] 11.689 [-17.473] 8.266 [-52.982] 0 [-88.492] <p>Status: Stabilized Analysis: 3D Wind Speed: 10.000 (m/s) Length: 915.364 (m) Width: 333.078 (m) Height: 153.359 (m) Voxel size: 2.396 (m)</p>
	Normal Section view (NS)	<p>Velocity (m/s) [Pressure (Pa)]</p> <ul style="list-style-type: none"> 16.531 [53.606] 14.334 [18.085] 11.703 [-17.437] 8.276 [-52.959] 0 [-88.481] <p>Status: Stabilized Analysis: 3D Wind Speed: 10.000 (m/s) Length: 915.364 (m) Width: 333.078 (m) Height: 153.359 (m) Voxel size: 2.396 (m)</p>
	Roof Level view (RL)	<p>Velocity (m/s) [Pressure (Pa)]</p> <ul style="list-style-type: none"> 16.533 [53.255] 14.335 [17.670] 11.705 [-17.915] 8.277 [-53.500] 0 [-89.084] <p>Status: Stabilized Analysis: 3D Wind Speed: 10.000 (m/s) Length: 915.364 (m) Width: 333.078 (m) Height: 153.359 (m) Voxel size: 2.396 (m)</p>
	Pedestrian Level view (PL)	<p>Velocity (m/s) [Pressure (Pa)]</p> <ul style="list-style-type: none"> 16.551 [53.540] 14.333 [17.994] 11.703 [-17.551] 8.275 [-53.096] 0 [-88.641] <p>Status: Stabilized Analysis: 3D Wind Speed: 10.000 (m/s) Length: 915.364 (m) Width: 333.078 (m) Height: 153.359 (m) Voxel size: 2.396 (m)</p>

Table 39 (continued)

Sample 47	Windward Sect. view (WS)		<p>Status: Transient</p> <p>Analysis: 3D</p> <p>Wind Speed: 10.000 (m/s)</p> <p>Length: 792.567 (m)</p> <p>Width: 213.056 (m)</p> <p>Height: 46.872 (m)</p> <p>Voxel size: 2.131 (m)</p>
	Normal Section view (NS)		<p>Status: Transient</p> <p>Analysis: 3D</p> <p>Wind Speed: 10.000 (m/s)</p> <p>Length: 792.567 (m)</p> <p>Width: 213.056 (m)</p> <p>Height: 46.872 (m)</p> <p>Voxel size: 2.131 (m)</p>
	Roof Level view (RL)		<p>Status: Transient</p> <p>Analysis: 3D</p> <p>Wind Speed: 10.000 (m/s)</p> <p>Length: 792.567 (m)</p> <p>Width: 213.056 (m)</p> <p>Height: 46.872 (m)</p> <p>Voxel size: 2.131 (m)</p>
	Pedestrian Level view (PL)		<p>Status: Transient</p> <p>Analysis: 3D</p> <p>Wind Speed: 10.000 (m/s)</p> <p>Length: 792.567 (m)</p> <p>Width: 213.056 (m)</p> <p>Height: 46.872 (m)</p> <p>Voxel size: 2.131 (m)</p>

Table 39 (continued)

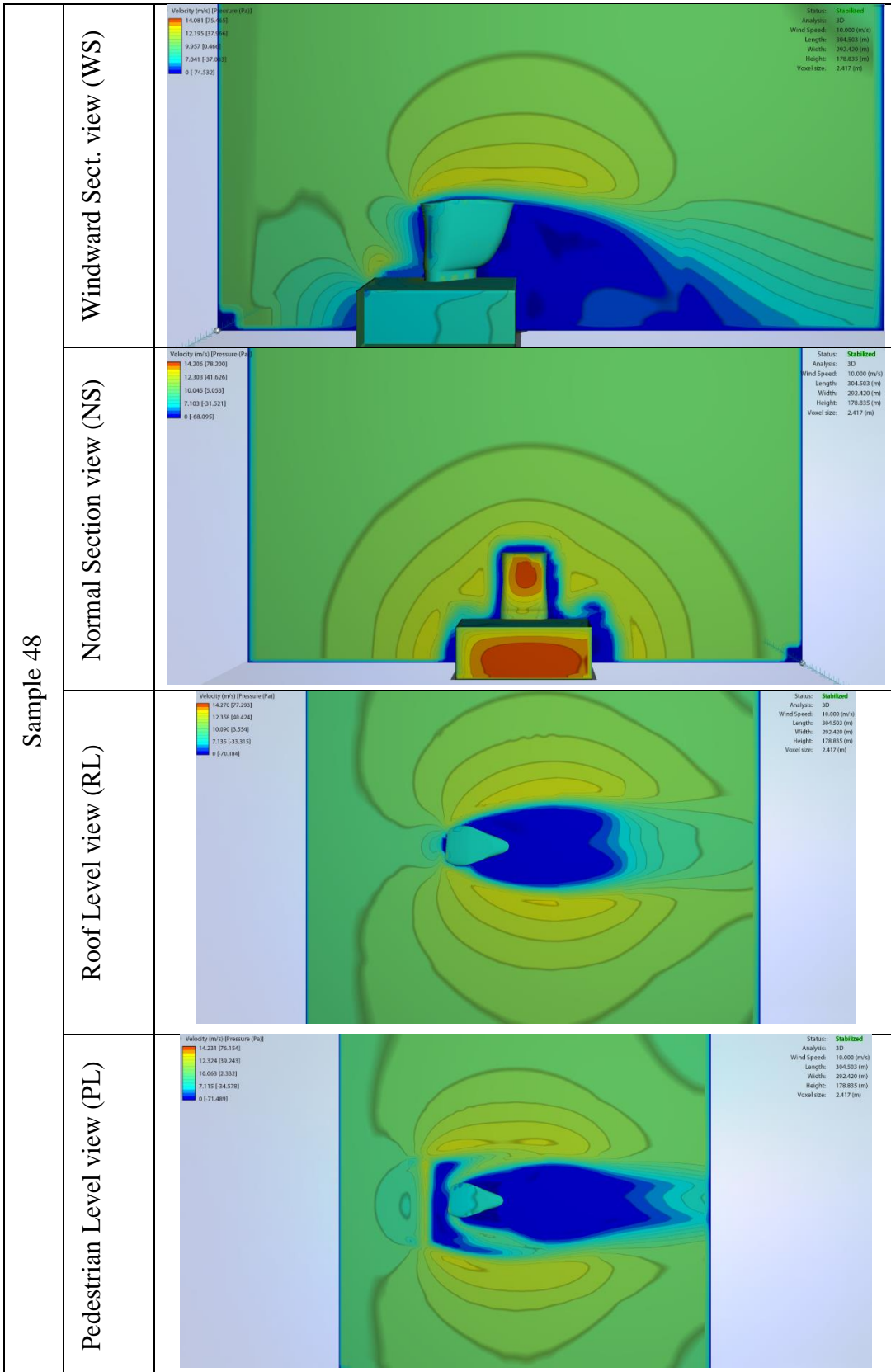


Table 39 (continued)

Sample 49	Windward Sect. view (WS)	<p>Velocity (m/s) (Pressure (Pa))</p> <ul style="list-style-type: none"> 13.29 (52.237) 11.367 (19.792) 9.281 (12.068) 6.562 (4.5769) 0 (1.78.550) <p>Status: Stabilized Analysis: 3D Wind Speed: 10.000 (m/s) Length: 1173.649 (m) Width: 385.901 (m) Height: 236.005 (m) Voxel size: 3.189 (m)</p>
	Normal Section view (NS)	<p>Velocity (m/s) (Pressure (Pa))</p> <ul style="list-style-type: none"> 13.129 (52.271) 11.340 (20.000) 9.280 (12.722) 6.561 (4.543) 0 (1.78.015) <p>Status: Stabilized Analysis: 3D Wind Speed: 10.000 (m/s) Length: 1173.649 (m) Width: 385.901 (m) Height: 236.005 (m) Voxel size: 3.189 (m)</p>
	Roof Level view (RL)	<p>Velocity (m/s) (Pressure (Pa))</p> <ul style="list-style-type: none"> 13.131 (53.043) 11.372 (20.160) 9.281 (12.220) 6.560 (4.611) 0 (1.78.496) <p>Status: Stabilized Analysis: 3D Wind Speed: 10.000 (m/s) Length: 1173.649 (m) Width: 385.901 (m) Height: 236.005 (m) Voxel size: 3.189 (m)</p>
	Pedestrian Level view (PL)	<p>Velocity (m/s) (Pressure (Pa))</p> <ul style="list-style-type: none"> 13.131 (53.215) 11.372 (20.438) 9.285 (12.338) 6.566 (4.5115) 0 (1.77.891) <p>Status: Stabilized Analysis: 3D Wind Speed: 10.000 (m/s) Length: 1173.649 (m) Width: 385.901 (m) Height: 236.005 (m) Voxel size: 3.189 (m)</p>

Table 39 (continued)

Sample 50	Windward Sect. view (WS)	<p>Velocity (m/s) [Pressure (Pa)]</p> <ul style="list-style-type: none"> 15.851 [37.643] 13.727 [12.440] 11.208 [12.763] 7.925 [-37.965] 0 [-63.168] <p>Status: Transient Analysis: 3D Wind Speed: 10.000 (m/s) Length: 1164.343 (m) Width: 142.651 (m) Height: 57.832 (m) Voxel size: 1.928 (m)</p>
	Normal Section view (NS)	<p>Velocity (m/s) [Pressure (Pa)]</p> <ul style="list-style-type: none"> 15.796 [37.041] 13.680 [11.155] 11.169 [14.731] 7.898 [-40.617] 0 [-66.503] <p>Status: Transient Analysis: 3D Wind Speed: 10.000 (m/s) Length: 1164.343 (m) Width: 142.651 (m) Height: 57.832 (m) Voxel size: 1.928 (m)</p>
	Roof Level view (RL)	<p>Velocity (m/s) [Pressure (Pa)]</p> <ul style="list-style-type: none"> 15.718 [37.691] 13.612 [10.671] 11.114 [16.349] 7.659 [-43.369] 0 [70.389] <p>Status: Transient Analysis: 3D Wind Speed: 10.000 (m/s) Length: 1164.343 (m) Width: 142.651 (m) Height: 57.832 (m) Voxel size: 1.928 (m)</p>
	Pedestrian Level view (PL)	<p>Velocity (m/s) [Pressure (Pa)]</p> <ul style="list-style-type: none"> 13.780 [39.229] 11.934 [11.513] 9.744 [-16.203] 6.890 [-43.919] 0 [71.635] <p>Status: Transient Analysis: 3D Wind Speed: 10.000 (m/s) Length: 1164.343 (m) Width: 142.651 (m) Height: 57.832 (m) Voxel size: 1.928 (m)</p>

Table 40: Screenshots of simulations 51- 66

Sample 51	Windward Sect. view (WS)	<p>Velocity (m/s) [Pressure (Pa)]</p> <ul style="list-style-type: none"> 13.970 [75.677] 12.098 [45.917] 9.878 [16.157] 6.985 [-13.603] 0 [-43.363] <p>Status: Stabilized Analysis: 3D Wind Speed: 10.000 (m/s) Length: 271.271 (m) Width: 247.510 (m) Height: 144.546 (m) Voxel size: 1.980 (m)</p>
	Normal Section view (NS)	<p>Velocity (m/s) [Pressure (Pa)]</p> <ul style="list-style-type: none"> 13.497 [77.464] 11.689 [49.387] 9.544 [21.309] 6.749 [-6.708] 0 [-34.845] <p>Status: Stabilized Analysis: 3D Wind Speed: 10.000 (m/s) Length: 271.271 (m) Width: 247.510 (m) Height: 144.546 (m) Voxel size: 1.980 (m)</p>
	Roof Level view (RL)	<p>Velocity (m/s) [Pressure (Pa)]</p> <ul style="list-style-type: none"> 13.208 [78.556] 11.438 [50.728] 9.339 [22.900] 6.604 [-4.928] 0 [-32.736] <p>Status: Stabilized Analysis: 3D Wind Speed: 10.000 (m/s) Length: 271.271 (m) Width: 247.510 (m) Height: 144.546 (m) Voxel size: 1.980 (m)</p>
	Pedestrian Level view (PL)	<p>Velocity (m/s) [Pressure (Pa)]</p> <ul style="list-style-type: none"> 13.172 [78.751] 11.408 [51.300] 9.314 [23.850] 6.586 [-3.600] 0 [-31.051] <p>Status: Stabilized Analysis: 3D Wind Speed: 10.000 (m/s) Length: 271.271 (m) Width: 247.510 (m) Height: 144.546 (m) Voxel size: 1.980 (m)</p>

Table 40 (continued)

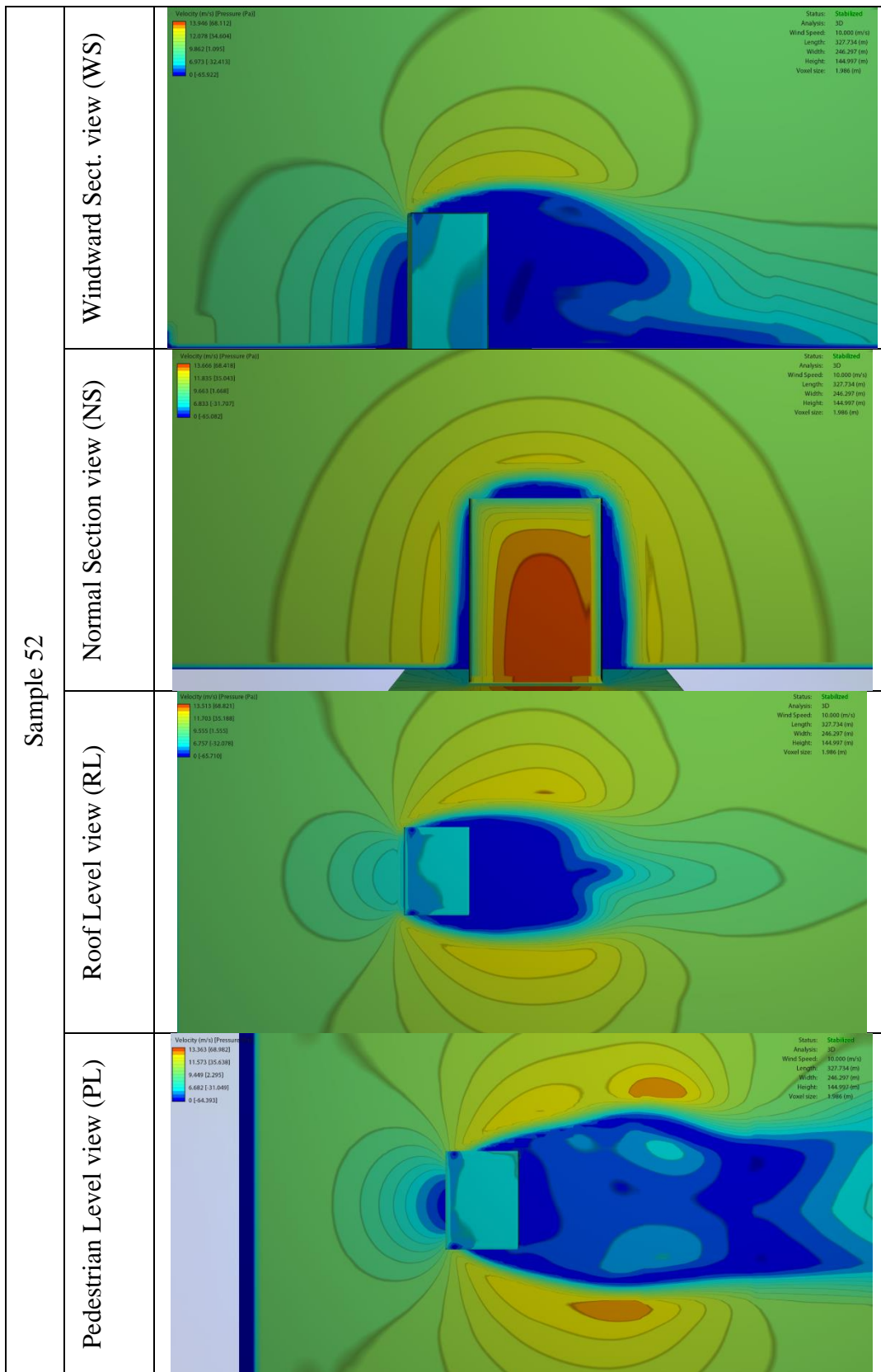


Table 40 (continued)

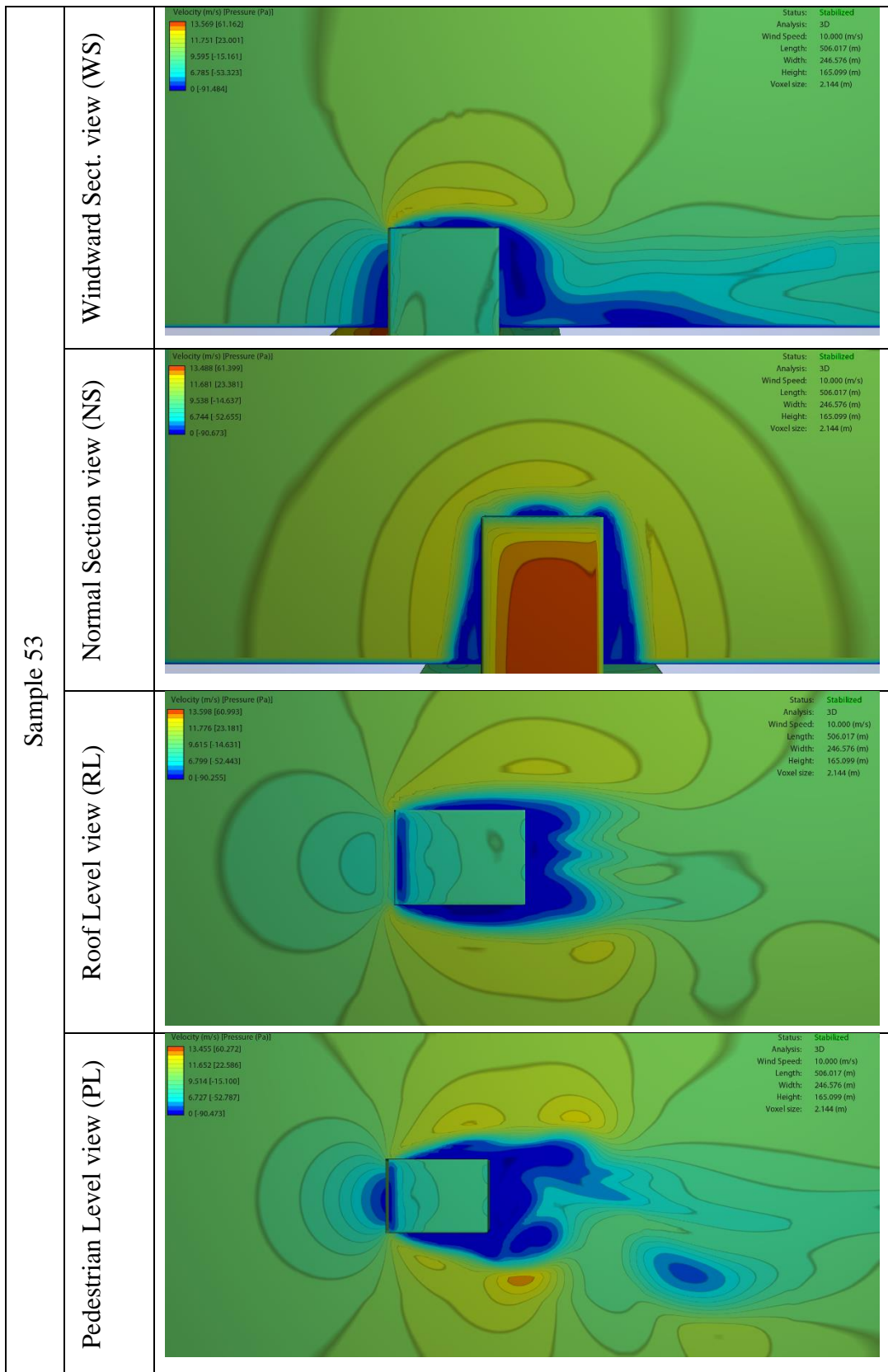


Table 40 (continued)

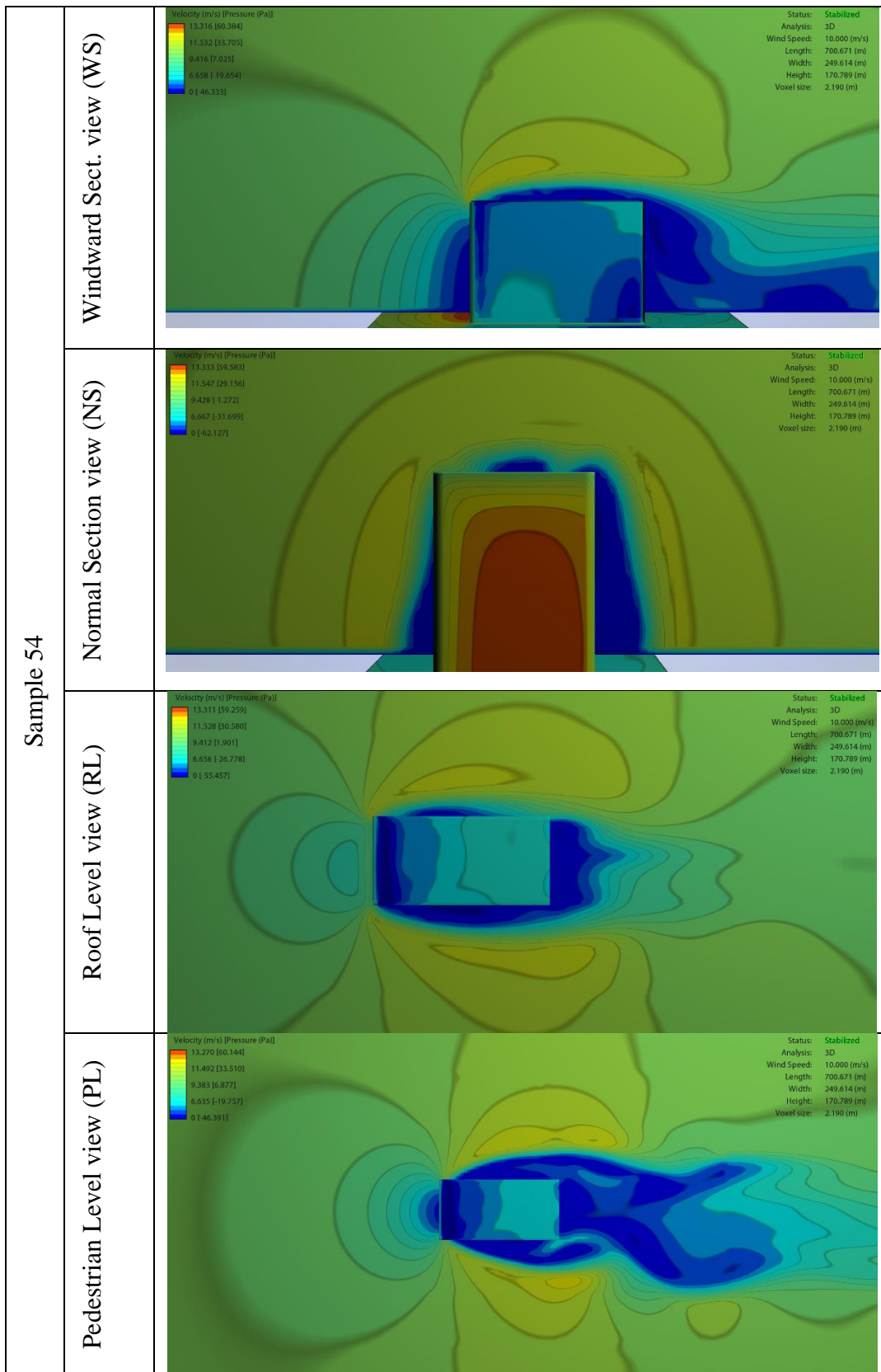


Table 40 (continued)

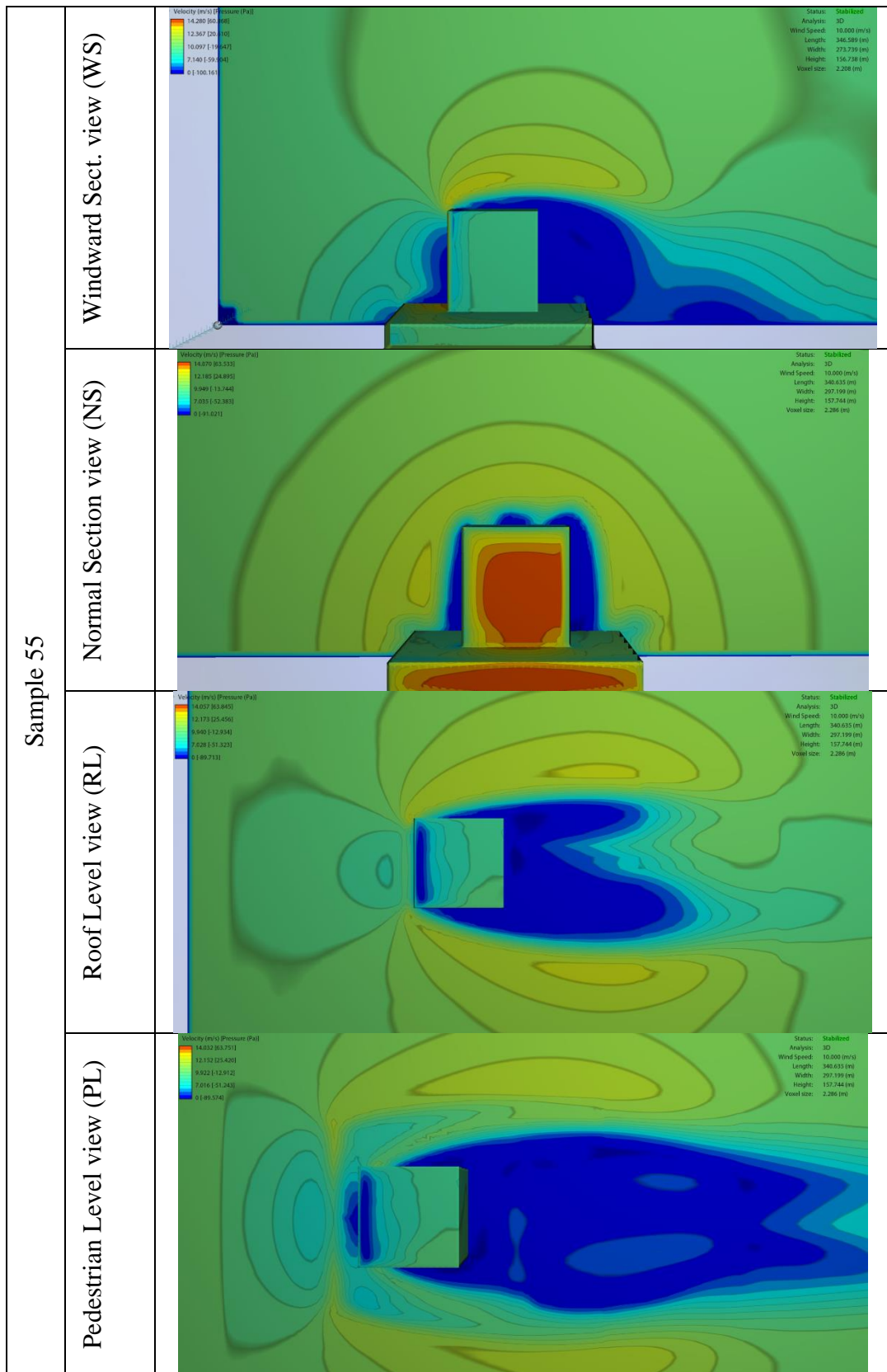


Table 40 (continued)

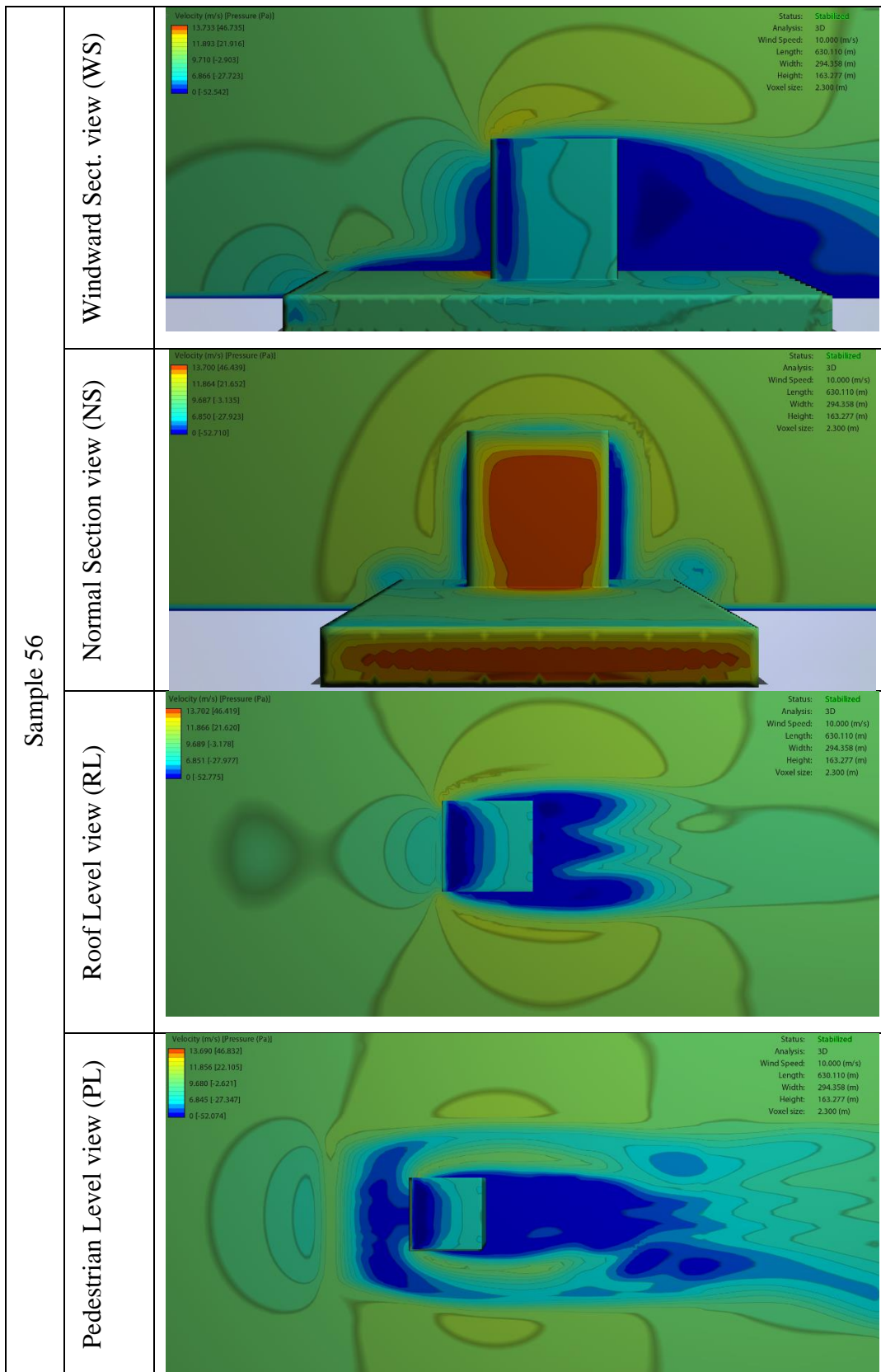


Table 40 (continued)

Sample 57	Windward Sect. view (WS)	<p>Velocity (m/s) Pressure (Pa)</p> <p>12.243 (85.000) 11.464 (82.958) 8.364 (60.998) 5.822 (42.142) 0.143 (1.032)</p> <p>Status: Stabilized Analysis: 30 Wind Speed: 10.000 (m/s) Length: 903.212 (m) Width: 292.834 (m) Height: 185.525 (m) Voxel size: 2.441 (m)</p>
	Normal Section view (NS)	<p>Velocity (m/s) Pressure (Pa)</p> <p>11.426 (82.580) 10.24 (74.476) 5.393 (39.462) 0.143 (1.032)</p> <p>Status: Stabilized Analysis: 30 Wind Speed: 10.000 (m/s) Length: 903.212 (m) Width: 292.834 (m) Height: 185.525 (m) Voxel size: 2.441 (m)</p>
	Roof Level view (RL)	<p>Velocity (m/s) Pressure (Pa)</p> <p>11.202 (82.196) 5.387 (39.416) 5.377 (39.402) 0.143 (1.032)</p> <p>Status: Stabilized Analysis: 30 Wind Speed: 10.000 (m/s) Length: 903.212 (m) Width: 292.834 (m) Height: 185.525 (m) Voxel size: 2.441 (m)</p>
	Pedestrian Level view (PL)	<p>Velocity (m/s) Pressure (Pa)</p> <p>11.382 (82.540) 9.293 (68.832) 6.071 (44.835) 0.142 (1.032)</p> <p>Status: Stabilized Analysis: 30 Wind Speed: 10.000 (m/s) Length: 903.212 (m) Width: 292.834 (m) Height: 185.525 (m) Voxel size: 2.441 (m)</p>

Table 40 (continued)

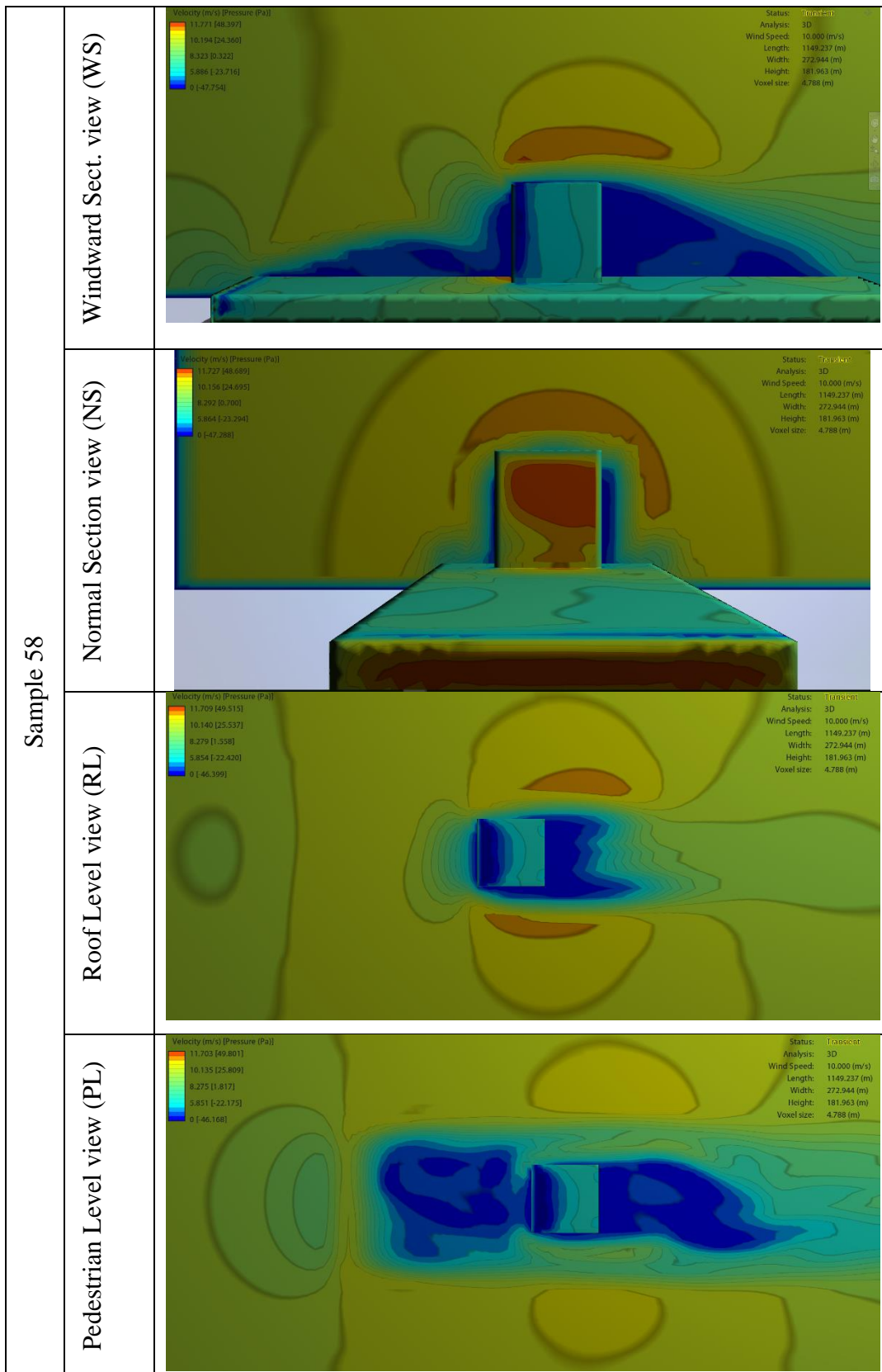


Table 40 (continued)

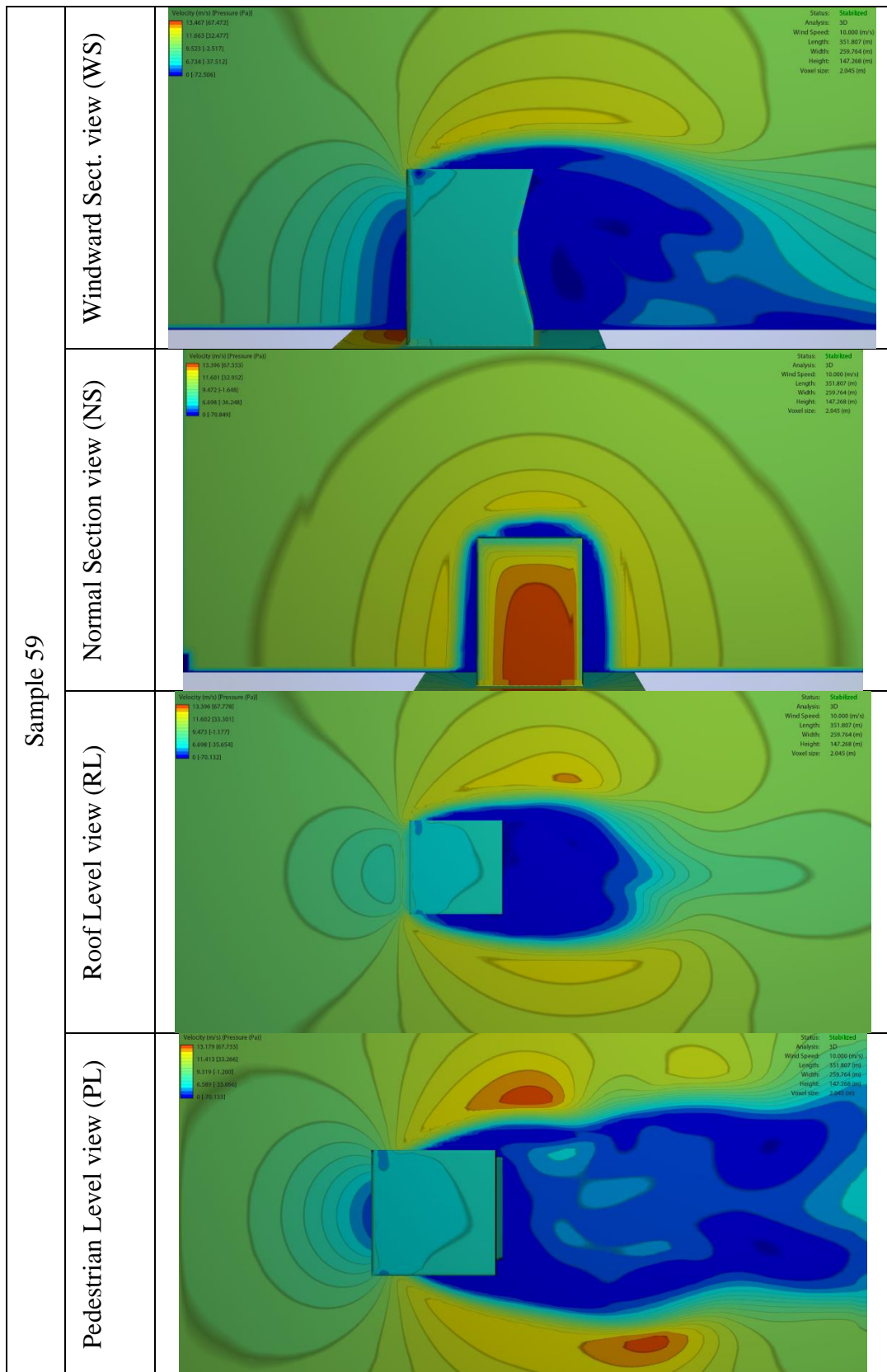


Table 40 (continued)

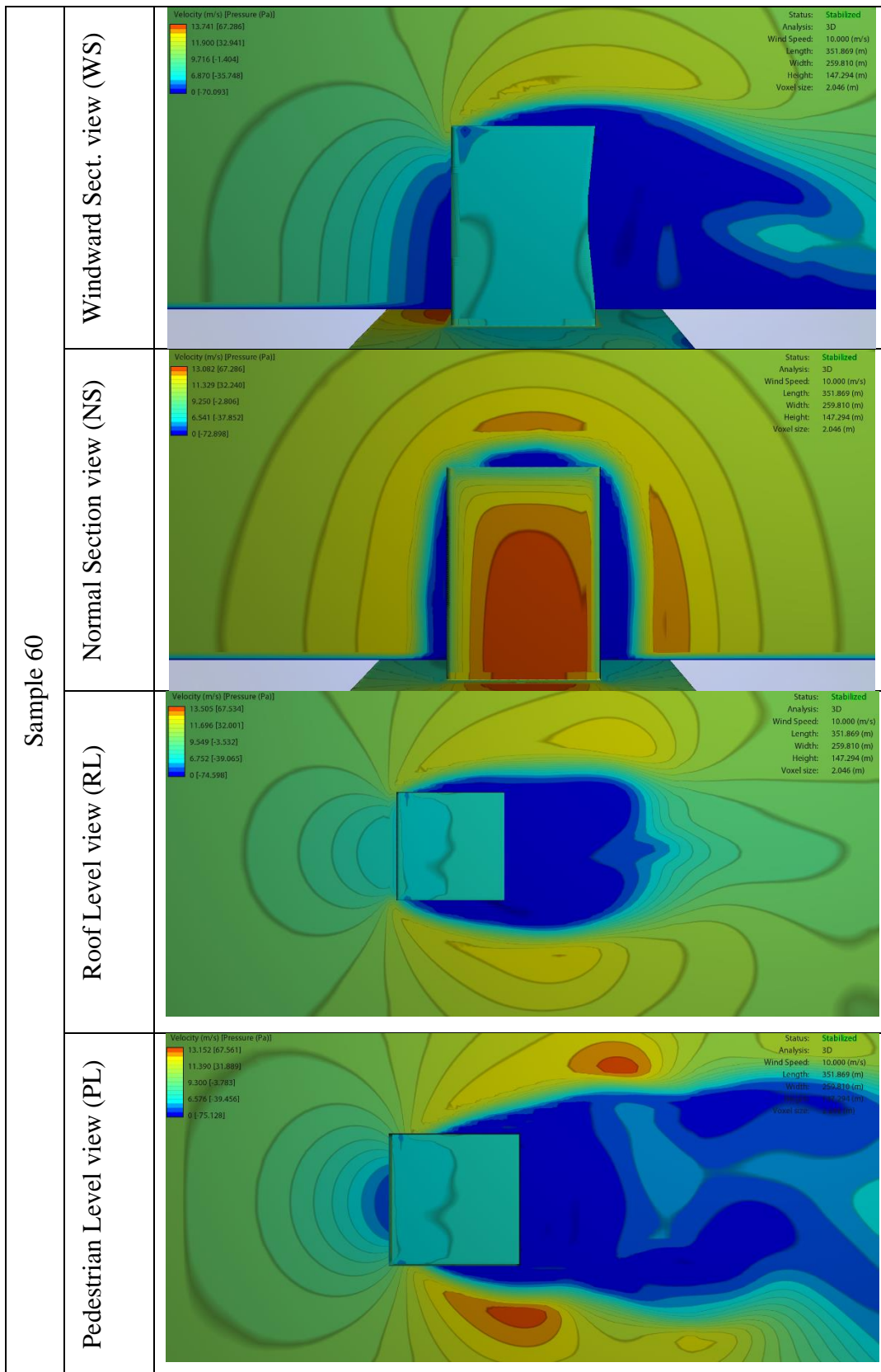


Table 40 (continued)

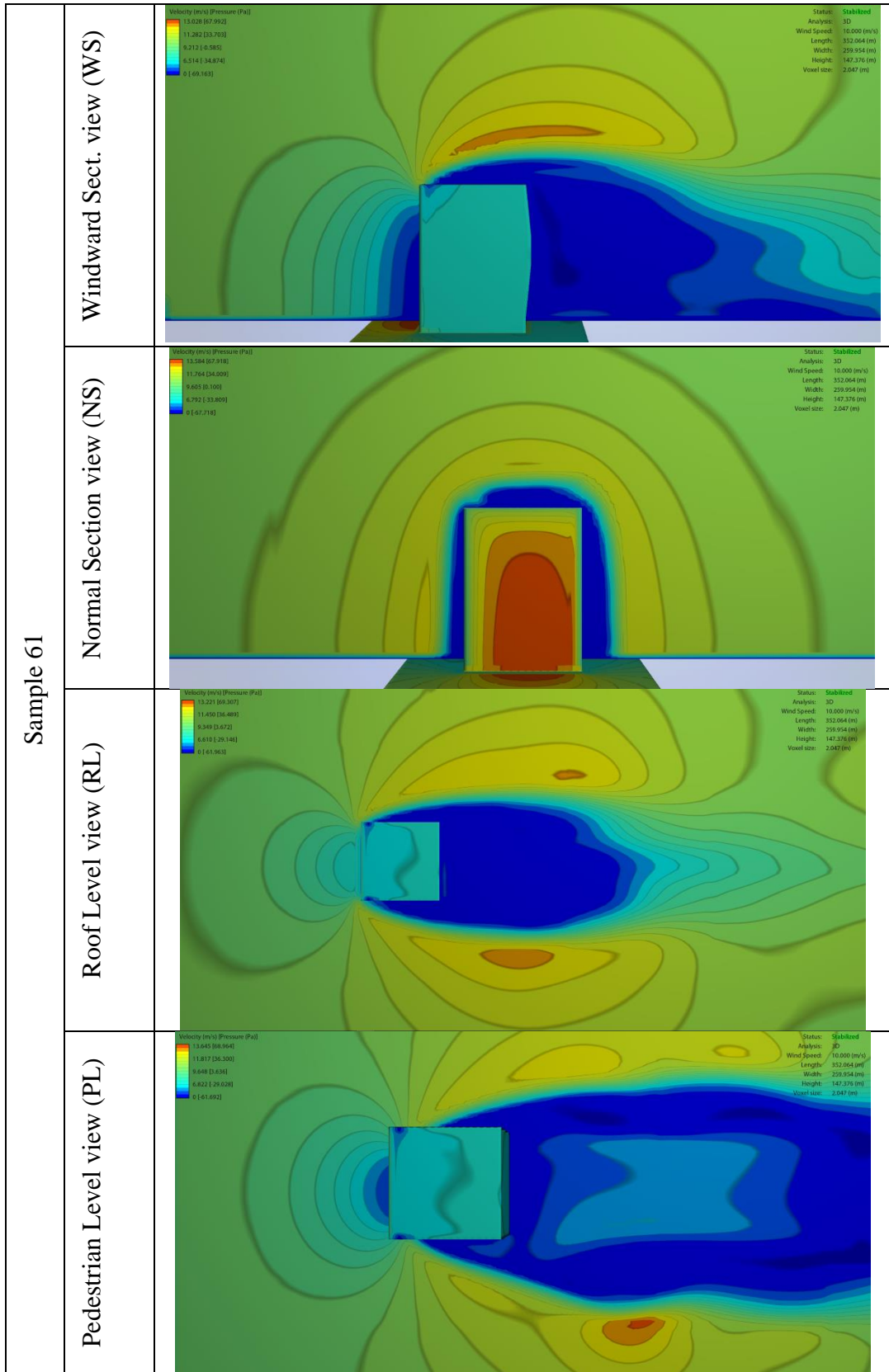


Table 40 (continued)

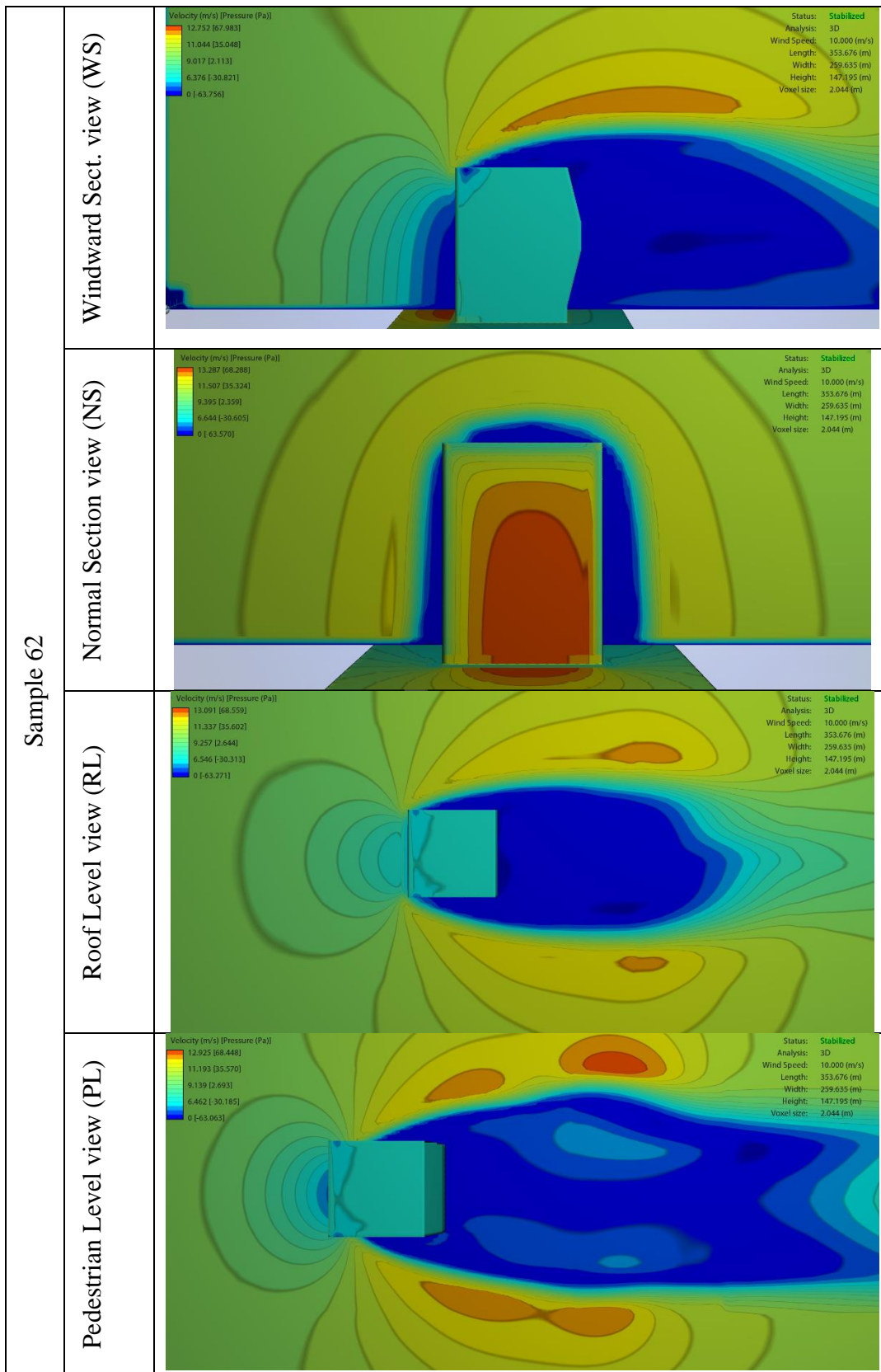


Table 40 (continued)

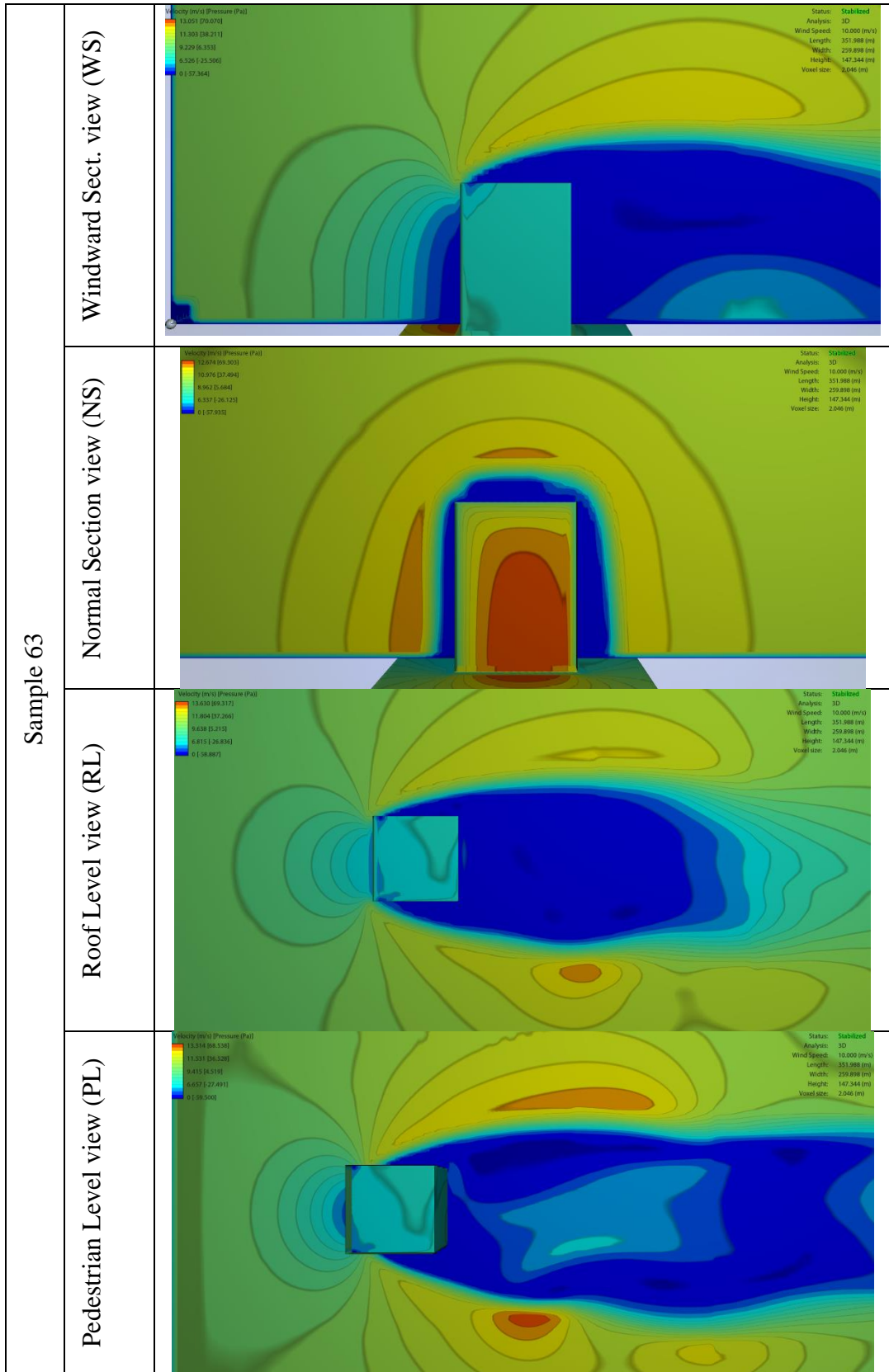


Table 40 (continued)

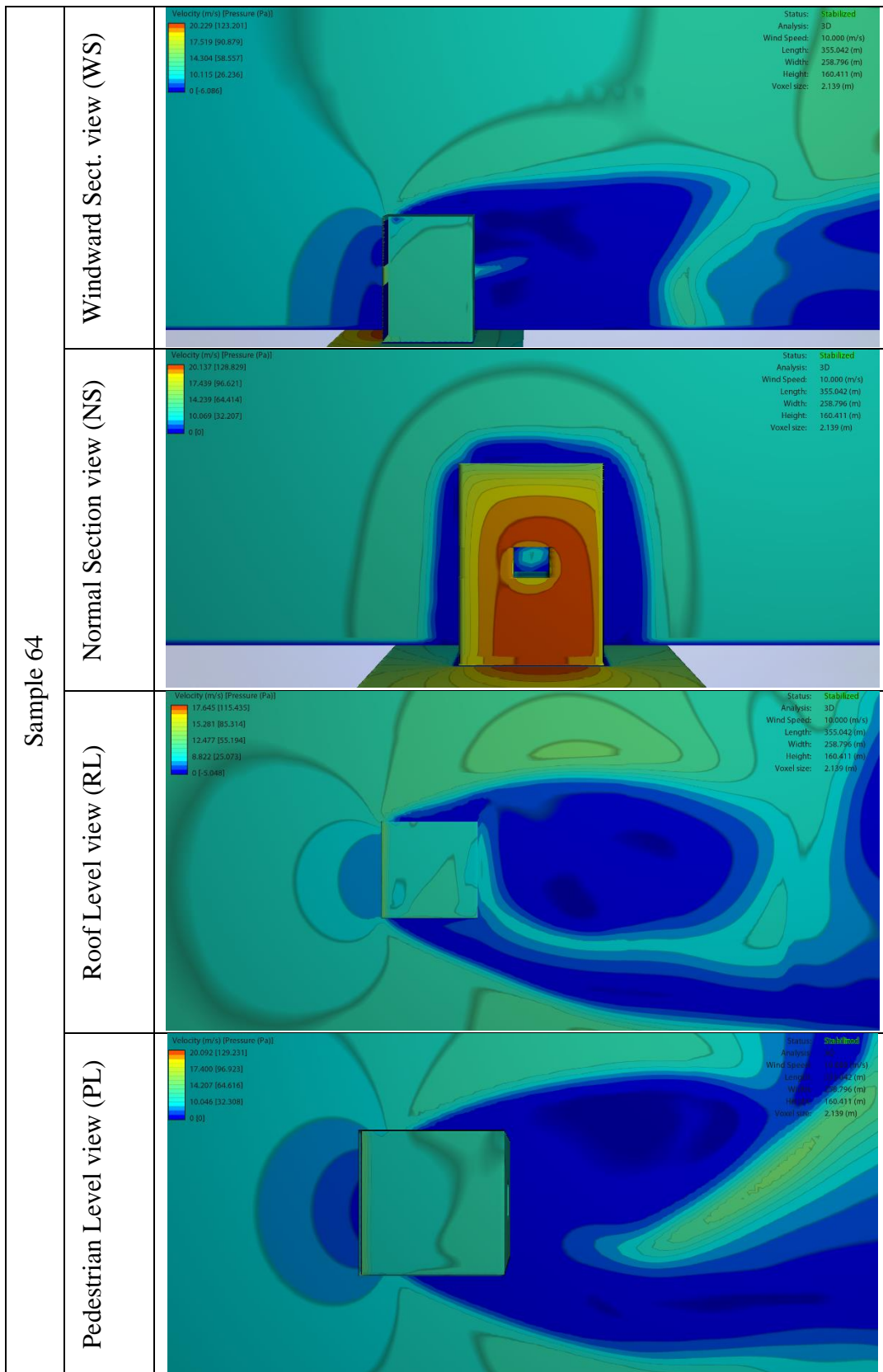


Table 40 (continued)

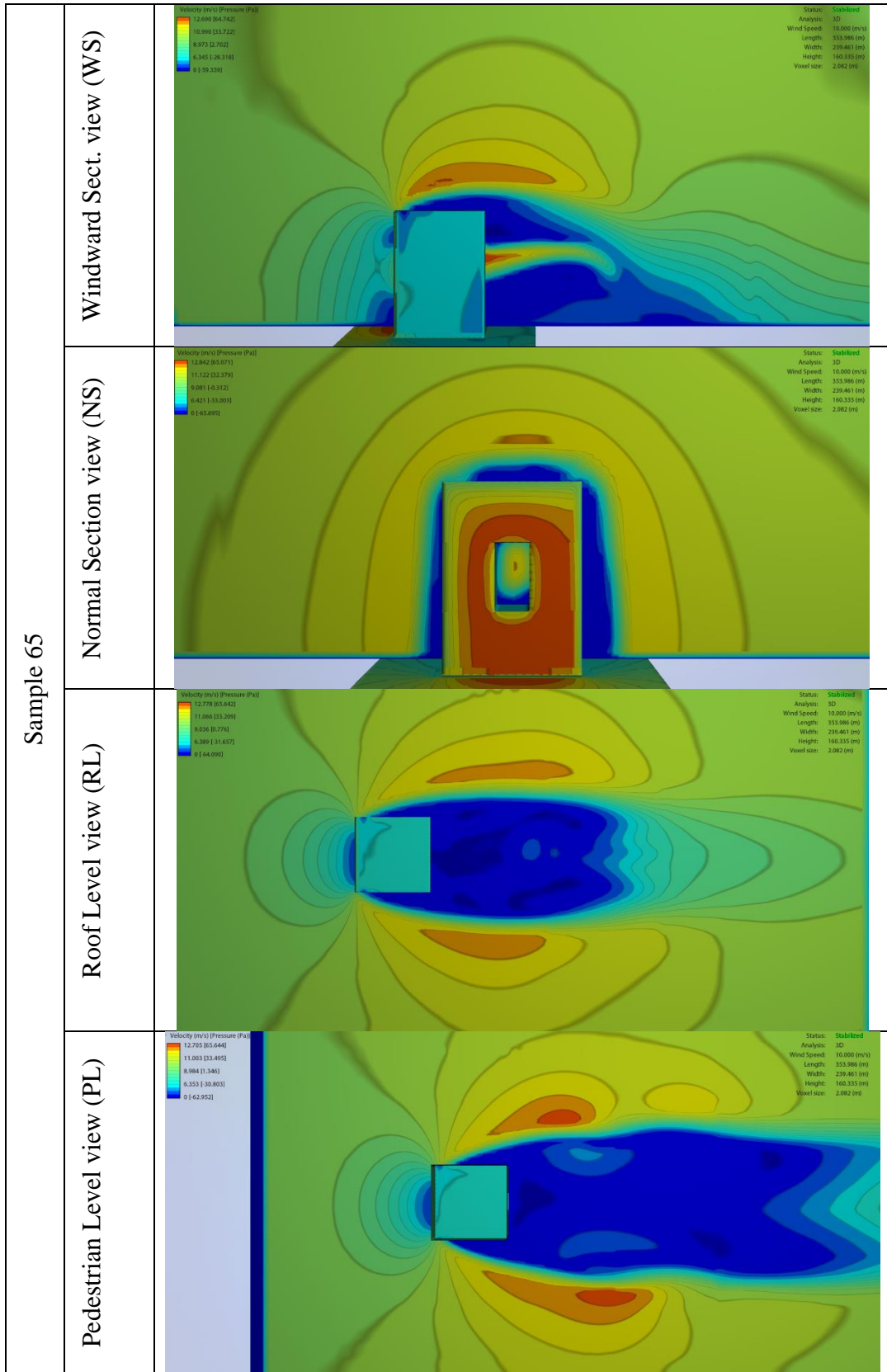
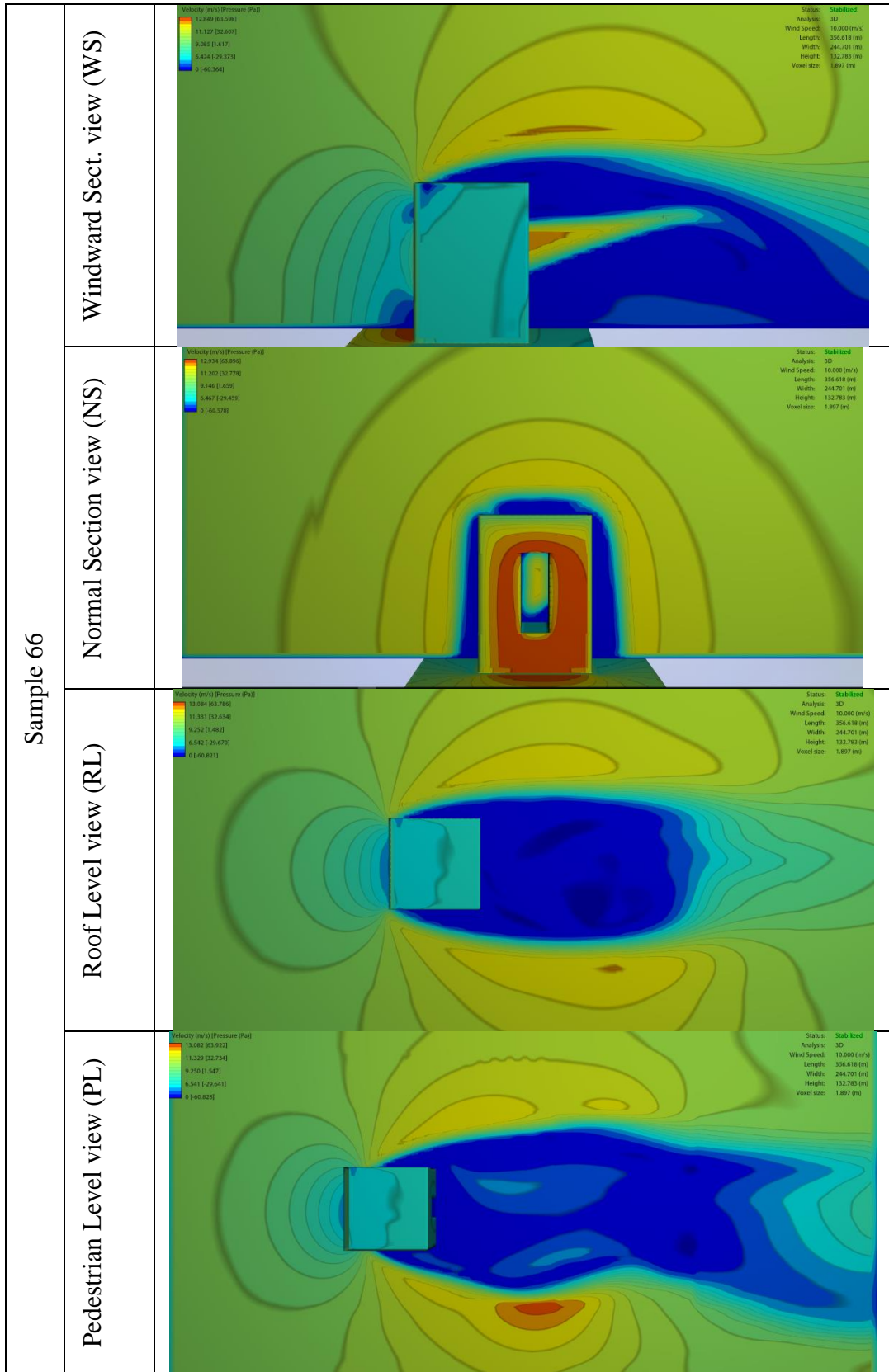


Table 40 (continued)



APPENDIX D

DATA ANALYSIS RESULTS

D.1 Multiple Regression Analyses

Summary of multiple regression analyses (by Automatic Linear Modeling via SPSS Statistics) results are presented in this appendix. All charts include values of top ten significant predictors for each target.

Some notes for the interpretations of contents:

- Automatic data preparation: This means the data prepared for regression analysis by SPSS Statistics using Trim Outliers function.
- Information Criterion: It is a measure of the accuracy for statistical models, smaller values shows better fits. It is a key control factor for the reliability of analysis.
- In the “Effects” table, higher “Sum of Square” values refers stronger predictor effect on target. “Importance” columns are another measure for this in a scale of 100.
- Type of the correlation between predictors and the target is deducible from the “Coefficient” values in the “Coefficients” table. Negative values suggests negative correlations, whereas positive values suggest positive correlations.

Other analytical results which are gathered by same process but not presented in this part are:

- Predicted by observed charts,
- P-P Plots for residuals,
- List of outliers with Cook’s distance values.
- Estimated means.
- Model building summary, showing the existence of effects per each model steps.

Regression Model 1, Target: Average Drag Coefficient

Table 41. Model summary for Regression Model 1

Target	Average Drag Coefficient
Automatic Data Preparation	On
Model Selection Method	Forward Stepwise
Information Criterion	-412.420,856
Accuracy	81,90%

Table 42: Effects, Regression Model 1

Source	Sum of Squares	df	Mean Square	F	Sig.	Importance
Corrected Model	7.318,003	25	292,720	18.104,812	0,000	
TF.X	1.369,809	1	1.369,809	84.723,041	0,000	0,295
B.Yratio	959,670	1	959,670	59.355,852	0,000	0,207
SC.EaveDepthRatioBack	411,716	1	411,716	25.464,727	0,000	0,089
H.TotalHeight	261,357	1	261,357	16.165,017	0,000	0,056
SC.VertexPositionRatio	217,408	1	217,408	13.446,722	0,000	0,047
V.ElevationRatio	173,096	1	173,096	10.706,038	0,000	0,037
SC.ConcavityTranslationRatioBack	144,485	1	144,485	8.936,438	0,000	0,031
V.HeightRatio	140,787	1	140,787	8.707,686	0,000	0,030
V.WidthRatio	130,062	1	130,062	8.044,380	0,000	0,028
TF.Roundness	126,675	1	126,675	7.834,885	0,000	0,027
Residual	1.616,291	99.968	0,016			
Corrected Total	8.934,294	99.993				

Table 43: Coefficients, Regression Model 1

Model Term	Coefficient	Std. Error	t	Sig.	95% Confidence Interval	
					Lower	Upper
Intercept	1,015	0,008	122,010	0,000	1,031	
TF.X	-0,006	0,000	-291,072	0,000	-0,005	0,295
BY.Ratio	-0,124	0,001	-243,631	0,000	-0,123	0,207
SC.EaveDepthRatio	-1,184	0,007	-159,577	0,000	-1,169	0,089
H.TotalHeight	0,004	0,000	127,142	0,000	0,004	0,056
SC.VertexPosition Ratio	-0,235	0,000	-115,960	0,000	-0,231	0,047
V.ElevationRatio	-0,279	0,000	-103,470	0,000	-0,273	0,037
SC.Concavity TranslationRatioBack	-0,518	0,000	-94,533	0,000	-0,507	0,031
V.HeightRatio	0,478	0,000	93,315	0,000	0,488	0,030
V.WidthRatio	0,335	0,000	89,690	0,000	0,342	0,028
TF.Roundness	-0,896	0,000	-88,515	0,000	-0,876	0,027

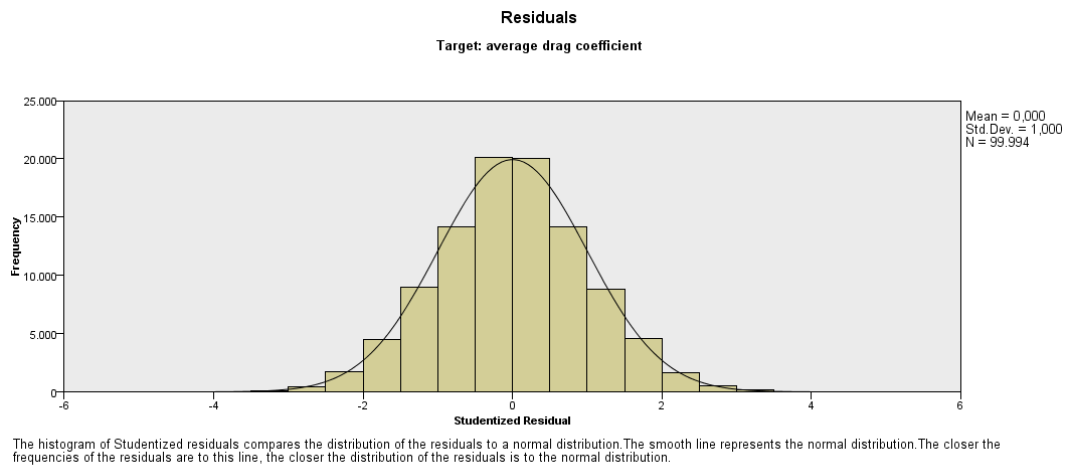


Figure 74: Residuals graph compared to a normal distribution, Regression Model 1

Regression Model 2, Target: WS Speed Up Regions

Table 44. Model summary for Regression Model 2

Target	WS. SpeedUp Regions
Automatic Data Preparation	On
Model Selection Method	Forward Stepwise
Information Criterion	-190.563,241
Accuracy	65,8%

Table 45: Effects, Regression Model 2

Source	Sum of Squares	df	Mean Square	F	Sig.	Importance
Corrected Model	28.622,456	25	1.144,898	7.700,788	0,000	
SC.ConcavityTranslationRatioFront	5.319,624	1	5.319,624	35.780,733	0,000	0,200
SC.VertexPositionRatio	4.185,430	1	4.185,430	28.151,943	0,000	0,157
TF.Y	2.591,639	1	2.591,639	17.431,824	0,000	0,097
SC.SetbackDepthRatioBack	2.045,003	1	2.045,003	13.755,051	0,000	0,077
H.TotalHeight	1.883,049	1	1.883,049	12.665,719	0,000	0,071
SC.FacadeEndpointTranslationRatioBack	1.797,422	1	1.797,422	12.089,779	0,000	0,067
SC.EaveDepthRatioBack	1.510,166	1	1.510,166	10.157,646	0,000	0,057
SC.ConcavityTranslationRatioBack	1.398,399	1	1.398,399	9.405,878	0,000	0,052
SC.SetbackDepthRatioFront	1.300,373	1	1.300,373	8.746,540	0,000	0,049
V.WidthRatio	1.289,790	1	1.289,790	8.675,353	0,000	0,048
Residual	14.862,530	99.968	0,149			
Corrected Total	43.484,986	99.993				

Table 46: Coefficients, Regression Model 2

Model Term	Coefficient	Std. Error	t	Sig.	95% Confidence Interval	
					Lower	Upper
Intercept	0,745	0,025	29,545	0,000	0,696	0,795
SC.ConcavityTranslation RatioFront	2,215	0,012	189,158	0,000	2,192	2,238
SC.VertexPositionRatio	-1,030	0,006	-167,785	0,000	-1,042	-1,018
TF.Y	-0,009	0,000	-132,030	0,000	-0,009	-0,009
SC.SetbackDepthRatio Back	1,740	0,015	117,282	0,000	1,711	1,769
H.TotalHeight	0,010	0,000	112,542	0,000	0,010	0,011
SC.FacadeEndpoint TranslationRatioBack	0,415	0,004	109,954	0,000	0,408	0,422
SC.EaveDepthRatioBack	-2,268	0,022	-100,785	0,000	-2,312	-2,224
SC.ConcavityTranslation RatioBack	1,611	0,017	96,984	0,000	1,579	1,644
SC.SetbackDepthRatio Front	1,339	0,014	93,523	0,000	1,311	1,367
V.WidthRatio	1,054	0,011	93,142	0,000	1,032	1,076

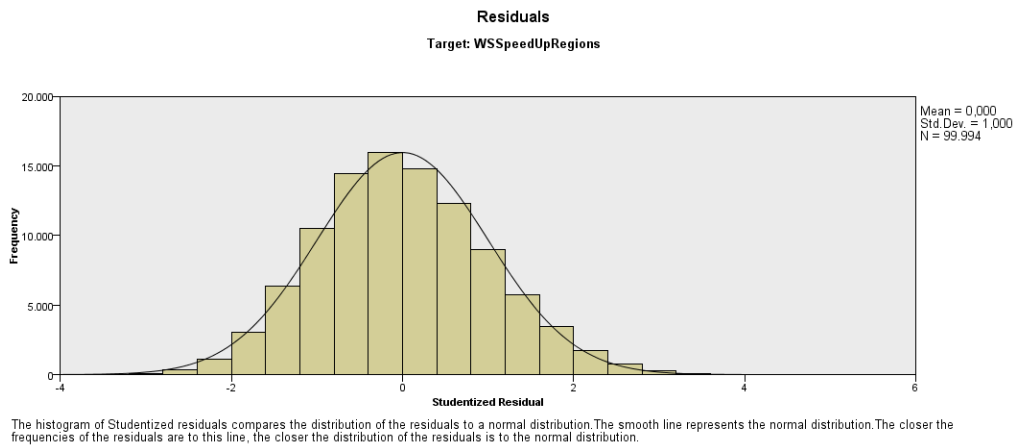


Figure 75: Residuals graph compared to a normal distribution, Regression Model 2

Regression Model 3, Target: WS Max Speed

Table 47. Model summary for Regression Model 3

Target	WS.MaxSpeed
Automatic Data Preparation	On
Model Selection Method	Forward Stepwise
Information Criterion	-185.333,568
Accuracy	61,9%

Table 48: Effects, Regression Model 3

Source	Sum of Squares	df	Mean Square	F	Sig.	Importance
Corrected Model	25.403,245	25	1.016,403	6.486,403	0,000	
SC.EaveDepthRatioFront	4.751,436	1	4.751,436	30.330,500	0,000	0,248
SC.FacadeEndpoint TranslationRatioFront	2.459,436	1	2.459,547	15.700,366	0,000	0,129
B.XRatio	1.895,547	1	1.895,263	12.098,298	0,000	0,099
B.YRatio	1.817,014	1	1.817,014	11.598,799	0,000	0,095
SC.FacadeEndpoint TranslationRatioBack	1.610,441	1	1.610,441	10.280,154	0,000	0,084
V.HeightRatio	1.292,079	1	1.292,079	8.247,907	0,000	0,068
SC.EaveDepthRatioBack	1.192,093	1	1.192,093	7.609,655	0,000	0,062
TF.Roundness	604,904	1	604,904	3.861,367	0,000	0,032
B.HeightRatio	529,033	1	529,033	3.377,052	0,000	0,028
TF.Vertice	376,275	1	376,275	2.401,931	0,000	0,020
Residual	15.660,524	99.968	0,157			
Corrected Total	41.063,769	99.993				

Table 49: Coefficients, Regression Model 3

Model Term	Coefficient	Std. Error	t	Sig.	95% Confidence Interval	
					Lower	Upper
Intercept	13,140	0,026	507,561	0,000	13,089	13,191
SC.EaveDepthRatioFront	-4,153	0,024	-174,157	0,000	-4,200	-4,106
SC.FacadeEndpoint TranslationRatioFront	0,541	0,004	125,301	0,000	0,532	0,549
B.XRatio	-0,168	0,002	-109,992	0,000	-0,171	-0,165
B.YRatio	-0,170	0,002	-107,698	0,000	-0,173	-0,167
SC.FacadeEndpoint TranslationRatioBack	0,393	0,004	101,391	0,000	0,385	0,400
V.HeightRatio	1,447	0,016	90,818	0,000	1,415	1,478
SC.EaveDepthRatioBack	-2,015	0,023	-87,233	0,000	-2,060	-1,969
TF.Roundness	-1,957	0,031	-62,140	0,000	-2,019	-1,895
B.HeightRatio	-1,083	0,019	-58,112	0,000	-1,119	-1,046
TF.Vertice	0,074	0,002	49,009	0,000	0,071	0,077

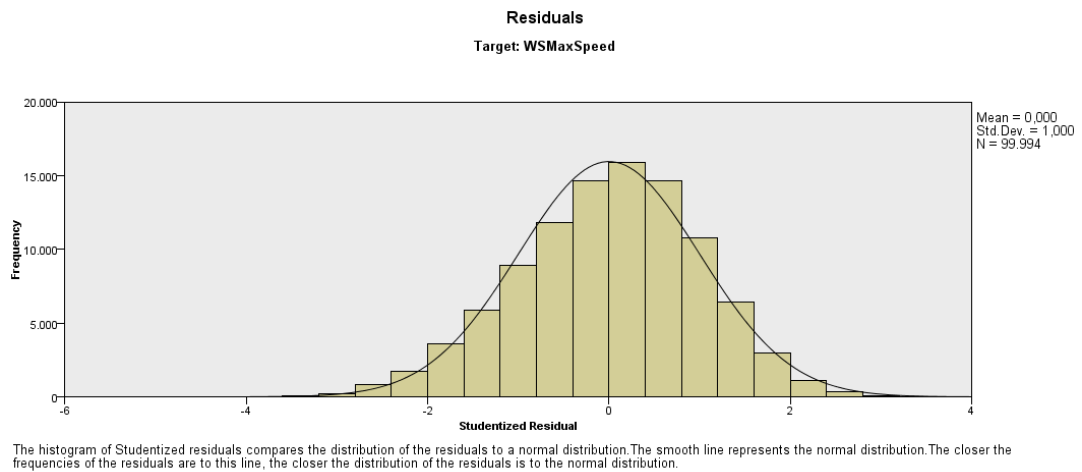


Figure 76: Residuals graph compared to a normal distribution, Regression Model 3

Regression Model 4, Target: WS Max Location

Table 50. Model summary for Regression Model 4

Target	WS. Max Location
Automatic Data Preparation	On
Model Selection Method	Forward Stepwise
Information Criterion	-72.987,595
Accuracy	76,9%

Table 51: Effects, Regression Model 4

Source	Sum of Squares	df	Mean Square	F	Sig.	Importance
Corrected Model	160.336,424	25	6.413,457	13.310,834	0,000	
TF.X	65.183,262	1	65.183,26	135.284,85	0,000	0,561
SC.SetbackDepthRatio Front	6.744,663	1	6.744,663	13.998,237	0,000	0,058
SC.VertexHeightRatio	6.572,733	1	6.572,733	13.641,403	0,000	0,057
SC.FacadeEndpoint TranslationRatioBack	4.718,058	1	4.718,058	9.792,111	0,000	0,041
SC.ConcavityTranslation RatioFront	4.407,020	1	4.407,020	9.146,567	0,000	0,038
V.ElevationRatio	3.895,085	1	3.895,085	8.084,935	0,000	0,034
TF.Irregularity	3.703,008	1	3.703,008	7.685,423	0,000	0,032
H.TotalHeight	3.202,432	1	3.202,432	6.646,499	0,000	0,028
SC.EaveDepthRatioFront	3.085,595	1	3.085,595	6.404,011	0,000	0,027
SC.SetbackHeightRatio	2.874,751	1	2.874,751	5.966,413	0,000	0,025
Residual	48.166,813	99.968	0,482			
Corrected Total	208.503,238	99.993				

Table 52: Coefficients, Regression Model 4

Model Term	Coefficient	Std. Error	t	Sig.	95% Confidence Interval	
					Lower	Upper
Intercept	1,373	0,045	30,240	0,000	1,284	1,462
TF.X	0,038	0,000	-367,811	0,000	-0,038	-0,038
SC.SetbackDepthRatio Front	3,050	0,026	118,314	0,000	3,000	3,101
SC.VertexHeightRatio	2,318	0,020	116,796	0,000	2,279	2,357
SC.FacadeEndpoint TranslationRatioBack	-0,672	0,007	-98,955	0,000	-0,686	-0,659
SC.ConcavityTranslation RatioFront	2,016	0,021	95,638	0,000	1,975	2,057
V.ElevationRatio	1,322	0,015	89,916	0,000	1,294	1,351
TF.Irregularity	-1,445	0,016	-87,667	0,000	-1,477	-1,413
H.TotalHeight	0,014	0,000	81,526	0,000	0,013	0,014
SC.EaveDepthRatioFront	3,347	0,042	80,025	0,000	3,265	3,429
SC.SetbackHeightRatio	-4,073	0,053	-77,243	0,000	-4,176	-3,969

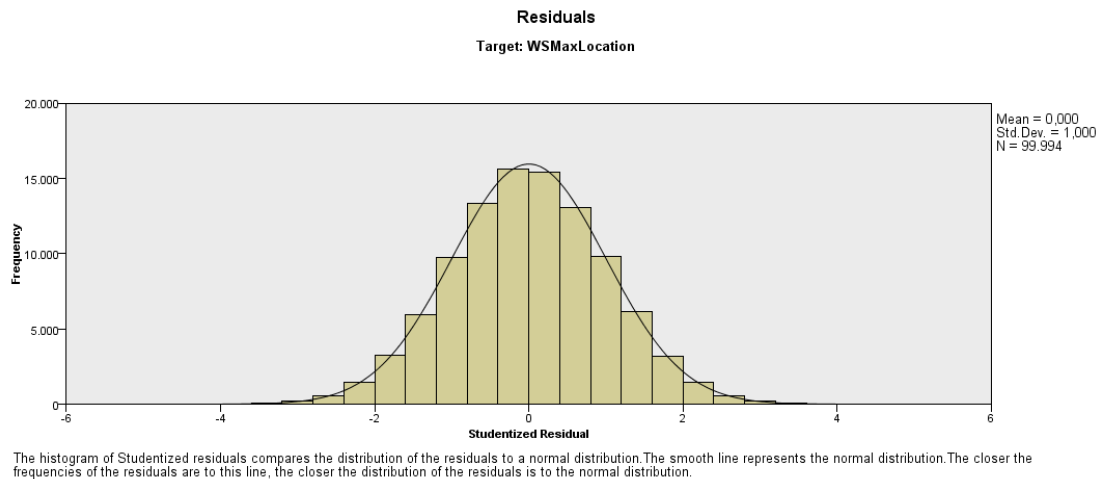


Figure 77: Residuals graph compared to a normal distribution, Regression Model 4

Regression Model 5, Target: NS Speed Up Regions

Table 53. Model summary for Regression Model 5

Target	NS.SpeedUp Regions
Automatic Data Preparation	On
Model Selection Method	Forward Stepwise
Information Criterion	-167.919,531
Accuracy	72,9%

Table 54: Effects, Regression Model 5

Source	Sum of Squares	df	Mean Square	F	Sig.	Importance
Corrected Model	50.130,443	25	2.088,768	11.202,319	0,000	
TF.X	12.251,880	1	12.251,880	65.708,321	0,000	0,225
SC.SetbackDepthRatio Front	10.467,602	1	10.467,602	56.139,020	0,000	0,192
SC.VertexHeightRatio	8.356,143	1	8.356,143	44.815,010	0,000	0,153
SC.FacadeEndpoint TranslationRatioBack	4.014,604	1	4.014,604	21.530,809	0,000	0,074
SC.Concavity TranslationRatioFront	3.265,859	1	3.265,859	17.515,198	0,000	0,060
V.ElevationRatio	2.797,070	1	2.797,070	15.001,024	0,000	0,051
TF.Irregularity	2.007,716	1	2.007,716	10.767,627	0,000	0,037
H.TotalHeight	1.918,058	1	1.918,058	10.268,778	0,000	0,035
SC.EaveDepthRatio Front	1.802,234	1	1.802,234	9.665,599	0,000	0,033
SC.SetbackHeigh Ratio	1.648,223	1	1.648,223	8.839,622	0,000	0,030
Residual	18.640,77	99.968	0,186			
Corrected Total	68.770,520	99.993				

Table 55: Coefficients, Regression Model 5

Model Term	Coefficient	Std. Error	t	Sig.	95% Confidence Interval	
					Lower	Upper
Intercept	-2,032	0,026	-78,567	0,000	-2,082	-1,981
SC.EaveDepthRatioFront	0,024	0,000	265,336	0,000	0,024	0,024
SC.FacadeEndpoint TranslationRatioFront	3,397	0,017	236,937	0,000	3,905	3,970
B.XRatio	-0,014	0,000	-211,696	0,000	-0,014	-0,013
B.YRatio	-0,640	0,004	-146,734	0,000	-0,649	-0,631
SC.FacadeEndpoint TranslationRatioBack	0,216	0,002	132,345	0,000	0,213	0,220
V.HeightRatio	0,412	0,003	122,479	0,000	0,405	0,418
SC.EaveDepthRatioBack	0,175	0,002	103,767	0,000	0,172	0,178
TF.Roundness	1,526	0,015	101,424	0,000	1,497	1,556
B.HeightRatio	1,286	0,013	98,314	0,000	1,261	1,312
TF.Vertice	3,134	0,033	94,019	0,000	3,069	3,200

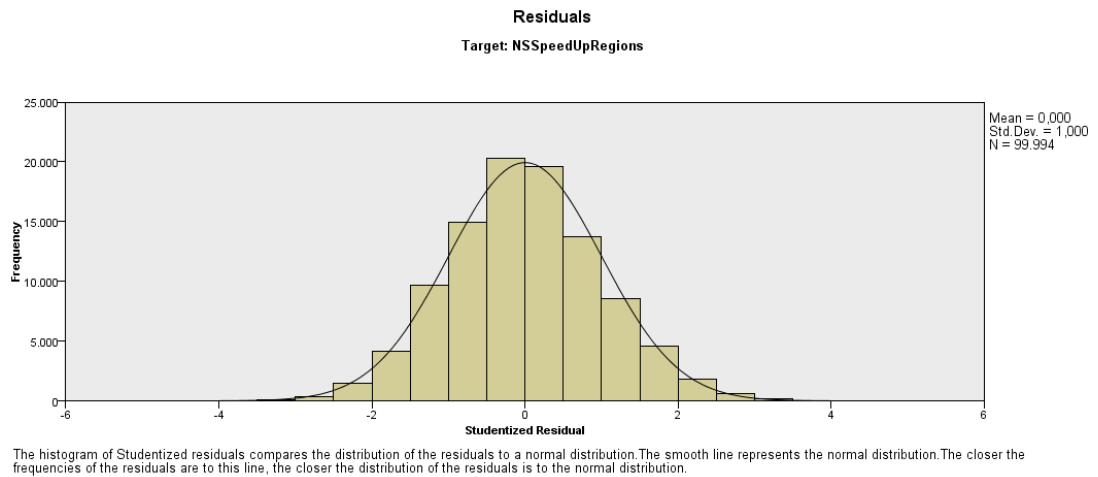


Figure 78: Residuals graph compared to a normal distribution, Regression Model 5

Regression Model 6, Target: NS Max Speed

Table 56. Model summary for Regression Model 6

Target	NS.Max Speed
Automatic Data Preparation	On
Model Selection Method	Forward Stepwise
Information Criterion	-169.270,760
Accuracy	63,5%

Table 57: Effects, Regression Model 6

Source	Sum of Squares	df	Mean Square	F	Sig.	Importance
Corrected Model	31.950,888	25	1.278,036	6.947,580	0,000	
TF.X	6.112,416	1	6.112,416	33.227,952	0,000	0,234
H.TotalHeight	4.419,120	1	4.419,120	24.022,957	0,000	0,169
B.YRatio	3.932,363	1	3.932,363	21.376,879	0,000	0,151
SC.DegreeOfCurve	2.371,069	1	2.371,069	12.889,466	0,000	0,091
B.XRatio	2.102,643	1	2.102,643	11.430,260	0,000	0,081
TF.Vertice	1.382,976	1	1.382,976	7.518,053	0,000	0,053
SC.FacadeEndpoint TranslationRatioBack	1.110,581	1	1.110,581	6.037,273	0,000	0,043
SC.VertexPositionRatio	956,749	1	956,749	5.201,021	0,000	0,037
SC.EaveDepthRatioBack	895,162	1	895,162	4.866,225	0,000	0,034
SC.FacadeEndpoint TranslationRatioFront	876,583	1	876,583	4.765,231	0,000	0,034
Residual	18.389,518	99.968	0,184			
Corrected Total	50.340,406	99.993				

Table 58: Coefficients, Regression Model 6

Model Term	Coefficient	Std. Error	t	Sig.	95% Confidence Interval	
					Lower	Upper
Intercept	9,279	0,028	330,763	0,000	9,224	9,334
TF.X	-0,012	0,000	-182,285	0,000	-0,012	-0,012
H.TotalHeight	0,016	0,000	154,993	0,000	0,016	0,016
B.YRatio	-0,250	0,002	-146,208	0,000	-0,254	-0,247
SC.DegreeOfCurve	0,299	0,003	113,532	0,000	0,294	0,304
B.XRatio	0,177	0,002	106,912	0,000	0,174	0,181
TF.Vertice	0,141	0,002	85,707	0,000	0,138	0,144
SC.FacadeEndpoint TranslationRatioBack	-0,326	0,004	-77,700	0,000	-0,334	-0,318
SC.VertexPositionRatio	0,493	0,007	72,118	0,000	0,479	0,506
SC.EaveDepthRatioBack	-1,746	0,025	-69,758	0,000	-1,795	-1,697
SC.FacadeEndpoint TranlsationRatioFront	-0,323	0,005	-69,031	0,000	-0,332	-0,314

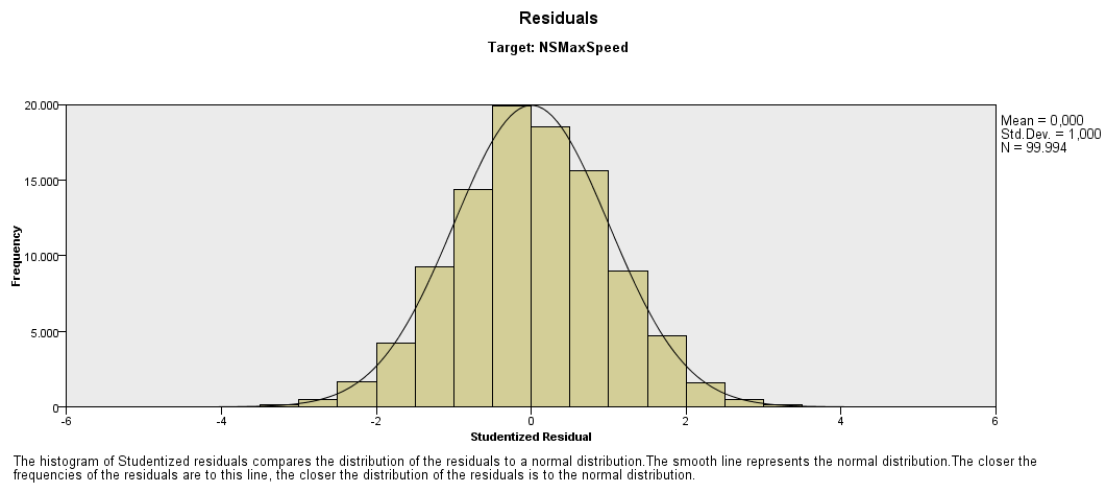


Figure 79: Residuals graph compared to a normal distribution, Regression Model 6

Regression Model 7, Target: RL Speed Up Regions

Table 59. Model summary for Regression Model 7

Target	RL.SpeedUp Regions
Automatic Data Preparation	On
Model Selection Method	Forward Stepwise
Information Criterion	-118.829,910
Accuracy	71,3%

Table 60: Effects, Regression Model 7

Source	Sum of Squares	df	Mean Square	F	Sig.	Importance
Corrected Model	75.708,399	25	3.028,336	9.940,763	0,000	
S.NormalTapering	19.166,630	1	19.166,630	62.916,048	0,000	0,240
V.WidthRatio	12.342,298	1	12.342,298	40.514,615	0,000	0,155
TF.Y	7.617,34	1	7.617,34	25.005,184	0,000	0,095
SC.SetbackDepthRatio Back	5.844,135	1	5.844,135	19.183,855	0,000	0,073
SC.FacadeEndpoint TranslationRatioFront	5.111,419	1	5.111,419	16.778,657	0,000	0,064
SC.SetbackDepthRatio Front	4.942,424	1	4.942,424	16.223,916	0,000	0,062
B.HeightRatio	4.564,997	1	4.564,997	14.984,982	0,000	0,057
SC.VertexHeightRatio	3.726,323	1	3.726,323	12.231,964	0,000	0,047
SC.EaveDepthRatio Front	2.799,025	1	2.799,025	9.188,030	0,000	0,035
H.TotalHeight	2.677,912	1	2.677,912	8.790,468	0,000	0,034
Residual	30.454,069	99.968	0,305			
Corrected Total	106.162,47	99.993				

Table 61: Coefficients, Regression Model 7

Model Term	Coefficient	Std. Error	t	Sig.	95% Confidence Interval	
					Lower	Upper
Intercept	-4,650	0,036	-128,791	0,000	-4,720	-4,579
S.NormalTapering	1,107	0,004	250,831	0,000	1,098	1,116
V.WidthRatio	3,261	0,016	201,282	0,000	3,229	3,292
TF.Y	0,015	0,000	158,130	0,000	0,015	0,015
SC.SetbackDepthRatio Back	2,942	0,021	138,506	0,000	2,900	2,984
SC.FacadeEndpoint TranslationRatioFront	-0,780	0,006	-129,532	0,000	-0,791	-0,768
SC.SetbackDepthRatio Front	-2,611	0,020	-127,373	0,000	-2,651	-2,571
B.HeightRatio	3,180	0,026	122,413	0,000	3,129	3,231
SC.VertexHeightRatio	1,745	0,016	110,598	0,000	1,714	1,776
SC.EaveDepthRatio Front	3,188	0,033	95,854	0,000	3,122	3,253
H.TotalHeight	0,012	0,000	93,757	0,000	0,012	0,013

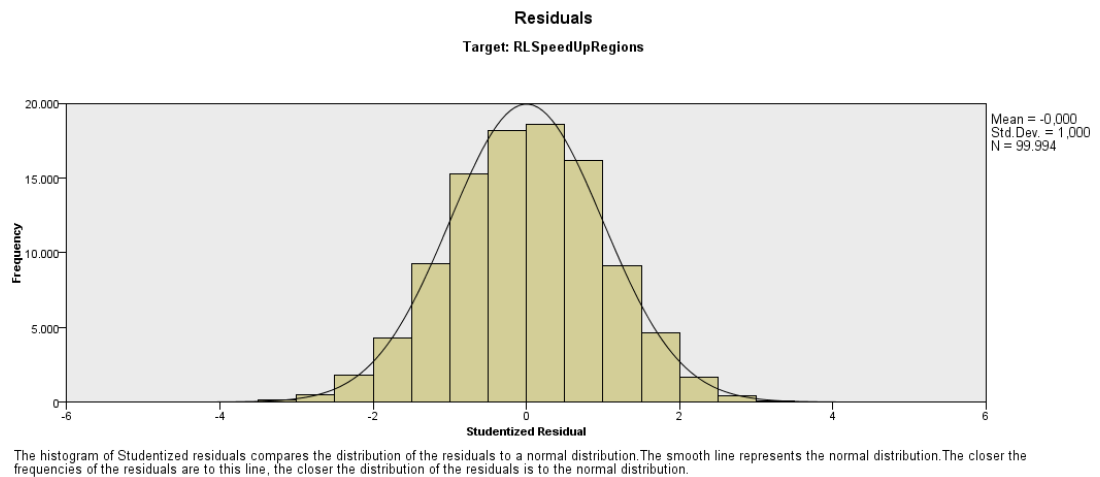


Figure 80: Residuals graph compared to a normal distribution, Regression Model 7

Regression Model 8, Target: RL Max Speed

Table 62. Model summary for Regression Model 8

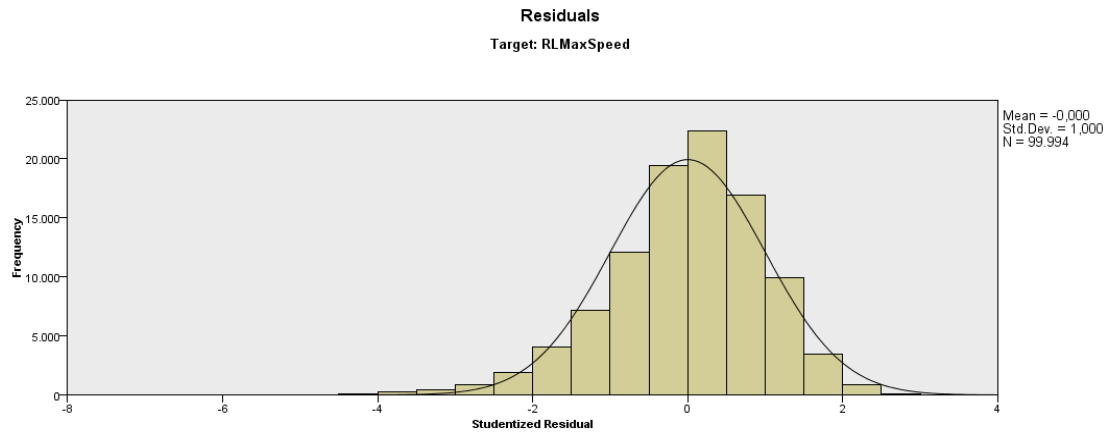
Target	RL. Max Speed
Automatic Data Preparation	On
Model Selection Method	Forward Stepwise
Information Criterion	-117.181,896
Accuracy	49,3%

Table 63: Effects, Regression Model 8

Source	Sum of Squares	df	Mean Square	F	Sig.	Importance
Corrected Model	30.095,136	25	1.253,964	4.048,916	0,000	
TF.Y	3.816,477	1	3.816,477	12.322,995	0,000	0,164
B.YRatio	3.688,492	1	3.688,492	11.909,745	0,000	0,159
SC.ConcavityRatio Front	2.578,730	1	2.578,730	8.326,443	0,000	0,111
TF.Vertice	2.471,218	1	2.471,218	7.979,299	0,000	0,106
TF.Irregularity	2.156,114	1	2.156,114	6.961,862	0,000	0,093
TF.X	1.071,552	1	1.071,552	3.459,927	0,000	0,046
B.HeightRatio	1.000,504	1	1.000,504	3.230,519	0,000	0,043
SC.SetbackDepthRatio Front	957,106	1	957,106	3.090,393	0,000	0,041
SC.FacadeEndpoint TranslationRatio Front	807,231	1	807,231	2.606,461	0,000	0,035
SC.FacadeEndpoint TranslationRatio Front	709,928	1	709,928	2.292,283	0,000	0,031
Residual	30.960,765	99.968	0,310			
Corrected Total	61.055,901	99.993				

Table 64: Coefficients, Regression Model 8

Model Term	Coefficient	Std. Error	t	Sig.	95% Confidence Interval	
					Lower	Upper
Intercept	11,694	0,036	328,956	0,000	11,624	11,763
TF.Y	-4,439	0,040	-111,009	0,000	-4,518	-4,361
B.YRatio	0,011	0,000	109,132	0,000	0,010	0,011
SC.ConcavityRatio Front	-0,202	0,002	-91,249	0,000	-0,206	-0,198
TF.Vertice	-1,496	0,017	-89,327	0,000	-1,528	-1,463
TF.Irregularity	0,175	0,002	83,438	0,000	0,171	0,179
TF.X	-0,750	0,013	-58,821	0,000	-0,775	-0,725
B.HeightRatio	-0,005	0,000	-56,838	0,000	-0,005	-0,005
SC.SetbackDepthRatio Front	1,367	0,025	55,591	0,000	1,319	1,415
SC.FacadeEndpoint TranslationRatio Front	-1,003	0,020	-51,054	0,000	-1,041	-0,964
SC.FacadeEndpoint TranslationRatio Front	-0,290	0,006	-47,878	0,000	-0,302	-0,278



The histogram of Studentized residuals compares the distribution of the residuals to a normal distribution. The smooth line represents the normal distribution. The closer the frequencies of the residuals are to this line, the closer the distribution of the residuals is to the normal distribution.

Figure 81: Residuals graph compared to a normal distribution, Regression Model 8

Regression Model 9, Target: PL Speed Up Regions

Table 65. Model summary for Regression Model 9

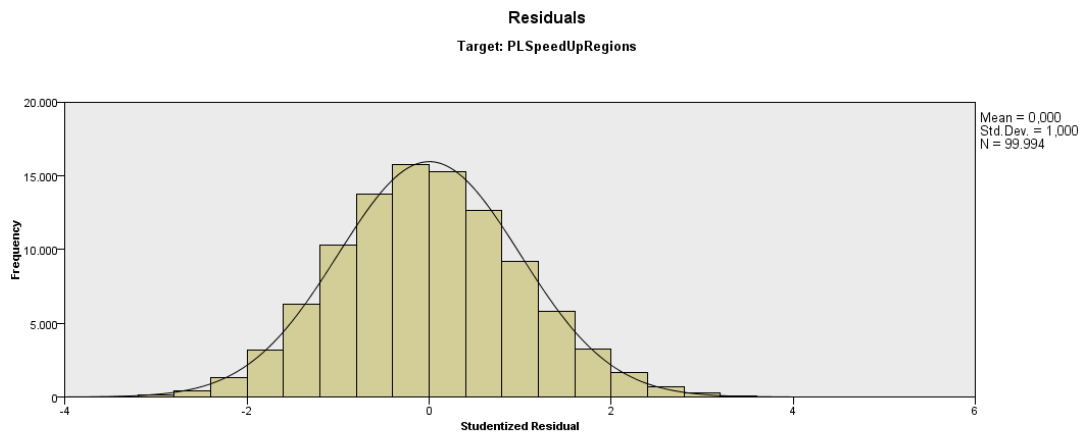
Target	PL.SpeedUp Regions
Automatic Data Preparation	On
Model Selection Method	Forward Stepwise
Information Criterion	1.329,606
Accuracy	55,7%

Table 66: Effects, Regression Model 9

Source	Sum of Squares	df	Mean Square	F	Sig.	Importance
Corrected Model	127.454,94	25	5.098,197	5.032,165	0,000	
SC.DegreeOfCurve	27.127,381	1	27.127,381	26.776,024	0,000	0,232
SC.SetbackDepthRatio Front	19.571,801	1	19.571,801	19.318,305	0,000	0,168
TF.Irregularity	8.769,771	1	8.769,771	8.656,184	0,000	0,075
SC.EaveDepthRatio Back	8.176,290	1	8.176,290	8.070,390	0,000	0,070
SC.Concavity TranslationRatioFront	6.667,195	1	6.667,195	6.580,841	0,000	0,057
SC.SetbackHeight Ratio	6.135,097	1	6.135,097	6.055,635	0,000	0,053
B.HeightRatio	6.105,809	1	6.105,809	6.026,726	0,000	0,052
SC.VertexHeightRatio	5.890,822	1	5.890,822	5.814,523	0,000	0,050
SC.VertexPosition Ratio	8.246,521	1	8.246,521	5.178,568	0,000	0,045
S.NormalTapering	3.788,027	1	3.788,027	3.738,964	0,000	0,032
Residual	101.279,79	99.968	1,013			
Corrected Total	228.734,72	99.993				

Table 67: Coefficients, Regression Model 9

Model Term	Coefficient	Std. Error	t	Sig.	95% Confidence Interval	
					Lower	Upper
Intercept	-2,067	0,066	-31,400	0,000	-2,196	-1,932
SC.DegreeOfCurve	1,012	0,006	163,634	0,000	1,000	1,024
SC.SetbackDepthRatio Front	-5,196	0,037	-138,990	0,000	-5,269	-5,123
TF.Irregularity	2,224	0,024	93,039	0,000	2,177	2,270
SC.EaveDepthRatio Back	5,276	0,059	89,835	0,000	5,161	5,392
SC.Concavity TranslationRatioFront	-2,480	0,031	-81,122	0,000	-2,540	-2,420
SC.SetbackHeight Ratio	-5,949	0,076	-77,818	0,000	-6,099	-5,800
B.HeightRatio	3,678	0,047	77,632	0,000	3,585	3,771
SC.VertexHeightRatio	2,194	0,029	76,253	0,000	2,138	2,251
SC.VertexPosition Ratio	1,153	0,016	71,962	0,000	1,122	1,185
S.NormalTapering	-0,492	0,008	-61,147	0,000	-0,508	-0,476



The histogram of Studentized residuals compares the distribution of the residuals to a normal distribution. The smooth line represents the normal distribution. The closer the frequencies of the residuals are to this line, the closer the distribution of the residuals is to the normal distribution.

Figure 82: Residuals graph compared to a normal distribution, Regression Model 9

Regression Model 10: Target: PL Max Speed

Table 68. Model summary for Regression Model 10

Target	PL.Max Speed
Automatic Data Preparation	On
Model Selection Method	Forward Stepwise
Information Criterion	-137.923,614
Accuracy	57,0%

Table 69: Effects, Regression Model 10

Source	Sum of Squares	df	Mean Square	F	Sig.	Importance
Corrected Model	33.324,500	25	1.388,521	5.516,855	0,000	
SC.Concavity TranslationRatioFront	6.010,579	1	6.010,579	23.881,166	0,000	0,213
SC.EaveDepthRatio Front	3.669,676	1	3.669,676	14.580,316	0,000	0,130
V.ElevationRatio	2.873,701	1	2.873,701	11.417,756	0,000	0,102
B.YRatio	2.507,722	1	2.507,722	9.963,653	0,000	0,089
SC.SetbackDepthRatio Back	2.223,396	1	2.223,396	8.833,971	0,000	0,079
H.TotalHeight	1.988,349	1	1.988,349	7.900,088	0,000	0,070
SC.VertexHeightRatio	1.605,200	1	1.605,200	6.377,761	0,000	0,057
TF.Irregularity	1.440,224	1	1.440,224	5.722,282	0,000	0,051
TF.Roundness	1.233,019	1	1.233,019	4.899,019	0,000	0,044
B.HeightRatio	1.088,461	1	1.088,461	4.324,662	0,000	0,038
Residual	25.160,898	99.968	0,252			
Corrected Total	58.485,398	99.993				

Table 70: Coefficients, Regression Model 10

Model Term	Coefficient	Std. Error	t	Sig.	95% Confidence Interval	
					Lower	Upper
Intercept	14,140	0,031	455,273	0,000	14,079	14,201
SC.Concavity TranslationRatioFront	-2,350	0,015	-154,535	0,000	-2,380	-2,320
SC.EaveDepthRatio Front	-3,646	0,030	-120,749	0,000	-3,705	-3,587
V.ElevationRatio	-1,119	0,010	-106,854	0,000	-1,140	-1,098
B.YRatio	-0,195	0,002	-99,818	0,000	-0,199	-0,191
SC.SetbackDepthRatio Back	-1,813	0,019	-93,989	0,000	-1,851	-1,775
H.TotalHeight	-0,010	0,000	-88,882	0,000	-0,010	-0,010
SC.VertexHeightRatio	1,135	0,014	79,861	0,000	1,107	1,163
TF.Irregularity	-0,875	0,012	-75,646	0,000	-0,897	-0,852
TF.Roundness	-2,775	0,040	-69,993	0,000	-2,853	-2,698
B.HeightRatio	1,478	0,022	65,762	0,000	1,434	1,522

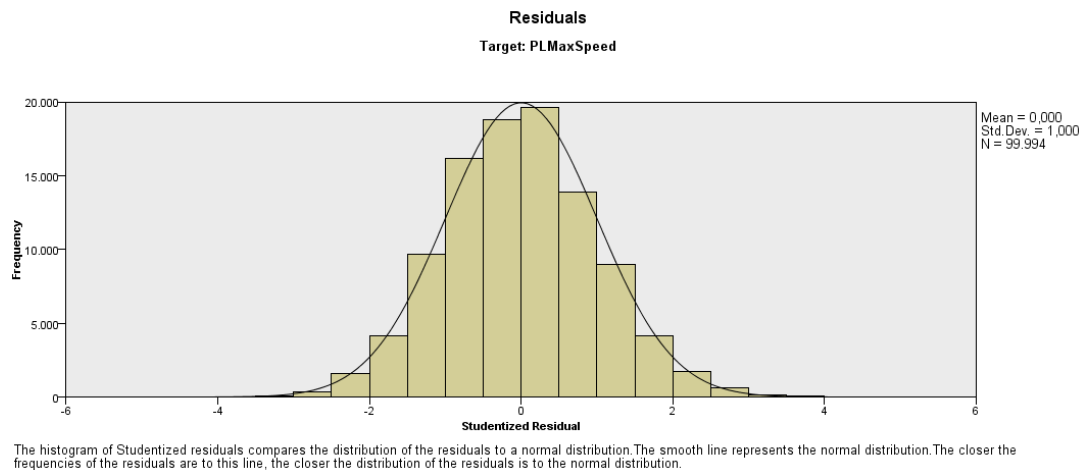


Figure 83: Residuals graph compared to a normal distribution, Regression Model 10

D.2 Correlation Matrices

Table 71: Correlation matrix of simulated dataset. (Simplified as columns are only outputs, rows are only inputs.)

PART 1		WS. Max Location	WS. Max Speed	WS. SpeedUp Regions	NS. MaxSpeed	NS. SpeedUp Regions
B.HR	Pearson Correlation	-,175**	,080**	,146**	,099**	-,052**
	Sig. (2-tailed)	0,000	0,000	0,000	0,000	0,000
	N	100000	100000	100000	100000	100000
B.XR	Pearson Correlation	-,156**	-,310**	,090**	-,120**	-,224**
	Sig. (2-tailed)	0,000	0,000	0,000	0,000	0,000
	N	100000	100000	100000	100000	100000
B.YR	Pearson Correlation	0,002	-,360**	0,000	-,374**	,120**
	Sig. (2-tailed)	0,546	0,000	0,979	0,000	0,000
	N	100000	100000	100000	100000	100000
H. Total Height	Pearson Correlation	,118**	,262**	,174**	,316**	,389**
	Sig. (2-tailed)	0,000	0,000	0,000	0,000	0,000
	N	100000	100000	100000	100000	100000
SC. Concavity Translation Ratio Front	Pearson Correlation	,177**	-,176**	,195**	-,072**	-0,004
	Sig. (2-tailed)	0,000	0,000	0,000	0,000	0,265
	N	100000	100000	100000	100000	100000
SC. Concavity Translation Ratio Back	Pearson Correlation	,127**	,032**	,117**	0,000	,077**
	Sig. (2-tailed)	0,000	0,000	0,000	0,886	0,000
	N	100000	100000	100000	100000	100000
SC .Degree Of Curve	Pearson Correlation	-,122**	-0,002	,254**	,240**	,132**
	Sig. (2-tailed)	0,000	0,592	0,000	0,000	0,000
	N	100000	100000	100000	100000	100000
SC. Eave Depth Ratio Back	Pearson Correlation	-0,006	-,232**	-,122**	-,217**	,007*
	Sig. (2-tailed)	0,060	0,000	0,000	0,000	0,024
	N	100000	100000	100000	100000	100000
SC. Eave Depth Ratio Front	Pearson Correlation	-0,005	-,310**	,115**	-,134**	-,314**
	Sig. (2-tailed)	0,142	0,000	0,000	0,000	0,000
	N	100000	100000	100000	100000	100000

Table 71 (continued)

SC. Facade Endpoint Translation Ratio Back	Pearson Correlation	-,148**	,175**	,121**	,036**	-0,004
	Sig. (2-tailed)	0,000	0,000	0,000	0,000	0,188
	N	100000	100000	100000	100000	100000
SC. Facade Endpoint Translation Ratio Front	Pearson Correlation	,048**	,185**	,093**	,043**	0,001
	Sig. (2-tailed)	0,000	0,000	0,000	0,000	0,707
	N	100000	100000	100000	100000	100000
SC. Setback Depth Ratio Back	Pearson Correlation	-,122**	-,094**	-0,006	-,149**	,174**
	Sig. (2-tailed)	0,000	0,000	0,074	0,000	0,000
	N	100000	100000	100000	100000	100000
SC. Setback Depth Ratio Front	Pearson Correlation	,169**	-,092**	-0,001	,077**	,093**
	Sig. (2-tailed)	0,000	0,000	0,692	0,000	0,000
	N	100000	100000	100000	100000	100000
SC. Setback Height Ratio	Pearson Correlation	-,057**	,060**	,033**	0,005	-,201**
	Sig. (2-tailed)	0,000	0,000	0,000	0,093	0,000
	N	100000	100000	100000	100000	100000
SC. Vertex Height Ratio	Pearson Correlation	,246**	-,031**	,148**	,060**	,121**
	Sig. (2-tailed)	0,000	0,000	0,000	0,000	0,000
	N	100000	100000	100000	100000	100000
SC. Vertex Positioning Ratio	Pearson Correlation	,062**	-,119**	-,332**	,119**	-,026**
	Sig. (2-tailed)	0,000	0,000	0,000	0,000	0,000
	N	100000	100000	100000	100000	100000
S. Normal Tapering	Pearson Correlation	,018**	,096**	0,002	-0,002	-,017**
	Sig. (2-tailed)	0,000	0,000	0,605	0,484	0,000
	N	100000	100000	100000	100000	100000
TF. Irregularity Ratio	Pearson Correlation	,075**	-,210**	-,122**	,066**	,036**
	Sig. (2-tailed)	0,000	0,000	0,000	0,000	0,000
	N	100000	100000	100000	100000	100000
TF. Roundness	Pearson Correlation	-,271**	-,095**	,123**	-,148**	0,001
	Sig. (2-tailed)	0,000	0,000	0,000	0,000	0,783
	N	100000	100000	100000	100000	100000
TF. Vertice	Pearson Correlation	,273**	,089**	-,081**	,167**	,168**
	Sig. (2-tailed)	0,000	0,000	0,000	0,000	0,000
	N	100000	100000	100000	100000	100000

Table 71 (continued)

TF.X	Pearson Correlation	-,667**	-,154**	,316**	-,418**	-,378**
	Sig. (2-tailed)	0,000	0,000	0,000	0,000	0,000
	N	100000	100000	100000	100000	100000
TF.Y	Pearson Correlation	,294**	,144**	-,394**	,055**	-,041**
	Sig. (2-tailed)	0,000	0,000	0,000	0,000	0,000
	N	100000	100000	100000	100000	100000
V. Elevation Ratio	Pearson Correlation	,126**	,225**	,008*	-,043**	-,143**
	Sig. (2-tailed)	0,000	0,000	0,011	0,000	0,000
	N	100000	100000	100000	100000	100000
V. Height Ratio	Pearson Correlation	,054**	,110**	,055**	-,015**	,155**
	Sig. (2-tailed)	0,000	0,000	0,000	0,000	0,000
	N	100000	100000	100000	100000	100000
V. Width Ratio	Pearson Correlation	,103**	,056**	,118**	-,106**	-0,002
	Sig. (2-tailed)	0,000	0,000	0,000	0,000	0,463
	N	100000	100000	100000	100000	100000
PART 2		Average Drag Coefficient	PL. MaxSpeed	PL. SpeedUp Regions	RL. MaxSpeed	RL. SpeedUp Regions
B.HR	Pearson Correlation	,120**	,292**	,188**	,163**	,086**
	Sig. (2-tailed)	0,000	0,000	0,000	0,000	0,000
	N	100000	100000	100000	100000	100000
B.XR	Pearson Correlation	-,275**	-,030**	-,060**	-,149**	,120**
	Sig. (2-tailed)	0,000	0,000	0,000	0,000	0,000
	N	100000	100000	100000	100000	100000
B.YR	Pearson Correlation	-,459**	-,309**	,032**	-,302**	,098**
	Sig. (2-tailed)	0,000	0,000	0,000	0,000	0,000
	N	100000	100000	100000	100000	100000
H. Total Height	Pearson Correlation	,394**	,017**	-,032**	,188**	-,157**
	Sig. (2-tailed)	0,000	0,000	0,000	0,000	0,000
	N	100000	100000	100000	100000	100000
SC. Concavity Translation Ratio Front	Pearson Correlation	-,119**	-,253**	,036**	-,181**	,183**
	Sig. (2-tailed)	0,000	0,000	0,000	0,000	0,000
	N	100000	100000	100000	100000	100000
SC. Concavity Translation Ratio Back	Pearson Correlation	-,056**	,074**	-,111**	,044**	-,120**
	Sig. (2-tailed)	0,000	0,000	0,000	0,000	0,000
	N	100000	100000	100000	100000	100000

Table 71 (continued)

SC .Degree Of Curve	Pearson Correlation	,180**	-,068**	,371**	0,005	-,130**
	Sig. (2-tailed)	0,000	0,000	0,000	0,115	0,000
	N	100000	100000	100000	100000	100000
SC. Eave Depth Ratio Back	Pearson Correlation	-,146**	-,115**	,120**	-,154**	-,103**
	Sig. (2-tailed)	0,000	0,000	0,000	0,000	0,000
	N	100000	100000	100000	100000	100000
SC. Eave Depth Ratio Front	Pearson Correlation	0,000	-,311**	,146**	-,240**	,248**
	Sig. (2-tailed)	0,973	0,000	0,000	0,000	0,000
	N	100000	100000	100000	100000	100000
SC. Facade Endpoint Tranlation Ratio Back	Pearson Correlation	,047**	-,102**	,244**	,090**	0,006
	Sig. (2-tailed)	0,000	0,000	0,000	0,000	0,070
	N	100000	100000	100000	100000	100000
SC. Facade Endpoint Translation Ratio Front	Pearson Correlation	,232**	,065**	-0,001	0,002	-0,001
	Sig. (2-tailed)	0,000	0,000	0,858	0,601	0,721
	N	100000	100000	100000	100000	100000
SC. Setback Depth Ratio Back	Pearson Correlation	-0,006	-,125**	,130**	-,072**	,109**
	Sig. (2-tailed)	0,053	0,000	0,000	0,000	0,000
	N	100000	100000	100000	100000	100000
SC. Setback Depth Ratio Front	Pearson Correlation	,062**	-,014**	-,117**	-,187**	-,264**
	Sig. (2-tailed)	0,000	0,000	0,000	0,000	0,000
	N	100000	100000	100000	100000	100000
SC. Setback Height Ratio	Pearson Correlation	,131**	0,002	-,122**	-,204**	-,118**
	Sig. (2-tailed)	0,000	0,597	0,000	0,000	0,000
	N	100000	100000	100000	100000	100000
SC. Vertex Height Ratio	Pearson Correlation	,120**	,065**	,024**	-,041**	,194**
	Sig. (2-tailed)	0,000	0,000	0,000	0,000	0,000
	N	100000	100000	100000	100000	100000
SC. Vertex Positioning Ratio	Pearson Correlation	-,140**	-,122**	,179**	-,110**	-,119**
	Sig. (2-tailed)	0,000	0,000	0,000	0,000	0,000
	N	100000	100000	100000	100000	100000
S. Normal Tapering	Pearson Correlation	,027**	,150**	-,201**	-,025**	,413**
	Sig. (2-tailed)	0,000	0,000	0,000	0,000	0,000
	N	100000	100000	100000	100000	100000
TF. Irregularity Ratio	Pearson Correlation	-,096**	-,246**	,128**	-,175**	,073**
	Sig. (2-tailed)	0,000	0,000	0,000	0,000	0,000
	N	100000	100000	100000	100000	100000
TF. Roundness	Pearson Correlation	-,224**	-,045**	,015**	-,135**	-,121**
	Sig. (2-tailed)	0,000	0,000	0,000	0,000	0,000
	N	100000	100000	100000	100000	100000

Table 71 (continued)

TF. Vertice	Pearson Correlation	,090**	,015**	,065**	,183**	,015**
	Sig. (2-tailed)	0,000	0,000	0,000	0,000	0,000
	N	100000	100000	100000	100000	100000
TF.X	Pearson Correlation	-,480**	-,007*	-,154**	-,264**	-,094**
	Sig. (2-tailed)	0,000	0,024	0,000	0,000	0,000
	N	100000	100000	100000	100000	100000
TF.Y	Pearson Correlation	,118**	,109**	-,045**	,242**	,249**
	Sig. (2-tailed)	0,000	0,000	0,000	0,000	0,000
	N	100000	100000	100000	100000	100000
V. Elevation Ratio	Pearson Correlation	-,016**	-,125**	-,096**	,030**	,064**
	Sig. (2-tailed)	0,000	0,000	0,000	0,000	0,000
	N	100000	100000	100000	100000	100000
V. Height Ratio	Pearson Correlation	,122**	,121**	-,122**	,046**	,147**
	Sig. (2-tailed)	0,000	0,000	0,000	0,000	0,000
	N	100000	100000	100000	100000	100000
V. Width Ratio	Pearson Correlation	,041**	-,143**	-,086**	-,112**	,375**
	Sig. (2-tailed)	0,000	0,000	0,000	0,000	0,000
	N	100000	100000	100000	100000	100000
**. Correlation is significant at the 0.01 level (2-tailed).						
*. Correlation is significant at the 0.05 level (2-tailed).						

Table 72: Correlation matrix for samples 51-54 (Simplified as columns are only outputs, row is TF.X)

		Average Drag Coefficient	WS Speed Up Regions	WS Max Speed	WS Max Location	NS Speed Up Regions	NS Max Speed	RL Speed Up Regions	RL Max Speed	PL Speed Up Regions	PL Max Speed
TF.X	Pearson Correlation	-,995**	. ^b	-,899*	-,890*	-,896	0,089	. ^b	-,960*	0,265	-,834
	Sig. (2-tailed)	0,005		0,101	0,110	0,104	0,911		0,040	0,735	0,166
	N	4	4	4	4	4	4	4	4	4	4
**. Correlation is significant at the 0.01 level (2-tailed).											
*. Correlation is significant at the 0.05 level (2-tailed).											
b. Cannot be computed because at least one of the variables is constant.											

Table 73: Correlation matrix for samples 55-58. (Simplified as columns are only inputs, the row is B.YRatio)

		Average Drag Coefficient	WS Speed Up Regions	WS Max Speed	WS Max Location	NS Speed Up Regions	NS Max Speed	RL Speed Up Regions	RL Max Speed	PL Speed Up Regions	PL Max Speed
B.YR	Pearson Correlation	-0,536	0,000	-,964**	. ^a	. ^a	-,941*	-,779	-,942*	0,779	-,899*
	Sig. (2-tailed)	0,464	1,000	0,036			0,059	0,221	0,058	0,221	0,101
	N	4	4	4	4	4	4	4	4	4	4
*. Correlation is significant at the 0.05 level (2-tailed).											
**. Correlation is significant at the 0.01 level (2-tailed).											

Table 74: Correlation matrix for samples 59 – 62 (Simplified as columns are only inputs, the row is SC.CTRB)

		Average Drag Coefficient	WS SpeedUp Regions	WS Max Speed	WS Max Location	NS Speed Up Regions	NS Max Speed	RL Speed Up Regions	RL Max Speed	PL Speed Up Regions	PL Max Speed
SC.CTRB	Pearson Correlation	-0,049	0,000	-0,139	0,407*	-0,084	-0,040	0,503*	0,000	0,274	-,561*
	Sig. (2-tailed)	0,858	1,000	0,608	0,118	0,757	0,884	0,358	1,000	0,304	0,024
	N	4	4	4	4	4	4	4	4	4	4
*. Correlation is significant at the 0.05 level (2-tailed).											
**. Correlation is significant at the 0.01 level (2-tailed).											

Table 75: Correlation Matrix for Samples 63 – 66 (Simplified as columns are only inputs, the row is V.HR)

		Average Drag Coefficient	WS SpeedUp Regions	WS Max Speed	WS Max Location	NS Speed Up Regions	NS Max Speed	RL Speed Up Regions	RL Max Speed	PL Speed Up Regions	PL Max Speed
V. HR	Pearson Correlation	0,303	0,758*	0,012	-0,919**	-0,758	-0,203	-0,303	-0,944	-0,303	-0,303
	Sig. (2-tailed)	0,697	0,242	0,988	0,081	0,242	0,797	0,697	0,056	0,697	0,697
	N	4	4	4	4	4	4	4	4	4	4
*. Correlation is significant at the 0.05 level (2-tailed).											
**. Correlation is significant at the 0.01 level (2-tailed).											

TEZ FOTOKOPİ İZİN FORMU

ENSTİTÜ

Fen Bilimleri Enstitüsü

Sosyal Bilimler Enstitüsü

Uygulamalı Matematik Enstitüsü

Enformatik Enstitüsü

Deniz Bilimleri Enstitüsü

YAZARIN

Soyadı :

Adı :

Bölümü :

TEZİN ADI (İngilizce) :

.....

.....

.....

.....

TEZİN TÜRÜ : Yüksek Lisans Doktora

1. Tezimin tamamı dünya çapında erişime açılsın ve kaynak gösterilmek şartıyla tezimin bir kısmı veya tamamının fotokopisi alınsın.
2. Tezimin tamamı yalnızca Orta Doğu Teknik Üniversitesi kullanıcılarının erişimine açılsın. (Bu seçenekle tezinizin fotokopisi ya da elektronik kopyası Kütüphane aracılığı ile ODTÜ dışına dağıtılmayacaktır.)
3. Tezim bir (1) yıl süreyle erişime kapalı olsun. (Bu seçenekle tezinizin fotokopisi ya da elektronik kopyası Kütüphane aracılığı ile ODTÜ dışına dağıtılmayacaktır.)

Yazarın imzası

Tarih